Effectiveness of Dampers in Response of Structures to Near-Fault Earthquakes

Xiao Qing Xu

A Thesis

in

The Department

of

Building, Civil and Environmental Engineering

Presented in Partial Fulfillment of the Requirements

for the Degree of Master of Applied Science (Civil Engineering) at

Concordia University

Montreal, Quebec, Canada

June 2006

Your file Votre référence
ISBN: 978-0-494-20736-9
Our file Notre référence
ISBN: 978-0-494-20736-9

ABSTRACT

Effectiveness of Dampers in Response of Structures to Near-Fault Earthquakes

Xiao Qing Xu

Using the nonlinear dynamic analysis program DRAIN-2DX, a detailed investigation for a one-story single-degree-of-freedom steel moment-resistant frame and a ten-story multi-degree-of-freedom steel moment-resistant frame with and without added dampers is performed. Three types of dampers - friction damper, viscoelastic damper and fluid viscous damper - are investigated. Comparisons of each damper under far-fault and near-fault ground motions are carried out. It is found that, when subjected to the same peak acceleration of ground motion, the dynamic responses of all damped structures under near-fault earthquakes with high pulse-type velocity are generally stronger than those under far-fault earthquakes. Moreover, from the energy point of view, comparison of effectiveness of different dampers subjected to earthquakes is performed. It is found that the friction-damped structure is relatively more effective than the other two dampers when subjected to selected earthquake records. However, the difference in the effectiveness among the three dampers is not large, which shows that all three types of dampers can be used to mitigate structural dynamic response effectively.

ACKNOWLEDGEMENTS

The author is deeply grateful to his supervisor Dr. O.A. Pekau. His expert guidance, thoughtful suggestions and constant support are indispensable for the progress of this research.

The author gratefully acknowledges the financial support for this work provided by the Natural Sciences and Engineering Research Council of Canada under Grant A8258 and by the Faculty of Engineering and Computer Science of Concordia University.

In addition, acknowledgement is also due to Dr. Xueye Zhu for his helpful advice.

Finally, the author extends deepest appreciation to his wife Ling Chen and his lovely son Steven for their infinite patience, love, understanding and support.

TABLE OF CONTENTS

LIST OF FIGURES

LIST OF TABLES

LIST OF SYMBOLS

A_{eq}	equivalent truss element cross section
$c,[c]$	damping coefficient, damping coefficient matrix
E	the Young's modulus of elasticity
E_D	damping energy
E_k	kinetic energy
E_s	elastic strain energy
E_Y	yielding energy
$f_D(t), F_D(t)$	damping force, damping force matrix
$f_I(t), F_I(t)$	inertia force , inertia force matrix
$f_s(t), F_s(t)$	structural internal force, structural internal force matrix
F_y	material yield strength
$G^{'}$	shear storage modulus of viscoelastic material
$G^{''}$	shear loss modulus of viscoelastic material
h	structural story height
I_b, I_c	moments of inertia of beam and column
$k,[k]$	structural stiffness, structural stiffness matrix
k_d	damper storage stiffness

k_{eq}	equivalent truss element stiffness
L, L_b	frame bay length, brace length
$m,[m]$	structural mass, structural mass matrix
M_{pb}, M_{pc}	yield moment of beam and column
N	exponent
$P(t)$	external load or external load vector
P_d	slip force of friction damper
T_n, T_d	structural vibration period without and with damper
$u(t)$	relative displacement
$\dot{u}(t)$	relative velocity
$\ddot{u}(t)$	relative acceleration
$\ddot{u}_g(t)$	ground acceleration
V_d	story shear force undertaken by friction damper
V_f	story shear force
α	mass-dependent damping coefficient
β	stiffness-dependent damping coefficient
ρ	stiffness ratio of the beam to the column
η_{VE}	viscoelastic material loss factor
ζ, ζ_i	damping ratio, modal damping ratio
$\zeta_{mass}, \zeta_{stiff}$	mass-dependent damping ratio, stiffness-dependent damping ratio

ω_n, ω_d	structural circular frequency without and with damper
λ	stiffness ratio of added brace to pure frame without brace
ϕ_i	The i th mode shape vector
{1}	unity vector

CHAPTER 1

INTRODUCTION

1.1 GENERAL

According to the earthquake-resistant design requirements, conventional building structures should be designed to resist minor and moderate earthquakes without significant damage and to resist major earthquakes without collapse. This means that the structure should keep in elastic state and its response is linear under moderate earthquakes. Under strong ground motions, the structure is allowed to have yielding in some specified components, such as the area of the beams near the columns and of the beam-column panel joints. Hence, the response of the structure is nonlinear. However, repairing damages caused by yielding under strong ground motions is usually very difficult and expensive; therefore, how to reduce the degree of structural damage is becoming an important issue.

Since structural damages result from the building structures absorbed a large amount of seismic energy, many researchers have tried to find effective ways to solve this problem from the energy point of view. Therefore, the concept of the supplement energy-dissipating devices has been raised over the past two decades. The purpose of energy-dissipating devices is to absorb added energy caused by the earthquake through incorporating specially designed members to the building in order to reduce the structural response and the degree of damage under random magnitude of ground movements. In this paper, three types of energy-dissipating devices namely friction-damped device,

viscoelastic-damped device and fluid-viscous-damped device have been studied, which will be discussed in detail in the following chapters.

With the development of monitor technology and the improvement of recording instruments, a lot of ground motions, especially for earthquake sites close to the fault rupture have been recorded. Research found that the characteristics of near-fault and far-fault earthquakes are obviously different. The near-fault ground movement displays a long-period pulse in its acceleration, velocity and displacement history records, which cannot be found for far-fault ground movement records. The different characteristics may lead to different responses in the structures.

1.2 OBJECTIVE OF THE RESEARCH

Although there is difference between the two types of earthquakes, little research has concerned about the difference of the effectiveness among different types of energy-dissipating devices to near-fault and far-fault earthquakes. Therefore, the major objective of this paper is to study dynamic responses, especially the nonlinear response, of a building structure with added dampers under strong ground motions. Comparing with its corresponding moment-resistant frame structure, the effectiveness of different dampers are analyzed and compared.

1.3 SCOPE

1.3.1 Types of Structural Models

In order to study the dynamic response of structures, two basic models are considered for the moment-resistant steel structural frames. One model is of a single-bay, one-storey, single-degree-of-freedom steel frame studied by Er Mao Gong [2004]. Another model is a single-bay, ten-storey, multi-degree-of-freedom steel frame studied by Parvaneh Baktash [1989]. With these two structural models, three types of energy-dissipating devices are investigated by studying the corresponding seismic behavior under different ground motion records.

1.3.2 Time History Dynamic Analysis Procedure

During the methods to study the dynamic response of the structures under earthquakes, the time history dynamic analysis, which provides accurate and detailed results, has been confirmed that it is much better than any other simplified equivalent static analysis. Therefore, many structural analysis programs have utilized this method. Here, two programs, i.e. inelastic time history dynamic analysis program DRAIN-2DX and three-dimensional static and dynamic finite element analysis program SAP2000 are used in the research.

SAP2000 is a powerful multi-purpose computer program for static and dynamic analysis and design of 2D and 3D structures. It performs nonlinear dynamic analysis with modeling a finite number of predefined special nonlinear elements. Therefore, it is not a completely general nonlinear analysis program, but its accuracy meets the design requirements of engineering practice.

DRAIN-2DX is a general-purpose computer program for static and dynamic analysis of plane frames. It performs dynamic analysis including nonlinear material properties. The structure is modeled as a plane assemblage of nonlinear elements connected at nodes [Prakash et al., 1993]. Of course, when compared with results of SAP2000, only the part of linear response from DRAIN-2DX is selected and analyzed.

The same as static analysis where static force should meet the requirement of equilibrium, structural dynamic analysis should also satisfy the force equilibrium conditions in its deformed position. Taking a single-degree-of-freedom system (SDOF) for example, the dynamic equilibrium equation is:

$$f_I(t) + f_D(t) + f_s(t) = P(t) \tag{1.1}$$

in which

$f_I(t)$ is the inertia force acting on the node mass

$f_D(t)$ is the damping force

$f_s(t)$ is the structural internal force

$P(t)$ is the external load

Equation (1.1) is suitable for both linear and nonlinear systems. However, for most structural buildings, which are only subjected to seismic motions, Equation (1.1) can be rewritten as follows:

$$m \cdot \ddot{u}(t) + c \cdot \dot{u}(t) + k \cdot u(t) = -m \cdot \ddot{u}_g(t) \tag{1.2}$$

or

$$m \cdot \Delta\ddot{u}(t)_i + c(t)_i \cdot \Delta\dot{u}(t)_i + k(t)_i \cdot \Delta u(t)_i = -m \cdot \Delta\ddot{u}_g(t)_i \tag{1.3}$$

where m is the nodal mass, $u(t)$ is the relative displacement, $\dot{u}(t)$ is the relative velocity, $\ddot{u}(t)$ is the relative acceleration, and $\ddot{u}_g(t)$ is the ground acceleration. However, Equation (1.2) is only valid for linear elastic structures because the damping and stiffness properties are constant. For nonlinear structures, it is better to use incremental form (1.3) to express inelastic behavior because the damping and stiffness properties are nonlinear. At the same time, it is assumed that the mass property remains unchanged. Of course, Equation (1.3) is also applicable to linear structures if the damping and stiffness properties become constant.

Although a lot of numerical methods can be used to solve Equation (1.2) and (1.3), due to limited to linear condition, the approximate Fast Fourier Transformation method and the Duhamel integral are not applicable to nonlinear systems. For convenience of calculation, in fact, no matter if the structure is linear or nonlinear; the incremental form of Equation (1.3) is used and solved by a direct step-by-step method in many computer programs including DRAIN-2DX and SAP2000. Nowadays, the direct step-by-step method is considered as the most powerful technique for dynamic analysis, particularly for nonlinear analysis. In this method, the equation of motion is integrated in the time domain without transformation of the equation into a different form. During each incremental time Δt_i, the damping $C(t)_i$ and stiffness $K(t)_i$ are assumed constant, and the calculated response at the end of each interval is considered as the initial condition for the next interval. At the same time, it checks the yield state of each element. The tangent stiffness and damping property modifications due to any change are applied at the end of each time step. In order to avoid error accumulation of any imbalance caused by

calculating assumptions, the equilibrium corrections and energy balance are also performed at the end of each step. Therefore, a nonlinear problem can be solved through an assembly of linearized incremental steps. Obviously the procedure can be carried out for any desired number of time increments. Linear structures can also be treated by the same process, which just becomes a little simpler than nonlinear analysis. The accuracy of this step-by-step procedure will depend on the length of the time increment Δt. An accurate solution can be obtained if a sufficient small increment Δt is used. The main factors that influence increment Δt are the natural period of the structure, the rate of variation of the applied loading $P(t)$, and the rate of variation of the nonlinear damping and stiffness properties [Clough, 1993]. In general, the time step should be no longer than one tenth of the fundamental period T of the structure. The following example and Table 1.1 clearly shows the effect of time step.

Example: Basic parameters of model

For a one-bay, single-degree-of –freedom structure, the basic parameters of the model are: concentrated mass of $m = 17319kg$, the fundamental period $T = 0.50192\sec$.

Time step Δt varies from 0.5sec to 0.001sec. The corresponding dynamic responses to the EL-Centro Earthquake, North-South Component (1940.5) are illustrated in Table 1.1.

It is found that the magnitude of time step greatly affects the accuracy of calculating results. Too large time step Δt will cause large calculating errors, and too small time step Δt will increase time to calculate. Therefore, it is very important to choose a correct and reasonable time step. From the Table 1.1, it is clearly to see that when the time step

is smaller than 0.01 sec, all the results are gradually close to constants, considering the influence of time interval of the input earthquake, time step of 0.005sec, which is also consistent with minimal time interval of selected earthquake records, is defined as a basic calculating parameter to use in the calculation.

1.4 ORGANIZATION OF THE THESIS

Chapter 1 Introduction

The objective of the research is presented.

Chapter 2 Literature Review

The previous research on supplement dampers is reviewed. The behavior of different types of supplement dampers, especially friction, viscoelastic and fluid-viscous damper, is presented.

Chapter 3 Characteristics of Earthquakes

Literature on previous research on behavior of structure under near-fault and far-fault earthquakes is reviewed. The earthquakes chosen in this paper are presented with time-history curves and corresponding frequency composition using Forward Fourier Transform method.

Chapter 4 Single-Degree-of-Freedom Systems

Linear and nonlinear time history analysis of a one-story moment-resisting frame (MRF) model, friction-damped model, viscoelastic-damped model and fluid viscous-damped

model are conducted using DRAIN-2DX programs. Their dynamic responses, such as interstory drift, top floor displacement, base shear force etc., are studied and compared.

Chapter 5 Multi-Degree-of-Freedom Systems

Linear and nonlinear time history analyses of a ten-story MRF model, friction-damped model, viscoelastic-damped and fluid-viscous-damped model under different earthquakes are conducted using DRAIN-2DX programs. Their dynamic responses are studied and compared.

Chapter 6 Conclusions

The conclusions of the research are presented.

Table 1.1 Accuracy Comparisons of Results under Different Time Steps

Dynamic Response of SDOF MRF to EL-Centro Ground Motion

Time Step	Time Ratio	Floor Displacement	Column Moment	Column Axial Force	Column Shear Force	Beam Moment
Δt	$T/\Delta t$	(mm)	(kN-m)	(kN)	(kN)	(kN-m)
0.5	1	19.955	50.97	6.113	39.92	22.07
0.1	5	12.933	56.42	7.389	44.44	24.85
0.09	5.6	14.916	55.65	7.864	43.7	24.43
0.07	7.2	18.714	54.18	7.283	42.64	23.69
0.05	10	18.692	54.48	7.305	42.86	23.84
0.03	16.7	19.542	54.34	7.206	42.74	23.77
0.01	50.2	19.609	54.41	7.705	42.8	23.81
0.007	71.7	19.612	54.4	7.704	42.8	23.81
0.005	100.4	19.632	54.4	7.073	42.8	23.81
0.003	167.3	19.631	54.4	7.073	42.8	23.81
0.001	502	19.63	54.4	7.073	42.8	23.81

SDOF: Single-Degree-of-Freedom; **MRF**: Moment-Resisting Frame; **T**: Period

CHAPTER 2

LITERATURE REVIEW

Earthquakes, especially strong ground motions, usually cause devastating consequence to the development of modern society. For example, the Pakistan earthquake of magnitude 7.6; happened on Oct. 8, 2005, and directly led to enormous loss of life and property: more than 40,000 people dead, a lot of residential and office buildings destroyed or reduced to rubble within the hazardous zone, and more than two million people homeless. Therefore, how to find better methods to protect structures, together with their occupants and contents, from these hazards of destructive earthquakes is one of the constant challenges in structural engineering.

Faced with earthquakes, the conventional structures are designed to resist ground motions through a combination of material strength, structural elements' energy-consuming ability, and overall structure deformability. During major earthquakes, the structures are permitted to have significant inelastic deformation, which is designed to occur in critical regions of the structure, usually in the beam or near to the beam-column joints. This significant inelastic behavior is able to absorb additional energy input by external ground motions. However, such permitted inelastic behavior also results in significant damage to the structural members in the form of plastic hinges induced in the connections. This kind of damage is usually difficult to repair although the structure may survive a severe earthquake, but is no longer able to meet practical requirements. On the other hand, excessive deformation in the structure will directly lead to collapse, which is not

permitted by codes and regulations. Therefore the structural ability to withstand earthquakes is restricted by the limit of structural deformability. It may be better to find other ways to improve the seismic-resistant ability of the structure.

When a structure is subjected to an earthquake, immense amount of kinetic energy will be fed into the building. Therefore, energy is a fundamental factor in earthquake-resistant dynamic analysis. The method to increase supplemental energy dissipation may be a suitable technology to reduce damage. In fact, the energy approach has been widely used by many researchers [Uang and Bertero, 1990; Aiken et al., 1993; Symans and Constantinou, 1994]. According to the energy balance principle, input energy provided by external work must be equal to internal energy. Therefore, the energy conservation relationship can be expressed as follows [Soong and Constantinou, 1994]:

$$E = E_k + E_s + E_Y + E_D \tag{2.1}$$

where E is the total input energy from the earthquake, E_k is the absolute kinetic energy, E_s is the recoverable elastic strain energy, E_Y is the irrecoverable energy dissipated by the structure through inelastic deformation, E_D is damping energy dissipated by inherent structural damping and supplemental damper devices. From the above equation, it is found that, the structural dynamic response will be reduced if other damping devices are added to dissipate part of input the energy. Therefore, from the energy point of view, using supplemental damping devices is an alternative to reduce dynamic response and to improve structural earthquake-resistant ability. As special designed members, these devices are incorporated into the structure. They can function only when passively induced by external force, and cannot adjust themselves to the change of either external

loading conditions or structural dynamic responses. Therefore these kinds of devices are called passive control systems. Based on this fundamental concept, many passive control systems, such as friction dampers, fluid viscous dampers, viscoelastic dampers, and metallic yield dampers, have been researched, developed and used over the past three decades.

2.1 FRICTION DAMPERS

2.1.1 Behavior of Friction Dampers

Friction damper (FD) mainly dissipates energy by means of heat that is generated by Coulomb friction through two surfaces sliding past each other. The slipping load provided by friction damper, which overcomes friction force, should be predetermined according to the practical designed requirements of the structural response. Usually, when inserted into the structure, the damper does not work or is not permitted to slip under wind and moderate earthquakes. It should slip at a given value of force during severe earthquakes. Therefore, the force-displacement relationship of a friction damper is that, before the damper force reaches its slipping force, the damper force is increased linearly with increase of displacement; when the damper force reaches its slipping value, the damper will keep its slipping force with the increase of displacement. Through this slipping process, the friction damper transforms seismic energy into friction heat and dissipates energy. When unloading from the maximum displacement, the force-displacement relationship is changed to a path parallel to the initial non-slipping state until the damper works in the opposite direction. The hysteretic loop of friction damper is

a rectangular loop as illustrated in Fig. 2.1a, similar to that of an ideal elasto-plastic material.

2.1.2 Types of Friction Dampers

There has been considerable progress in the research on friction dampers in recent years, and a variety of friction devices have been developed. Among them, the Sumitomo Friction Damper, the Pall Friction Damper, and the Slotted Bolted Connection Damper are widely used in earthquake-resistance structural engineering.

The Sumitomo Friction Damper, as seen in Fig. 2.2, is developed by Sumitomo Metal Industries of Japan [Soong and Constantinou, 1994]. The device utilizes a metal cylindrical casing with friction pads that slide against the inner surface of the device. The sliding surface consists of a bronze friction pad sliding against a steel casing. The steel casing also has a graphite coating to ensure a stable frictional force and to help prevent corrosion over time. The friction force may be altered and calibrated in advance by the manufacturer.

The Pall Friction Damper, as shown in Fig. 2.3, is designed by Pall Dynamics Limited [Soong and Constantinou, 1994]. The device is usually incorporated at the intersection of cross bracing. The device consists of a series of steel plates with slotted holes. They are clamped together with high-strength bolts. When seismic load is applied, the compression brace buckles while the tension brace induces slippage at the friction joint. This in turn activates the four links that force the compression brace to slip. The links are specially

designed to ensure that a stable friction force can be developed. The friction force of the device can be adjusted by tightening or loosening the bolts.

The Slotted Bolted Connection Damper, as shown in Fig. 2.4, is proposed by Fitzgerald [Soong and Constantinou, 1994]. Similar to the Pall Friction Damper, the device is also inserted at the concentrically braced connections. The device consists of similar sized steel bracing arms that are interlocked through bolts passing through slots in each arm. The friction force of the device can be changed by varying the pretension in the bolts.

No matter what kind of device, the concept of the energy dissipation in all the three devices is the same: all of them utilize the mechanism of solid friction to dissipate external seismic energy.

2.1.3 Previous Research and Application of Friction Dampers

In the past thirty years, a lot of time and energy have been paid to the study of the behavior of supplemental friction dampers and their applications in engineering.

In 1982, a ten-story braced frame model with the Pall Friction Damper was firstly proposed by Pall and Marsh [1982]. The hysteretic mechanics of the friction damper was investigated. The behavior of a friction-damped frame with no other type of damping was compared with the behavior of moment-resisting frame (MRF) and ordinary cross-braced frame (CBF). The study shows that when MRF is equipped with friction dampers, its ability to resist earthquake can be increased efficiently. In 1989, the Pall Friction Damper

was further modeled by Baktash [1989]. From the energy point of view, a direct static method to calculate the optimum slip forced was proposed in the study. The results confirmed the opinions proposed by Pall that friction dampers are very effective to reduce the dynamic response of structures especially the floor drift and the top floor displacement. A more detailed parameter study about optimum slip load of the Pall Friction damper was conducted by Tan [1992]. A response spectrum was developed for the Pall Friction Damped bracing frame (FDBF) for modal analysis and compared with a series of analytical calculations. A force reduction factor of the friction damped systems for engineering design was proposed by the author.

In order to examine the reliability of friction dampers, Colajanni and Papia [1995] paid more attention to study the dynamic response of FDBF and ordinary cross-braced frames (CBF). Based on two different cyclic force-displacement hysteretic relationships, the study demonstrated that FDBF shows more stable dynamic response than CBF. In 1997, Colajanni and Papia [1997] further studied the structural parameters that influence the dissipative capacity of the friction damper when inserted in a structure. Research found that the period of vibration T of the structure, the structural lateral stiffness ratio, and slip load are three important factors. They analyzed the response of a one story single-degree-of-freedom frame and developed approximate analytical expressions to characterize the hysteretic behavior of the structure and defined global slip loads. Based on the global parameter concept, a possible simplified design criterion was proposed such that the behavior of multistory braced systems may be evaluated from the one-story system.

In order to simplify the design procedure for the use of dampers, Levy et al. [2001] proposed a simple method to analyze the structural response with the slotted bolted connection dampers (SBC). The study showed that equivalent SDOF frames could be used to model MDOF frames. The results were satisfactory when compared with those of MDOF frames by a full nonlinear analysis based on certain assumptions.

In addition to many analytical studies, there also have extensive applications of the friction damper in practical engineering. Taking the Pall Friction Damper for example, many new engineering projects selected this kind of damper as their main energy-absorbing device. A total of 88 friction dampers were mounted in Concordia University's Engineering, Computer Science and Visual Arts Complex in 2004. More than 50%of the project cost was saved compared to conventional structural design. The Desjardins Life Insurance Building having a six-story concrete frame constructed in1996, an eleven-storey concrete frame condominium building finished in 1995, the headquarters of the Canadian Space Agency built in 1992, and a ten-story Concordia University Library Building completed in 1991 all chose friction dampers as supplemental energy-dissipating devices to reduce the structural dynamic response and obtained good usage and economical benefits. Moreover, friction damper can also be used in seismic rehabilitation work. A sixteen-story Quebec Provincial Police Headquarters built in 1964, Boeing Commercial Airplane Factory in America, and a four-story steel frame, the Moscone West Convention Center located in downtown San Francisco, which is 110 feet high with clear spans of 40 to 90 feet, were upgraded for seismic-resistance ability

through installing the friction dampers. Other types of friction damper were also widely used around the world over the past three decades.

2.2 FLUID VISCOUS DAMPERS

2.2.1 Behavior of Fluid Viscous Dampers

Fluid viscous dampers (VD) dissipate energy through a finite movement of a piston in a highly viscous fluid. By pushing viscous fluid through small orifices, mechanical kinetic energy can be transferred to heat and dissipated. The VD damper provides a resistant force, which is usually out of phase with the displacement of the structure. Therefore, it acts in a direction opposite to that of the input motion. This means that the damping force does not significantly increase the seismic loads for a comparable degree of structural deformation. Moreover, research found that VD dampers have no apparent storage stiffness when the excitation frequency is within a low frequency, e.g. 0 to 3 Hz, which is usually sufficient to cover the first mode vibration frequency of most building structures. Hence, when a VD damper is incorporated into a structure, the influence to the fundamental natural period and mode shape of the structure can be ignored.

The VD damper force is proportional to the relative velocity between the ends of the damper. The damping law is as follows:

$$f_d = c\dot{u}^N \tag{2.2}$$

Where:

f_d is the damper force, c is damping coefficient, $\dot{u}$ is deformation velocity, and N is an exponent that can range from 0.1~1.0 for seismic applications.

Noting that there is no spring force in the Equation (2.2), damper force varies only with velocity. Because of no restoring force provided by VD damper, the structure itself must resist all static lateral loads. The hysteretic loop of VD damper is an elliptical type loop as illustrated in Fig. 2.1b.

2.2.2 Types of Fluid Viscous Dampers

According to Equation (2.2), when $N = 1$, $f_d = c\dot{u}$ indicating that the damping force is linear; whereas, when $N \neq 1$, the damping force is non-linear. Therefore, there are two basic types of VD dampers: linear VD dampers and non-linear VD dampers.

Fig. 2.5 shows one of the typical fluid viscous dampers provided by Taylor Devices Inc. It consists of a stainless steel piston with a bronze orifice head and an accumulator. The stainless container is filled with silicone oil, which is non-flammable, non-toxic and stable for extremely long periods of time.

2.2.3 Previous Research and Application of Viscous Dampers

As an energy-dissipating device for the purpose of mitigating seismic response in building structures, fluid viscous damper began to be studied in the University of New York at Buffalo by Soong and Constantinou [1994]. In 1998, a fluid damper was tested by Symans and Constantinou [1998]. Two influential parameters, frequency and temperature were investigated. A kind of mathematical model for fluid damper behavior was proposed and compared with experimental results. Energy response history, peak structural deformation and peak structural force were analyzed. Test simulation and

analytical research clearly demonstrated that the use of fluid dampers, especially non-linear fluid dampers resulted in reduction of structural dynamic response.

Although linear fluid dampers can simply be modeled and analyzed, studies show that the damper may develop excessive damper force than a non-linear damper when the structural velocity is very large under strong or near-fault earthquakes [Lin and Chopra, 2002]. Therefore, researchers paid more attention to study the behavior of the non-linear fluid damper. Pekcan et al. [1999] investigated the behavior of the non-linear damper under spectral pseudo-velocity and actual relative velocity. Analysis showed that it is suitable to use actual relative velocity to design the damper. Based on comparison and analysis, an empirical expression was proposed to transform pseudo-velocity to actual relative velocity. A simplified design procedure was proposed based on equivalent power consumption formulation. In 2002, Lin and Chopra [2002] investigated the earthquake response of SDOF systems with a non-linear fluid damper. The study showed that the non-linearity of the damper has little influence on the peak response of systems in the velocity sensitive region.

More researchers investigated the efficacy of using fluid dampers to reduce dynamic response of symmetric-plan and asymmetric-plan one-story or multi-story structures [Lin and Chopra, 2001]. Studies confirmed that fluid damper is a very effective energy-dissipating device to mitigate the structural response induced by ground motions.

Fluid viscous dampers have many engineering applications. It can be used in parallel with base isolation (Fig. 2.6a), in the diagonal member (Fig. 2.6b), in chevron brace (Fig. 2.6c), horizontally at the top of a chevron brace (Fig. 2.6d), in toggle brace (Fig. 2.6e) and horizontally between adjacent structures (Fig. 2.6f). The seismic upgrade of an 8-story concrete building located in Los Angeles using fluid damper was conducted and investigated by Naeim and Rhaman [2000]. More detailed investigations about using fluid viscous dampers can be found in the paper [Symans and Constantinou, 1998].

2.3 VISCOELASTIC DAMPERS

2.3.1 Behavior of Viscoelastic Dampers

The viscoelastic damper (VE) dissipates energy through shear deformation of viscoelastic materials. The most commonly used VE materials are acrylic polymers, which are known to be very stable with good aging properties, and good chemical ability to resist environmental pollutants. Studies found that the behavior of the VE material is influenced by its shear storage modulus $G^{'}$, the shear loss modulus $G^{''}$, their ratio $\gamma = G^{'}/G^{''}$, and material loss factor $\eta = G^{''}/G^{'}$ [Mahmoodi, 1969]. The loss modulus controls the energy dissipation capacity of the material. The storage modulus affects the stiffness of the structure to which the VE damper is added. The VE damper properties are dependent on excitation frequency, ambient temperature, and allowed material shear strain level.

Similar to the VD damper, the VE damper also exhibits an elliptically hysteretic loop, as in Fig. 2.1c, which is dependent on velocity. The damping law is as follows:

$$f_d = k_d u + c\dot{u}^N \tag{2.3}$$

where:

f_d is the damper force, k_d is damper storage stiffness, c is damping coefficient, u is damper deformation, $\dot{u}$ is damper deformation velocity, and N is an exponent. From Equation (2.3), it is seen that the VE damper also adds additional stiffness when it is inserted to a structure, unlike the VD damper.

2.3.2 Type of Viscoelastic Dampers

VE materials are manufactured by the 3M Company. Fig. 2.7 and Fig. 2.8 shows two basic configurations used as a VE damper in seismic-resistant structures. The VE materials are bonded to a central and two exterior steel plates and the damper can be installed in the diagonal bracing element. When relative motion between the exterior steel plates and the center plate is caused by structural vibration, the damper produces shear deformation and then energy is dissipated.

2.3.3 Previous Research and Application of Viscoelastic Dampers

In order to evaluate the suitability of VE dampers for seismic design application, many experiments have been carried out for steel frames.

A nine-story, three bay, 1/4-scale model with two types of VE material dampers was tested by Aiken et al. [1990]. Test results demonstrated the effectiveness of VE dampers in reduction of the structural dynamic response under earthquakes.

An examination of a five-story, single bay, 2/5-scale model with VE dampers was conducted by Chang et al. [1992]. Only one key factor about ambient temperature with different excitation frequency and strain level, which influence the properties of VE material, was considered and tested in the study. The examination showed that environmental temperature is an important factor to determine the property of the VE material. Based on the test data, empirical equations to estimate the stiffness and loss factors of the VE damper were proposed.

One model of a 2/5-scale ,five-story, single bay steel frame; one model of a 2/5-scale, three-story steel frame and one model of a 1/3-scale, three-story reinforced concrete frame with VE dampers to different earthquakes were separately tested by Chang et al. [1995], Chang et al. [1996] and Shen et al. [1995]. The tests confirmed the reasonableness of the modal strain energy method to predict the modal damping ratio of the structure.

Moreover, a series of full-scale experiments were developed by Zhang et al. [1989], Lai et al. [1995], Chang and Lin [2004], and Min et al. [2004]. All the test results confirmed that the effectiveness of VE dampers is similar to that of using small-scale model. At the same time, the modal strain energy method also can be used to analyze the damping ratio of structures with practical dimensions. Therefore, it is feasible to use VE dampers in practical applications.

As well experimental studies, analytical research was also developed. In 1995, Shen and Soong [1995] proposed an analytical model to evaluate the hysteretic behavior of VE damper. Tezcan and Uluca [2003] analyzed three different models based on the Maxwell model using SAP2000 program. The results demonstrated the feasibility and reasonableness of analytical models.

Seismic retrofit of a four-story steel frame with viscoelastic damper in the Los Angeles area was developed by Kanitkar et al. [1998]. Detailed design method of VE dampers, design requirements and design procedures were presented in the paper. It was confirmed that VE damper was an effective energy-dissipating device to control deformation of the structure.

2.4 PREVIOUS COMPARATIVE RESEARCH OF PASSIVE CONTROL DEVICES

In 1990, Aiken and Kelly [1990] conducted earthquake simulator tests and analytical analysis on dynamic behavior of a three-bay, nine-story steel structure with two different dampers, a friction damper and a viscoelastic damper. The effectiveness of each damper was evaluated and confirmed. However, direct comparisons of effectiveness of two dampers were not performed.

In 1997, Fu and Kasai [1997] proposed a consistent mathematical expression for both viscoelastic damper and pure viscous damper. Parameter analysis and analytical comparison of a ten-story steel frame with VE damper and VD damper to the artificial

earthquake record was performed. Research found that VD damped frames have a little higher efficiency in energy dissipation than VE damped frame when damper is subjected to the same deformation.

In conclusion, different type of dampers have been extensively tested, studied and some of them have been used in practical.

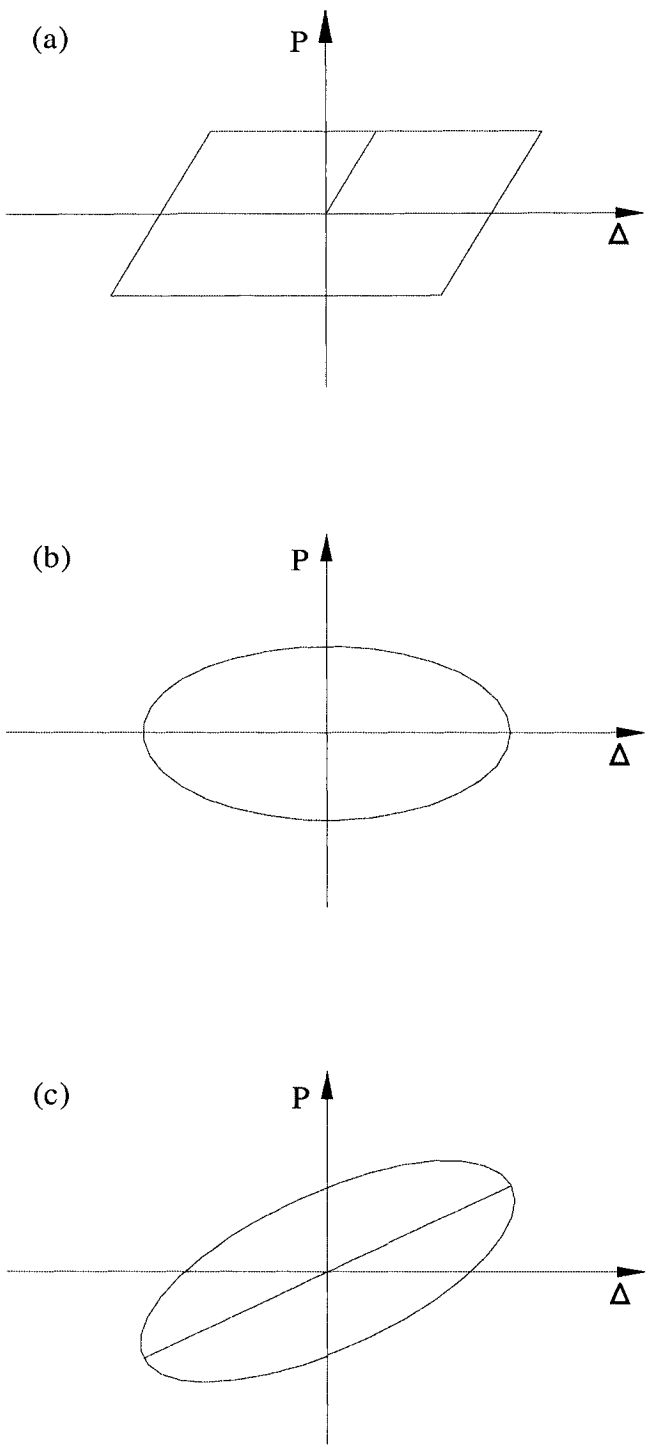

Fig. 2.1 Hysteretic Loops of Force-Displacement Relationship (a) Friction Damper; (b) Fluid Viscous Damper (c) Viscoelastic Damper

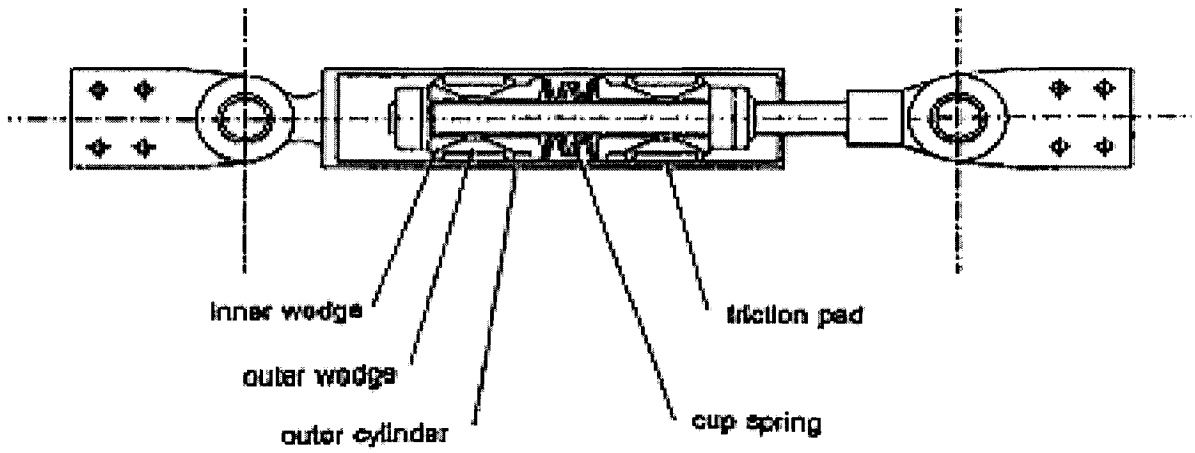

Fig. 2.2 Sumitomo Friction Damper [Ian D. Aiken, 1990]

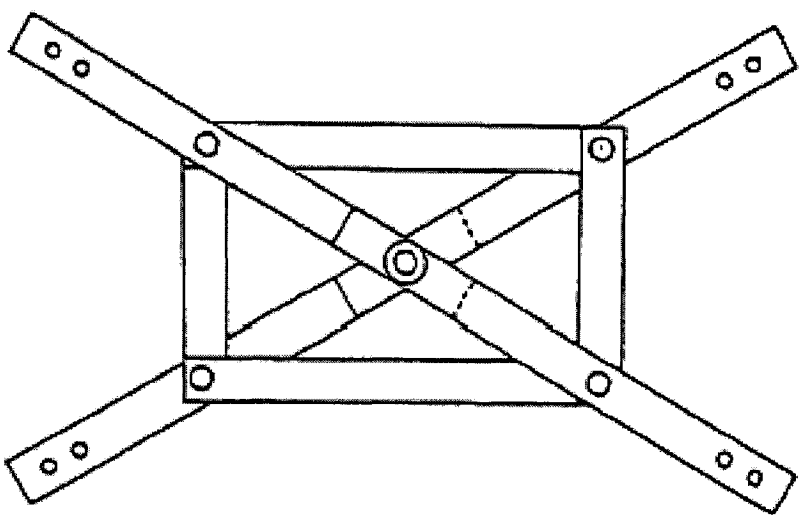

Fig. 2.3 Pall Friction Damper [A.S. Pall and C. Marsh, 1982]

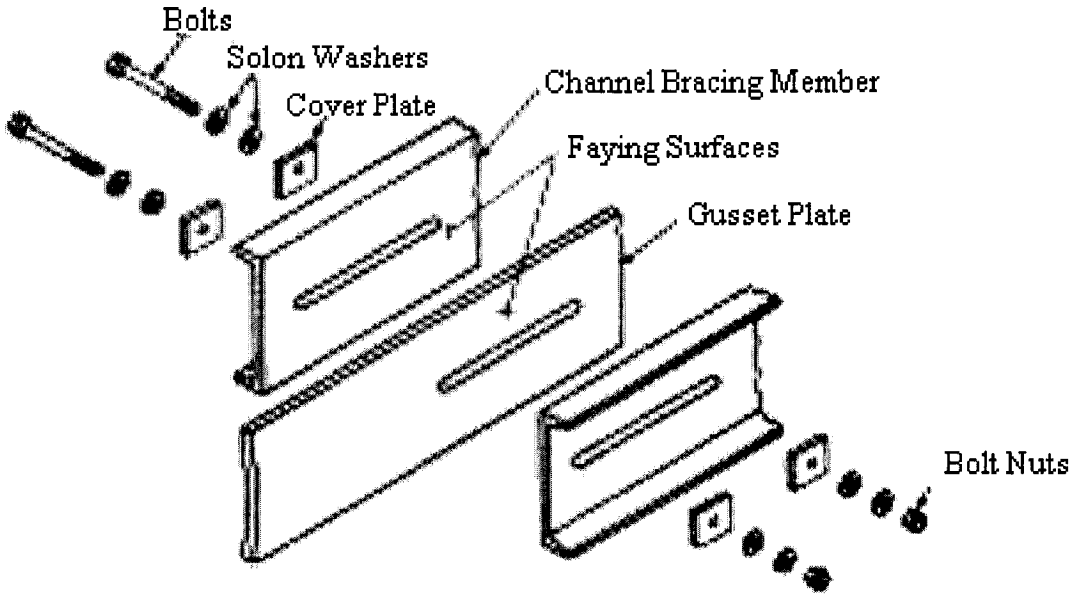

Fig. 2.4 Slotted Bolted Connection Damper [M.C. Constantinou, 1994]

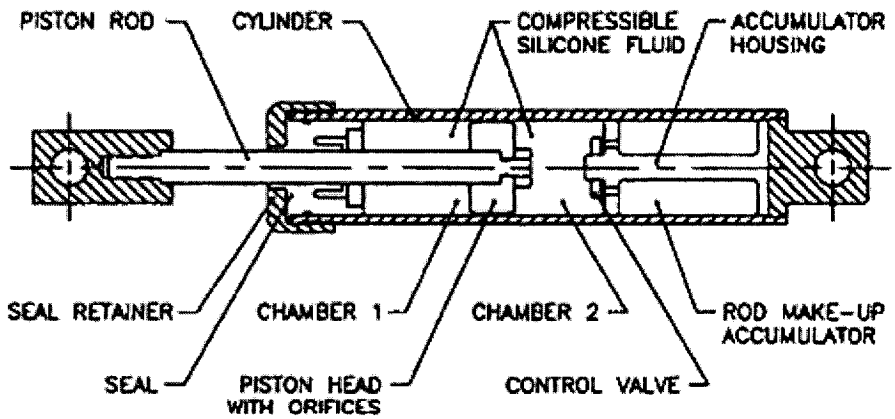

Fig. 2.5 Fluid Viscous Damper [M.C. Constantinou, 1992]

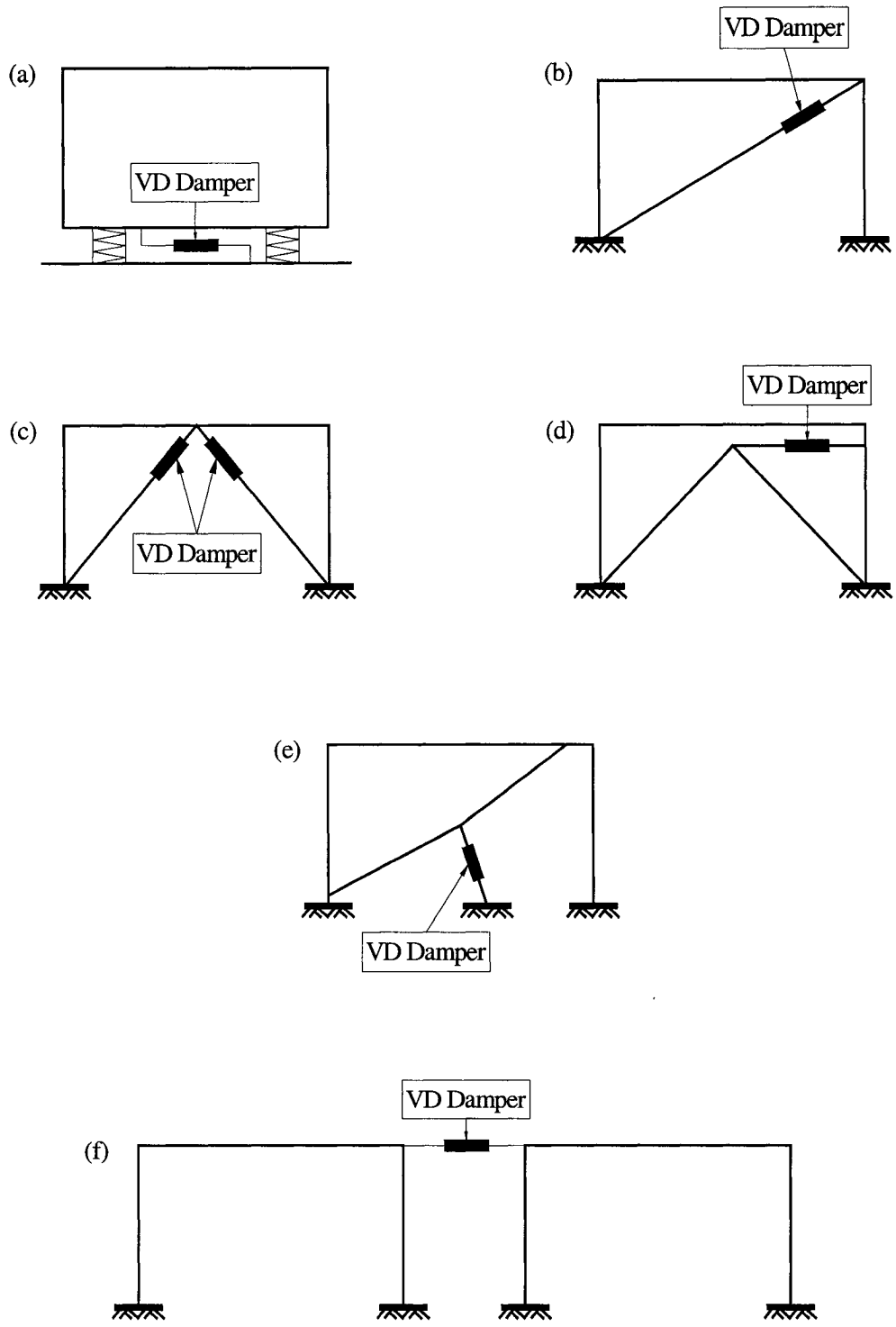

Fig. 2.6 Fluid Viscous Damper Applications
(a) Base Isolation (b) Diagonal Brace (c) Chevron Brace
(d) Horizontal Chevron Brace (e) Toggle Brace
(f) Horizontal connection Between Adjacent Buildings

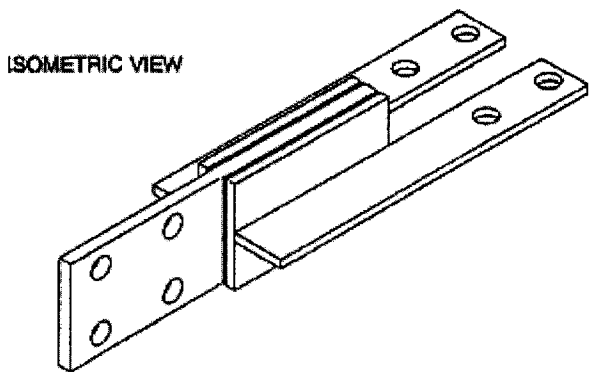

Fig. 2.7 Viscoelastic Damper [Ian D. Aiken 1990]

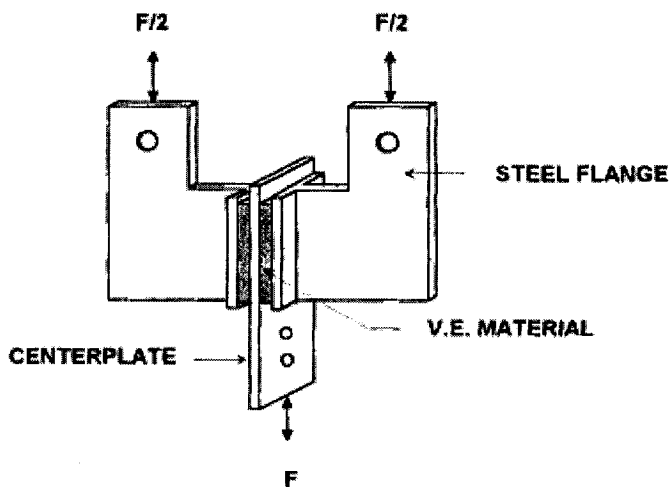

Fig. 2.8 Viscoelastic Damper [P. Mahmoodi, 1969]

CHAPTER 3

CHARACTERISTICS OF EARTHQUAKES

According to the theory of plate tectonics, the earth is composed of several large plates. Usually, an earthquake takes place at the boundaries of adjacent plates because of their interaction induced by plate motion. Different plate tectonic movement forms different geologic fault. There are two typical geologic fault types: the strike-slip fault and the dip-slip fault. The dip-slip fault also can be classified into two types: the normal-slip fault and the reverse-slip fault. The strike-slip fault, which is caused by shear forces, produces relative horizontal movement of the plates. The normal-slip fault, which is induced by tensional forces, produces relative vertical downward motion of the plates. The reverse-slip fault, which is caused by compression forces, produces relative vertical upward motion of the plates. Fig. 3.1 clearly expresses different kinds of faults and their relative relationships of motion. When an earthquake occurs, the accumulated energy in the rock is released, through rupture of the fault, in the form of waves such as body waves, which are traveling in the earth, and surface waves which are traveling on the ground surface, causing what are known as an earthquake. There are three components: two horizontal components and one vertical component to describe a ground motion. Two horizontal components respectively are fault-normal component, whose component is perpendicular to the fault, and fault-parallel component whose component is parallel to the fault. Usually, the point where the earthquake originally occurs is called the hypocenter or the seismic source. The vertical projection of hypocenter to the ground surface is called the epicenter. The specific place distant away from the epicenter and influenced by the

seismic source is called the site. Fig. 3.2 clearly shows their spatial relationships, and Fig. 3.3 shows different types of earthquake waves. The characteristics of an earthquake can be influenced by many factors such as the fault mechanism, the wave propagation path, the epicenter distance and the local site condition. Usually, the seismic source, which is close to a site, produces a near-fault earthquake at the site, and the seismic source, which is far away from a site, induces a far-fault earthquake at the site.

Buildings under the two types of earthquakes exhibit different dynamic response behaviors, which show that the two types of earthquakes have different characteristics. Due to long-term investigation on far-fault earthquakes and limited number of observed strong near-fault earthquake records, the following will pay more attention on the research of near-fault earthquakes.

3.1 Previous Seismological Research on Near-Fault Earthquakes

Field observations and investigations in seismic zones found that the dynamic response of a structure is stronger in a near-fault earthquake than in a far-fault earthquake. More serious structural damages have been found in the site close to an earthquake fault. This phenomenon attracts many researchers to study the characteristics of near-fault ground motions, which cause different degree of damage than far-fault earthquakes.

3.1.1 Characteristics of Near-Fault Earthquakes

Different from far-fault earthquake records, near-fault earthquake recordings such as the 1966 Parkfield, the 1979 Imperial Valley, the 1992 Landers and the 1994 Northridge

earthquakes in the United States, the 1995 Hyogo-ken Nanbu (Kobe) earthquake in Japan, the 1999 Kacaeli earthquake in Turkey and the 1999 Chi-Chi earthquake in Taiwan contain strong long-period pulses and permanent ground displacements. Such large peak ground displacements, ground velocities or ground acceleration pulses have been studied and confirmed by many researchers such as Aki [1968], Abrahamson [2000], Chen et al. [2001], and Akkar et al. [2005]. Nowadays, researchers have recognized and attributed such significant characteristics of near-fault records to the two near-fault effects: rupture directivity effect and fling effect [Malhotra, 1999; Somerville, 2000; Abrahamson, 2000; Loh et al., 2002; Makris and Black, 2004].

Directivity effect occurs when the velocity of the fault rupture propagation toward a site is close to the shear wave velocity of the rock near the source, which causes the accumulated energy from the rupture to be in the form of a large long-period shock wave that occurs at the beginning of the record [Abrahamson, 2000]. Directivity effect causes large two-sided velocity pulse. According to direction of rupture propagation to the site, directivity has two basic forms: forward directivity and backward directivity. Forward directivity occurs when the rupture propagates toward a site and the direction of slip on the fault is also toward the site, which is away from the epicenter. Forward directivity causes larger and impulsive horizontal ground motion of the fault-normal component than that of the fault-parallel component in both the strike-slip fault and the dip-slip fault. Backward directivity occurs when the rupture propagates away from a site, which is near the epicenter [Somerville, 2000; Abrahamson, 2000].

Fling effect is due to the static tectonic deformation of the ground. It induces permanent ground displacements, which, at the same time, result in a one-sided velocity pulse. Fling effect causes larger fault-parallel peak velocity for the dip-slip fault than that for strike-slip fault; and it causes larger fault-normal component for the strike-slip fault mechanism than that for the dip-slip fault mechanism [Abrahamson, 2000]. Table 3.1 clearly shows the above-mentioned relationships between different near-fault effect and fault mechanism.

3.1.2 Previous Theoretical Research on Near-Fault Earthquakes

Since near-fault earthquake records show significantly different characteristics from far-fault earthquakes, the response spectrum method used in the conventional seismic design regulations for far-field earthquakes may not sufficiently exhibit the seismic demand presented by a near-field ground motion. Therefore, many new models considering near-fault effects have been proposed during the past a few decades.

In order to consider the directivity effect, Somerville [2000] proposed a preliminary model for forward directivity effect. In the model, two pulse parameters (the period and the amplitude of velocity of the largest cycle) are considered. The model revised the relationship between the pulse period T and the moment magnitude M_w and set up a relationship between PGV, M_w and the closest distance R. This model showed that it is helpful to build probabilistic maps of near-fault ground motion using pulse parameters.

The investigations also found that great difference in amplitude exists among three components of strong near-fault ground motions due to directivity effects, which indicates that it may be more reasonable to use three-components of an earthquake to completely consider the influence of near-fault earthquakes on structures. Based on a modified model considering source effects, propagation effects, and the local site conditions, Onishi, et al. [2004] proposed a revised simulation method to construct three-components of near-fault ground motions used for earthquake-resistant structural analysis. The research showed that this method is only effective for near-fault earthquakes in horizontal components.

3.2 Previous Structural Dynamic Response Research on Near-Fault Earthquakes

Using a displacement amplification method, MacRae et al. [2001] investigated the rupture directivity effects on the inelastic behavior of SDOF systems with elastic-perfectly plastic hysteretic behavior. Through studying of a few parameters such as the vibration period, the ductility and the lateral force reduction factor, it was found that near-fault ground motion records, which although have similar elastic response spectra, may cause different inelastic responses of the structures, and near-fault earthquakes with forward directivity effects can cause stronger response for the structures with the period of 1-3 sec than those structures with too-short or too-long period.

Since the structural damages due to the insufficient lateral displacement ability during the near-fault earthquakes show more displacement demands than those in the far-fault earthquakes, Akkar et al. [2005] paid more attention to near-fault earthquake effects on

the MRF dynamic response, especially the ground story drift and the inter-story drift. Based on the first-mode-control assumption and parameter study of beam-column stiffness ratio, it was found that the pulse effect on the ground story drift (GSDR) and maximum inter-storey drift (MIDR) tends to increase when the fundamental period of the structure is near the pulse period of the ground motion. Finally, two simple formulas were proposed to estimate GSDR and MIDR for the purpose of preliminary design.

A ten-storey, three-bay moment-resisting steel frame has been investigated by Anderson and Bertero [1987]. Non-linear dynamic responses of the frame under four near-field earthquake records were analyzed and compared with that under EL-Centro 1940 earthquake. The study found that, in general, there are more structural damages associated with directivity effects of near-fault earthquakes. Different from damages under far-fault earthquakes, the lower floors of buildings can receive more damages under near-fault earthquakes. At the same time, only using the peak ground acceleration method to analyze structural dynamic response, especially inelastic behavior, may not be adequate. The design response spectrum method needs to be revised due to near-fault effects and increased ductility requirement under near-fault ground motions.

In order to evaluate the validity of current response spectra used in structural design, Chopra and Chintanapakdee [2001] studied the responses of SDOF systems under near-fault and far-fault earthquake records. The investigations found that under near-fault ground motions, due to the larger peak pulse, the fault-normal component of earthquake needs more deformation and strength requirements than the fault-parallel component,

completely different from far-fault earthquakes. Moreover, response spectra of near-fault and far-fault ground motions are also different. It is found that the width of the velocity-sensitive region of near-fault ground motions is narrow and the widths of the acceleration-sensitive region and the displacement-sensitive region of near-fault records become wider when compared with those of far-fault records.

3.3 Previous Structural Dynamic Response Research with Added-Damper on Near-Fault Earthquakes

Dynamic response of a six-storey three-bay moment-resisting frame with added friction dampers was analyzed by Tremblay et al. [1998]. The efficiency of two friction dampers, slotted-bolted connection dampers and the ring-spring dampers was investigated and compared with each other under near-field and far-field earthquakes. The optimum slip force was based on the method proposed by Filiatrault and Cherry [1990]. Research found that the friction damper can reduce structural dynamic response such as the inter-story drifts and accelerations. However, only increasing the slip load cannot reduce the response economically. It should be carefully calculated when using friction damper under near-fault earthquakes. Finally, the authors suggested that further research work is required to evaluate the influence of near-fault ground motions on friction-damped braced frame.

All in all, although the research about near-fault earthquakes and their effects on the dynamic response of structures has been received much attention, little research is involved with damped structure, especially comparison of far-fault and near-fault effect

of different dampers. Therefore, the purpose of this study is to try to do some investigation in this direction.

3.4 Selected Earthquake Records

In order to conduct time-history analysis, a total of 18 strong earthquake records are selected. Among them, one is EL-Centro 1940 record, considered as a far-fault record. 9 records are strong near-fault ground motions on firm ground with magnitude from 6.0 to 8.0 at distance less than 20 km. The other 8 near-fault records refer to research paper Makris and Roussos [2000]. Only horizontal components of ground motions with velocity over 20cm/sec are used. All the data of the near-fault records was downloaded from website of PEER strong motion database (http://peer.berkeley.edu/smcat).

Table 3.2 simply shows the important characteristics of selected earthquakes. Fig. 3.4 to Fig. 3.21 clearly show time-history record curves of ground motions. Fig. 3.22 to Fig. 3.39 also shows the curves of Forward Fourier Transform of the ground acceleration to selected earthquake records, which provide useful information of earthquake frequency composition. The selected earthquakes have following features:

Coalinga D-TSM270, D-TSM360, 22 July 1983: the records have distinct long-period acceleration pulses, which have maximum amplitude of 0.84 and 1.083 of gravity separately for two horizontal directions. It is noted that the principal amplitudes of motion occur between 1~2 Hz in the Fig. 3.22 and Fig. 3.23.

Parkfield TMB205, 28, June 1966: the record has obvious acceleration pulse. Its principal amplitudes of motion occur between 2~3 Hz in the Fig. 3.24.

Mammoth Lakes I-LUL000, 25, May 1980: the record has distinct displacement pulse, which has maximum amplitude of 75.2 mm and its principal amplitudes of motion occur between 2~3 Hz in the Fig. 3.25.

Mammoth Lakes L-LUL000, L-LUL090, 27, May 1980: the records have obvious acceleration pulses and velocity pulses. Its principal amplitudes of motion occur between 1~3 Hz in the Fig. 3.26 and Fig. 3.27.

Northridge PAC175, PAC265, 17, January 1994: the records have obvious acceleration pulses, peak displacements and distinct velocity pulses. Its principal amplitudes of motion occur between 1~2 Hz in the Fig. 3.28 and Fig. 3.29.

Northridge PUL104, 17, January 1994: the record has distinct acceleration pulses and velocity pulses. The peak acceleration is 1.585 of gravity; the peak velocity is 55.7 cm/sec. Its principal amplitudes of motion occur between 3~4 Hz in the Fig. 3.30.

Landers LCN000, LCN275, 28, June 1992: the records have distinct velocity pulses and large displacements. The peak velocity is 97.6 cm/sec. The peak displacement is 703.1 mm. Its principal amplitudes of motion occur between 11~12 Hz in the Fig. 3.31, 0~1and 9~10 Hz in the Fig. 3.32.

Northridge RRS228, RRS318, 17, January 1994: the records have distinct velocity pulses and large displacements. The peak velocity is 166.1 cm/sec; the peak displacement is 287.8 mm. Its principal amplitudes of motion occur between 0~2 Hz in the Fig. 3.33 and 0~4 Hz in the Fig. 3.34.

Northridge SCE018, SCE288, 17, April 1994: the records have distinct velocity pulses and large displacements. The peak velocity is 117.5 cm/sec; the peak displacement is

342.2mm. Its principal amplitudes of motion occur between 0~2 Hz in the Fig. 3.33 and 0~2 Hz in the Fig. 3.35 and Fig. 3.36.

Imperial Valley H-E05140, H-E05230, 15, October 1979: the records have distinct acceleration, velocity pulses and large displacements. The peak velocity is 90.5 cm/sec. the peak displacement is 630.3 mm. Its principal amplitudes of motion occur between 0~4 Hz in the Fig. 3.37 and 0~1 Hz in the Fig. 3.38.

3.5 Objective

Although many researchers have investigated different seismic characteristics and structural dynamic responses to the near-fault ground motions with those to the far-fault records, little research has concerned about dynamic behavior of structures with supplement dampers, especially under strong near-fault earthquakes. Therefore, the major objective of this study is to investigate the working efficiency of supplement dampers for strong near-fault earthquakes and compare them with that to the strong far-fault earthquakes. Three different types of damper, i.e. friction damper, fluid-viscous damper and viscoelastic damper, are selected and investigated to determine which one is more effective for the near-fault ground motions. The nonlinear time-history analysis method is employed to analyze the dynamic response of the moment-resisting frame with and without added dampers. The results under near-fault and far-fault ground motions are studied and compared.

Table 3.1 Different Near-Fault Effects on Different Fault Mechanisms

Fault Mechanism / Near-Fault Effect	Strike-Slip Fault	Dip-Slip Fault
Directivity Effect	Stronger motion in the fault-normal direction	Stronger motion in the fault-normal direction
Fling Effect	Stronger motion in the fault-normal direction	Stronger motion in the fault-parallel direction

Table 3.2 Selected Earthquake Records:

Number	Earthquake Record	Distance(km)	Magnitude	PGA(g)	PGV(cm/s)	PGD(cm)
1	EL-Centro			0.32		
2	Coalinga270	9.2(f)	M5.8	0.84	44.1	6.8
3	Coalinga360	9.2(f)	M5.8	1.083	39.7	5.41
4	Parkfield205	9.9(f)	M6.1	0.357	21.5	3.87
5	Mammothlake-I-000	15.5(h)	M6.3	0.43	23.6	7.52
6	Mammothlake-L-000	20(h)	M6.0	0.921	28.9	3.17
7	Mammothlake-L-090	20(h)	M6.0	0.408	33.9	6.41
8	Northridge175	8(f)	M6.7	0.415	45.6	5.06
9	Northridge265	8(f)	M6.7	0.434	31.3	4.8
10	Northridge104	8(f)	M6.7	1.585	55.7	6.06
11	Lander000	1.1(f)	M7.3	0.785	31.9	16.42
12	Lander275	1.1(f)	M7.3	0.721	97.6	70.31
13	Northridge228	7.1(f)	M6.7	0.838	166.1	28.78
14	Northridge318	7.1(f)	M6.7	0.472	73	19.76
15	Northridge018	6.1(f)	M6.7	0.828	117.5	34.22
16	Northridge288	6.1(f)	M6.7	0.493	74.6	28.69
17	Imperial514	1(f)	M6.5	0.519	46.9	35.35
18	Imperial523	1(f)	M6.5	0.379	90.5	63.03

Note: f------distance to fault rupture h------distance to hypocenter

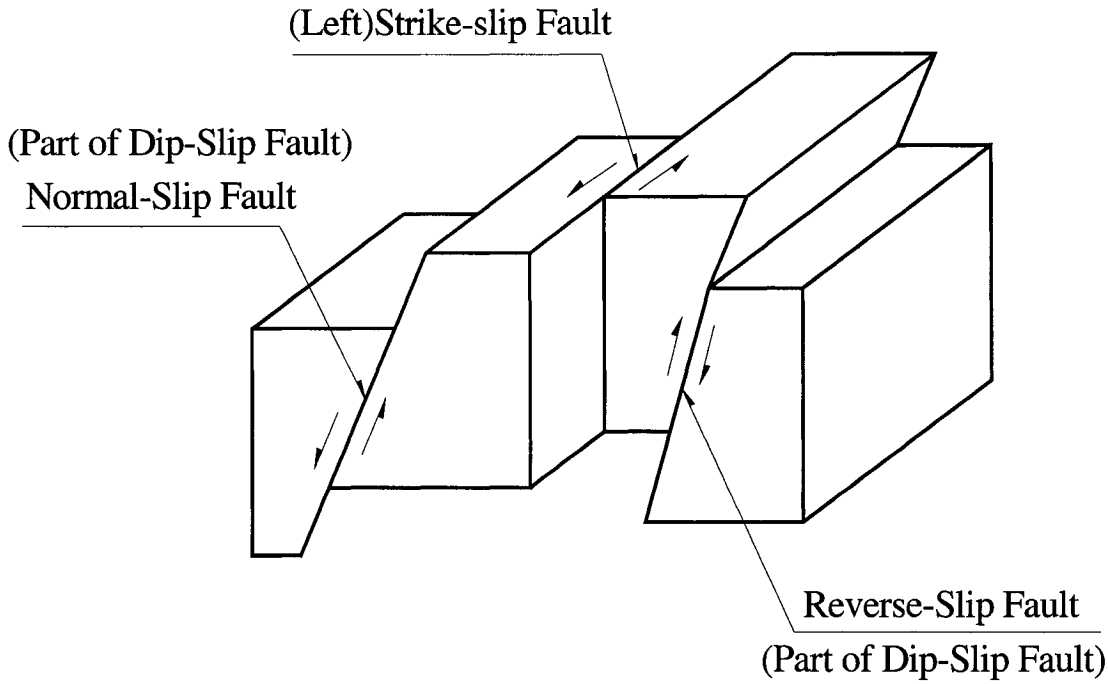

Fig. 3.1 Geology Fault Mechanisms [Filiatrault, 2002]

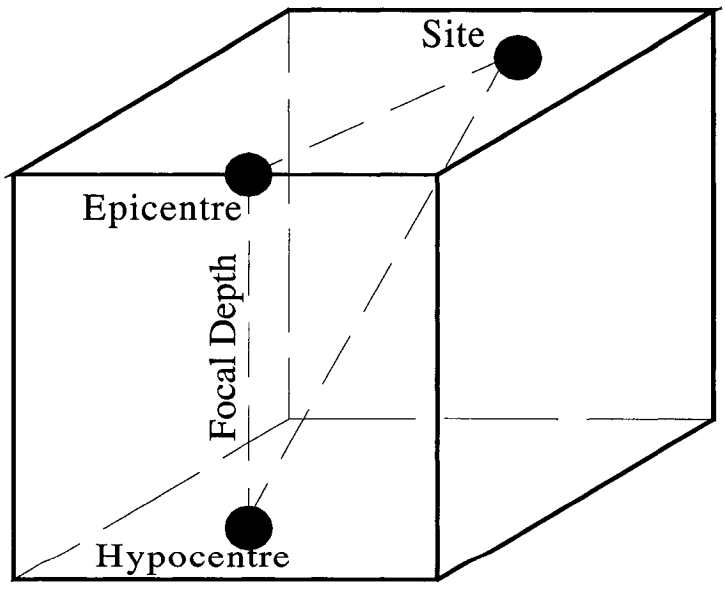

Fig. 3.2 Spatial Relationship [Filiatrault, 2002]

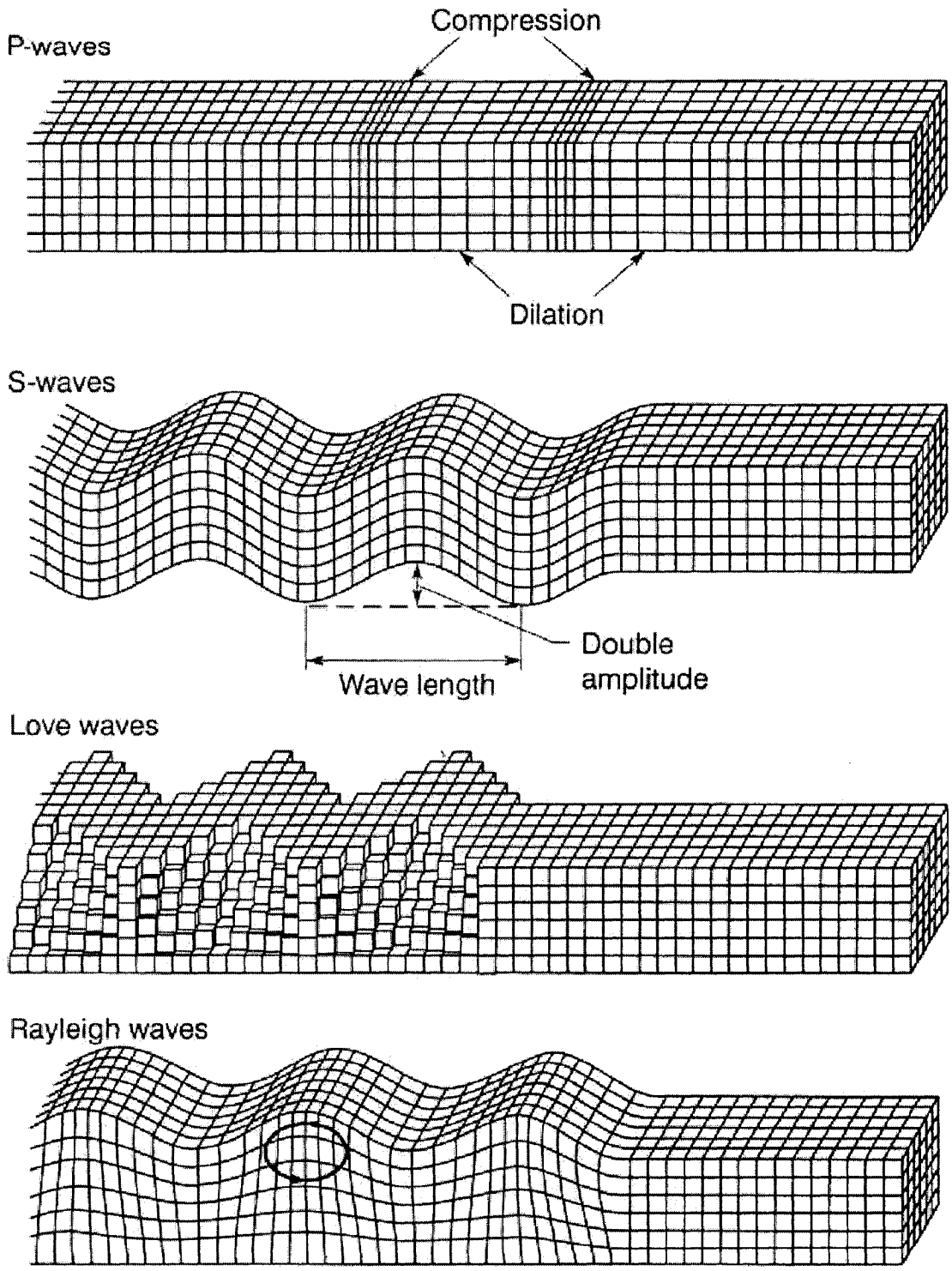

Fig. 3.3 Types of Earthquake Waves [Filiatrault, 2002]
Body Waves: P-waves and S-waves
Surface Waves: Love waves and Rayleigh waves

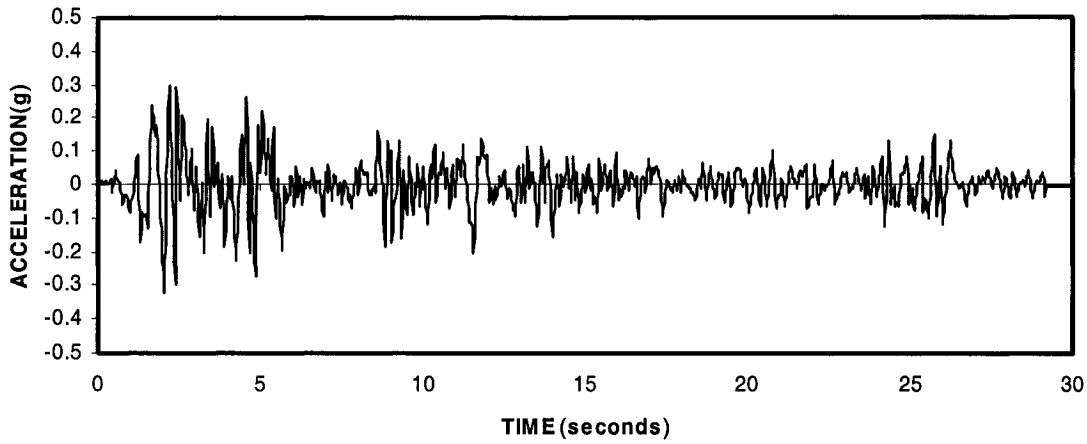

Fig. 3.4 Acceleration Time-History Record of El-Centro (N.S. Component) 1940/05/18

(a)

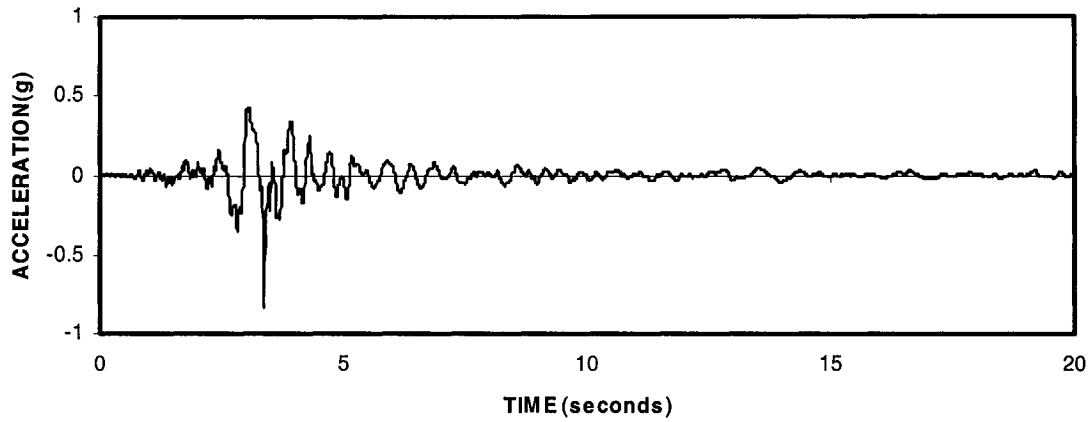

(b)

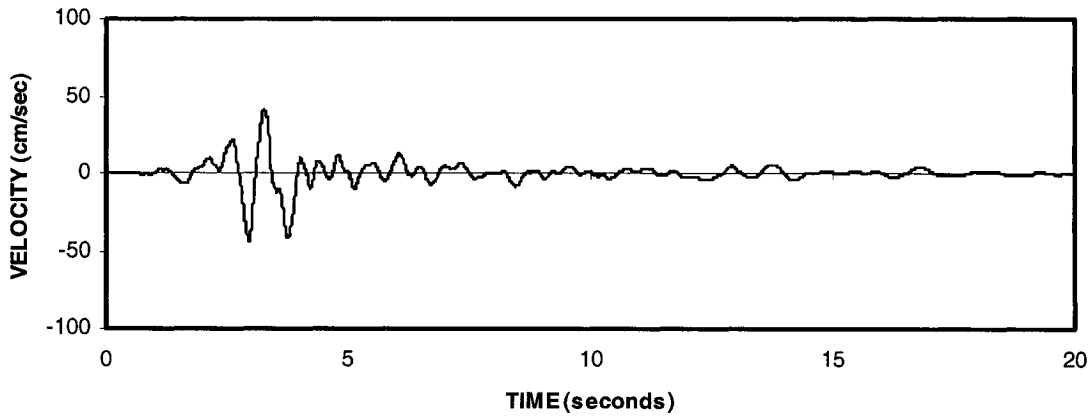

(c)

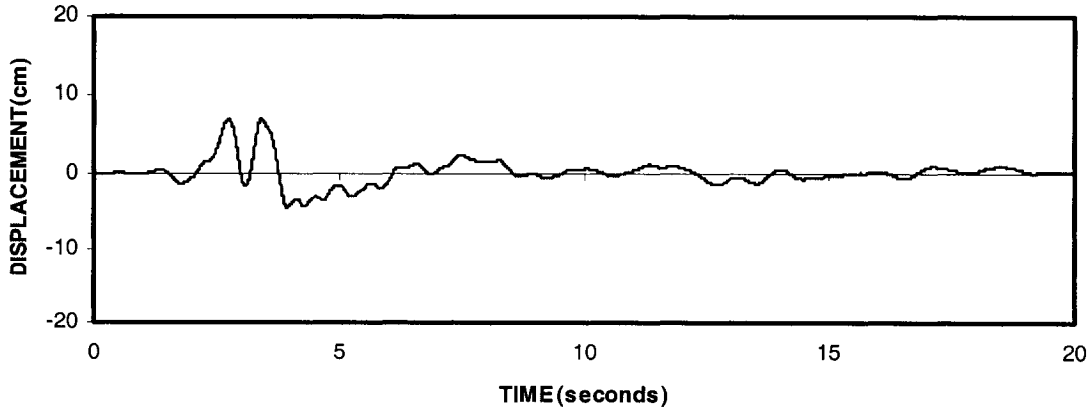

Fig. 3.5 Time-History Record of Coalinga (D-TSM270 Component) 1983/07/22 (a) Acceleration; (b) Velocity; (c) Displacement

(a)

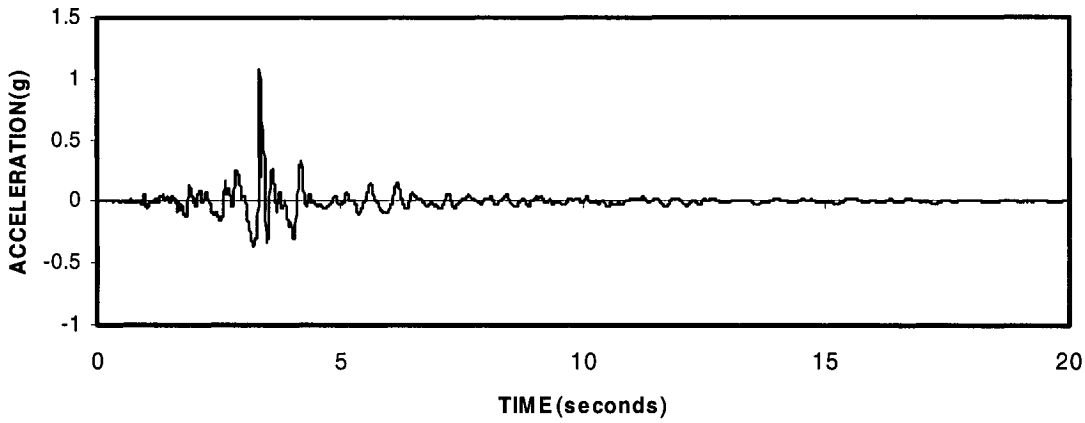

(b)

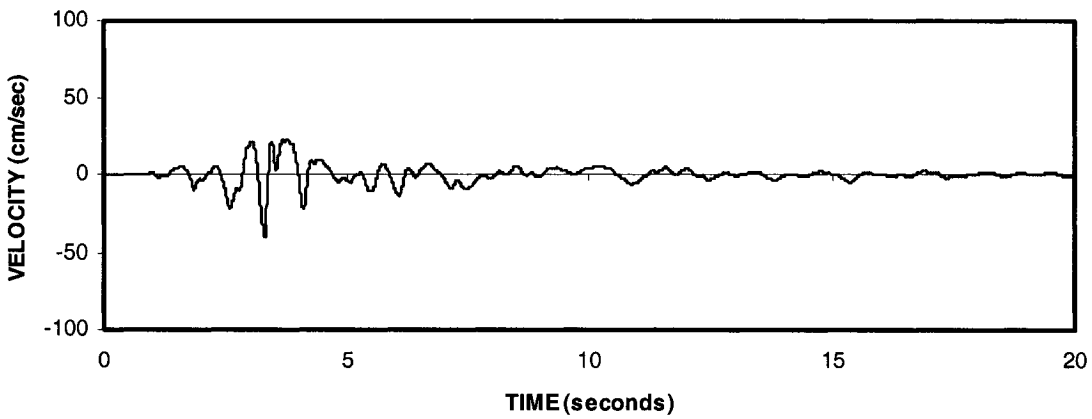

(c)

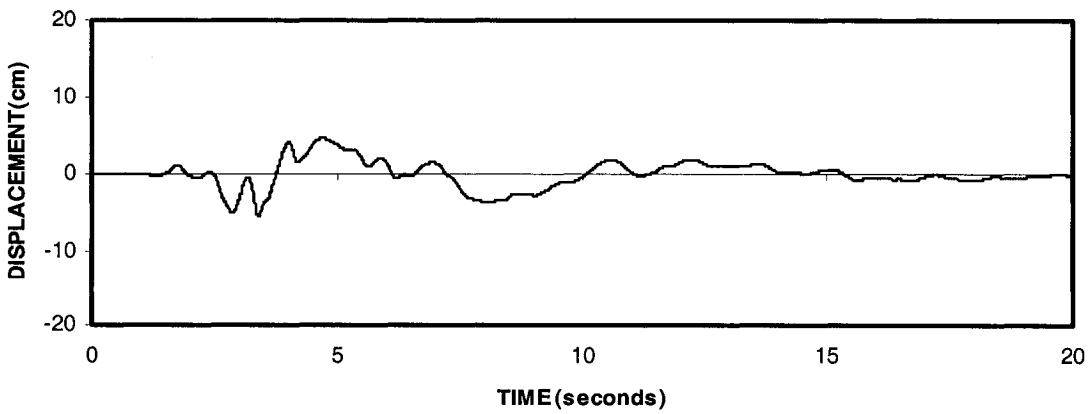

Fig. 3.6 Time-History Record of Coalinga (D-TSM360 Component) 1983/07/22 (a) Acceleration; (b) Velocity; (c) Displacement

(a)

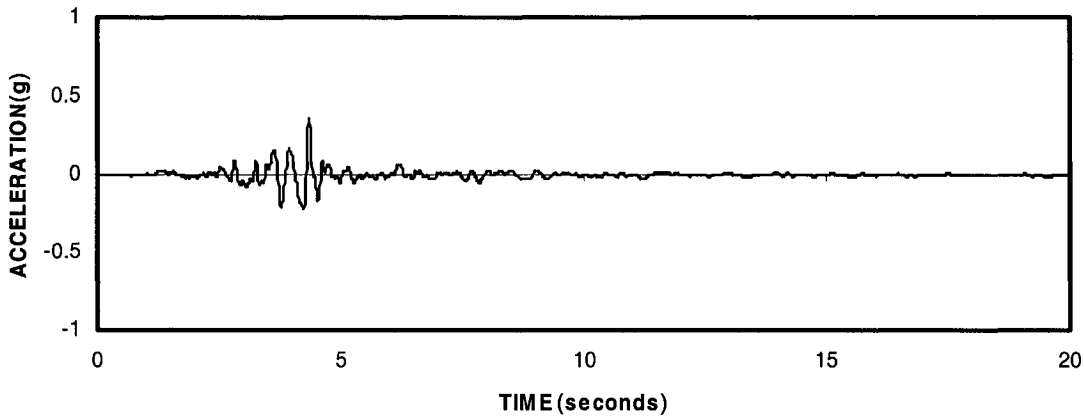

(b)

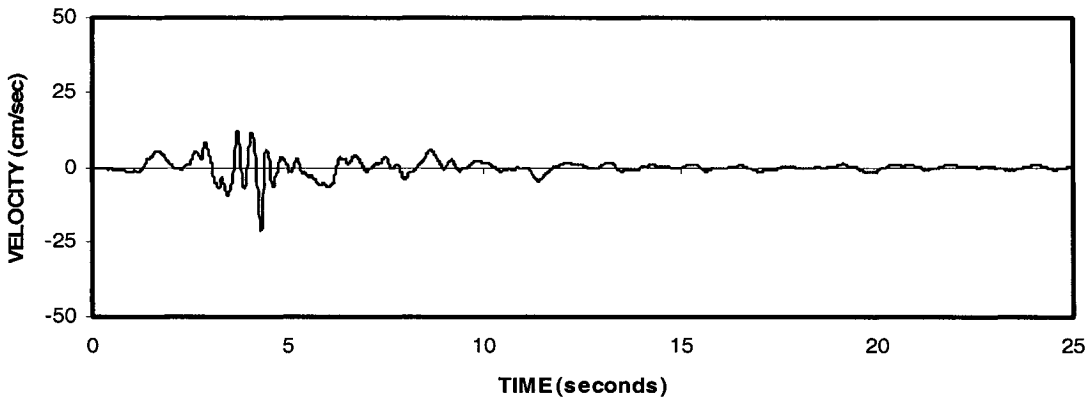

(c)

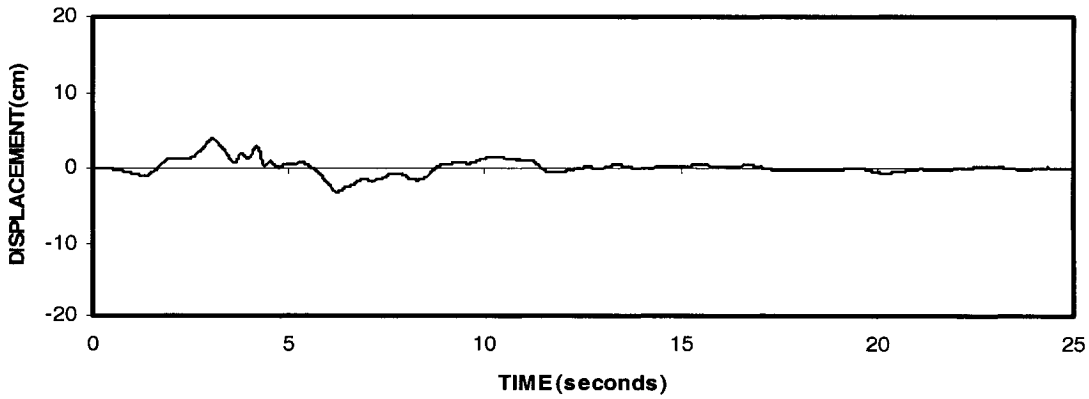

Fig. 3.7 Time-History Record of Parkfield (TMB205 Component) 1966/06/28 (a) Acceleration; (b) Velocity; (c) Displacement

(a)

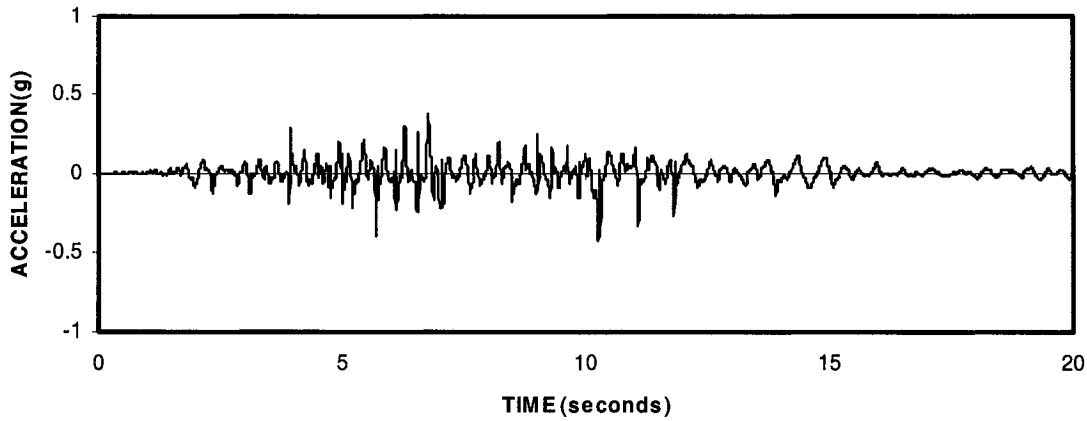

(b)

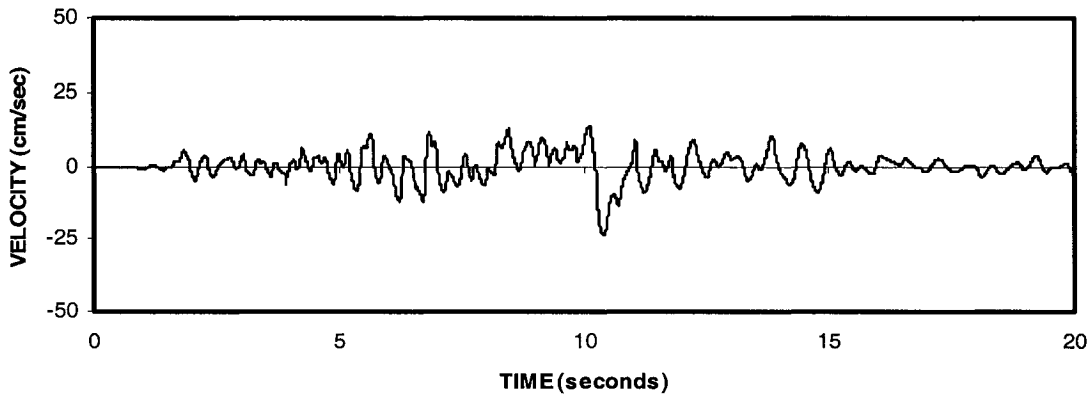

(c)

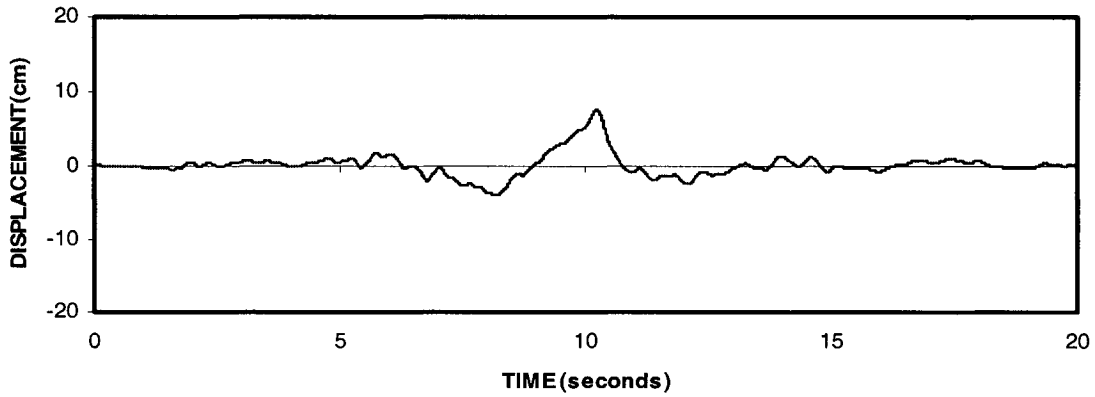

Fig. 3.8 Time-History Record of Mammoth Lakes (I-LUL000) 1980/05/25 (a)Acceleration; (b) Velocity; (c) Displacement

(a)

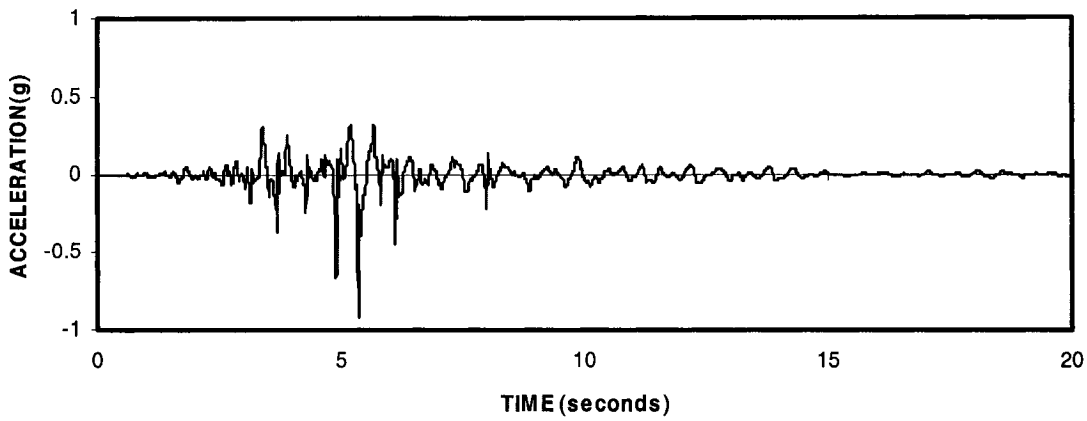

(b)

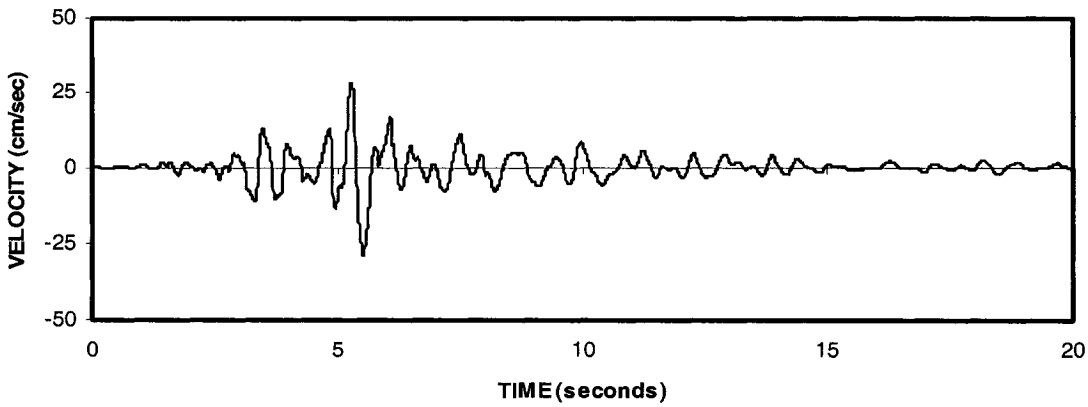

(c)

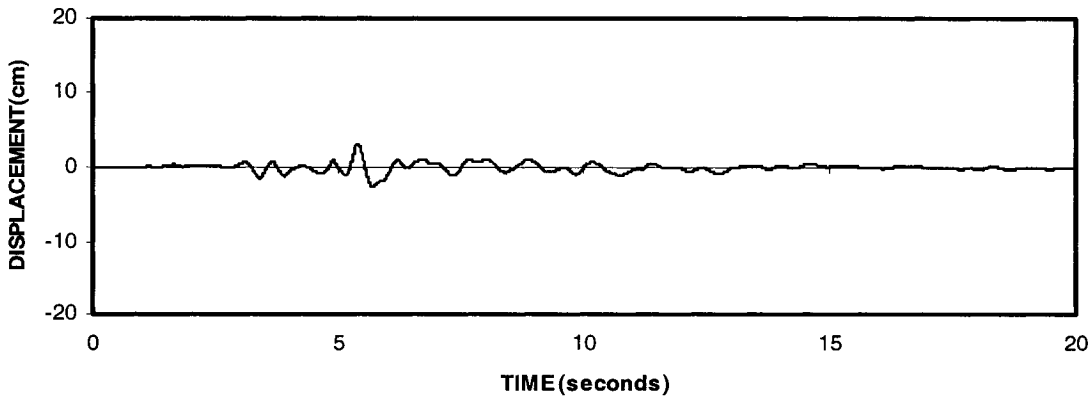

Fig. 3.9 Time-History Record of Mammoth Lakes (L-LUL000) 1980/05/27 (a) Acceleration; (b) Velocity; (c) Displacement

(a)

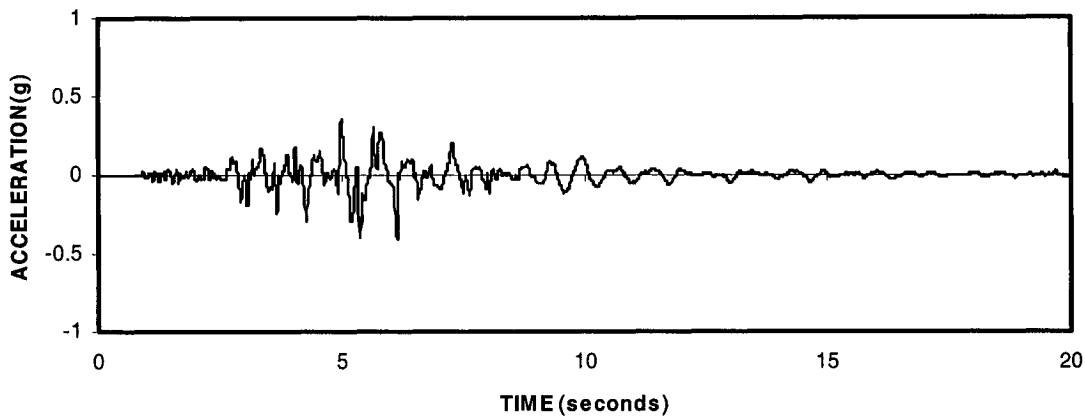

(b)

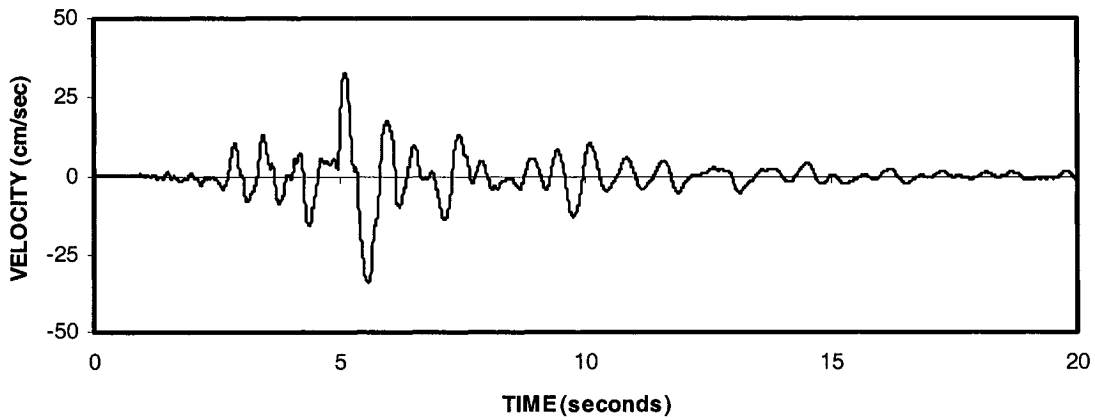

(c)

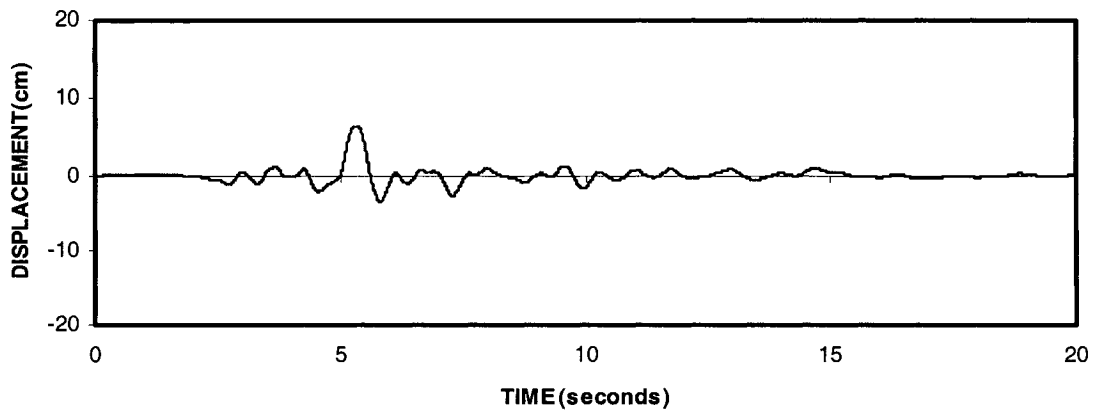

Fig. 3.10 Time-History Record of Mammoth Lakes (L-LUL090) 1980/05/27 (a) Acceleration; (b) Velocity; (c) Displacement

(a)

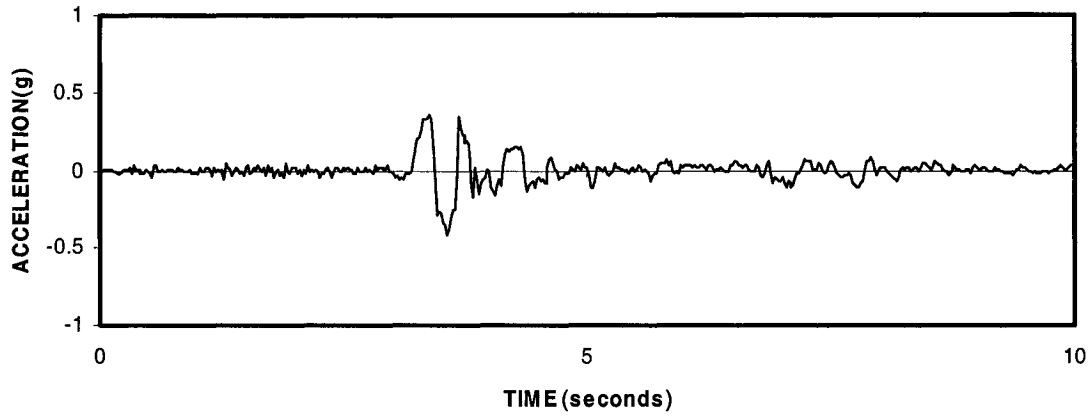

(b)

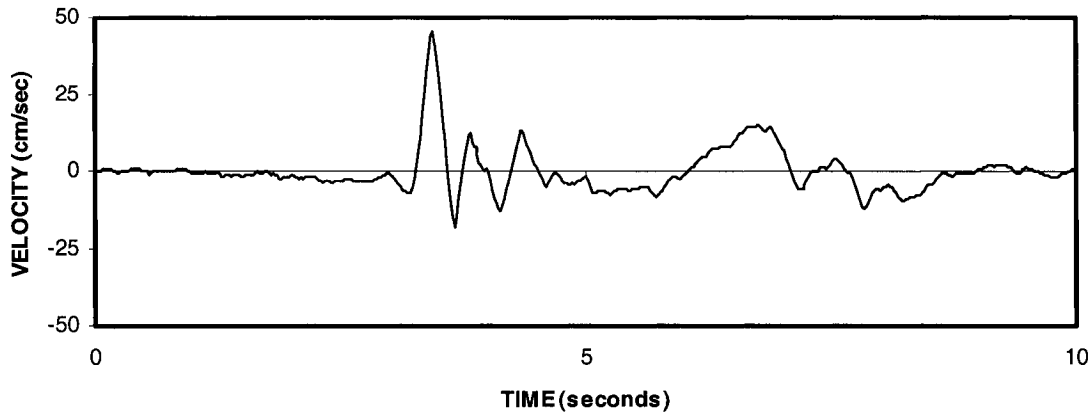

(c)

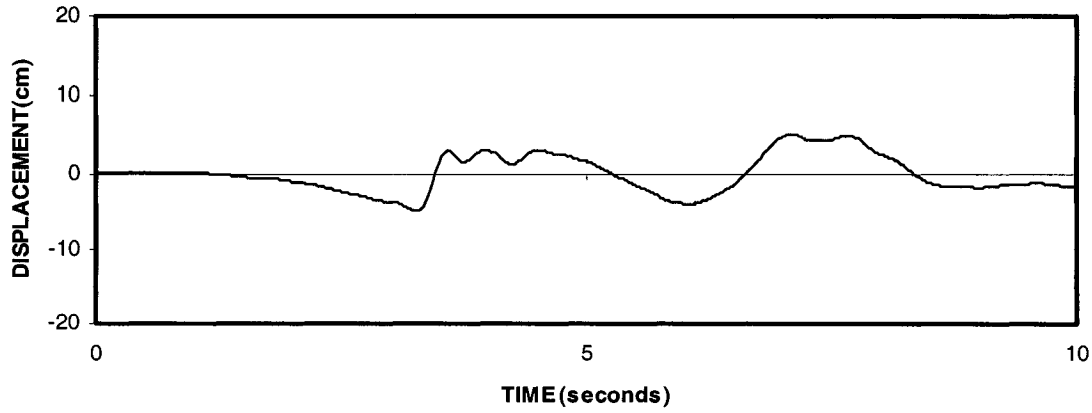

Fig. 3.11 Time-History Record of Northridge (PAC175 Component) 1994/01/17 (a) Acceleration; (b) Velocity; (c) Displacement

(a)

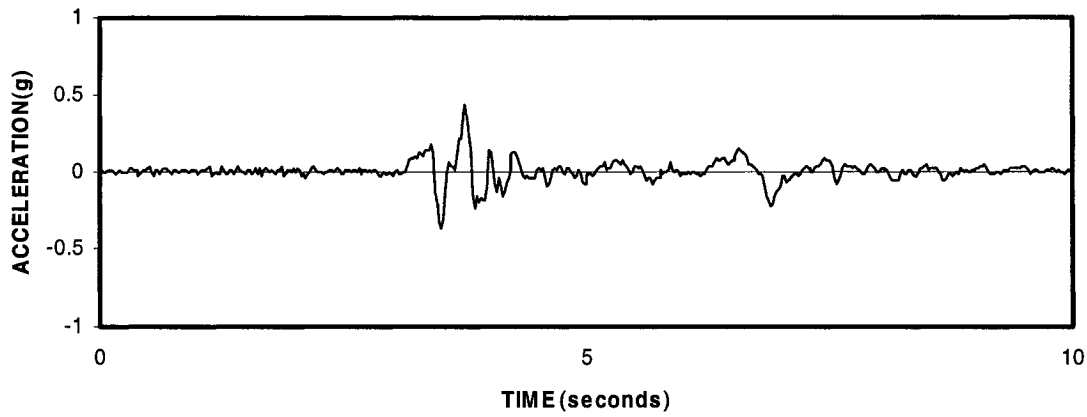

(b)

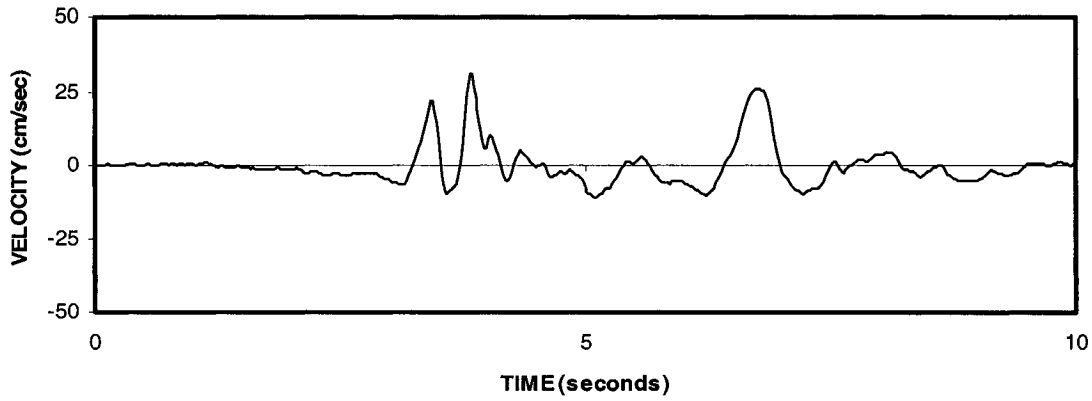

(c)

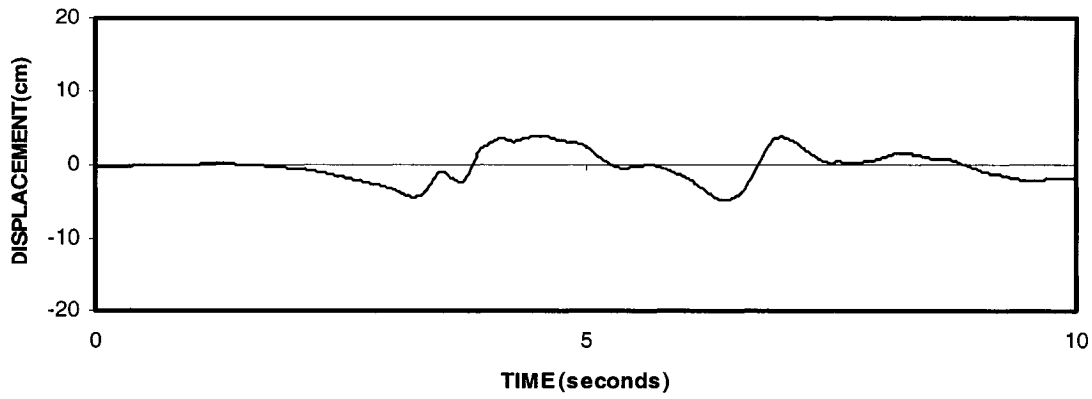

Fig. 3.12 Time-History Record of Northridge (PAC265 Component) 1994/01/17 (a) Acceleration; (b) Velocity; (c) Displacement

(a)

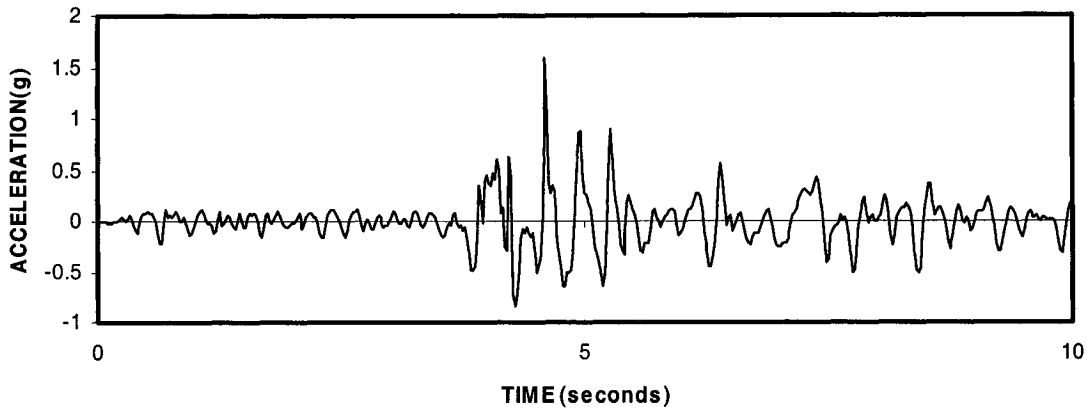

(b)

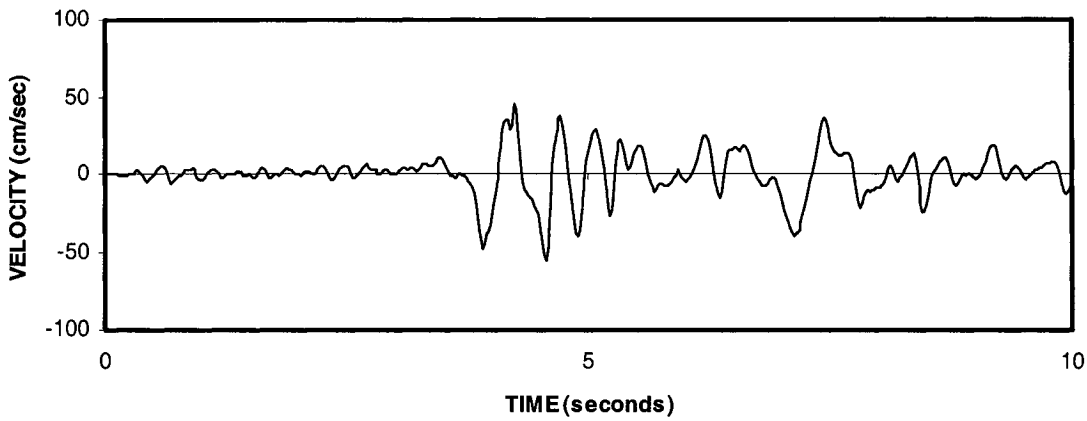

(c)

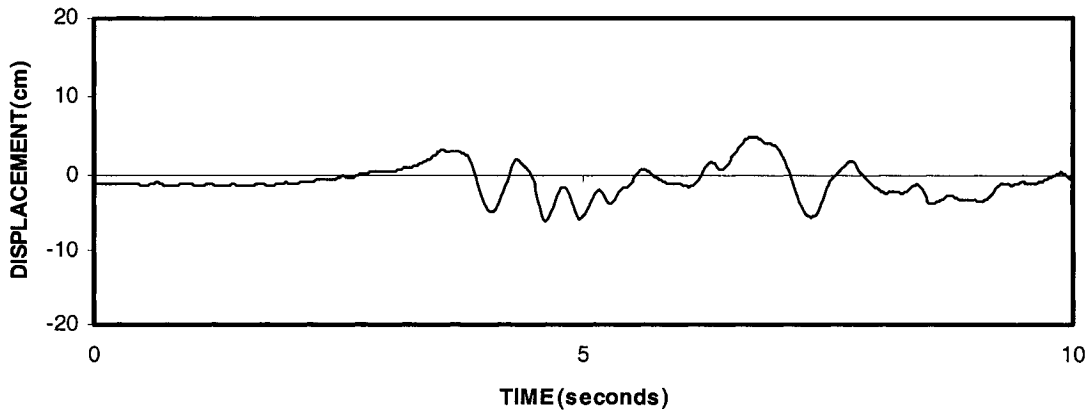

Fig. 3.13 Time-History Record of Northridge (PUL104 Component) 1994/01/17 (a) Acceleration; (b) Velocity; (c) Displacement

(a)

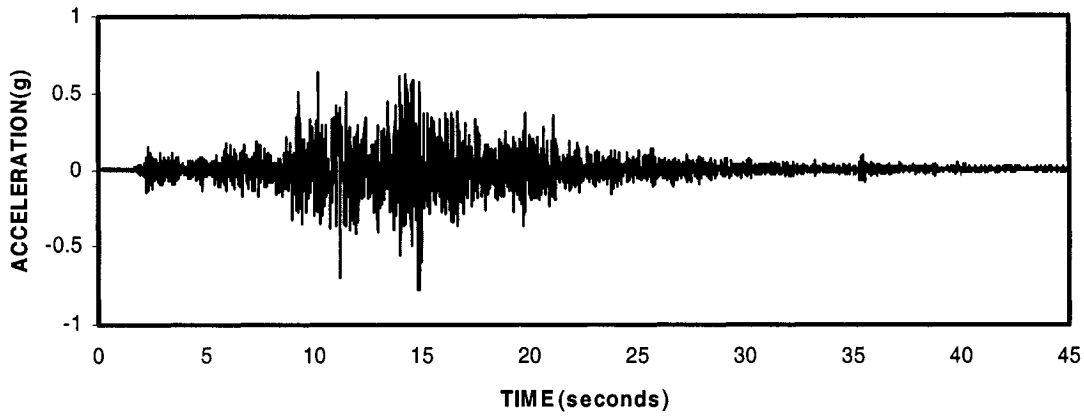

(b)

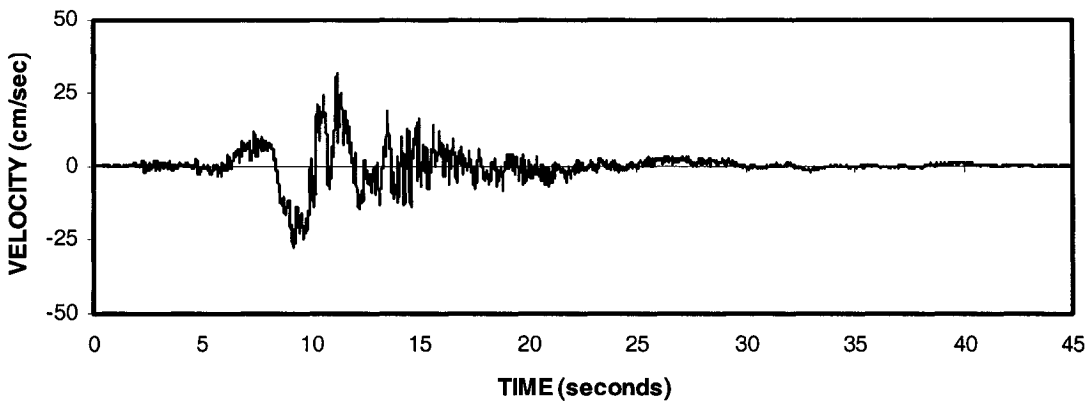

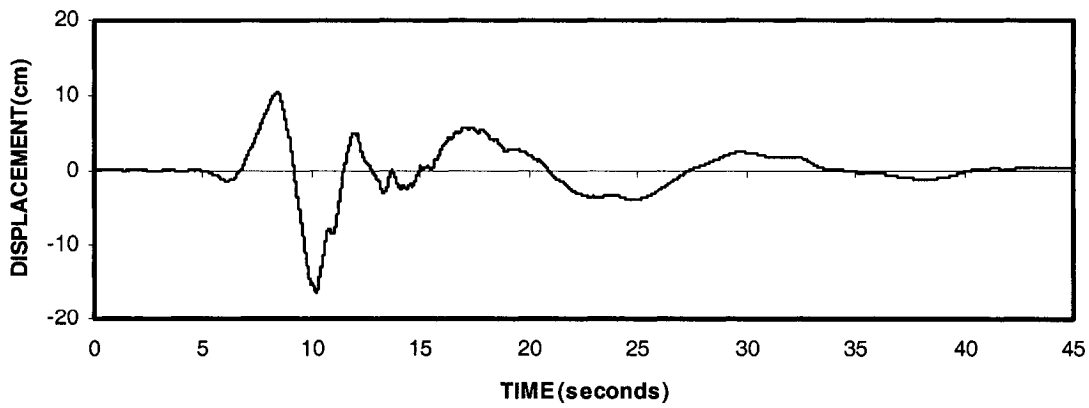

Fig. 3.14 Time-History Record of Landers (LCN000 Component) 1992/06/28 (a) Acceleration; (b) Velocity; (c) Displacement

(a)

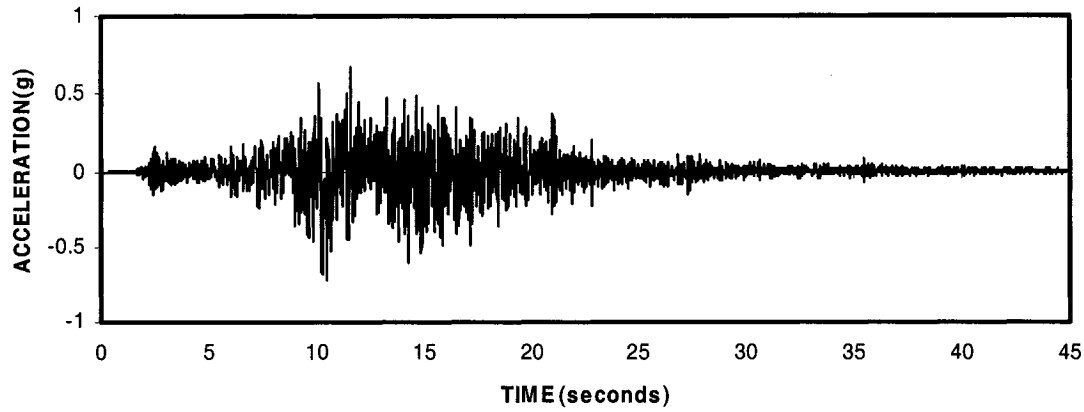

(b)

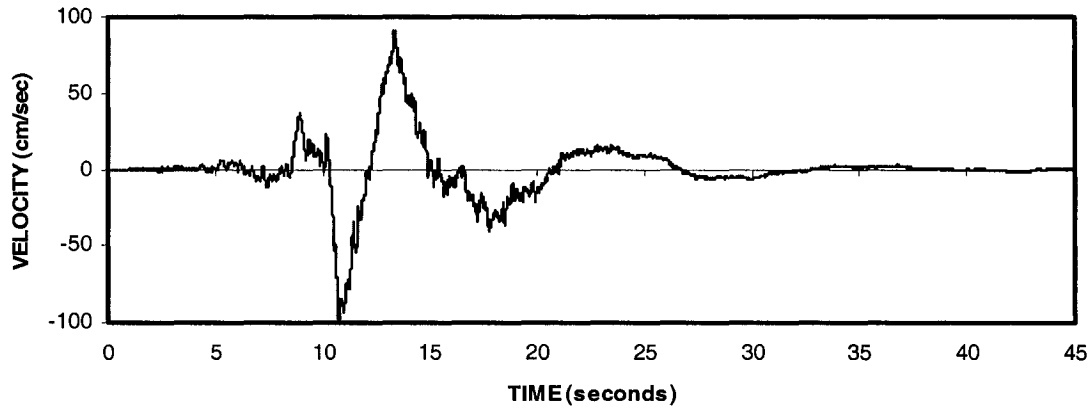

(c)

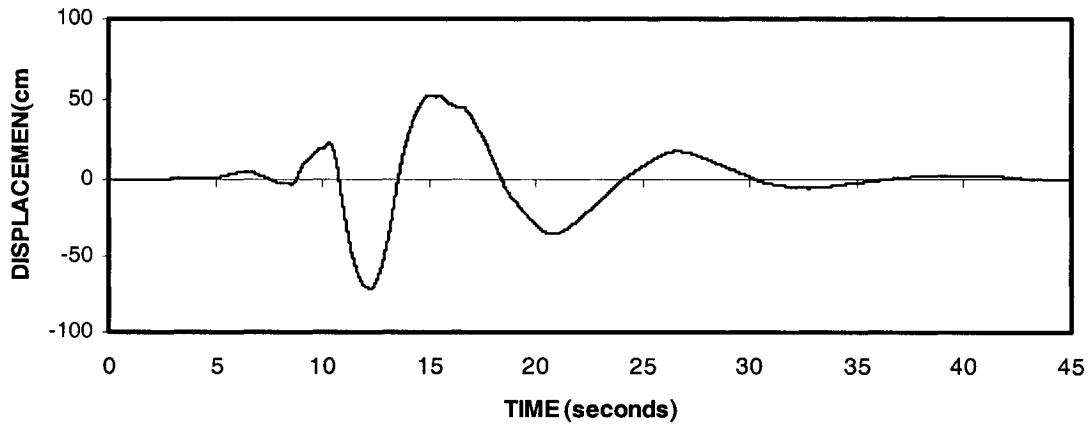

Fig. 3.15 Time-History Record of Landers (LCN275 Component) 1992/06/28 (a) Acceleration; (b) Velocity; (c) Displacement

(a)

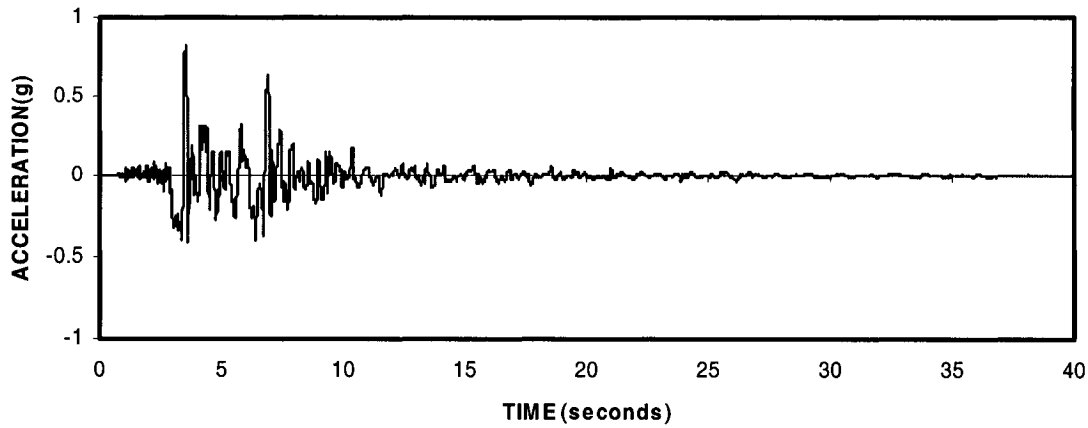

(b)

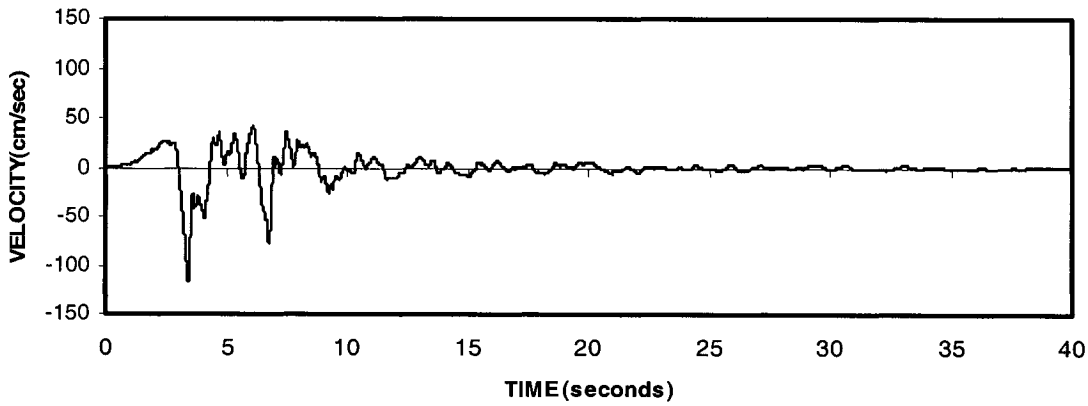

(c)

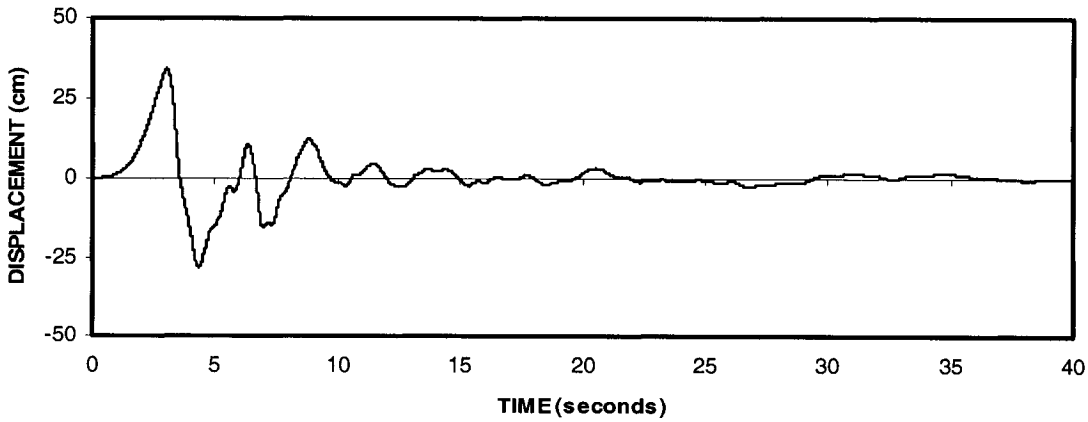

Fig. 3.16 Time-History Record of Northridge (SCE018 Component) 1994/04/17 (a) Acceleration; (b) Velocity; (c) Displacement

(a)

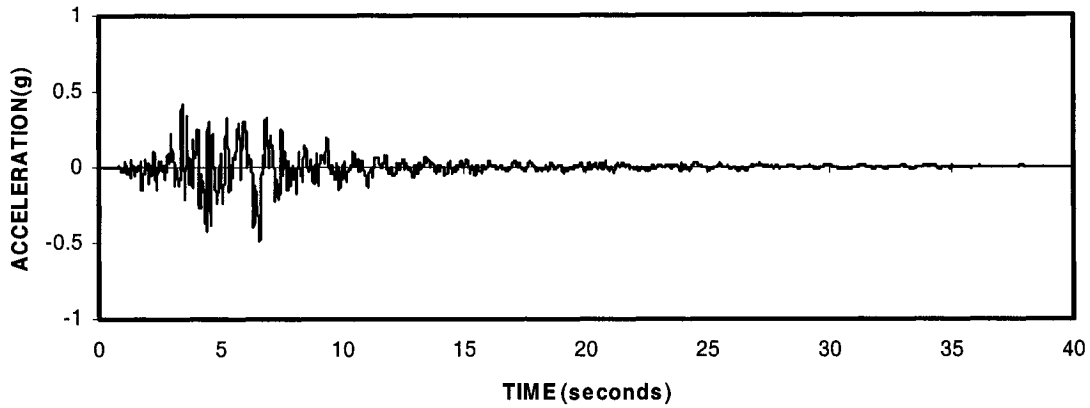

(b)

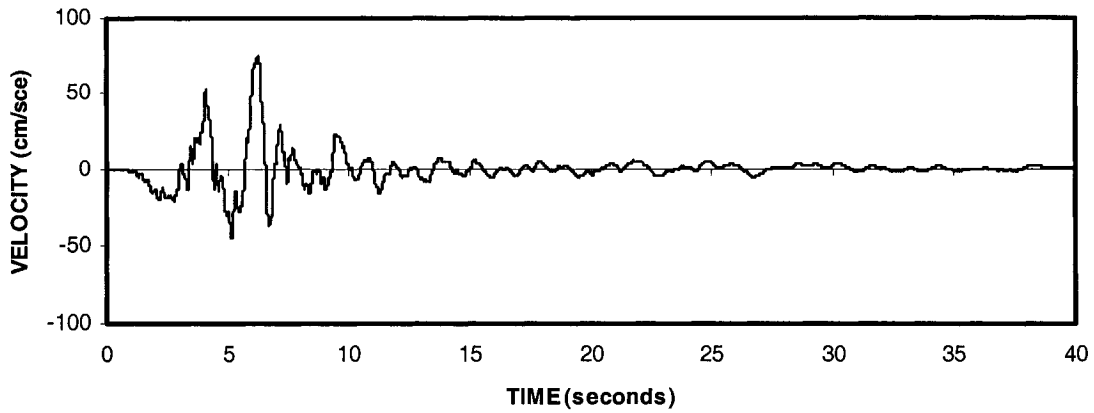

(c)

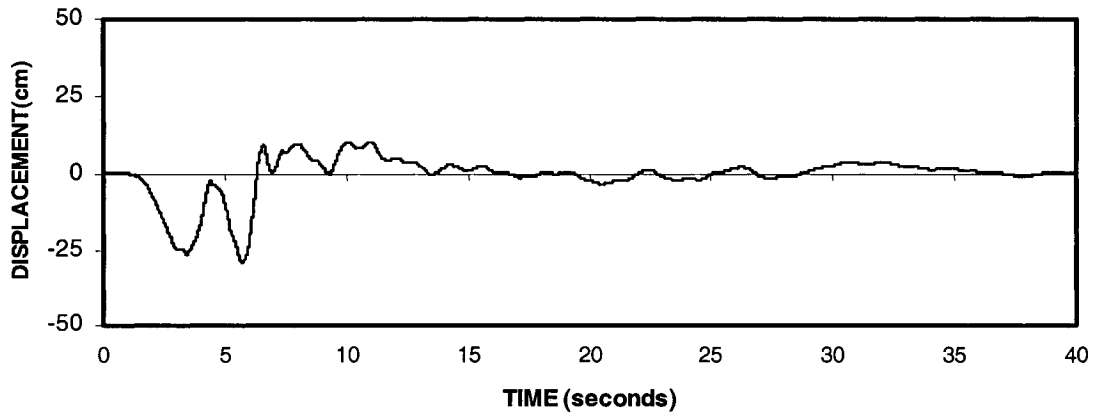

Fig. 3.17 Time-History Record of Northridge (SCE288 Component) 1994/04/17 (a) Acceleration; (b) Velocity; (c) Displacement

(a)

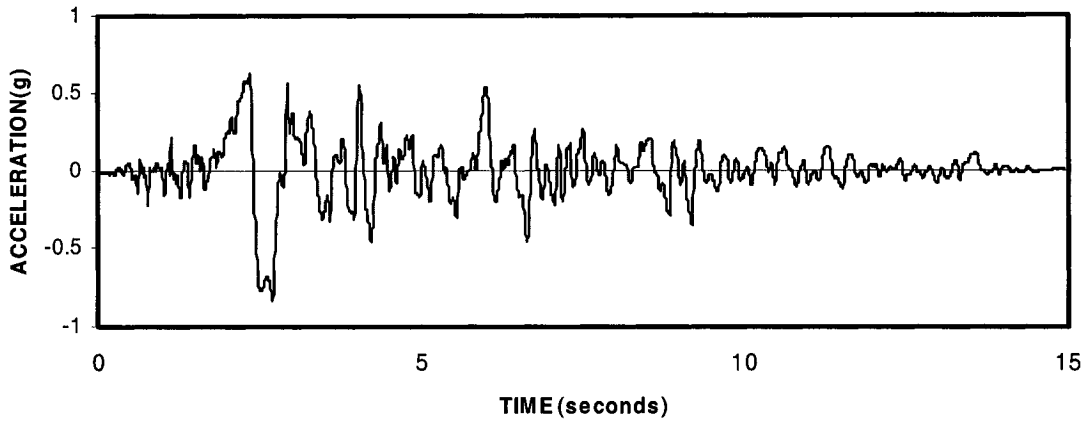

(b)

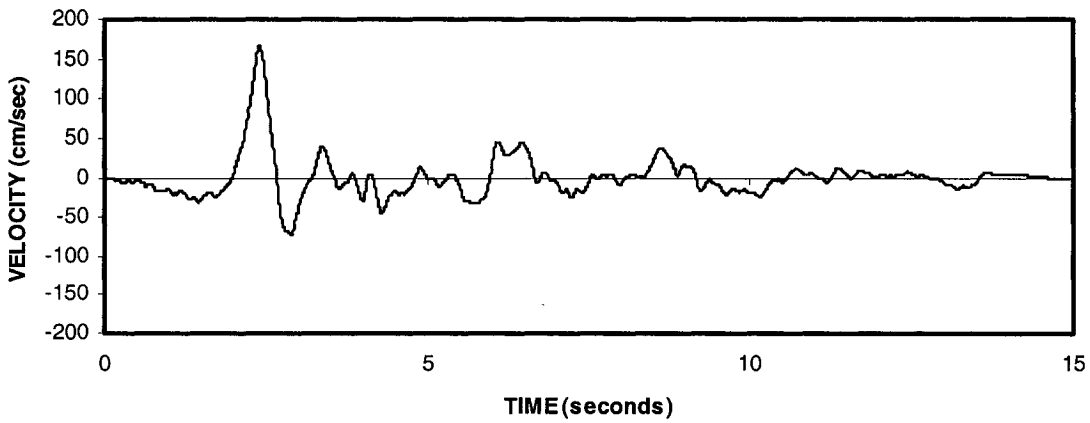

(c)

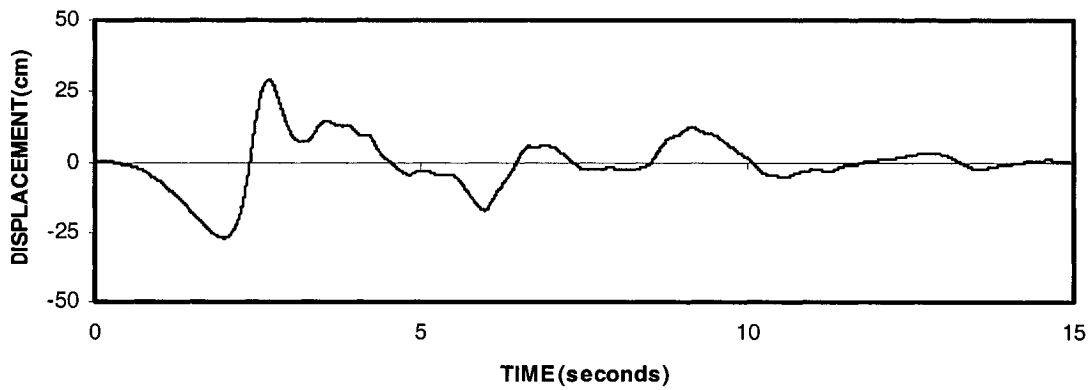

Fig. 3.18 Time-History Record of Northridge (RRS228 component) 1994/01/17 (a) Acceleration; (b) Velocity; (c) Displacement

(a)

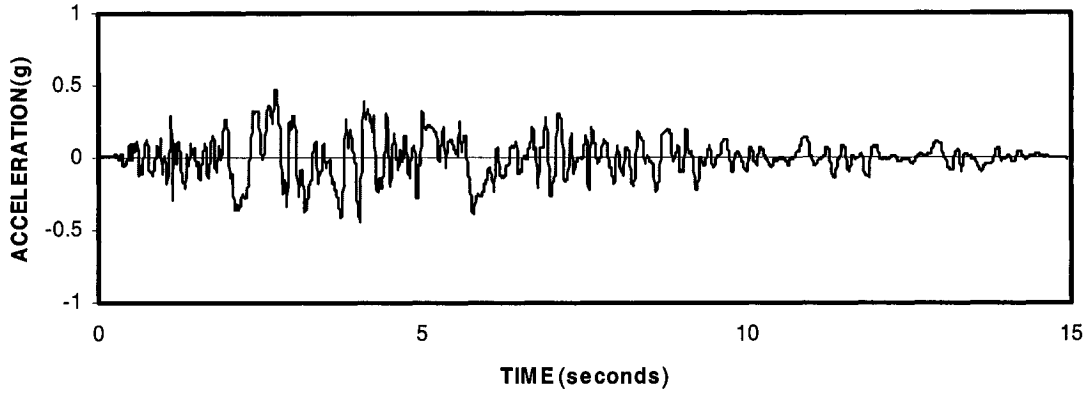

(b)

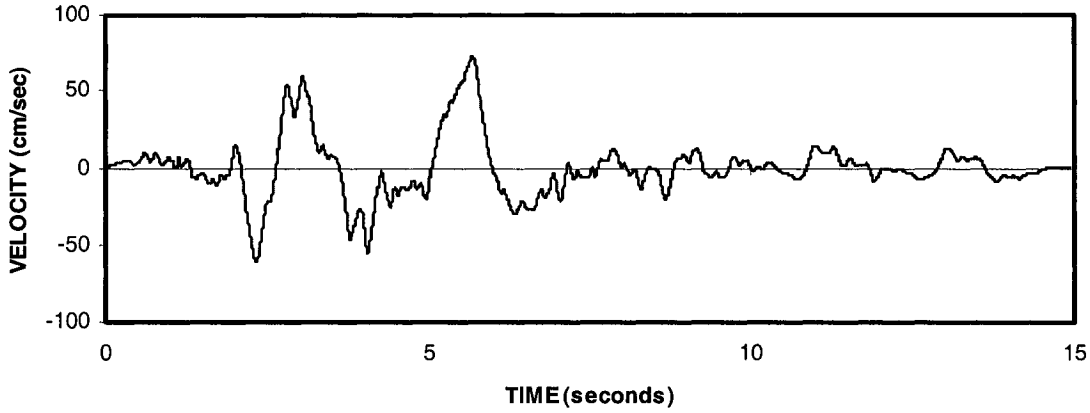

(c)

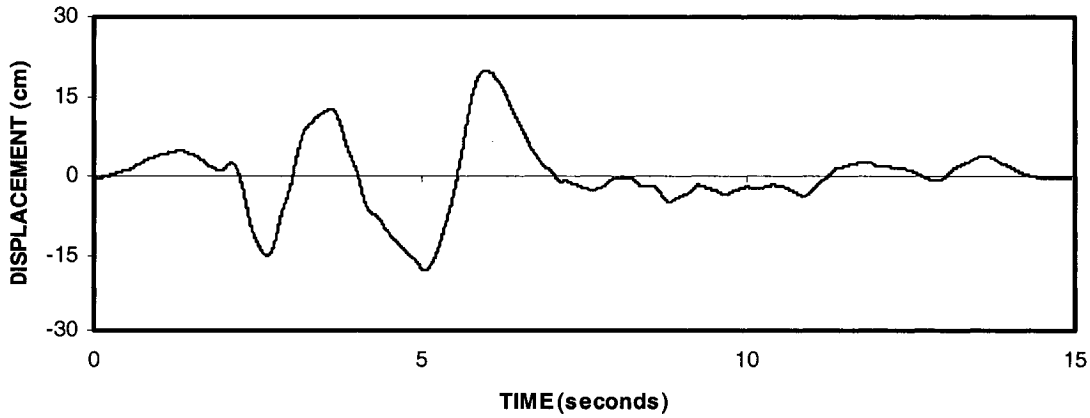

Fig. 3.19 Time-History Record of Northridge (RRS318 component) 1994/01/17 (a) Acceleration; (b) Velocity; (c) Displacement

(a)

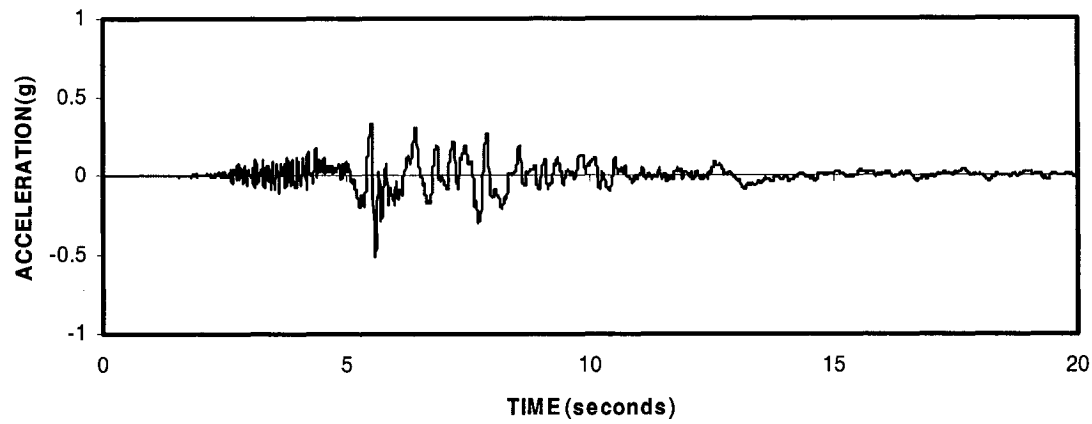

(b)

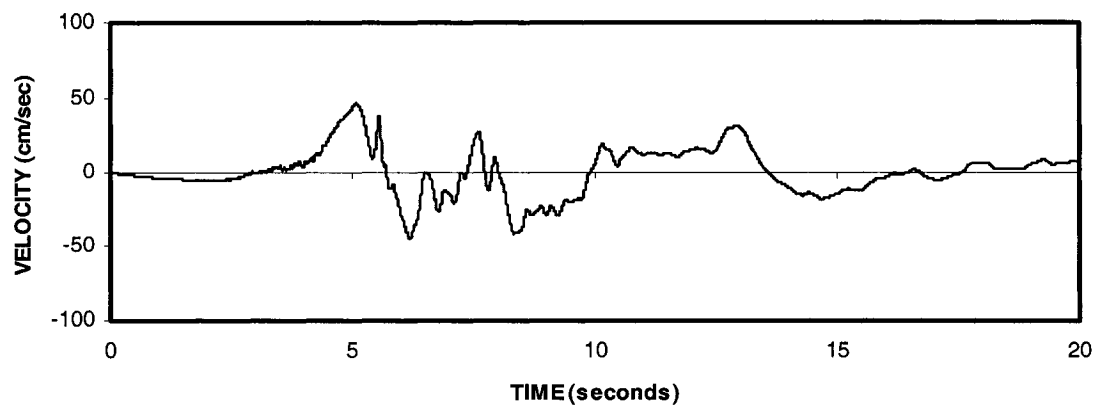

(c)

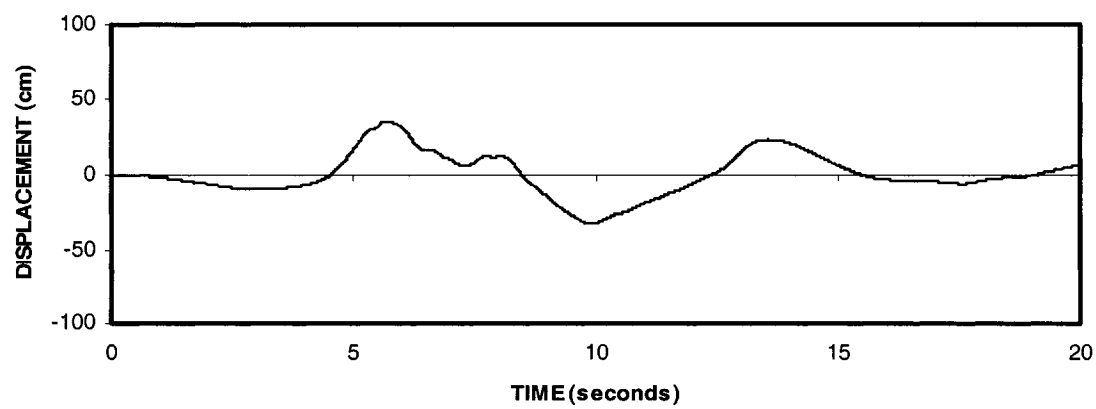

Fig. 3.20 Time-History Record of Imperial Valley (H-E05140) 1979/10/15 (a) Acceleration; (b) Velocity; (c) Displacement

(a)

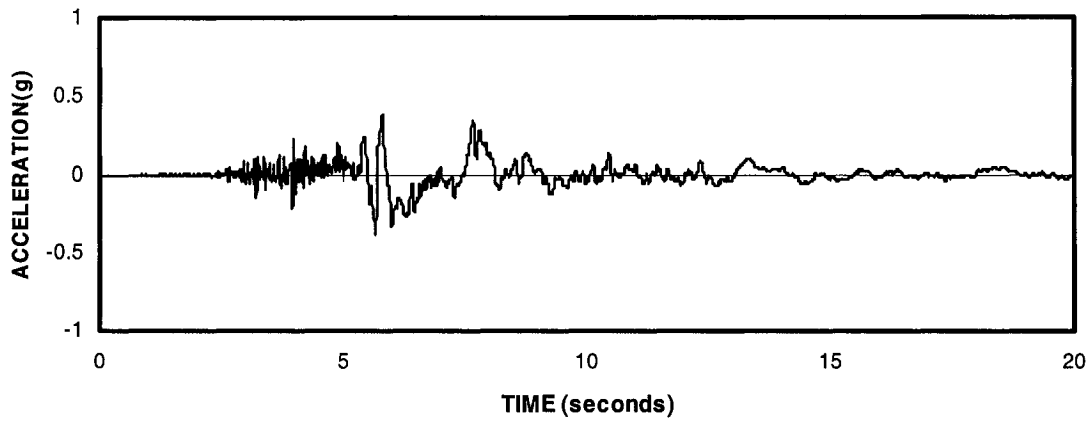

(b)

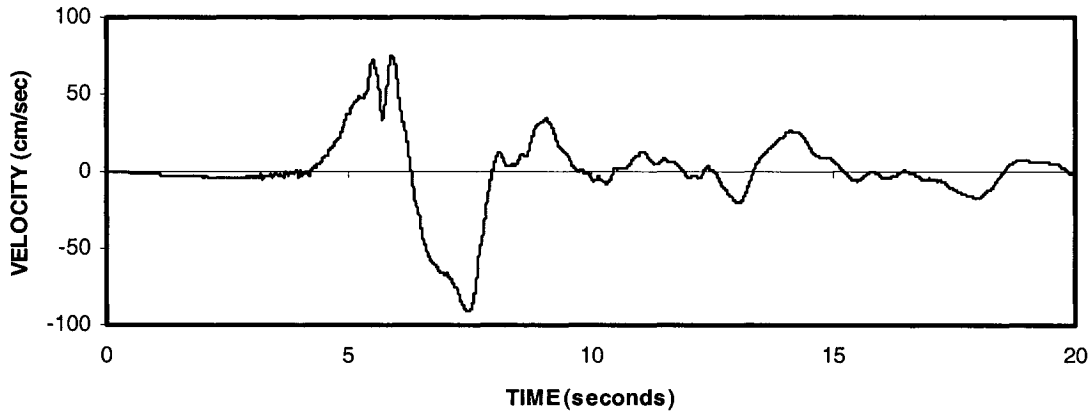

(c)

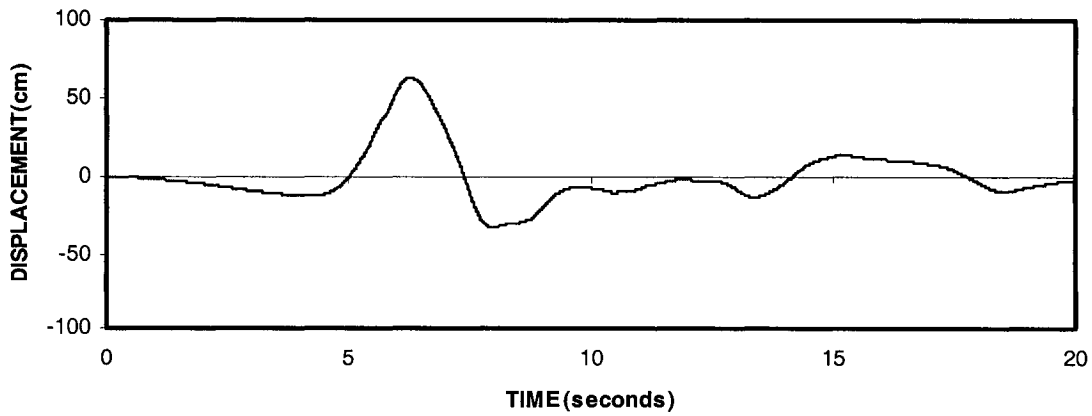

Fig. 3.21 Time-History Record of Imperial Valley (H-E05230) 1979/10/15 (a) Acceleration; (b) Velocity; (c) Displacement

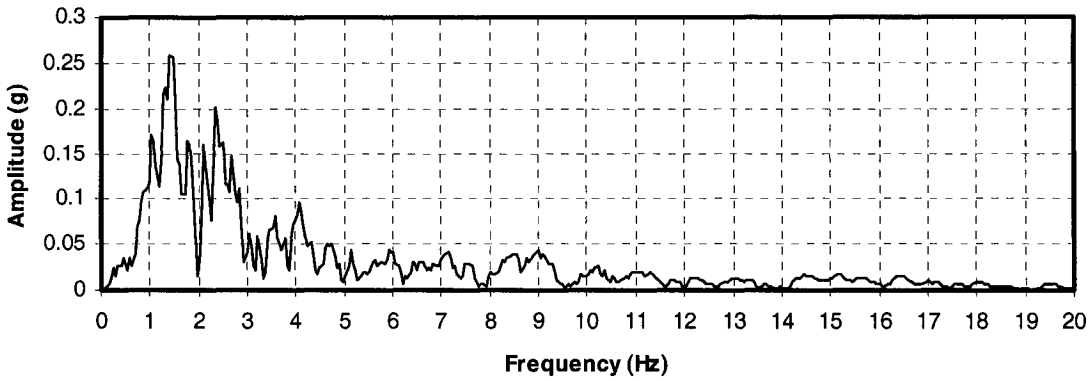

Fig. 3.22 Forward Fourier Transform of the Ground Acceleration to Coalinga270 Earthquake

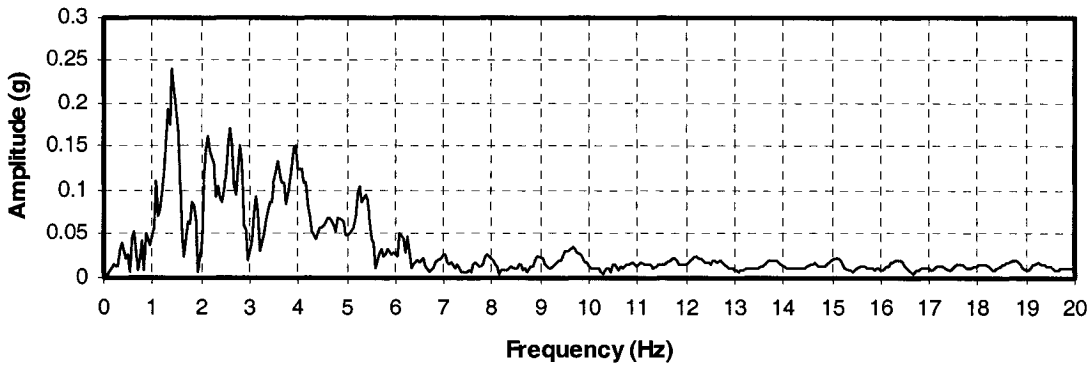

Fig. 3.23 Forward Fourier Transform of the Ground Acceleration to Coalinga360 Earthquake

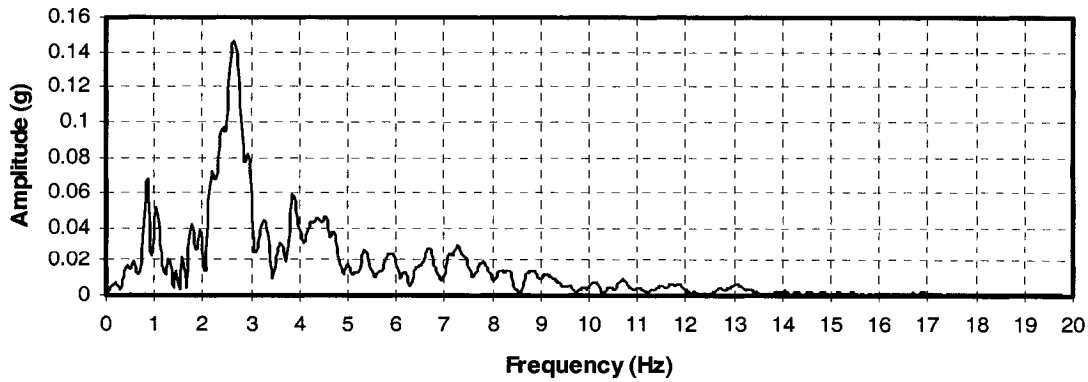

Fig. 3.24 Forward Fourier Transform of the Ground Acceleration to Parkfield205 Earthquake

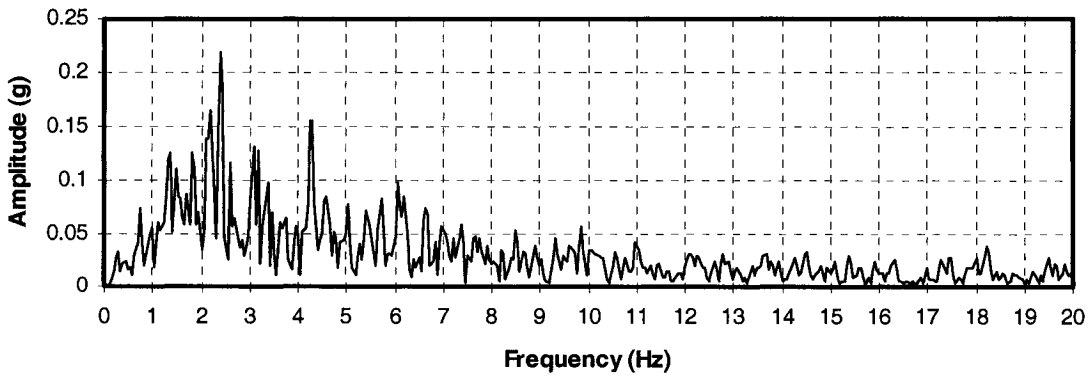

Fig. 3.25 Forward Fourier Transform of the Ground Acceleration to Mammothlake-I-00 Earthquake

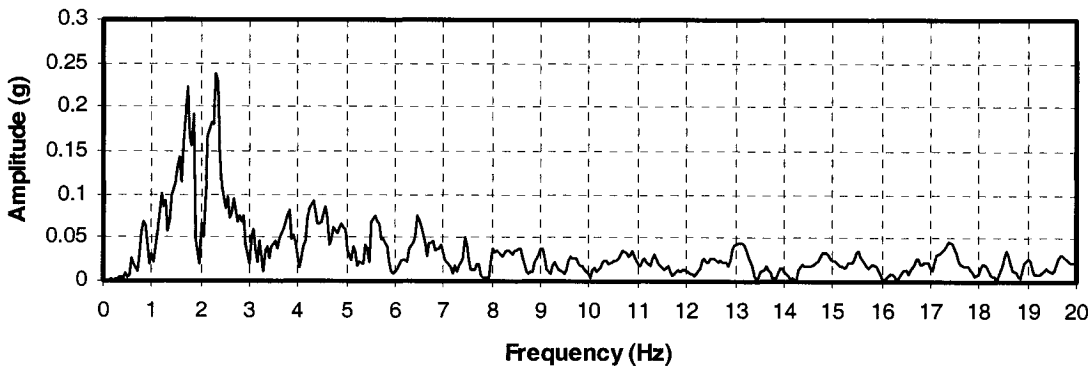

Fig. 3.26 Forward Fourier Transform of the Ground Acceleration to Mammothlake-L-00 Earthquake

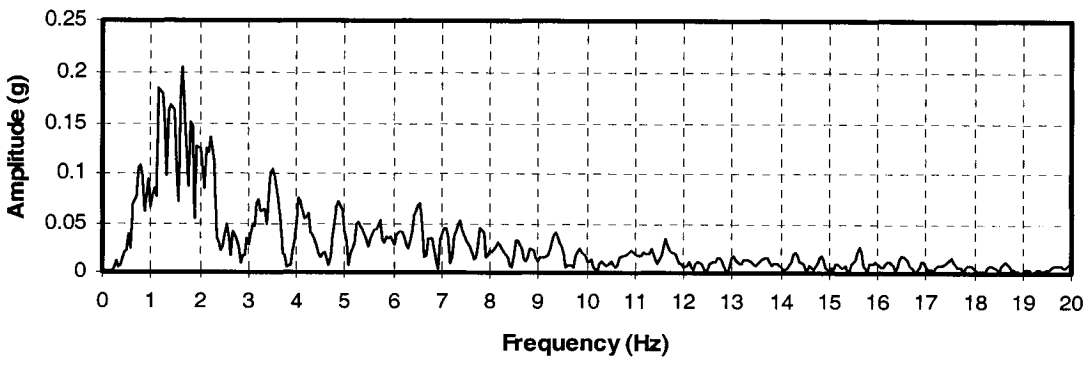

Fig. 3.27 Forward Fourier Transform of the Ground Acceleration to Mammothlake-L-90 Earthquake

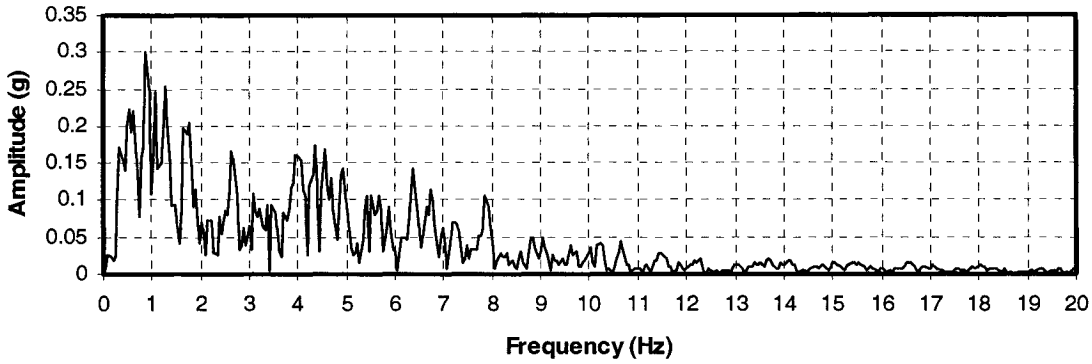

Fig. 3.28 Forward Fourier Transform of the Ground Acceleration to Northridge175 Earthquake

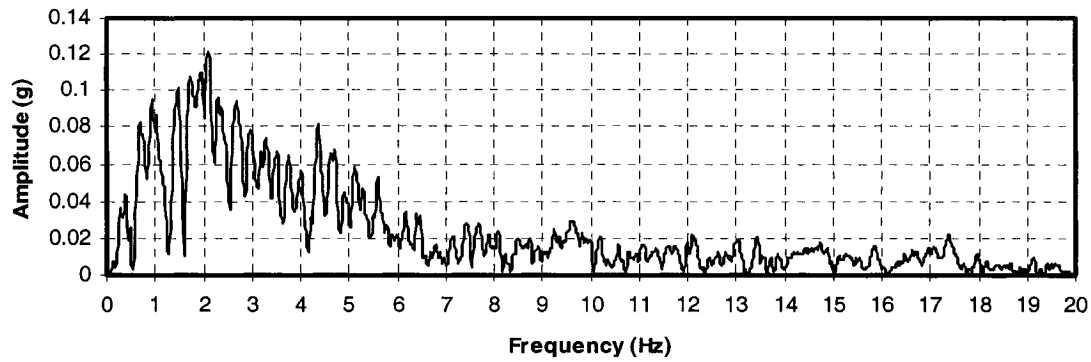

Fig. 3.29 Forward Fourier Transform of the Ground Acceleration to Northridge265 Earthquake

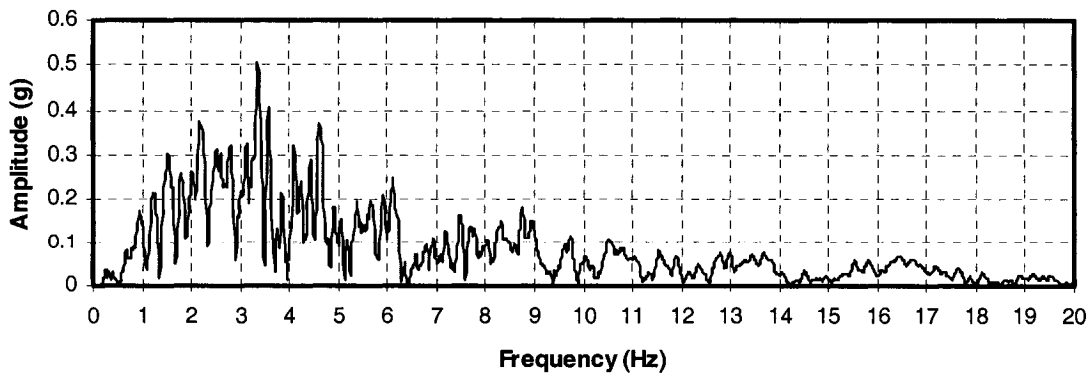

Fig. 3.30 Forward Fourier Transform of the Ground Acceleration to Northridge104 Earthquake

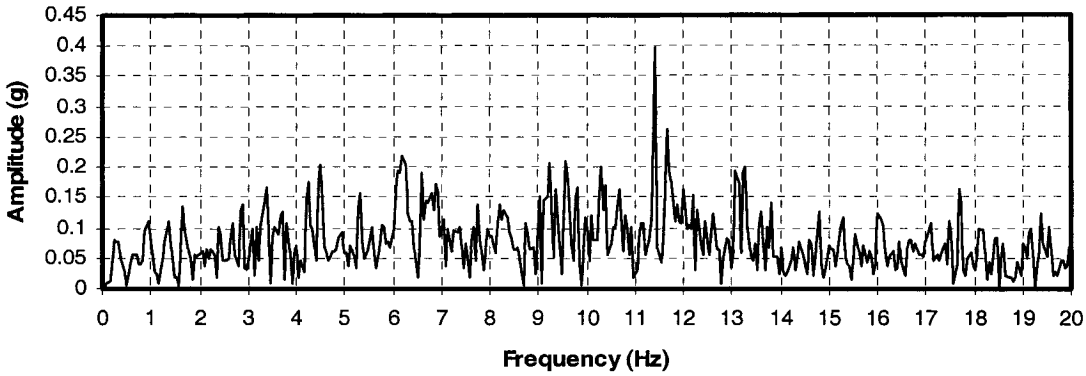

Fig. 3.31 Forward Fourier Transform of the Ground Acceleration to Lander000 Earthquake

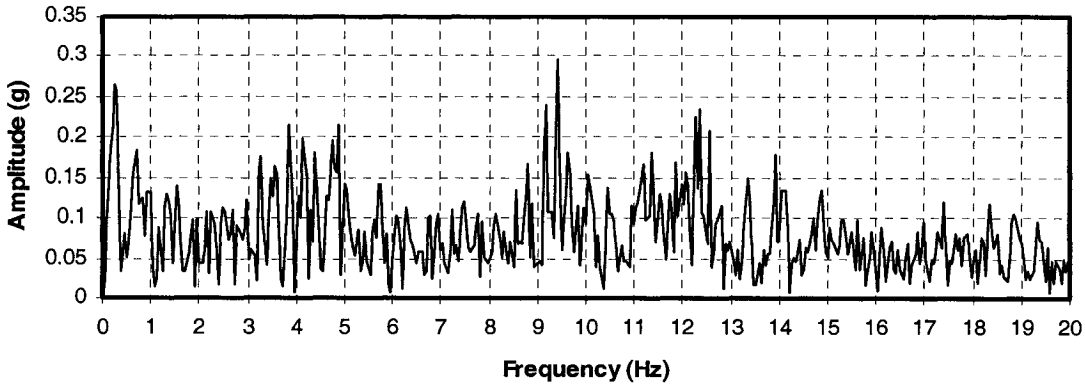

Fig. 3.32 Forward Fourier Transform of the Ground Acceleration to Lander275 Earthquake

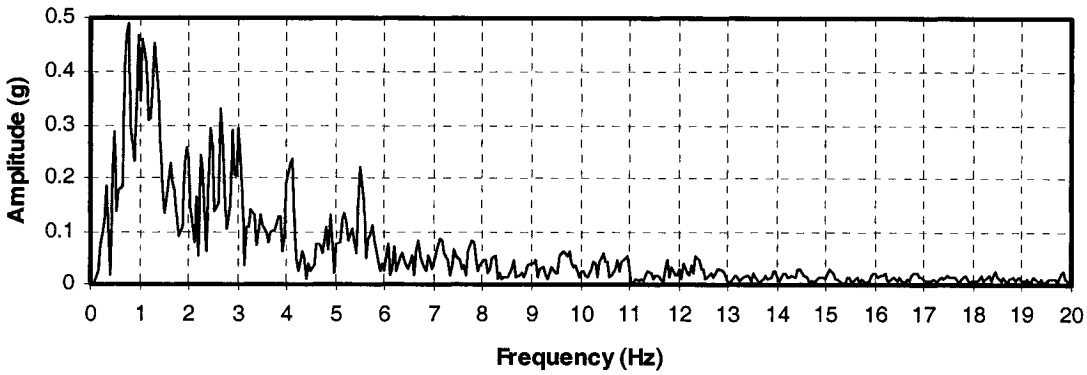

Fig. 3.33 Forward Fourier Transform of the Ground Acceleration to Northridge228 Earthquake

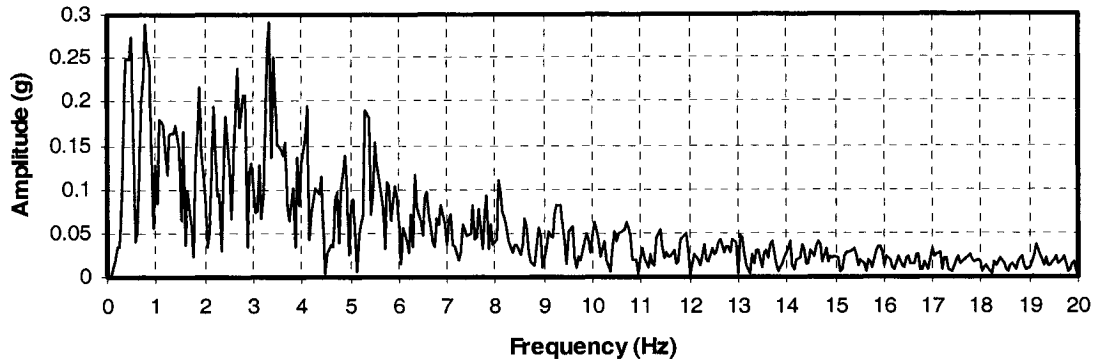

Fig. 3.34 Forward Fourier Transform of the Ground Acceleration to Northridge318 Earthquake

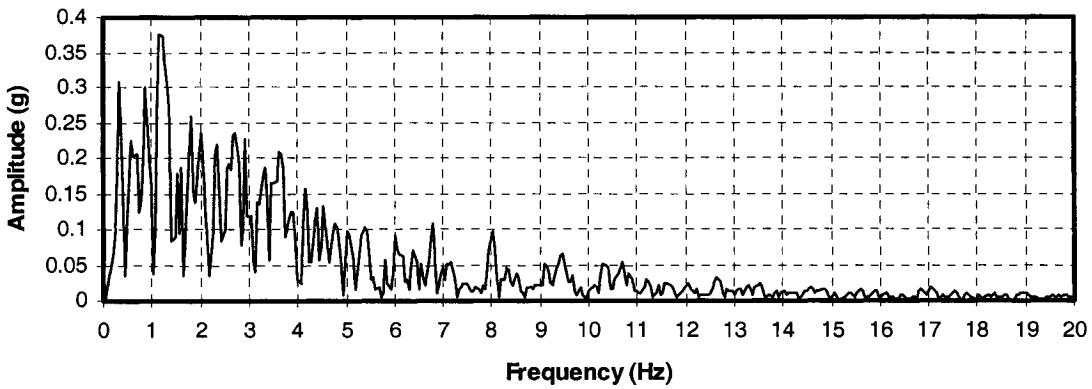

Fig. 3.35 Forward Fourier Transform of the Ground Acceleration to Northridge018 Earthquake

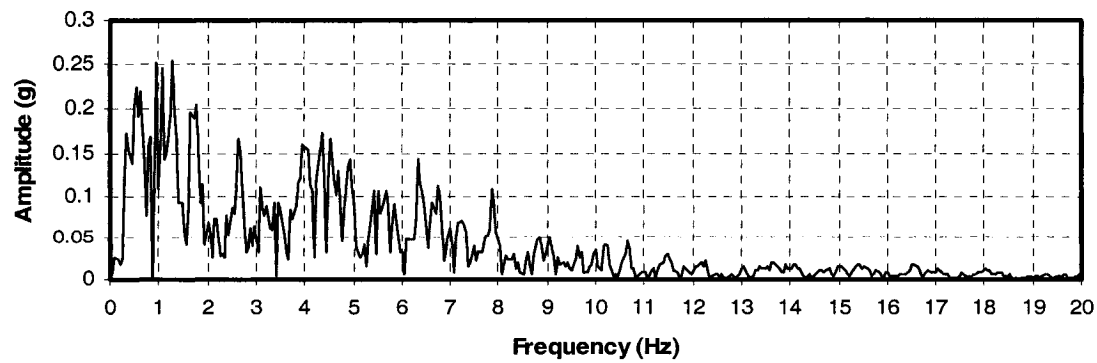

Fig. 3.36 Forward Fourier Transform of the Ground Acceleration to Northridge288 Earthquake

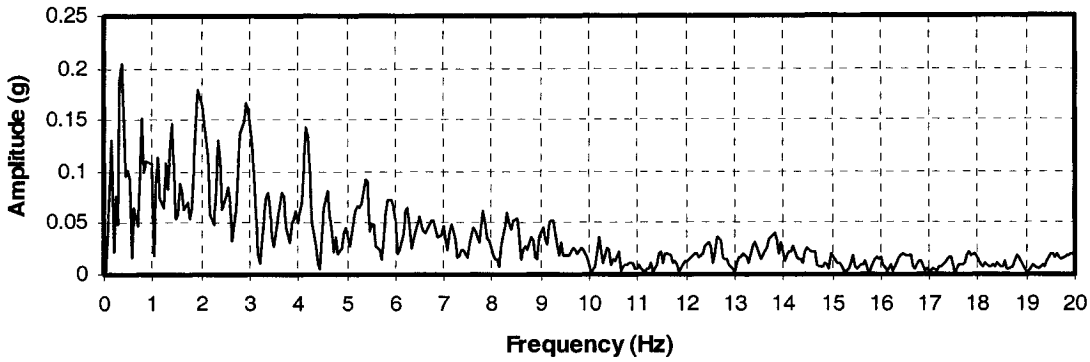

Fig. 3.37 Forward Fourier Transform of the Ground Acceleration to Imperial514 Earthquake

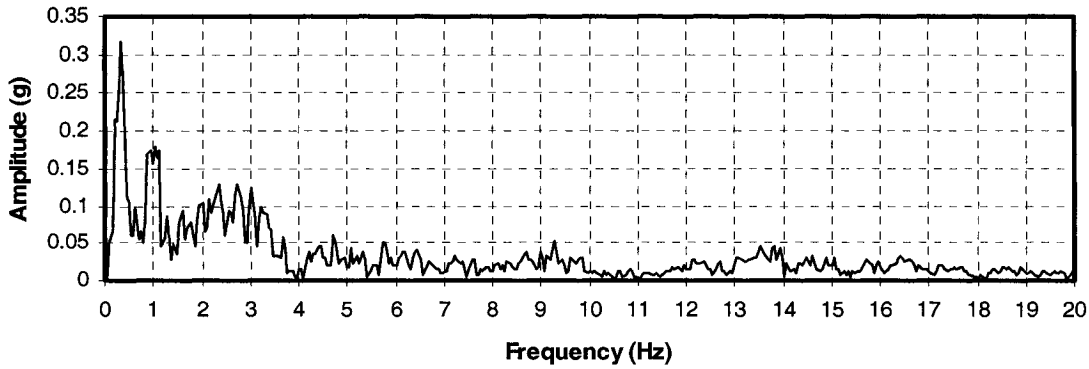

Fig. 3.38 Forward Fourier Transform of the Ground Acceleration to Imperial523 Earthquake

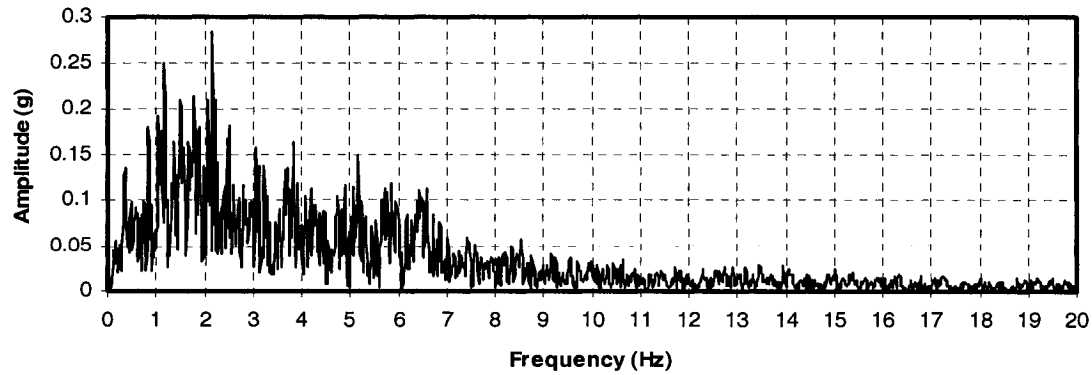

Fig. 3.39 Forward Fourier Transform of the Ground Acceleration to El-Centro Earthquake

CHAPTER 4

SINGLE DEGREE-OF-FREEDOM SYSTEMS

4.1 GENERAL EQUATION OF MOTION

With reasonable conditions, a complicated dynamic problem is usually simplified as a single-degree-of-freedom system (SDOF), neglecting some inferior factors. Therefore, for a one-bay one-story frame, it is usually assumed that the total mass m of the structure is concentrated at the middle of the roof floor, and the frame itself is massless and provides stiffness k in the lateral direction. In order to study the dynamic response of the frame, the necessity is to set up the equation of motion, given by

$$f_I(t) + f_D(t) + f_s(t) = P(t) \tag{4.1}$$

where $f_I(t) = m \cdot \ddot{u}(t)$ is the inertia force, $f_s(t) = k \cdot u(t)$ is the elastic restoring force of the structure, and $f_D(t) = f_h + f_d$ is the damping force, including structural inherent damping force $f_h = c \cdot \dot{u}(t)$ and added damping force f_d provided by desired additional dampers, $P(t) = -m \cdot \ddot{u}_g(t)$ is the external load, due to ground earthquake motions. If dynamic response of the structure is linearly elastic, the mass m, the damping coefficient c and the stiffness k of the SDOF system are constant. The formula (4.1) can be also re-written as follows:

$$m \cdot \ddot{u}(t) + c \cdot \dot{u}(t) + k \cdot u(t) = -m \cdot \ddot{u}_g(t) \tag{4.2}$$

However, yielding can usually be induced in the building by an earthquake, especially under a major earthquake. The structural parameters such as structural stiffness k and

damping coefficient c are no longer constant. It is more suitable to set up an incremental form of the equation as follows:

At time t_i:

$$m \cdot \ddot{u}(t_i) + c(t_i) \cdot \dot{u}(t_i) + k(t_i) \cdot u(t_i) = -m \cdot \ddot{u}_g(t_i)$$

At time $t_i + \Delta t$:

$$m \cdot \ddot{u}(t_{i+\Delta t}) + c(t_i) \cdot \dot{u}(t_{i+\Delta t}) + k(t_i) \cdot u(t_{i+\Delta t}) = -m \cdot \ddot{u}_g(t_{i+\Delta t})$$

Subtracting the first equation from the second:

$$m \cdot \Delta\ddot{u}(t_i) + c(t_i) \cdot \Delta\dot{u}(t_i) + k(t_i) \cdot \Delta u(t_i) = -m \cdot \Delta\ddot{u}_g(t_i) \qquad (4.3)$$

Above formula (4.3) is an incremental form of the equation used for nonlinear analysis of SDOF systems. In the following we will discuss how to set up models with and without dampers to analyze the dynamic properties of the SDOF systems.

4.2 MODEL OF MOMENT-RESISTING FRAME

4.2.1 System Configuration

The one-story one-bay steel moment-resistant frame (MRF1) shown in Fig. 4.1 is chosen from [Gong, 2004]. Overall dimensions of the frame are $7.32m$ in plan and story height is $3.66m$. The system has a mass of $m = 17319kg$, which is lumped at the roof floor. The cross section properties of beam and column, respectively, are: moments of inertia $I_b = 3.134 \times 10^7 mm^4$ and $I_c = 6.077 \times 10^7 mm^4$; yield moments $M_{pb} = 21.65kN - m$ and $M_{pc} = 50.18kN - m$; the Young's modulus of elasticity $E = 2.0 \times 10^5 MPa$; and the material yield strength $F_y = 250MPa$.

4.2.2 Calculation of Control Parameters

4.2.2.1 The Lateral Stiffness

According to the formula provided by [Chopra, 2001], the lateral stiffness of a frame can be calculated as follows:

$$k_{frame} = \frac{24EI_c}{h^3} \times \frac{12\rho + 1}{12\rho + 4} \tag{4.6}$$

where $\rho = {}^{I_b}\!/_{4I_c}$ is stiffness ratio of the beam to the column. Accordingly, $\rho = 0.1289$, and overall lateral stiffness $k_{frame} = 2732kN/m$, then the period of the SDOF can be obtained $(T_n)^*_{frame} = 2\pi \cdot \sqrt{\frac{m}{k_f}} = 0.5\sec$, which is very close to the period $(T_n)_{frame} = 0.5019\sec$ calculated by the program.

4.2.2.2 Structural Damping and Damping Coefficient

The structural inherent damping is an important parameter to influence the dynamic behavior of the building. However, in practice, the actual damping mechanisms lead to relatively complicated mathematics to describe the associated energy-dissipating mechanisms. Therefore, for the convenience of dynamic analysis, structural damping is usually idealized as a linear viscous damper or dashpot. What we need is to calculate the equivalent viscous damping, which represents the energy dissipation in all the damping mechanisms existing in the structure. For the ordinary steel structure, critical damping ratio $\zeta = 5\%$ is usually assumed, which is confirmed to be enough to include the effect of the structural inherent damping. Here the Rayleigh damping is defined to describe

characteristics of the structural inherent damping, which is also used by the programs DRAIN-2DX and SAP2000. The following is the Rayleigh damping expression:

$$C = \alpha \times M + \beta \times K \tag{4.7}$$

which shows that Rayleigh damping matrix C is proportional to nodal mass matrix M and element stiffness matrix K. If needed, transnational or rotational dampers can be specified at each node when mass-dependent damping αM is defined and stiffness-dependent damping βK defines a damper in parallel with each element.

For the SDOF moment-resisting frame, we may define stiffness-dependent damping $c = \beta k$ for the convenience of calculation. Since the critical damping $c_r = 2m\omega_n$, the initial stiffness $k = m\omega_n{}^2$, and critical damping ratio $\zeta = \frac{c}{c_r} = \frac{\beta k}{2m\omega_n} = \frac{m\omega_n{}^2\beta}{2m\omega_n} = \frac{\omega_n\beta}{2}$, the stiffness-dependent damping coefficient $\beta = \frac{2\zeta}{\omega_n} = \frac{2\times 5\%}{2\pi} \times 0.5019 = 0.007988$, which will be used in the computation to consider the influence of structural inherent viscous damping itself.

4.3 MODEL OF FRICTION-DAMPED FRAME

4.3.1 System Configuration

Based on the MRF1 model, a friction-damped brace element is added to the structure, as shown in Fig. 4.2. The cross-section properties of beam and column elements are the same as the MRF1 model. Later, symbol FD1 is used to refer to one-story friction-damped frame model.

4.3.2 Calculation of Control Parameters

4.3.2.1 Optimum Slip Force of Friction Damper

Baktash [1989] proposed a simple method to find out the optimum slip force. For a SDOF friction-damped braced frame, when the shear force V_f undertaken by the frame is equal to that of the friction damper, the capacity of the system's energy dissipation is maximal. That means the slip force is optimum under that condition.

For a one-story one-bay frame, the maximum shear force is:

$$V_f = \frac{2(M_{pb} + M_{pc})}{h} \tag{4.8}$$

where M_{pb} and M_{pc} are the yield moments for the beam and column, respectively, given before; h is story height. Then, the shear force undertaken by the friction damper is $V_d = V_f = 39.26kN$. According to the geometric relationship of the friction-damped brace shown in Fig. 4.2, the slip force P_d of the damper is $P_d = V_d / \cos\alpha$, where $\cos\alpha = 0.8944$. So that the optimum slip load is $P_d = 43.89kN$.

4.3.2.2 Stiffness of Friction-Damper Brace

Since hysteretic loop of friction damper is similar to that of an ideal elastic-plastic material, in the DRAIN-2DX program, the friction damper can be modeled as a truss element with elastic-plastic yielding behavior. The yield strength $F_y = 250\ MPa$ for steel material is selected here. Therefore, the equivalent cross-section of the truss element

is $A_{eq} = P_d / F_y = 175.6mm^2$. The corresponding equivalent stiffness of the truss element is $k_{eq} = \frac{EA_d}{L_b} \times \cos^2 \alpha$; the truss element length $L_b = \sqrt{7.32^2 + 3.66^2} = 8.184m$; and $k_{eq} = 3432kN/m$. The stiffness ratio of truss element to the pure frame is $\lambda = k_{eq} / k_{frame} = 1.256$, which is relatively small. Usually, the friction damper does not work or is not activated under service load. The brace connected with the damper should be stiff enough under service conditions. The stiffness of the brace should satisfy the optimum condition $\lambda = 4 \sim 5$. Then, the design stiffness of the truss element is $k_{eq} = 4k_{frame} = 10928kN/m$. We can see that the stiffness of the truss element is dependent only on the stiffness of the brace, and the yield stress of the truss element is dependent on damper slip force and is equal to the slip force divided by the brace area. The adjusted equivalent cross-section of the truss element is $A_{eq} = \frac{k_{eq} L_b}{E} \times \frac{1}{\cos^2 \alpha} = 559.0mm^2$, and the yield stress $\sigma_d = P_d / A_{eq} = 78.5\ MPa$, which is used in the computation.

Using the DRAIN-2DX program analysis, the natural vibration period of the friction-damped frame is $(T_d)_{friction} = 0.23\sec$, which is smaller than that of MRF1. It is reasonable because the friction damper adds additional stiffness to the structure at the same time.

4.3.2.3 Structural Damping and Damping Coefficient

In order to keep the structural inherent viscous damping with critical damping ratio $\zeta = 5\%$, which is the same as for the MRF1 model, here, we define damping $c = \beta k$, so that, damping coefficient $\beta = \frac{2\zeta}{\omega_d} = \frac{\zeta}{\pi} \times T_d = \frac{5\%}{\pi} \times 0.23006 = 0.003662$.

The corresponding stiffness-dependent damping ratio is $\zeta_{stiff} = 0.01262$. In fact, the structural damping ratio should be $\zeta = \zeta_{stiff} + \zeta_{mass} = 0.05$. So that the mass-dependent damping ratio $\zeta_{mass} = \zeta - \zeta_{stiff} = 0.05 - 0.01262 = 0.03738$.

Secondly, defining $c = \alpha m + \beta k$,

the critical damping ratio

$$\zeta = \frac{c}{c_r} = \frac{\alpha m + \beta k}{c_r} = \frac{\alpha m}{c_r} + \frac{\beta k}{c_r} = \zeta_{mass} + \zeta_{stiff}$$

Then $\frac{\alpha m}{c_r} = \zeta_{mass} \Rightarrow \alpha = \frac{\zeta_{mass} \cdot c_r}{M} = 2\zeta_{mass} \cdot \omega_n = 2.0418$

Therefore, the damping coefficients $\alpha = 2.0418$ and $\beta = 0.003662$ have been obtained to consider the structural inherent viscous damping.

4.4 MODEL OF VISCOELASTIC-DAMPED FRAME

4.4.1 System Configuration

Based on the MRF1 model, a viscoelastic-damped brace element is added to the structure, as shown as in Fig. 4.2. The cross-section properties of the beam and the column elements are the same as for the MRF1 model. For the convenience of analysis later, symbol VE1 is defined to represent a one-story viscoelastic-damped frame model.

4.4.2 Calculation of Control Parameters

4.4.2.1 Procedure to Model Viscoelastic Damper

Step 1: Determination of stiffness k_d of viscoelastic damper

Usually, the storage modulus, the loss modulus and the loss factor are the three basic parameters to describe the properties of a viscoelastic damper. It was found that the frequency of the viscoelastic damped structure decreases when increasing ambient temperature. Although the viscoelastic damper is made of frequency and temperature sensitive material, many tests confirmed that the change of temperature and structural frequency caused by an earthquake is not large, so that the properties of VE material can be considered as constant.

Step 2: Determination of equivalent stiffness k_{vb} of VE-damped brace element

The stiffness of the brace connecting the VE damper to the structure influences the damper efficiency. Therefore, the combined equivalent stiffness of damper-brace element should be determined. The following formula is selected from Chang and Lin [2004]:

$$\text{Equivalent loss factor } \eta_{vb} = \frac{k_b}{k_d(1+\eta_{ve}^2)+k_b} \times \eta_v \tag{4.9}$$

$$\text{Equivalent stiffness } k_{vb} = \frac{k_d k_b (1+\eta_{ve}^2)}{k_d(1+\eta_{ve}^2)+k_b} \times \frac{1}{1+\eta_{vb}^2} \tag{4.10}$$

where k_b is the stiffness of the brace, k_d is the stiffness of the VE damper, k_{vb} is equivalent combined stiffness, η_{ve} are the loss factor of the VE material, and η_{vb} is equivalent loss factor of combined damper-brace element.

Step 3: Determination of structural damping ratio

The modal strain energy method is used to determine the structural damping ratio ζ_i, which is corresponding to each mode. The purpose of modal strain energy method is to use the modal damping ratio containing the mechanical property of the VE damper. For a SDOF system, we have the relationship $\zeta = \frac{\eta_{ve}}{2}(1-\frac{\omega_n}{\omega_d})$ [Chang et al., 1995], where ω_n is the circular frequency of the MRF1 without the VE damper, and ω_d is the circular frequency of the MRF1 with the VE damper. If given design damping ratio $\zeta = 15\%$, and loss factor $\eta_{ve} = 0.9$, the period of the VE damped model is:

$$(T_d)_{viscoelastic} = \sqrt{1-\frac{2\zeta}{\eta_{ve}}} \times (T_n)_{frame} = 0.4098 \sec .$$

Step 4: Determination of equivalent axial cross section

In the DRAIN-2DX program, the VE damped braced element is modeled as a truss element with equivalent cross section A_{eq} and combined with corresponding calculated modal damping ratio. Because $k_{eq} = \frac{EA_{eq}}{L_b} \cdot \cos\alpha^2$, and total model stiffness $k = k_{frame} + k_{eq}$, the equivalent stiffness:

$$k_{eq} = k - k_{frame} = m\omega_d^2 - k_{frame} = [17.319 \times (\frac{2\pi}{0.4098})^2 - 2732]kN/m = 1339kN/m .$$

Therefore, the equivalent damper-brace cross section $A_{eq} = \frac{k_{eq}L_b}{E\cos\alpha^2} = 68.5mm^2$ is obtained.

4.4.2.2 Structural Damping and Damping Coefficient

In order to compare with MRF1 and FD1 model under the same condition, viscoelastic-damped model also assumes having $\zeta = 5\%$ inherent viscous damping ratio. The mass-dependent damping coefficient is $\alpha = 0.5075$, and stiffness-dependent damping coefficient is $\beta = 0.006522$. The method of calculation is the same as for friction-damped model above mentioned.

4.5 MODEL OF FLUID-VISCOUS DAMPED FRAME

4.5.1 System Configuration

Based on the MRF1 model, a fluid viscous damped brace element is added to the structure, as shown as in Fig. 4.2. The cross-section properties of beam and column elements are the same as for the MRF1 model, and symbol VD1 is defined to refer to a one-story fluid viscous-damped frame model.

4.5.2 Calculation of Control Parameters

4.5.2.1 Additional Damping Ratio

In the DRAIN-2DX program, it is relatively easy to model the fluid viscous damper as a truss element with assumed equivalent additional damping ratio $\zeta = 15\%$. At the same time, the brace should be stiff enough to connect the damper to the structure; however, in practice, the stiffness of the brace does not provide any contribution to the structure. Therefore, the natural period of model remains $(T_d)_{viscous} = 0.5019\,\text{sec}$, the same as that of the MRF1 model.

4.5.2.2 Structural Damping and Damping Coefficient

The same condition with other three models, the inherent viscous damping ratio of VD1 model also assumes $\zeta = 5\%$. The corresponding stiffness-dependent damping coefficient is $\beta = 0.007988$.

4.6 MODEL CALCULATION AND RESULTS ANALYSIS

Nonlinear analysis using the program DRAIN-2DX is conducted for the four different structural models under near-fault and far-fault ground motions. Detailed dynamic response quantities of each model, such as maximum roof displacements, developed plastic hinges, magnitudes of base shear force, axial forces in column, column moments and beam moments, are shown in Tables 4.3~ 4.6. Table 4.2 indicates structural state of each model under near-fault ground motions. In order to analyze structural responses conveniently, two basic parameters are firstly defined. One is an earthquake coefficient EVA, which is the ratio of peak ground velocity to peak ground acceleration. It reflects characteristics of different near-fault ground motions. Another is response coefficient RNF, which is the ratio of response under near-fault earthquake to response under far-fault earthquakes.

4.6.1. Dynamic Responses of Three Models to Different Ground Motions

a. From the Table 4.3~ 4.6, it is found that, one the hand, for the same ground motion, a different model has different dynamic response, which means that structural dynamic character such as stiffness and natural vibration period significantly affects the model dynamic response; on the other hand, for the same model, its dynamic response also varies to different earthquake records, which means that the characteristics of the

input ground motion such as peak magnitude and duration of motion greatly influences the model dynamic response at the same time.

b. Compared with the single-story MRF1 model, generally speaking, the structural dynamic response especially roof displacement is reduced once the frame incorporates an additional damper. For example, Table 4.7 clearly shows that the peak roof displacements of FD1 model, VE1 model and VD1 model are reduced respectively: ranges from 20% to 76%, 26% to 76%, and 55% to 81%.

4.6.2. Comparison of Dynamic Response to Far-Fault and Near-Fault Earthquakes

In order to conveniently compare structural dynamic response to near-fault earthquakes with far-fault earthquakes, we choose the El-Centro time history record as a representative of far-fault earthquakes, and adjust its peak acceleration to the peak acceleration of corresponding near-fault record. The detailed time history analysis results are shown in Fig. 4.3 ~ Fig. 4.4 and discussed below.

4.6.2.1 Dynamic Response of Model with Added Friction Damper

Roof Displacement:

Compared with roof displacement to El-Centro far-fault earthquake, Fig. 4.3a shows two different dynamic responses to friction-damped model. In most of cases, when the FD1 model is subjected to near-fault earthquakes with earthquake coefficient EVA< 0.1, corresponding response coefficient RNF<1.0, which means the roof displacement of friction-damped model is smaller than that under El-Centro earthquake. On the contrary, if earthquake coefficient EVA>1.0, the response coefficient RNF is generally larger than

1.0, which means the roof displacement of friction-damped model is larger than that under El-Centro earthquake.

Base Shear:

Fig. 4.4a shows that change of base shear force of FD1 model is similar to the change of roof displacement of FD1 model. If earthquake coefficient EVA>1.0, the response coefficient RNF is close or larger than 1.0, which means the response of friction-damped model is larger than that under El-Centro earthquake.

4.6.2.2 Dynamic Response of Model with Added Viscoelastic Damper

Roof Displacement:

Compared with roof displacement to El-Centro far-fault earthquake, Fig. 4.3b also shows two different dynamic responses for the viscoelastic-damped model. When the VE1 model is subjected to near-fault earthquakes with earthquake coefficient EVA < 0.1, corresponding roof displacement of VE1 model is smaller than that under El-Centro earthquake, not including the case of Northridge265. The roof displacement of model is larger than that for El-Centro far-fault earthquake if earthquake coefficient EVA of near-fault earthquakes is larger than 0.1.

Base Shear:

Fig. 4.4b shows that change of base shear force of VE1 model is similar to the change of roof displacement of VE1 model.

4.6.2.3 Dynamic Response of Model with Added Fluid Viscous Damper

Roof Displacement:

Compared with roof displacement under El-Centro far-fault earthquake, Fig. 4.3c also indicates two different dynamic responses for fluid-viscous damped model. When the VD1 model is subjected to near-fault earthquakes with earthquake coefficient EVA< 0.1, corresponding roof displacement of VD1 model is smaller than that under El-Centro earthquake. The roof displacement of model is larger than that under El-Centro far-fault earthquake if earthquake coefficient EVA of near-fault earthquakes is larger than 0.1.

Base Shear:

Fig. 4.4c shows that change of base shear force of VD1 model is similar to that of roof displacement of VD1 model.

4.6.3. Effectiveness Comparison of Different Dampers

Influenced by vibration period, direct comparison of dynamic quantities of the model with different damper is difficult and explaining which damper is more effective is also difficult. Since damper is an energy-dissipating device, comparison of different damper from the energy point of view, which we emphasis many times before, may be a feasible method. Because the damper is used to dissipate energy during strong vibration, it is reasonable that if energy dissipated by added damper is large, the corresponding damper is more effective. For each model, we can respectively calculate total input energy and energy dissipated by the incorporation of the damper; then we can define the ratio of energy dissipated by damper to total energy input to measure capacity of each damper to

dissipate energy and compare the dampers' effectiveness. Therefore, the first step is to analyze energy time history of the structure.

Figs. 4.5 ~ 4.12 respectively show energy time history of models to El-Centro far-fault earthquake and Northridge228 near-fault earthquake. It is found that the input energy increases with the increase of duration; therefore, for each input earthquake, the total energy input which model receives is evaluated at the end of the ground motion duration. Figs. 4.5 ~ 4.12 also clearly indicate that, for the same earthquake, different model has different amount of energy input that is the reason why different model has different dynamic response. At the same time, each model also has different energy input when subjected to different ground motions. Therefore, in order to compare effectiveness of different damper, we have to measure energy-dissipating ability related to it own input energy.

Fig. 4.5 shows the energy time history of MRF1 model to El-Centro earthquake. It is found that, due to limit ability of structural damping, the yielding energy occupies a major part of the total energy input, which means the structure has yielded during the El-Centro earthquake. Fig. 4.6 shows the energy time history of FD1 model under El-Centro earthquake. There is no yielding energy in the figure, which is consistent with its elastic state. Although VE1 model and VD1 model have yielded under El-Centro ground motion, Fig. 4.7 and Fig. 4.8 show that the amount of yielding energy is smaller than that of damper energy, which indicates added dampers improve the ability of structure to resist earthquake, and the corresponding plastic deformation is reduced.

Fig. 4.9 ~ Fig. 4.12 show the energy time history of MRF1, FD1, VE1 and VD1 model under Northridge228 earthquake. It is also found that the amount of yielding energy of the structure is reduced when added damper to the structure. Therefore, the corresponding dynamic response is mitigated and degree of damage in the structure is reduced.

Table 4.8 digitally shows the proportion of damper energy to total input energy for each model to different earthquake records and Figs. 4.13~ 4.16 graphically indicate damper energy provided by each damper under different earthquake records. From Table 4.8 and Fig. 4.13, it is found that, for a moment-resistant structure, energy absorbed by structural yielding occupies a major proportion of total energy input, minimum is 56%, and maximum is 75%. That means the structure receives relatively high degree of damage during an earthquake. For a friction-damped structure, Table 4.8 and Fig. 4.14 also show that the proportion of damper energy is greatly improved and structural yielding energy is significantly reduced due to added damper. The minimum of proportion of yielding energy is zero and maximum is only 27%, which means structure may be in elastic state during an earthquake. Fig. 4.15 and Fig. 4.16 respectively show contributions provided by viscoelastic damper and fluid viscous damper. The minimum of proportion of damper energy is 71 and maximum is 99% for a viscoelastic-damped structure. The minimum of proportion of damper energy is 59% and maximum is 98% for a fluid viscous-damped structure. Therefore, the ability to resist seismic load of a damped-structure has greatly improved.

4.6.4. Analysis of Results

1. Through time-history analysis to near-fault and far-fault earthquakes, we find that the three types of dampers show similar function. Generally speaking, when subjected to near-fault earthquakes with relatively low impulse velocity, the damper's behavior under near-fault earthquakes is better or close to the behavior under far-fault earthquake. On the contrary, when subjected to relatively high impulse velocity during near-fault ground motion, the damper's behavior under far-fault earthquake is better than that under the near-fault earthquake condition.
2. From Fig. 4.17, we can clearly find that the capacity of friction damper to dissipate energy is relatively higher; therefore, the friction damper is the most effective device among three different dampers. The viscoelastic damper is better than fluid-viscous damper.
3. The main purpose of this study is to investigate the effectiveness of the damper to near-fault and far-fault earthquakes. Due to complicated earthquake conditions, the model dynamic responses are also very complicated. Generally, for a SDOF system, the friction damper and the viscoelastic damper are more effective than the fluid-viscous damper; however during near-fault earthquakes with large velocity, friction damper cannot function very well, and even is worse than fluid-viscous damper. Therefore, how to select proper damper in the design is dependent on the characteristics of earthquakes and should be considered carefully according to the practical situation.

Table 4.1 Model Definition of Different Dampers

Damper Type	Model Element	Brace-Damper Stiffness Definition	Yielding Stress Definition	Equivalent Damping Ratio Definition
Friction Damper	Truss	Only Brace Stiffness	Define Slip force	-
Viscoelastic Damper	Truss	Equivalent Stiffness including Brace and Damper	-	Define desired Damping Ratio
Fluid-Viscous Damper	Truss	-	-	Define desired Damping Ratio

Table 4.2 States of Different Models Subjected to Near-Fault Earthquake Motions

Earthquake Record	Type	Scale	PGA	PGV	PGD	EVA=PGV/PGA	Model of State			
			(g)	(cm/s)	(cm)		MRF1	FD1	VE1	VD1
Coalinga270	Near-Fault	1.0	0.84	44.1	6.8	0.05	Inelastic	Inelastic	Inelastic	Inelastic
Coalinga360	Near-Fault	1.0	1.083	39.7	5.41	0.04	Inelastic	Inelastic	Inelastic	Inelastic
Parkfield205	Near-Fault	1.0	0.357	21.5	3.87	0.06	Inelastic	elastic	Inelastic	Inelastic
Mammothlake-I-00	Near-Fault	1.0	0.43	23.6	7.52	0.06	Inelastic	elastic	Inelastic	Inelastic
Mammothlake-L-00	Near-Fault	1.0	0.921	28.9	3.17	0.03	Inelastic	Inelastic	Inelastic	Inelastic
Mammothlake-L-90	Near-Fault	1.0	0.408	33.9	6.41	0.08	Inelastic	elastic	Inelastic	Inelastic
Northridge175	Near-Fault	1.0	0.415	45.6	5.06	0.11	Inelastic	Inelastic	Inelastic	Inelastic
Northridge265	Near-Fault	1.0	0.434	31.3	4.8	0.07	Inelastic	elastic	Inelastic	Inelastic
Northridge104	Near-Fault	1.0	1.585	55.7	6.06	0.04	Inelastic	Inelastic	Inelastic	Inelastic
Lander000	Near-Fault	1.0	0.785	31.9	16.42	0.04	Inelastic	elastic	Inelastic	Inelastic
Lander275	Near-Fault	1.0	0.721	97.6	70.31	0.14	Inelastic	Inelastic	Inelastic	Inelastic
Northridge228	Near-Fault	1.0	0.838	166.1	28.78	0.20	Inelastic	Inelastic	Inelastic	Inelastic
Northridge318	Near-Fault	1.0	0.472	73	19.76	0.16	Inelastic	Inelastic	Inelastic	Inelastic
Northridge018	Near-Fault	1.0	0.828	117.5	34.22	0.14	Inelastic	Inelastic	Inelastic	Inelastic
Northridge288	Near-Fault	1.0	0.493	74.6	28.69	0.15	Inelastic	Inelastic	Inelastic	Inelastic
Imperial514	Near-Fault	1.0	0.519	46.9	35.35	0.09	Inelastic	Inelastic	Inelastic	Inelastic
Imperial523	Near-Fault	1.0	0.379	90.5	63.03	0.24	Inelastic	Inelastic	Inelastic	Inelastic

Table 4.3 Maximum Dynamic Response Quantities of the Single-Story Moment-Resisting Frame Model

Earthquake Record	Moment of Column	Moment of Beam	Shear Force of Column	Axial Force of Column	Displacement of Top Floor	Magnitude of Plastic Hinge		Record Scale
						Column	Beam	
Unit	Mc (kN-m)	Mb (kN-m)	Vc (kN)	Nc (kN)	(mm)	(Rotation)	(Rotation)	
El-Centro	54.40	23.81	42.80	7.70	43.63	2.54E-02	2.57E-02	1
Coalinga270	57.43	25.34	45.32	8.09	64.49	4.18E-02	4.16E-02	1
Coalinga360	56.15	24.68	44.28	7.59	55.66	1.97E-02	1.97E-02	1
Parkfield205	51.95	22.55	40.80	6.99	26.72	4.28E-03	4.31E-03	1
Northridge175	54.08	23.64	42.56	7.53	41.37	1.38E-02	1.37E-02	1
Northridge265	53.54	23.37	42.10	7.23	37.70	9.43E-03	9.58E-03	1
Northridge104	61.00	27.15	48.32	8.68	89.04	6.39E-02	6.34E-02	1
Lake-L-90	54.97	22.65	43.28	7.38	47.51	3.37E-02	3.42E-02	1
Lake-L-00	54.70	23.96	43.04	7.37	45.67	2.52E-02	2.55E-02	1
Lake-I-00	51.90	22.54	40.72	6.72	26.38	9.39E-03	1.03E-02	1
lander275	57.75	25.51	45.56	7.61	66.71	2.10E-02	2.10E-02	1
lander000	51.55	22.36	40.40	6.65	24.02	5.58E-03	5.81E-03	1
Northridge318	59.03	26.16	46.66	8.10	75.50	5.17E-02	5.13E-02	1
Northridge228	89.18	33.35	71.56	13.80	283.16	1.37E-01	1.36E-01	1
Northridge288	56.57	24.91	44.56	7.66	58.57	4.85E-02	4.82E-02	1
Northridge018	64.96	29.18	51.50	9.41	116.36	8.97E-02	8.90E-02	1
Imperial523	59.76	46.72	47.20	7.69	80.55	2.63E-03	2.62E-02	1
Imperial514	59.49	26.40	46.98	7.77	78.67	2.46E-02	2.47E-02	1

Table 4.4 Maximum Dynamic Response Quantities of the Single-Story Friction-Damped Frame Model

Earthquake Record	Moment of Column	Moment of Beam	Shear Force of Column	Axial Force of Column	Displacement of Top Floor	Magnitude of Plastic Hinge		Record Scale
						Column	Beam	
Unit	Mc (kN-m)	Mb (kN-m)	Vc (kN)	Nc (kN)	Disp. (mm)	Rotation	Rotation	
El-Centro	32.91	14.27	25.60	23.51	9.53	-	-	1
Coalinga270	51.06	22.11	39.99	25.81	20.61	1.66E-03	1.70E-03	1
Coalinga360	52.91	23.05	41.53	26.31	33.32	5.13E-03	5.11E-03	1
ParkField205	39.46	17.12	30.74	24.29	11.42	-	-	1
Northridge175	51.36	22.27	40.23	25.87	22.66	2.22E-03	2.25E-03	1
Northridge265	37.90	16.44	29.52	24.10	10.97	-	-	1
Northridge104	57.54	25.41	45.35	27.07	65.23	2.01E-02	2.01E-02	1
Lake-L-90	43.94	19.07	34.24	24.82	12.72	-	-	1
Lake-L-00	51.41	22.29	40.27	25.92	23.02	2.32E-03	2.34E-03	1
Lake-I-00	35.81	15.53	27.88	23.85	10.37	-	-	1
lander275	50.29	21.72	39.37	25.65	15.29	2.06E-04	2.57E-04	1
lander000	40.36	17.51	31.44	24.39	11.69	-	-	1
Northridge318	50.94	22.05	39.89	25.81	19.77	2.30E-03	2.38E-03	1
Northridge228	73.56	33.55	58.55	29.28	175.59	4.84E-02	4.79E-03	1
Northridge288	50.19	21.66	39.19	25.56	14.57	9.89E-06	5.37E-05	1
Northridge018	60.85	27.09	48.07	27.38	88.01	2.01E-02	1.98E-02	1
Imperial523	50.47	21.81	39.51	25.72	16.55	5.49E-04	5.94E-04	1
Imperial514	50.40	21.78	39.45	25.69	16.08	4.20E-04	4.74E-04	1

Table 4.5 Maximum Dynamic Response Quantities of the Viscoelastic-Damped Frame Model

Earthquake Record	Moment of Column	Moment of Beam	Shear Force of Column	Axial Force of Column	Displacement of Top Floor	Magnitude of Plastic Hinge		Record Scale
						Column	Beam	
Unit	Mc (kN-m)	Mb (kN-m)	Vc (kN)	Nc (kN)	Disp. (mm)	Rotation	Rotation	
1El-Centro	50.64	21.91	39.70	22.75	17.85	1.61E-03	1.68E-03	1
Coalinga270	52.76	22.97	40.51	31.99	32.31	8.73E-03	8.81E-03	1
Coalinga360	52.92	23.05	41.61	38.34	33.42	7.01E-02	7.03E-03	1
ParkField205	50.80	21.98	39.81	22.87	18.83	1.78E-03	1.84E-03	1
Northridge175	52.64	22.91	41.33	32.71	31.48	6.26E-03	-6.24E-03	1
Northridge265	51.50	22.34	40.42	27.27	23.82	3.25E-03	3.27E-03	1
Northridge104	55.02	24.13	43.38	49.49	48.20	3.40E-02	3.38E-02	1
Lake-L-090	51.06	22.11	40.03	24.79	20.58	1.65E-03	1.67E-03	1
Lake-L-000	52.65	22.91	41.33	33.28	31.51	5.89E-03	5.98E-03	1
Lake-I-000	50.30	21.72	39.38	18.92	15.37	2.79E-04	3.64E-04	1
lander275	50.74	21.95	39.73	21.64	18.43	1.06E-03	1.11E-03	1
lander000	50.19	21.67	39.31	19.23	14.59	1.68E-05	5.69E-05	1
Northridge318	51.95	22.55	40.73	27.59	26.72	1.06E-02	1.07E-02	1
Northridge228	61.18	27.25	48.35	35.41	90.30	4.06E-02	4.05E-02	1
Northridge288	51.16	22.16	40.10	23.70	21.27	3.70E-03	3.82E-03	1
Northridge018	50.71	24.25	43.58	50.88	49.85	1.84E-02	1.84E-02	1
Imperial523	51.34	22.25	40.25	26.72	22.49	5.73E-03	5.75E-03	1
Imperial514	51.08	22.12	40.02	23.38	20.72	2.54E-03	2.74E-03	1

Table 4.6 Maximum Dynamic Response Quantities of the Viscous-Damped Frame Model

Earthquake Record	Moment of Column	Moment of Beam	Shear Force of Column	Axial Force of Column	Displacement of Top Floor	Magnitude of Plastic Hinge		Record Scale
						Column	Beam	
Unit	Mc (kN-m)	Mb (kN-m)	Vc (kN)	Nc (kN)	Disp. (mm)	Rotation	Rotation	
El-Centro	51.92	22.55	40.72	14.48	26.53	7.38E-03	7.62E-03	1
Coalinga270	54.57	23.89	42.94	19.30	44.75	2.02E-02	2.01E-02	1
Coalinga360	53.91	23.55	42.40	20.97	40.19	8.85E-03	8.86E-03	1
Parkfield205	51.11	22.13	40.08	12.99	20.90	1.74E-03	3.32E-04	1
Northridge175	52.43	22.80	41.20	18.31	30.05	7.50E-03	7.44E-03	1
Northridge265	51.32	22.24	40.25	16.87	22.37	4.17E-03	4.18E-03	1
Northridge104	56.35	24.80	44.40	25.54	57.07	3.88E-02	3.84E-02	1
Lake-L-90	51.39	22.28	40.30	14.19	22.88	6.12E-03	6.32E-03	1
Lake-L-00	52.42	22.80	41.18	18.74	29.94	9.43E-03	9.55E-03	1
Lake-I-00	51.18	22.17	40.12	11.75	21.42	2.50E-03	2.61E-03	1
lander275	53.61	23.41	42.12	13.27	38.19	6.60E-03	6.63E-03	1
lander000	50.46	21.80	39.52	9.84	16.43	5.18E-04	5.84E-04	1
Northridge318	55.17	22.80	43.44	16.28	48.88	2.49E-02	2.47E-02	1
Northridge228	70.58	32.02	56.16	37.31	155.03	7.36E-02	7.30E-02	1
Northridge288	54.55	23.88	42.92	15.72	44.61	1.82E-02	1.83E-02	1
Northridge018	59.59	26.44	47.08	26.88	79.32	4.36E-02	4.34E-02	1
Imperial523	54.30	23.76	42.68	15.46	42.93	1.03E-02	1.03E-02	1
Imperial514	54.04	23.63	42.48	14.71	41.12	1.03E-02	1.04E-02	1

Table 4.7 Comparison of Roof Displacement of Damped Model with Non-Damped Model

Input Earthquake Records	Roof Displacement				Roof Displacement Comparison		
	MRF1 (mm)	FD1 (mm)	VE1 (mm)	VD1 (mm)	FD1/MRF1 (%)	VE1/MRF1 (%)	VE1/MRF1 (%)
El-Centro	43.63	9.53	17.85	26.53	22	41	61
Coalinga270	64.49	20.61	32.31	44.75	32	50	69
Coalinga360	55.66	33.32	33.42	40.19	60	60	72
Parkfield205	26.72	11.42	18.83	20.9	43	70	78
Northridge175	41.37	22.66	31.48	30.05	55	76	73
Northridge265	37.7	10.97	23.82	22.37	29	63	59
Northridge104	89.04	65.23	48.2	57.07	73	54	64
Lake-L-90	47.51	12.72	20.58	22.88	27	43	48
Lake-L-00	45.67	23.02	31.51	29.94	50	69	66
Lake-I-00	26.38	10.37	15.37	21.42	39	58	81
lander275	66.71	15.29	18.43	38.19	23	28	57
lander000	24.02	11.69	14.59	16.43	49	61	68
Northridge318	75.5	19.77	26.72	48.88	26	35	65
Northridge228	283.16	175.59	90.3	155.03	62	32	55
Northridge288	58.57	14.57	21.27	44.61	25	36	76
Northridge018	116.36	88.01	49.85	79.32	76	43	68
Imperial523	80.55	16.55	22.49	42.93	21	28	53
Imperial514	78.67	16.08	20.72	41.12	20	26	52

MRF1: One-Story Moment-Resistant Frame; FD1: One-Story Friction-Damped Frame;
VE1: One-Story Viscoelastic-Damped Frame; VD1: One-Story Fluid Viscous-Damped Frame

Table 4.8 Energy Calculations and Analysis of Different Models under Far-Fault and Near-Fault Ground Motions

Model	MRF1		FD1		VE1		VD1	
Earthquake Record	Yielding Energy Ratio (%)	Damping Energy Ratio (%)	Yielding Energy Ratio (%)	Damper Energy Ratio (%)	Yielding Energy Ratio (%)	Damper Energy Ratio (%)	Yielding Energy Ratio (%)	Damper Energy Ratio (%)
El-Centro	57	43	0	100	4	96	21	79
Coalinga270	71	29	5	95	24	76	36	64
Coalinga360	63	37	14	86	21	79	29	71
Parkfield205	57	42	0	100	10	90	11	89
Lake-L-00	60	40	9	91	18	82	24	76
Lake-L-90	67	32	0	100	6	94	19	81
Lake-I-00	60	40	0	100	1	99	7	93
Northridge175	60	40	9	91	25	75	30	70
Northridge265	57	43	0	100	21	79	23	77
Northridge104	71	29	15	85	25	75	33	67
Lander000	64	36	0	100	1	99	2	98
Lander275	56	44	1	99	3	97	15	85
Northridge228	66	34	27	73	28	71	37	63
Northridge318	73	27	3	97	19	81	38	62
Northridge018	74	26	22	78	26	74	41	59
Northridge288	75	25	0	100	21	79	23	77
Imperial514	67	33	1	99	9	91	26	74
Imperial523	71	29	3	97	26	74	39	61

Yielding Energy Ratio (%) = (Yielding Energy / Total Energy Input) ×100%
Damping Energy Ratio (%) = (Damping Energy / Total Energy Iinput) ×100%
Damper Energy Ratio (%) = (Damper Energy / Total Energy Input) ×100%

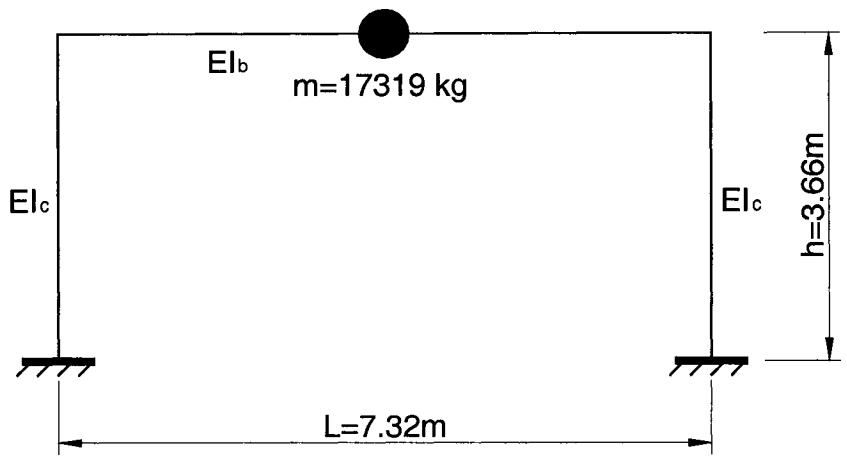

Fig. 4.1 Layout of Single-Degree-of Freedom of MRF

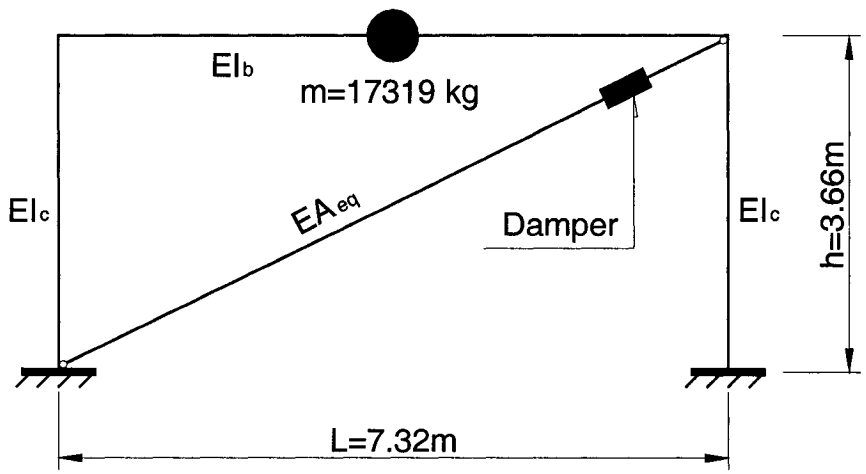

Fig. 4.2 Layout of Single-Degree-of Freedom of Damped Frame
Damper: Friction Damper;
Viscoelastic Damper;
Fluid Viscous Damper

a.

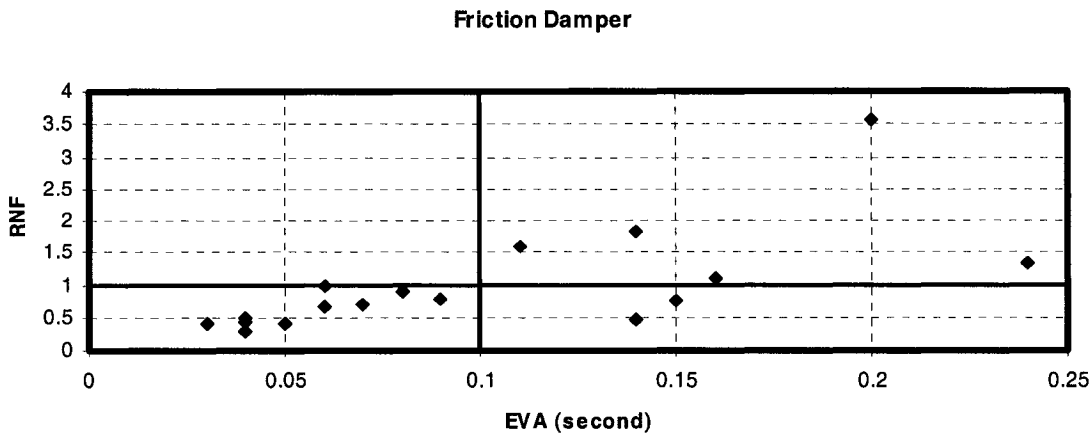

b.

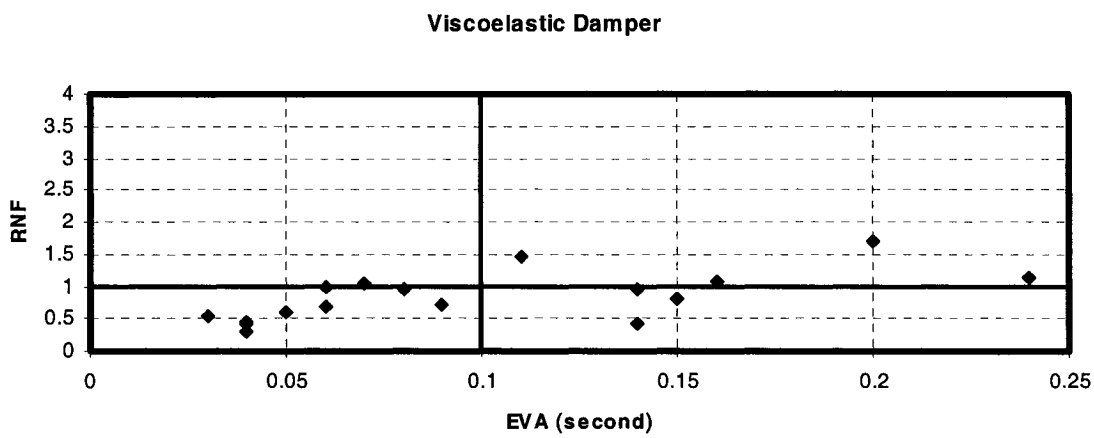

c.

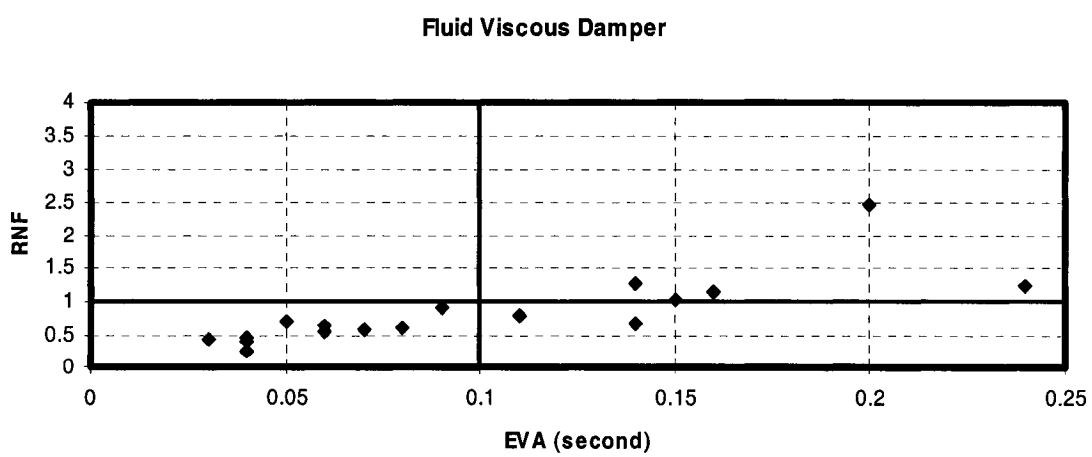

Fig. 4.3 Comparison of Roof Displacement under Near-Fault and Far-Fault Earthquakes a. FD1 Model b. VE1 Model c. VD1 Model

a.

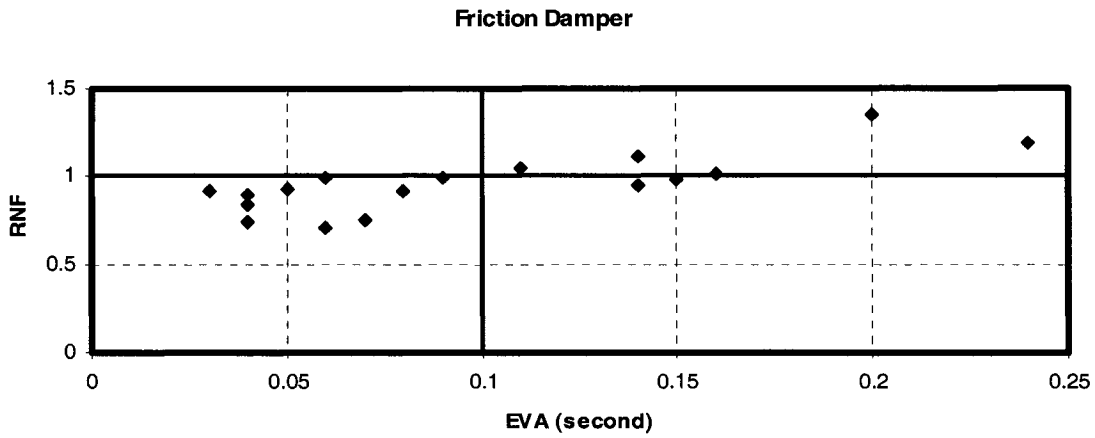

b.

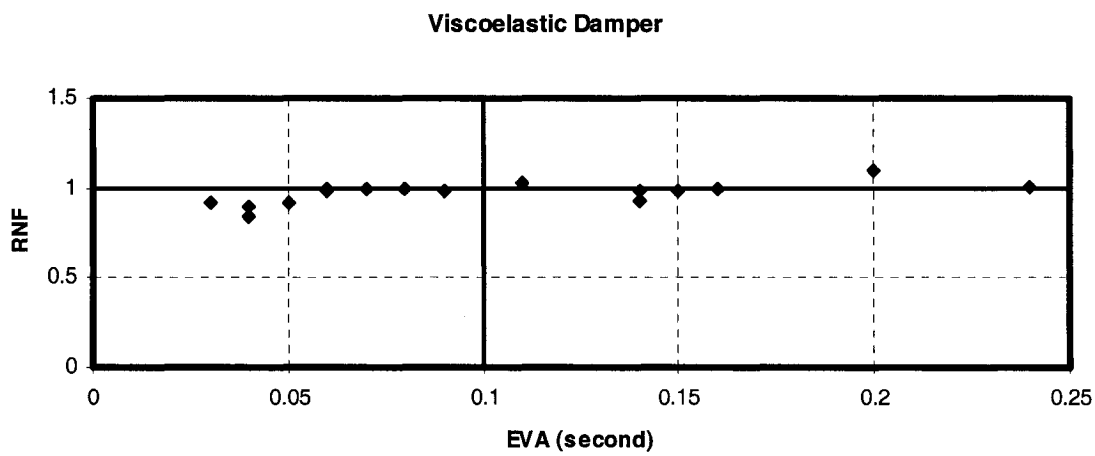

c.

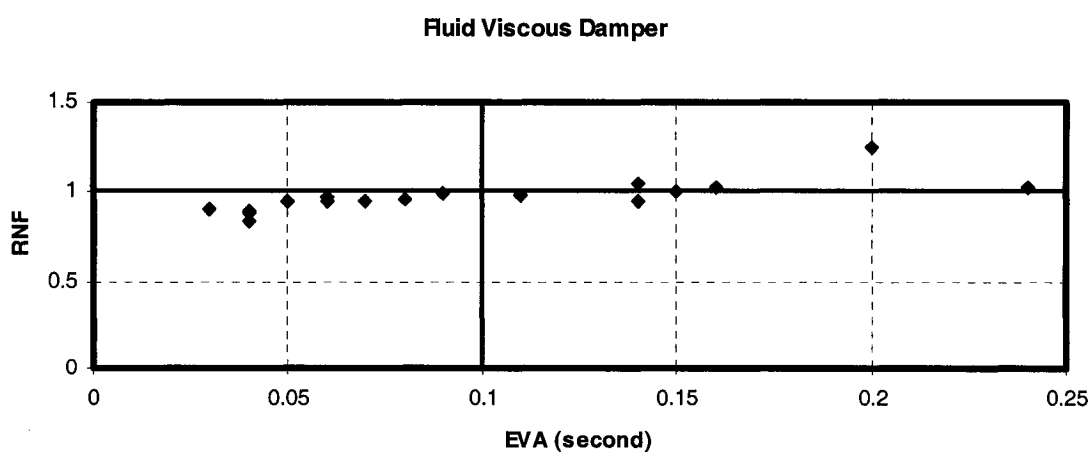

Fig. 4.4 Comparison of Base Shear Force under Near-Fault and Far-Fault Earthquakes a. FD1 Model b. VE1 Model c. VD1 Model

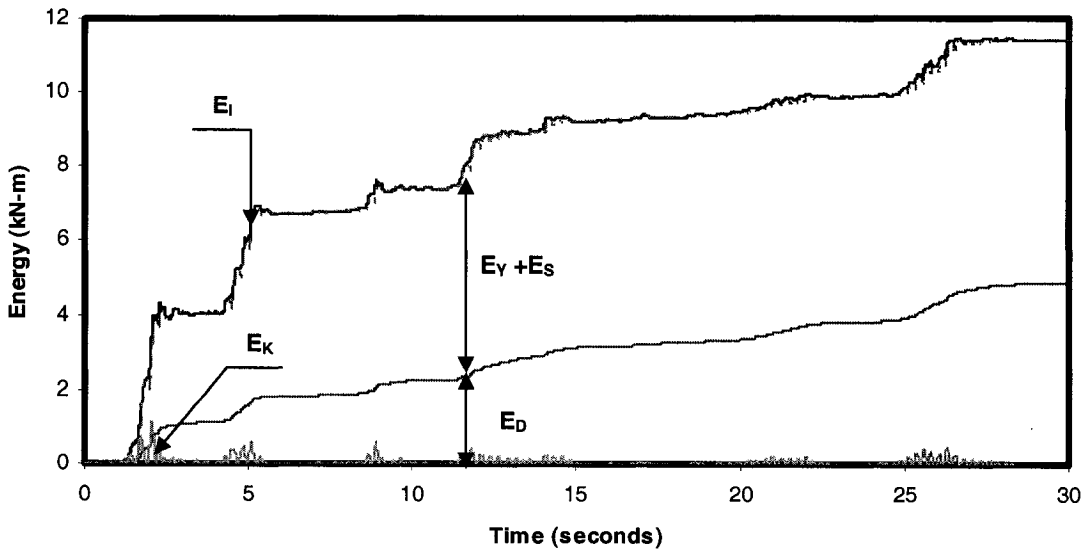

Fig. 4.5 Energy Time History of MRF1 Model to El-Centro Record
Note: E_I – Input Energy; E_k – Kinetic Energy; E_D – Damping Energy; E_S – Strain Energy; E_Y – Yielding Energy

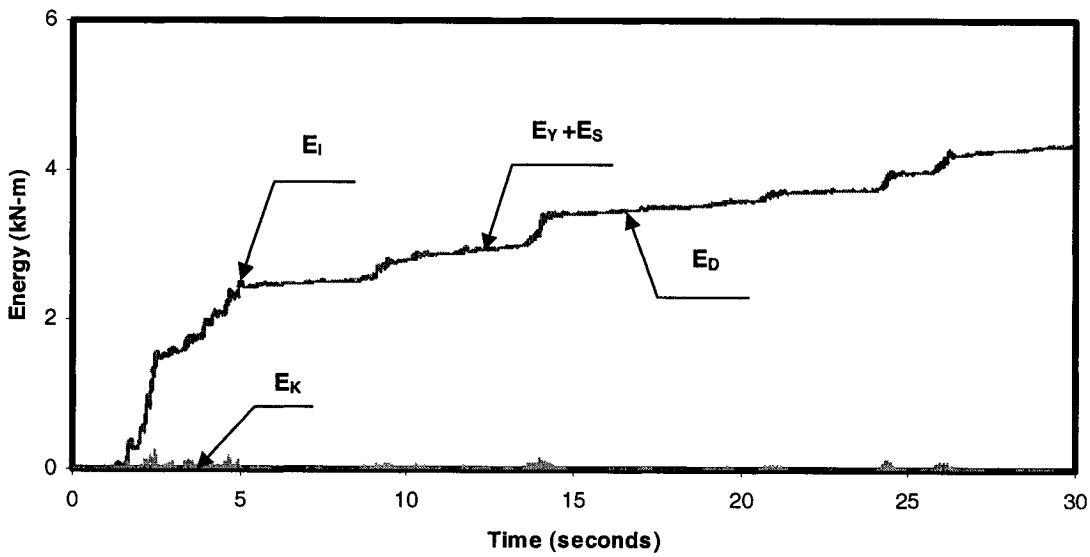

Fig. 4.6 Energy Time History of FD1 Model to El-Centro Record
Note: E_I – Input Energy; E_k – Kinetic Energy; E_D – Damper Energy; E_S – Strain Energy; E_Y – Yielding Energy

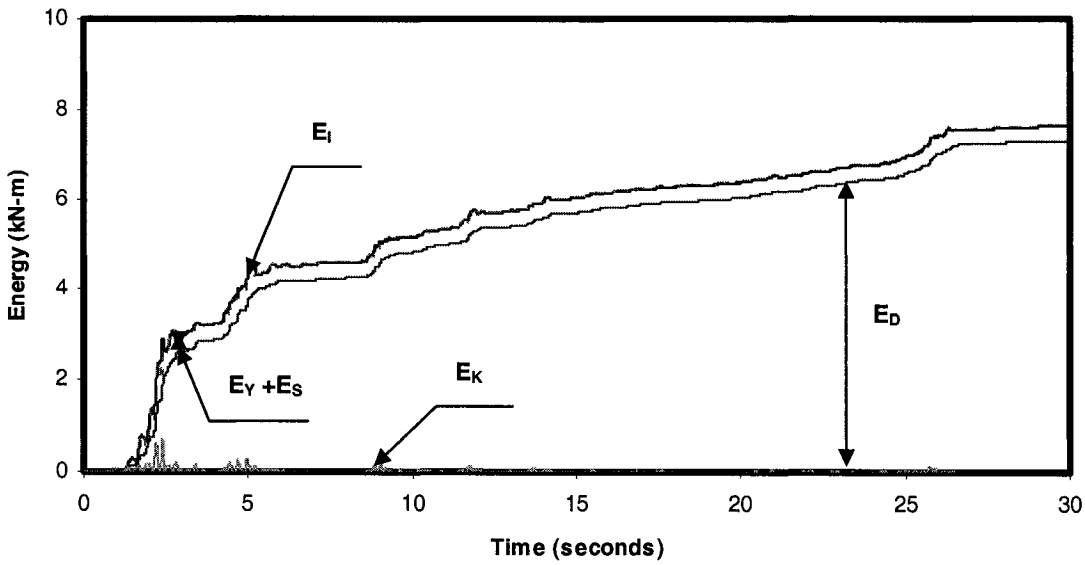

Fig. 4.7 Energy Time History of VE1 Model to El-Centro Record
Note: E_I – Input Energy; E_k – Kinetic Energy; E_D – Damper Energy;
E_S – Strain Energy; E_Y – Yielding Energy

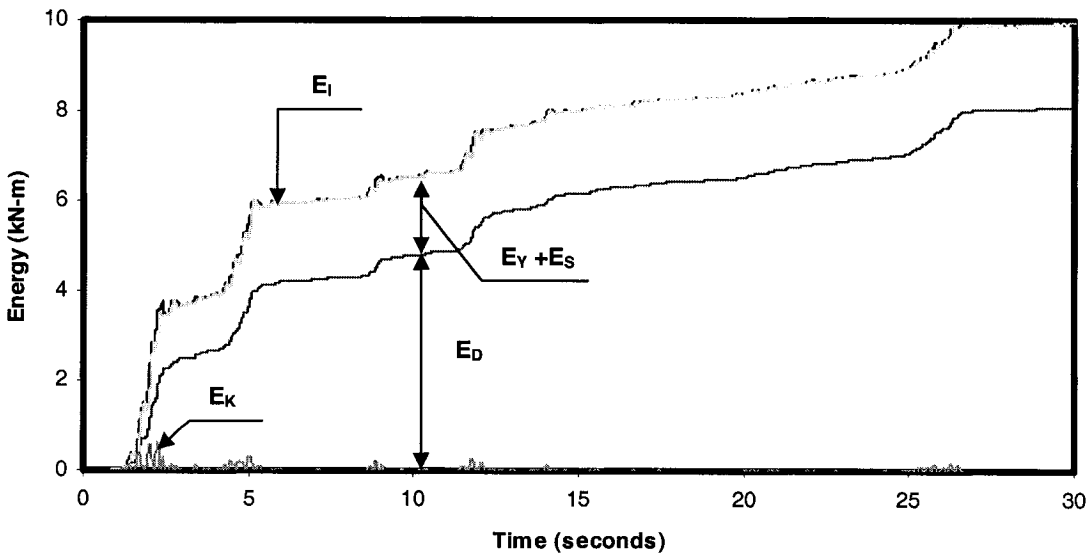

Fig. 4.8 Energy Time History of VD1 Model to El-Centro Record
Note: E_I – Input Energy; E_k – Kinetic Energy; E_D – Damper Energy;
E_S – Strain Energy; E_Y – Yielding Energy

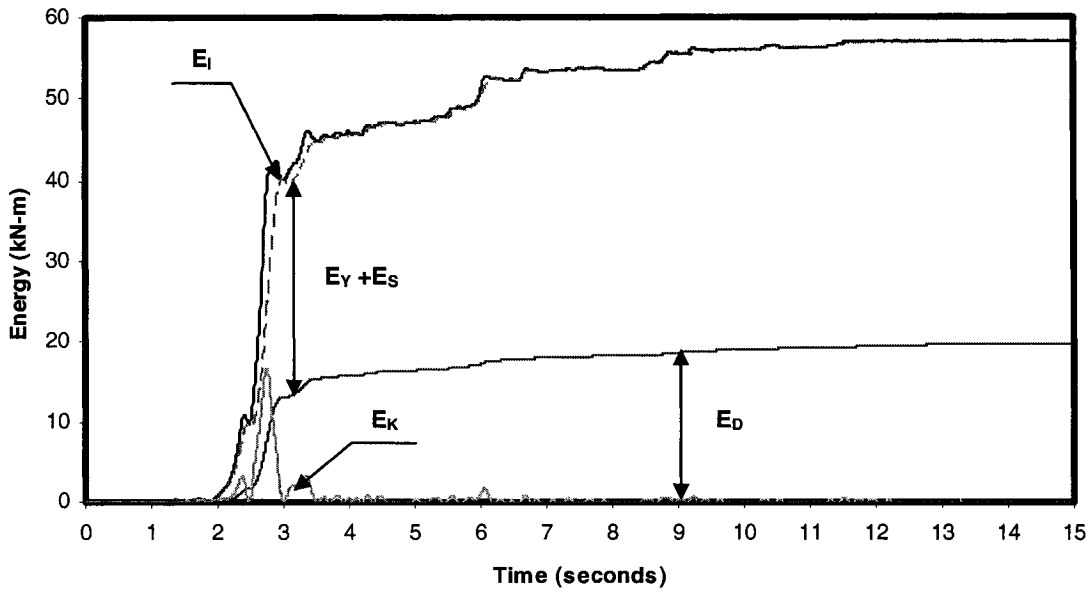

Fig. 4.9 Energy Time History of MRF1 Model to Northridge228 Record
Note: E_I – Input Energy; E_k – Kinetic Energy; E_D – Damping Energy;
E_S – Strain Energy; E_Y – Yielding Energy

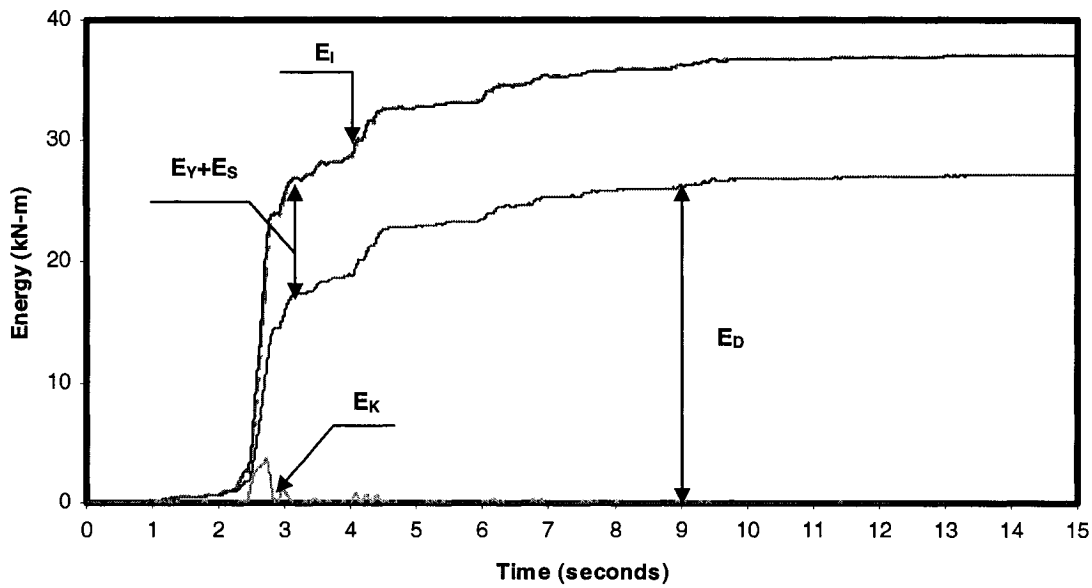

Fig. 4.10 Energy Time History of FD1 Model to Northridge228 Record
Note: E_I – Input Energy; E_k – Kinetic Energy; E_D – Damper Energy;
E_S – Strain Energy; E_Y – Yielding Energy

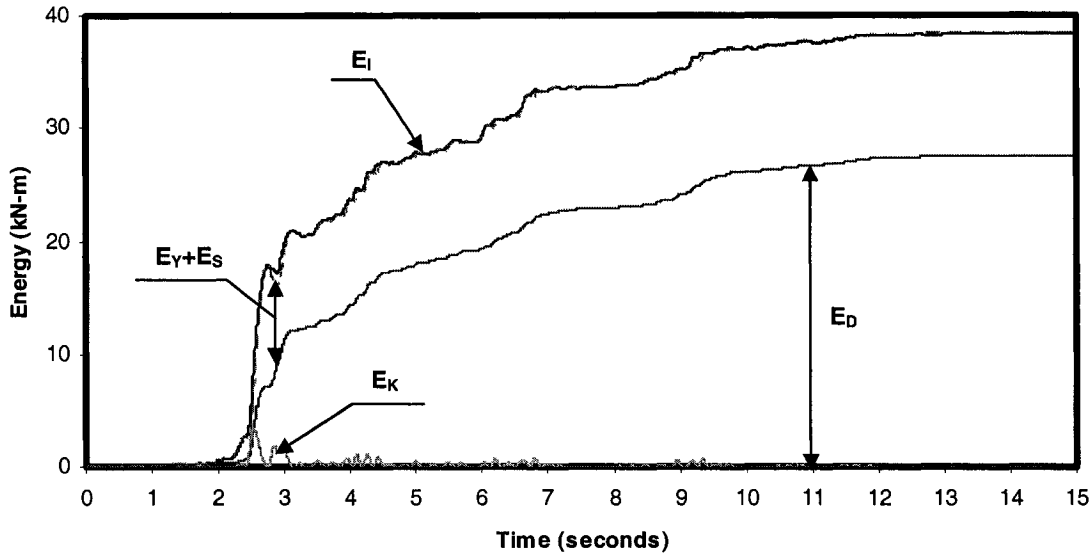

Fig. 4.11 Energy Time History of VE1 Model to Northridge228 Record
Note: E_I – Input Energy; E_k – Kinetic Energy; E_D – Damper Energy;
E_S – Strain Energy; E_Y – Yielding Energy

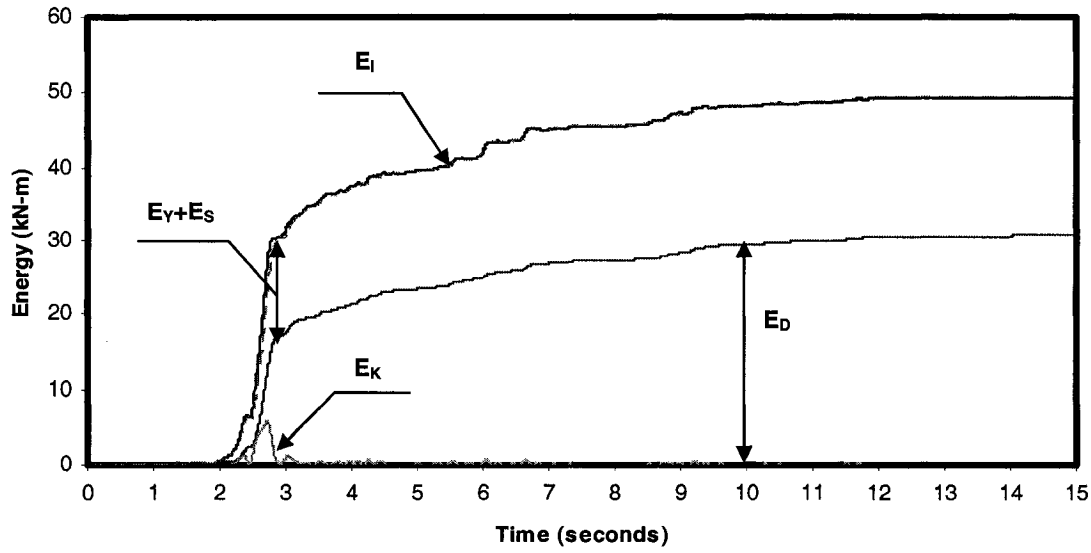

Fig. 4.12 Energy Time History of VD1 Model to Northridge228 Record
Note: E_I – Input Energy; E_k – Kinetic Energy; E_D – Damper Energy;
E_S – Strain Energy; E_Y – Yielding Energy

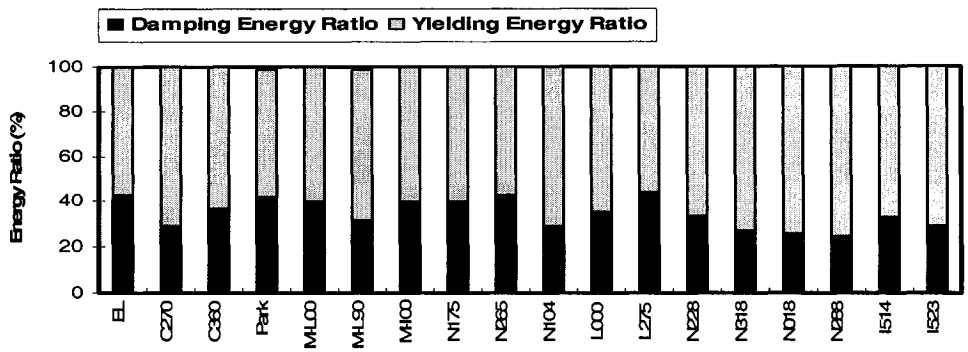

Fig. 4.13 Energy Ratio of MRF1 Model for Different Earthquakes (Evaluated at the end of the ground motion duration)

Damping Energy Ratio(%) = Damping Energy/ Total Energy Input×100%
Yielding Energy Ratio (%) = Yielding Energy/ Total Energy Input ×100%

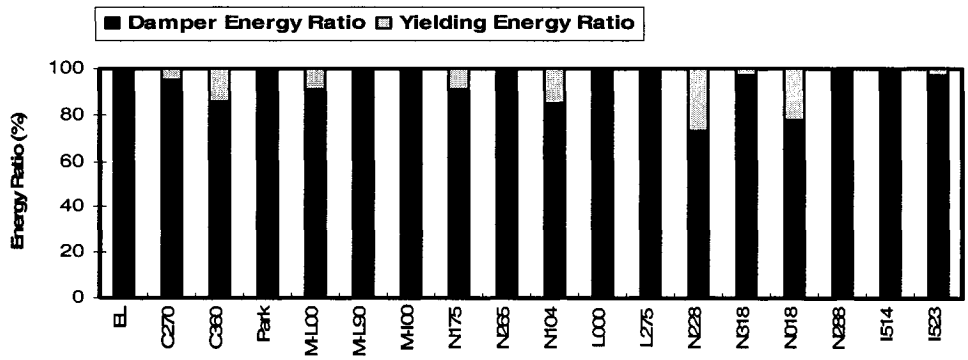

Fig. 4.14 Energy Ratio of FD1 Model for Different Earthquakes (Evaluated at the end of the ground motion duration)

Damper Energy Ratio (%) = Damper Energy/ Total Energy Input ×100%
Yielding Energy Ratio (%) = Yielding Energy/ Total Energy Input×100%

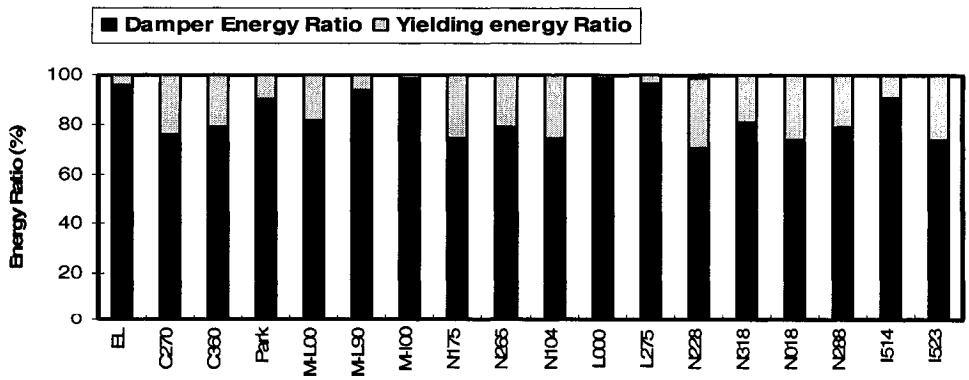

Fig. 4.15 Energy Ratio of VE1 Model for Different Earthquakes (Evaluated at the end of the ground motion duration)

Damper Energy Ratio (%) = Damper Energy/ Total Energy Input ×100%
Yielding Energy Ratio (%) = Yielding Energy/ Total Energy Input×100%

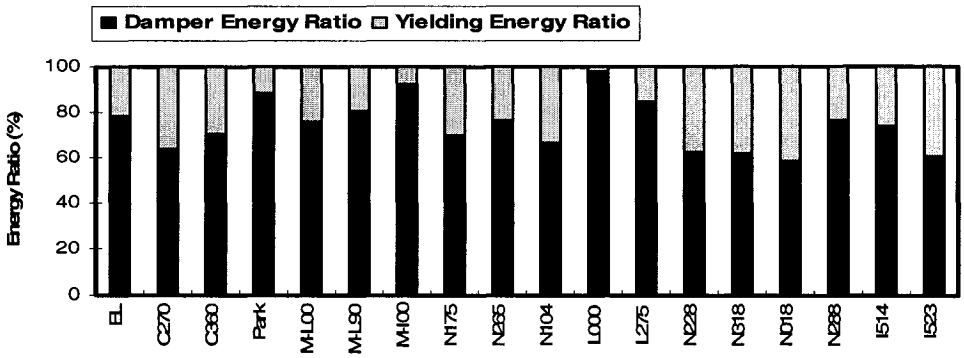

Fig. 4.16 Energy Ratio of VD1 Model for Different Earthquakes (Evaluated at the end of the ground motion duration)

Damper Energy Ratio (%) = Damper Energy/ Total Energy Input ×100%

Yielding Energy Ratio (%) = Yielding Energy/ Total Energy Input ×100%

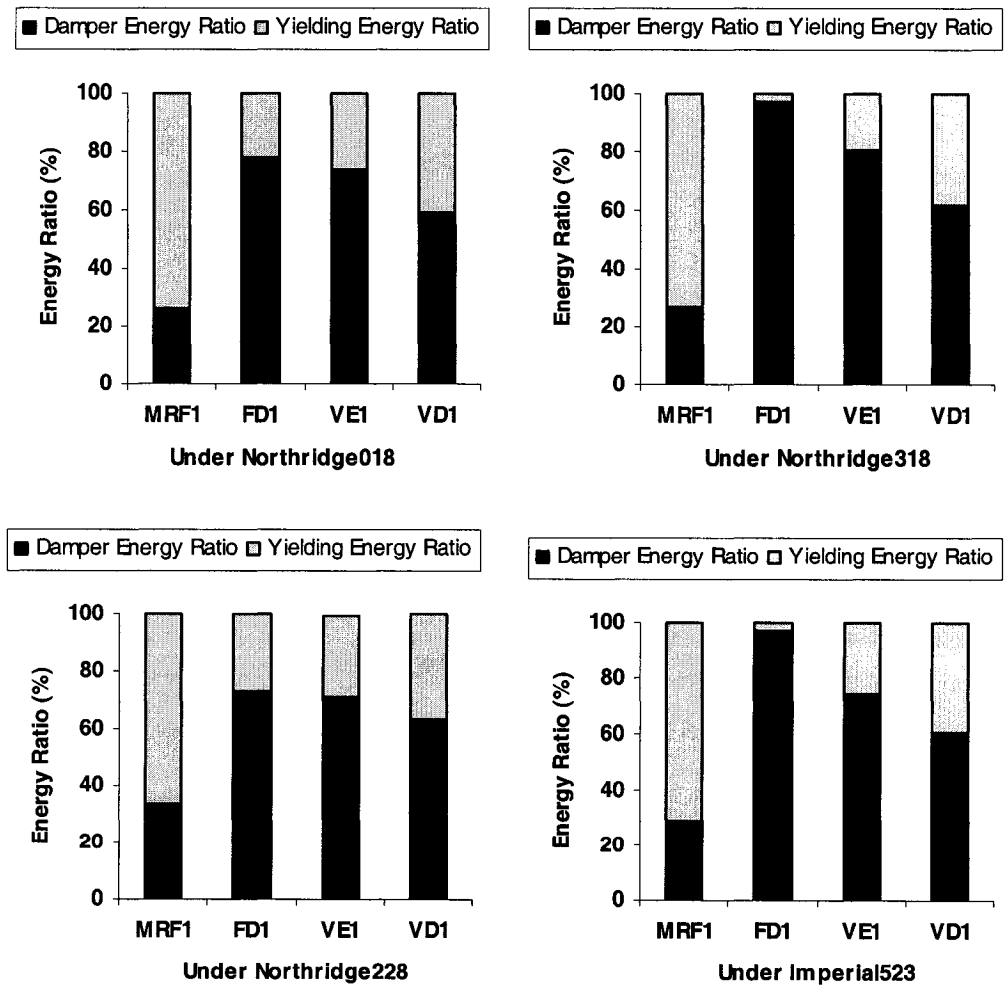

Fig. 4.17 Comparison of Energy Ratio for Different Damped Models

CHAPTER 5

MULTI-DEGREE-OF-FREEDOM SYSTEMS

5.1 GENERAL EQUATION OF MOTION

During the structural dynamic analysis, the number of independent displacements needed to completely define the position of all the masses is called the number of dynamic degrees of freedom. Similar to the single-degree-of-freedom system, a multistory single-bay frame can also be idealized as a discrete model with lumped mass concentrated at the each floor. Since the frame vibrates only in the horizontal direction, the horizontal displacement of each floor relative to the ground is enough to describe the motion of the concentrated mass. Therefore, the number of degrees of freedom in the dynamic analysis is equal to the number of stories. In addition, a single differential equation as SDOF system is no longer sufficient to describe the motion of a multistory frame. A group of differential equations is needed to define the vibration of a multistory building. The general governing equation of motion for linear MDOF systems is:

$$F_I(t) + F_D(t) + F_s(t) = P(t) \tag{5.1}$$

If a system is only subjected to the earthquake-induced ground motion, the governing equation of motion (5.1) can be rewritten as follows:

$$[m]\cdot\{\ddot{u}(t)\} + [c]\cdot\{\dot{u}(t)\} + [k]\cdot\{u(t)\} = -[m]\cdot\{1\}\cdot\ddot{u}_g(t) \tag{5.2}$$

where $[m]$ is the mass matrix, $[c]$ is the damping matrix, $[k]$ is the stiffness matrix, $\{\ddot{u}(t)\}$ is the relative acceleration vector, $\{\dot{u}(t)\}$ is the relative velocity vector, $\{u(t)\}$ is

the relative displacement vector, $\ddot{u}_g(t)$ is the ground acceleration, and {1} is the unity vector. For a nonlinear MDOF system, Equation (5.2) will be changed to

$$[m]\cdot\{\ddot{u}(t)\}+[c]\cdot\{\dot{u}(t)\}+\{f_s(u(t))\}=-[m]\cdot\{1\}\cdot\ddot{u}_g(t) \tag{5.3}$$

where $\{f_s(u(t))\}$ is the lateral restoring force vector having nonlinear relationship with the lateral displacements.

5.2 MODEL OF MOMENT-RESISTING FRAME

5.2.1 System Configuration

As a basic structure for dynamic analysis, a one-bay ten-story steel moment-resistant frame model (MRF10) shown in Fig. 5.1 was selected, which was studied by [Baktash, 1989]. The bay width of model is $6.10m$. The story height of model is $3.66m$. The lumped mass $m = 60{,}000kg$ is concentrated at the middle of the beam at each floor. The cross section properties of beams and columns are detailed in the Table 5.1. The Young's modulus of elasticity is $E = 2.0\times10^5 MPa$. The material yield strength is $F_y = 250MPa$. According to dynamic calculation, the natural vibration periods of the first two models are $(T_{1n})_{frame} = 3.2699\,\text{sec}$ and $(T_{2n})_{frame} = 1.1176\,\text{sec}$, respectively.

5.2.2 Calculation of Control Parameters

5.2.2.1 Structural Damping and Damping Coefficient

Similar to SDOF systems, structural inherent damping of MDOF systems is also assumed to have an equivalent viscous damping ratio of 5%. At the same time, Rayleigh damping $C = \alpha M + \beta K$ is selected to define the magnitude of structural damping.

Because the critical damping $c_r = 2m\omega_n$ and stiffness $k = m\omega_n{}^2$, the equivalent damping ratio is given by

$$\zeta = \frac{c}{c_r} = \frac{\alpha m + \beta k}{2m\omega_n} = \frac{\alpha}{2\omega_n} + \frac{m\omega_n{}^2\beta}{2m\omega_n} = \frac{\alpha}{2\omega_n} + \frac{\omega_n\beta}{2}$$

Therefore

$$\alpha + \beta\omega_n^2 = 2\omega_n\zeta \tag{5.4}$$

For a multi-degree-of-freedom MRF system, Equation (5.4) will be changed as follows:

$$\alpha + \beta\omega_{ni}^2 = 2\omega_{ni}\zeta_i \tag{5.5}$$

where ω_{ni} and ζ_i denote the mode frequency and the mode damping ratio, respectively.

Let $\zeta_1 = \zeta_2 = 5\%$, given $\omega_{1n} = \frac{2\pi}{T_{1n}} = 1.922 rad/\sec$ and $\omega_{2n} = \frac{2\pi}{T_{2n}} = 5.622 rad/\sec$,

Equation (5.5) yields

$$\begin{cases} \alpha + \beta \times 1.922^2 = 2 \times 1.922 \times 5\% \\ \alpha + \beta \times 5.622^2 = 2 \times 5.622 \times 5\% \end{cases} \tag{5.6}$$

Solving Equations in (5.6), mass-dependent damping coefficient $\alpha = 0.1432$ and the stiffness-dependent damping coefficient $\beta = 0.01326$ is obtained, which will be used in the computation to consider influence of the structural inherent viscous damping.

5.3 MODEL OF FRICTION-DAMPED FRAME

5.3.1 System Configuration

The model of a friction-damped frame is the modification of the MRF10 model with a friction-damped bracing element added to each story of the structure. Each of the bracing members consists of two double angles, detailed as shown as in Fig. 5.2. The basic cross

section properties of the beam and the column elements in the model of the ten-story friction-damped frame (FD10) are the same as the MRF10 model, shown in Table 5.1.

5.3.2 Calculation of Control Parameters

5.3.2.1 Optimum Slip Force of Friction Damper

Providing either over large slipping force or too small slipping force can not sufficiently take advantage of energy-dissipation capacity of a friction damper. Therefore, an appropriate method is needed to design a friction-damped structure based on the concept of optimum slip force, which means that the response of the system is at the minimum and the energy dissipation is at the maximum. Similar to SDOF friction-damped model, the method to find the optimum slip force of friction damper is based on plastic moment capacity of the beam proposed by [Baktash, 1989], the shear force V_d undertaken by the friction damper and the slip force P_d of the friction damper are given by

$$V_d = \frac{2M_{pb}}{h} \tag{5.7}$$

$$P_d = \frac{V_d}{\cos\alpha} = \frac{2M_{pb}}{h \cdot \cos\alpha} \tag{5.8}$$

where M_{pb} is yield moment of the beam, h is the story height, and α is the angle between the brace and the beam. According to the geometric relationship of FD10 model shown in Fig. 5.2, $\cos\alpha = 0.8575$. Therefore, the corresponding slip forces are obtained as shown in Table 5.2.

5.3.2.2 Stiffness of Friction-Damper Brace

The stiffness of the brace connecting the friction damper with the frame is also an important factor. On one hand, over flexibility of the brace will reduce the working efficiency of the damper, on the other hand, an over rigidity of the brace will directly lead to the increase of the cost. Therefore, an appropriate stiffness ratio of brace K_b to the lateral stiffness K_{frame} without brace is needed. Here an optimum value $\lambda = \frac{K_b}{K_{frame}} = 4$ is defined. Fig. 5.2 shows the brace dimensions used in the model. By using program DRAIN-2DX, the first two natural vibration periods of FD10 model are obtained: $(T_{1d})_{friction} = 1.4674\text{sec}$ and $(T_{2d})_{friction} = 0.4292\text{sec}$. Comparing with the MRF10 model, the stiffness ratio is given by:

$$\lambda = \frac{K_b}{K_{frame}} = \frac{K_{FD10} - K_{MRF10}}{K_{MRF10}} = \frac{K_{FD10}}{K_{MRF10}} - 1 \approx \frac{(\omega_{1d}^2)_{friction}}{(\omega_{1n}^2)_{frame}} - 1 = \frac{(T_{1d}^2)_{frame}}{(T_{1n}^2)_{friction}} - 1 = 3.97$$

which is close to the pre-defined optimum valve of 4, meaning that the selected brace can ensure friction damper to work efficiently.

5.3.2.3 Structural Damping and Damping Coefficients

In order to compare with MRF10 model, the structural inherent damping is also assumed to have an equivalent damping ratio of 5%, which is the same as in the MRF10 model. Given the modal damping ratio $\zeta_1 = \zeta_2 = \zeta = 5\%$, $\omega_{1d} = \frac{2\pi}{(T_{1d})_{friction}} = 4.282 rad/\text{sec}$ and $\omega_{2d} = \frac{2\pi}{(T_{2d})_{friction}} = 14.639 rad/\text{sec}$, Equation (5.5) yields

$$\begin{cases} \alpha + \beta \times 4.282^2 = 2 \times 4.282 \times 5\% \\ \alpha + \beta \times 14.639^2 = 2 \times 14.639 \times 5\% \end{cases} \tag{5.9}$$

Solving above Equations (5.9), the mass-dependent damping coefficient $\alpha = 0.3313$ and the stiffness-dependent damping coefficient $\beta = 0.005285$, which are used in the program to consider influence of the structural inherent viscous damping.

5.4 MODEL OF VISCOELASTIC-DAMPED FRAME

5.4.1 System Configuration

The model of a ten-story viscoelastic-damped frame (VE10) is the modification of the MRF10 model. The single-diagonal bracing member with the viscoelastic damper connects neighboring floors. Each floor has a VE damper connected at the upper one-third of the bracing, detailed as shown as in Fig. 5.2. The basic cross section properties of the beams and the columns are the same as the MRF10 model, shown in Table 5.1.

5.4.2 Design Procedure of Viscoelastic (VE) Damper

Step 1: Determination of material parameters

Because the material property of a VE damper is mainly dependent on environmental temperature, external excitation frequency and the magnitude of the material strain; it is an important step to obtain the basic material parameters, such as storage modulus $G^{'}$, loss modulus $G^{''}$ and loss factor η_{VE} to correctly represent the properties of VE damper. Usually these parameters are provided by the manufacturer based on experimental tests.

Step 2: Determination of dynamic properties of original structure without VE dampers.

Because VE dampers are used to reduce the dynamic response of the structure, the structure without VE dampers should firstly be analyzed to obtain basic dynamic

characteristics of the structure such as vibration frequency, mode shape, floor drift, and roof displacement in order to determine the degree of dynamic response reduction.

Step 3: Determination of the VE design curve of relationship between the structural damping ratio and the stiffness of VE damper or the equivalent stiffness of VE-damped brace member

As confirmed by many researchers, VE damping effects can usually be evaluated with the equivalent damping ratio using the modal strain energy method that comprehensively includes all kinds of influencing factors. According to Min [2004], the equivalent structural modal damping ratio ζ_i provided by VE damper is given by

$$\zeta_i = \frac{\eta_{VE}}{2}[1 - \frac{\phi_i^T K_{frame} \phi_i}{\phi_i^T K_{VE} \phi_i}] \tag{5.10}$$

where η_{VE} is the loss factor of VE material, ϕ_i is the i th mode shape vector of VE-damped structure, and K_{frame} and K_{VE} represent stiffness matrices of the structure with and without VE damper, respectively. For the detailed derivation sees Appendix A.

Step 4: Determination of Design Damping Ratio

Based on practical dynamic response characteristics of the structure, a value of design damping ratio is first assumed which will be re-examined later through detailed dynamic analysis to see if it meets design requirements and objectives, such as permitted floor drift and allowable maximum roof displacement.

Step 5: Determination of Dimension of VE Dampers

Once the dynamic response of the structure with added VE damper meets the design requirements, the formula to determine the dimensions of the VE dampers from the VE damper design curve can be obtained [Shen et al., 1995]

$$A_{VE} = \frac{k_d \cdot t}{n \cdot G'} \tag{5.11}$$

where n is the number of layer of VE material. A_{VE} is the area (cm^2) of the VE material k_d, G', t denote the storage stiffness (kN/cm), the storage modulus (kN/cm^2) and the thickness (cm) of VE damper, respectively.

5.4.3 Calculation of Control Parameters

5.4.3.1 Design Damping Ratio

The desired damping ratio is given by [Min et al., 2004]:

$$\zeta_{design} = \zeta_{frame} \cdot (R^{-2} - 1) \tag{5.12}$$

where R is the dynamic response reduction coefficient defined as ratio of added VE damping ratio to inherent structural damping ratio, and ζ_{design} , ζ_{frame} represent, respectively, equivalent additional damping ratio and inherent structure damping ratio. If let $R = 0.5$, then, $\zeta_{design} = \zeta_{frame} \cdot (R^{-2} - 1) = 5\% \times (0.5^{-2} - 1) = 15\%$, which we anticipate is the desired equivalent additional damping ratio provided by VE damper.

5.4.3.2 Structural Damping and Damping Coefficient

The equivalent stiffness of the VE damper can be obtained from the VE damper design curve, detailed as shown as in Appendix A. According to the model analysis, the first two

vibration periods of the VE-damped model are $(T_{1d})_{viscoelastic} = 2.6655\sec$ and $(T_{2d})_{viscoelastic} = 0.8928\sec$, separately. In order to compare with MRF10 model, the structural inherent damping is also assumed to have an equivalent damping ratio of $\zeta = 5\%$, which is the same as in the MRF10 model. Substituting into Equation (5.5) with mode damping ratios $\zeta_1 = \zeta_2 = \zeta = 5\%$, $\omega_{1d} = \dfrac{2\pi}{(T_{1d})_{viscoelastic}} = 2.3572 rad/\sec$ and $\omega_{2d} = \dfrac{2\pi}{(T_{2d})_{viscoelastic}} = 7.038 rad/\sec$. Thus,

$$\begin{cases} \alpha + \beta \times 2.3572^2 = 2 \times 2.3572 \times 5\% \\ \alpha + \beta \times 7.038^2 = 2 \times 7.038 \times 5\% \end{cases} \tag{5.13}$$

Solving above Equations (5.13), the mass-dependent damping coefficient $\alpha = 0.1766$ and stiffness-dependent damping coefficient $\beta = 0.01064$, which are used in the computation to simulate influence of the structural inherent viscous damping.

5.4.3.3 Equivalent Stiffness and Axial Area of VE Damper

According to the VE design damping curve of Fig. A.2 in Appendix A, the equivalent VE damper's stiffness corresponding to damping ratio $\zeta_{design} = 15\%$ is $(k_{eq})_{ve} = 84 kN/cm$. Accordingly, the equivalent axial area is $(A_{eq})_{ve} = \dfrac{(K_{eq})_{ve} L_b}{E} = 298.8 mm^2$. Therefore, the VE-damped braced member can be modeled as a truss element with equivalent cross section $(A_{eq})_{ve}$ and calculated model damping ratio $\zeta_{design} = \zeta_1 = 15\%$. Because the dynamic displacement response is controlled by the first mode, only the first mode damping ratio is used to evaluate the VE damping effect.

5.5 MODEL OF FLUID-VISCOUS DAMPED FRAME

5.5.1 System Configuration

The model of a ten-story fluid-viscous damped frame (VD10) is the modification of the MRF10 model with fluid viscous damped brace elements uniformly added to each story of the structure, as shown as in Fig. 5.2. The cross section properties of the beam and the column are the same as in the MRF10 model.

5.5.2 Calculation of Control Parameters

The brace should be stiff enough to connect the damper to the structure; however, the brace will not contribute to the structural stiffness because of the working mechanism of the fluid-viscous damper. Therefore, the natural period of the model remains $(T_{1d})_{fluid-viscous} = (T_{1n})_{frame} = 3.2699\,\text{sec}$, the same as that of the MRF10 model.

5.5.2.1 Structural Damping and Damping Coefficient

In order to compare with the MRF10 model, the structural inherent damping is also assumed to have an equivalent damping ratio of $\zeta = 5\%$, which is the same as in the MRF10 model. Because the vibration period is the same as MRF10 model, the inherent damping coefficients are also the same as MRF10 model, according to Equation (5.5). Therefore, the mass-dependent damping coefficient is $\alpha = 0.3313$ and the stiffness-dependent damping coefficient $\beta = 0.005285$, which are used in the program to consider the structural inherent viscous damping effect.

5.5.2.2 Equivalent Stiffness and Axial Area of Fluid Viscous Damper

The fluid-viscous-damped braced element is modeled as a truss element with equivalent cross section $(A_{eq})_{viscous} = 0.0$ and desired modal damping ratio assumed as anticipated $\zeta_{design} = \zeta_1 = 15\%$.

5.6 MODEL CALCULATION AND RESULTS ANALYSIS

The nonlinear time history analysis program DRAIN-2DX is used to calculate a single-bay, ten-story model with and without added dampers. Summary of dynamic response quantities are shown in Table 5.3 and Table 5.4, including state of model, floor deflections and floor interstory drifts. For the convenience of analysis later, an earthquake coefficient EVA is defined as a ratio of peak ground velocity to peak ground acceleration. A response coefficient RNF is defined as a ratio of structural response under near-fault earthquake to far-fault earthquake.

5.6.1. Four Models' Dynamic Responses to Different Ground Motions

Compared with the SDOF models, the MDOF models also show similar dynamic response behavior. Table 5.4 clearly indicates that, to the same ground motion, different damped-model has different dynamic response such as floor deflection and floor interstory drift, which reflects that the period of structural vibration and damping greatly influence structural dynamic response; to the same structural model, when subjected to different earthquakes, its response is also different, which shows the characteristic of earthquake ground motion such as the frequency components and duration time also significantly affect the response of structures. Therefore, structural dynamic response under ground motions is very complicated. Moreover, Table 5.4 apparently shows the

effect of additional damper. Once the structure incorporates dampers, the dynamic response such as floor deflections and floor interstory drifts are efficiently reduced.

5.6.2. Comparison of Dynamic Response to Far-Fault and Near-Fault Earthquakes

In order to compare the response of the damped model to near-fault and far-fault earthquakes, the peak acceleration of EL-Centro record is adjusted to the same peak acceleration as compared near-fault ground motion. Figs. 5.3 ~ 5.21 clearly show the comparison of responses.

5.6.2.1 Dynamic Response of Model with Added Friction Dampers

Figs. 5.3a ~ 5.19a indicate that the friction-damped model has two different response characteristics when compared with near-fault and far-fault earthquakes. During the near-fault earthquake whose velocity value is relative small or the earthquake coefficient EVA (shown in Table 5.3) is smaller than 0.1, the floor deflections of the model are smaller than those under EL-Centro ground motion, indicating that friction damper can work well in the near-fault earthquakes. However, if the near-fault earthquake has relatively large pulse velocity or its earthquake coefficient EVA is larger than 0.1, compared with the same intensity of far-fault earthquake, the floor deflections of model are larger than those subjected to EL-Centro, except two cases of Northridge175 and Lander275.

5.6.2.2 Dynamic Response of Model with Added Viscoelastic Dampers

Similar to the response behavior of the friction damper, compared with the response in the far-fault earthquake, Figs. 5.3b ~ 5.19b show that the viscoelastic damper subjected to

near-fault earthquakes also indicates two different response behavior. When the viscoelastic damper is subjected to a near-fault earthquake with relatively small pulse velocity, the damper's behavior in the near-fault ground motion is better than that in the far-fault earthquake. On the contrary, if a near-fault earthquake has relatively large velocity, the damper cannot work well compared with response in the far-fault earthquake, not including the case of Northridge175.

5.6.2.3 Dynamic Response of Model with Added Fluid Viscous Dampers

Fig. 5.3c ~ Fig. 5.19c shows the response of the fluid viscous damper to near-fault and far-fault earthquakes. Like the above two dampers, the fluid viscous damper behaves well in the near-fault earthquakes if its earthquake coefficient EVA < 0.1; otherwise, fluid viscous damper shows better behavior during the far-fault earthquake when subjected to near-fault earthquake with large pulse velocity, not including the case of Northridge175.

Fig. 5.20 shows comparison of mean floor deflection of each damped model under 17 near-fault records with that under El-Centro earthquake record. It is found that the response of each damped model under the near-fault earthquakes is smaller than that under the far-fault earthquake. In addition, the dynamic response of friction-damped model is smaller than those of the other two kinds of dampers. Moreover, Fig. 5.21 shows comparison of roof deflection of three types of damped models under near-fault and far-fault earthquakes. It is clearly found that, if the building is subjected to near-fault earthquake with EVA<0.1, the response coefficient RNF of all three damped models is smaller than 1.0, which means the response under near-fault earthquakes is smaller than

that under far-fault earthquake; otherwise, the response under near-fault earthquakes is stronger than that under far-fault earthquake if subjected to near-fault earthquake with earthquake coefficient EVA>1.0.

5.6.3. Comparison of Effectiveness of Different Dampers

A damper is a device dissipating energy. To discover whether a damper is effective, it is necessary to determine how much energy the damper dissipates. For a structure subjected to an earthquake, the total energy of the structure includes kinetic energy, elastic strain energy, yielding energy and damping energy. Therefore, we should determine the proportion of damping energy to total energy input to evaluate the energy-dissipating ability of a damper. From energy time history curves of Fig. 5.22 ~ Fig. 5.29, it is found that the total input energy increases with increase of the ground motion duration. Therefore, the magnitude of total energy input is dependent on the duration of earthquake. Figs. 5.22~ 5.29 also show that, to the same model, the total input energy is different under different earthquake ground motions; to the same earthquake, a different model also has different ability to absorb external energy, which further confirms the complication of response of the models.

During the calculation, two points should be carefully noted. One point involves definition of the time step emphasized in Chapter 1. The total amount of input energy is sensitive to time step. It is found that the amount of input energy increases with the decrease of time step. Therefore, time step is an important control parameter to affect the accuracy of calculation. The other point is about calculation of friction damper energy.

Since the friction damper is simulated as an ideal elastic-plastic material, the calculated energy dissipated by friction damper is in the form of yielding energy E_Y, hence calculated total yielding energy should be adjusted and the energy dissipated by friction damper should be withdrawn from yielding energy and added to damper energy. Therefore, the total damper Energy E_D includes two parts: one is E_Y of friction damper, the other is energy dissipated by structural inherent damping effect.

Figs. 5.22 ~ 5.25 show the energy time history of MRF10, FD10, VE10 and VD10 model to earthquake Coalinga270 ground motion. Checking Table 5.3 finds that MRF10 model is in inelastic state when subjected to Coalinga270 earthquake. During the whole time, it is found that, except for damper energy, kinetic energy and elastic energy, yielding energy is also a major part of the curve, which clearly confirms the response result of MRF10 model. Fig. 5.23, Fig. 5.24 and Fig. 5.25 show the total input energy is dissipated by damper energy. There is no yielding energy that is consistent with the elastic state shown in Table 5.3.

Figs. 5.26 ~ 5.29 show the energy time history of MRF10, FD10, VE10 and VD10 model to earthquake Northridge228 ground motion. Checking Table 5.3 finds that all models are in inelastic state when subjected to Northridge228 earthquake. These dynamic responses are consistent with results in Figs. 5.26 ~ 5.29, which show that the total input energy is controlled by yielding energy and damper energy, however, damper energy is a major component.

The energy time history indicates the energy accumulation input to the structure. Therefore, we consider the total input energy through the whole time of each earthquake and evaluate the energy at the end of the ground motion. At this specific time, the ground motion is almost over, the kinetic energy is becoming zero, and the elastic strain energy is also very small. The major ability of the structure to absorb or dissipate energy comes from damping effect and structural yielding deformation. Table 5.3 digitally shows the relationship of damping energy and yielding energy at the end of ground motion, and Fig. 5.30 ~ Fig. 5.33 show two energy relationships graphically. Take the friction-damped model subjected to Coalinga270 ground motion for example. Table 5.3 shows no yielding is produced during the whole duration; therefore, at the end of the earthquake, the input energy should all be dissipated by damper effect. This result is correctly confirmed by the data in Table 5.5 and Fig.5.30 ~ Fig. 5.33. Take another case for example. Table 5.3 shows the MDOF of the friction-damped model is yielding when subjected to Lander275 earthquake. Table 5.5 confirms that 9% of the total energy is indeed absorbed by the structural yielding deformation.

All in all, comparing proportion of damping energy for each model's total energy, as shown as in Fig. 5.34, it is found that, generally speaking, friction damper has relatively higher value than the other two dampers, which means friction damper is more effective than viscoelastic damper and fluid-viscous damper. The effectiveness of the viscoelastic damper is close to fluid-viscous damper, but seems a little better than fluid-viscous damper.

5.6.4. Analysis of Results

1. The response to near-fault and far-fault earthquakes, the three types of damper show similar function. If the near-fault earthquake has large pulse velocity, dampers cannot work very well compared with response under far-fault earthquake.

2. To all the near-fault and far-fault earthquakes, the effectiveness of the friction damper is a little higher than the other two dampers under selected earthquake records. The effectiveness of viscoelastic damper seems a little better than linear fluid-viscous damper.

Table 5.1 Cross Section Properties of MRF10 model

Beam ($f_y = 250N/mm^2$)				
Dimension	A	I_x	Z_x	$M_{pb} = Z_x \cdot f_y$
	(mm^2)	$(10^6 mm^6)$	$(10^3 mm^3)$	$(10^6 N \cdot mm)$
W460x74	9450	332	1650	412.5
W460x89	11400	409	2010	502.5
W460x113	14400	556	2670	667.5
Column ($f_y = 250N/mm^2$)				
Dimension	A	I_x	Z_x	$M_{pc} = Z_x \cdot f_y$
	(mm^2)	$(10^6 mm^6)$	$(10^3 mm^3)$	$(10^6 N \cdot mm)$
W360x51	6440	141	893	223.3
W360x79	10100	226	1430	357.5
W360x122	15500	365	2270	567.5
W360x162	20600	515	3140	785.0
W360x179	22800	574	3480	870.0
W360x287	36600	997	5810	1452.5

Table 5.2 Definition of Slip Force in the Friction Damper of FD10 Model

Floor	Beam	Yield Moment $(kN \cdot m)$	Slip Force (kN)
1	W460x74	412.5	263
2~5	W460x89	502.5	320
6~10	W460x113	667.5	425

Table 5.3 State of Models to Near-Fault Earthquake Records

Earthquake Record	Type	Scale	PGA	PGV	PGD	EVA=PGV/PGA	State of Model			
			(g)	(cm/s)	(cm)		MRF10	FD10	VE10	VD10
Coalinga270	Near-Fault	1.0	0.84	44.1	6.8	0.05	Inelastic	elastic	elastic	elastic
Coalinga360	Near-Fault	1.0	1.083	39.7	5.41	0.04	elastic	elastic	elastic	elastic
Parkfield205	Near-Fault	1.0	0.357	21.5	3.87	0.06	elastic	elastic	elastic	elastic
Mammothlake-I-00	Near-Fault	1.0	0.43	23.6	7.52	0.06	elastic	elastic	elastic	elastic
Mammothlake-L-00	Near-Fault	1.0	0.921	28.9	3.17	0.03	elastic	elastic	elastic	elastic
Mammothlake-L-90	Near-Fault	1.0	0.408	33.9	6.41	0.08	Inelastic	elastic	elastic	elastic
Northridge175	Near-Fault	1.0	0.415	45.6	5.06	0.11	Inelastic	elastic	elastic	elastic
Northridge265	Near-Fault	1.0	0.434	31.3	4.8	0.07	Inelastic	elastic	elastic	elastic
Northridge104	Near-Fault	1.0	1.585	55.7	6.06	0.04	Inelastic	elastic	elastic	elastic
Lander000	Near-Fault	1.0	0.785	31.9	16.42	0.04	Inelastic	elastic	elastic	Inelastic
Lander275	Near-Fault	1.0	0.721	97.6	70.31	0.14	Inelastic	Inelastic	Inelastic	Inelastic
Northridge228	Near-Fault	1.0	0.838	166.1	28.78	0.20	Inelastic	Inelastic	Inelastic	Inelastic
Northridge318	Near-Fault	1.0	0.472	73	19.76	0.16	Inelastic	Inelastic	Inelastic	Inelastic
Northridge018	Near-Fault	1.0	0.828	117.5	34.22	0.14	Inelastic	Inelastic	Inelastic	Inelastic
Northridge288	Near-Fault	1.0	0.493	74.6	28.69	0.15	Inelastic	Inelastic	Inelastic	Inelastic
Imperial514	Near-Fault	1.0	0.519	46.9	35.35	0.09	Inelastic	Inelastic	Inelastic	Inelastic
Imperial523	Near-Fault	1.0	0.379	90.5	63.03	0.24	Inelastic	Inelastic	Inelastic	Inelastic

Earthquake Coefficient: EVA= Peak Ground Velocity/Peak Ground Acceleration

Table 5.4 Dynamic Responses of Models to Near-Fault and Far-Fault Earthquake Motions

Record	EL-Centro				Coalinga270				Coalinga360			
Quantity	Floor Deflection (mm)				Floor Deflection (mm)				Floor Deflection (mm)			
Floor	MRF10	FD10	VE10	VD10	MRF10	FD10	VE10	VD10	MRF10	FD10	VE10	VD10)
10	311.21	143.35	218.86	219.79	163.27	160.56	109.20	111.37	131.82	84.59	94.77	99.26
9	287.54	134.17	204.81	207.34	137.62	151.33	102.15	107.54	125.40	75.30	88.72	94.61
8	258.44	123.21	186.54	190.15	133.68	139.99	94.09	103.41	116.09	65.23	81.16	88.57
7	226.37	105.93	164.13	168.11	151.25	121.67	85.39	98.63	115.06	53.06	72.19	80.91
6	194.83	86.39	139.65	144.15	151.19	102.54	76.03	92.04	100.92	45.52	62.37	71.86
5	169.36	67.97	113.32	117.92	134.64	85.49	65.74	82.74	79.03	37.62	51.74	61.05
4	142.82	54.45	87.18	91.44	106.76	71.18	54.49	70.14	60.32	30.93	40.91	48.98
3	103.41	42.60	60.30	63.13	71.84	54.19	41.63	53.50	42.68	24.66	29.94	35.04
2	54.64	25.89	35.70	36.14	38.79	33.14	27.24	33.28	26.53	16.21	18.07	21.96
1	15.00	7.92	12.45	12.06	12.26	10.75	10.68	11.88	9.87	5.39	6.69	9.45
Quantity	Interstory Drift (mm)				Interstory Drift (mm)				Interstory Drift (mm)			
Floor	MRF10	FD10	VE10	VD10	MRF10	FD10	VE10	VD10	MRF10	FD10	VE10	VD10
10	27.98	9.62	14.28	13.45	46.49	10.56	8.79	7.73	30.47	11.64	6.57	6.17
9	34.41	12.56	18.98	19.17	48.14	12.24	11.80	11.52	27.41	14.99	8.77	9.13
8	44.31	18.36	23.78	25.34	46.16	18.86	14.37	15.20	29.24	17.75	10.89	12.19
7	49.40	22.25	25.95	27.37	32.09	29.27	15.22	16.41	20.18	17.44	11.77	13.26
6	46.03	18.99	27.78	29.14	31.21	30.55	15.65	17.60	21.91	14.59	12.44	14.27
5	40.02	15.30	27.18	28.23	31.75	24.17	15.14	17.93	22.79	10.47	12.14	14.12
4	41.12	17.08	27.65	29.37	40.82	23.36	15.78	20.33	22.53	8.08	12.48	15.17
3	48.88	17.27	26.72	28.76	37.49	23.60	16.73	22.54	18.97	11.11	12.53	15.55
2	39.79	17.99	23.65	24.60	27.68	22.87	17.32	22.21	17.92	11.41	11.91	13.99
1	15.00	7.92	12.45	12.06	12.26	10.75	10.68	11.88	9.87	5.39	8.63	9.45

Table 5.4 Continued

Record	Parkfield205				Northridge175				Northridge265			
Quantity	Floor Deflection (mm)				Floor Deflection (mm)				Floor Deflection (mm)			
Floor	MRF10	FD10	VE10	VD10	MRF10	FD10	VE10	VD10	MRF10	FD10	VE10	VD10
10	69.05	49.03	43.72	48.25	231.22	95.33	98.23	129.89	225.68	125.46	114.30	144.42
9	60.08	45.03	40.98	45.86	217.38	87.69	93.22	122.80	208.96	118.12	107.59	137.16
8	55.47	41.20	37.49	42.64	201.53	79.41	86.75	112.96	192.54	106.66	99.27	127.63
7	49.84	36.72	33.25	38.50	183.64	71.63	78.45	99.91	175.86	93.22	89.29	115.62
6	44.45	34.79	28.60	33.71	164.40	65.47	70.87	85.45	156.45	76.15	78.15	101.94
5	41.81	33.46	23.57	28.22	141.98	60.35	63.22	69.50	132.75	57.54	65.74	86.12
4	43.46	30.34	18.51	22.43	115.99	55.26	53.77	59.58	106.31	41.94	52.60	68.96
3	37.22	22.74	13.24	16.74	82.24	46.99	41.88	46.82	74.92	32.52	38.07	49.42
2	23.86	11.11	8.42	12.34	44.16	30.01	27.46	30.35	41.28	23.08	22.64	28.43
1	8.15	2.91	4.01	5.24	12.77	10.08	11.01	11.62	12.49	7.58	7.90	9.19
Quantity	Interstory Drift (mm)				Interstory Drift (mm)				Interstory Drift (mm)			
Floor	MRF10	FD10	VE10	VD10	MRF10	FD10	VE10	VD10	MRF10	FD10	VE10	VD10
10	18.22	7.19	2.93	3.03	38.24	8.31	7.20	7.29	27.92	8.89	7.58	9.12
9	16.07	9.86	3.92	4.48	32.98	9.27	9.70	10.23	37.10	12.79	10.13	13.21
8	19.22	9.59	4.90	5.98	31.81	14.74	11.81	13.66	43.98	14.02	12.64	17.54
7	15.40	7.24	5.33	6.48	29.87	16.29	12.54	14.98	39.10	17.20	13.76	19.04
6	12.21	6.46	5.68	6.94	29.47	13.44	13.11	16.34	35.66	19.88	14.74	20.45
5	9.49	6.37	5.58	6.78	28.42	10.17	13.31	16.10	33.35	17.93	14.71	20.15
4	13.51	7.64	5.73	7.12	33.88	13.65	14.73	17.02	35.37	16.04	15.55	21.50
3	16.87	12.06	5.68	7.15	38.25	19.22	16.43	19.40	35.29	13.62	16.01	21.94
2	16.59	8.53	5.20	7.72	31.51	21.10	17.40	19.98	29.11	15.79	15.01	19.55
1	8.15	2.91	4.01	5.24	12.77	10.08	11.01	11.62	12.49	7.58	7.90	9.19

Table 5.4 Continued

Record	Northridge104				Lake-I-00				Lake-L-00			
Quantity	Floor Deflection (mm)				Floor Deflection (mm)				Floor Deflection (mm)			
Floor	MRF10	FD10	VE10	VD10	MRF10	FD10	VE10	VD10	MRF10	FD10	VE10	VD10
10	206.01	104.80	130.24	146.78	158.49	91.09	89.21	114.15	49.75	50.27	43.01	34.28
9	193.77	99.19	122.54	140.05	144.76	84.11	83.00	107.74	39.28	44.75	40.46	34.17
8	187.43	91.67	113.34	131.49	139.47	77.05	74.82	98.89	52.17	38.27	38.75	34.99
7	176.39	83.98	102.61	120.84	126.30	63.79	64.82	87.37	48.82	38.50	38.13	36.57
6	159.11	78.77	90.69	108.37	112.40	48.78	56.28	74.45	48.77	39.23	37.20	37.51
5	137.94	69.12	77.28	93.51	98.48	37.40	48.85	62.87	56.38	40.38	35.22	36.92
4	116.11	58.59	62.77	76.64	82.68	31.71	40.72	52.06	54.43	38.32	31.48	33.78
3	88.31	50.75	46.41	56.61	61.85	25.27	31.03	39.11	42.97	33.22	25.72	27.81
2	52.55	32.23	30.35	35.04	36.37	16.18	19.62	23.93	25.99	20.65	17.62	18.81
1	17.34	11.36	12.63	13.85	11.61	5.19	7.30	8.30	8.63	7.24	7.28	7.42
Quantity	Interstory Drift (mm)				Interstory Drift (mm)				Interstory Drift (mm)			
Floor	MRF10	FD10	VE10	VD10	MRF10	FD10	VE10	VD10	MRF10	FD10	VE10	VD10
10	47.69	8.42	9.26	9.42	28.61	8.99	6.21	7.04	33.95	8.29	4.30	2.95
9	46.35	12.33	12.43	13.99	29.00	9.03	8.23	10.07	27.77	12.39	5.75	4.47
8	61.58	14.66	15.38	18.65	27.32	17.77	10.14	13.34	21.84	15.60	6.81	5.82
7	50.63	17.43	16.57	20.26	24.19	19.44	10.90	14.43	21.50	11.14	7.01	6.19
6	43.27	14.85	17.54	21.77	24.84	14.54	11.40	15.37	20.96	8.38	6.97	6.61
5	40.95	17.73	17.43	21.66	23.88	7.28	10.95	14.72	14.87	5.66	6.93	7.24
4	39.39	20.75	18.43	23.46	25.86	7.55	11.50	15.66	17.00	7.28	7.99	9.07
3	39.87	23.24	19.21	24.62	26.07	10.19	12.43	16.74	19.69	13.23	9.64	11.19
2	36.31	21.59	18.61	23.01	24.83	11.15	12.68	16.11	18.13	14.86	11.01	12.27
1	17.34	11.36	12.63	13.85	11.61	5.19	7.30	8.30	8.63	7.24	7.28	7.42

Table 5.4 Continued

Record	Lake-L-90				Lander000				Lander275			
Quantity	Floor Deflection (mm)				Floor Deflection (mm)				Floor Deflection (mm)			
Floor	MRF10	FD10	VE10	VD10	MRF10	FD10	VE10	VD10	MRF10	FD10	VE10	VD10
10	113.90	115.08	103.88	83.99	384.42	73.33	200.55	254.73	842.70	339.90	410.29	569.95
9	81.97	107.25	95.60	79.93	362.79	68.84	188.76	240.56	823.21	326.80	390.62	548.53
8	80.86	99.41	85.34	74.97	332.11	63.08	173.26	220.92	792.00	308.73	364.40	518.88
7	84.67	90.21	73.81	69.45	290.77	56.56	153.81	195.27	726.70	281.36	330.78	476.41
6	81.39	73.88	62.55	62.85	245.71	49.01	132.26	166.92	632.95	245.49	292.37	422.52
5	79.33	58.09	53.96	55.55	198.04	40.87	108.73	135.87	521.70	203.49	247.39	355.59
4	74.29	53.04	44.39	48.27	150.04	35.61	85.01	105.05	399.89	158.49	197.64	279.72
3	59.46	45.27	33.36	37.92	99.46	28.30	59.92	72.40	264.30	106.47	140.06	191.93
2	36.04	28.71	20.89	23.84	52.60	16.99	34.59	40.29	132.75	56.12	78.59	100.65
1	11.51	9.24	7.84	8.38	15.55	5.51	11.75	12.80	36.74	16.17	25.00	30.55
Quantity	Interstory Drift (mm)				Interstory Drift (mm)				Interstory Drift (mm)			
Floor	MRF10	FD10	VE10	VD10	MRF10	FD10	VE10	VD10	MRF10	FD10	VE10	VD10
10	39.79	9.13	8.86	6.71	30.41	8.85	11.87	14.83	24.73	13.20	21.82	21.79
9	51.39	10.35	11.83	10.15	34.63	9.67	15.74	21.04	46.00	19.67	28.87	30.44
8	48.04	13.09	14.35	13.31	42.36	9.69	19.95	28.01	93.99	30.83	36.33	42.53
7	30.56	18.94	15.08	14.10	56.30	9.73	22.09	30.50	118.85	36.01	40.33	55.01
6	26.02	23.34	15.19	14.53	62.60	9.34	24.19	32.29	133.45	42.63	45.14	70.48
5	21.71	19.24	13.90	13.80	57.12	10.04	24.31	32.17	135.40	45.85	50.02	82.06
4	21.10	15.78	13.19	14.52	55.51	11.17	25.60	33.99	142.45	53.08	57.75	93.00
3	24.59	17.74	13.63	15.87	51.42	12.91	25.67	33.39	134.44	53.30	61.67	93.92
2	24.66	19.72	13.55	15.96	38.35	11.80	23.11	27.93	99.71	40.29	53.74	72.67
1	11.51	9.24	7.84	8.38	15.55	5.51	11.75	12.80	36.74	16.17	25.00	30.55

Table 5.4 Continued

Record	Northridge228				Northridge318				Northridge018			
Quantity	Floor Deflection (mm)				Floor Deflection (mm)				Floor Deflection (mm)			
Floor	MRF10	FD10	VE10	VD10	MRF10	FD10	VE10	VD10	MRF10	FD10	VE10	VD10
10	771.54	528.46	619.44	660.56	676.26	338.96	433.17	506.37	880.00	427.75	472.92	521.12
9	742.92	516.92	586.96	635.09	637.80	325.57	410.80	484.34	848.55	414.50	446.39	501.12
8	711.71	503.70	545.53	599.81	586.39	302.38	381.17	453.37	792.24	397.48	412.82	472.96
7	677.04	481.90	495.07	553.46	515.61	268.52	343.59	411.00	666.28	366.66	372.29	431.50
6	629.07	456.29	438.65	499.24	445.09	228.13	301.36	360.20	540.36	330.16	327.72	380.08
5	553.60	416.72	375.11	434.29	370.88	184.92	253.24	299.82	458.60	292.94	278.44	320.97
4	453.06	353.43	306.07	359.01	287.16	143.03	201.28	233.86	368.45	244.57	225.77	263.39
3	326.95	259.61	227.50	331.90	191.96	96.02	142.73	159.96	252.47	175.83	165.95	193.94
2	186.34	146.24	140.25	190.83	96.96	49.17	80.71	84.59	130.16	94.66	99.63	113.27
1	63.98	46.78	54.36	62.23	26.41	15.71	26.01	24.64	37.66	27.20	35.14	37.54
Quantity	Interstory Drift (mm)				Interstory Drift (mm)				Interstory Drift (mm)			
Floor	MRF10	FD10	VE10	VD10	MRF10	FD10	VE10	VD10	MRF10	FD10	VE10	VD10
10	52.19	20.04	33.51	26.41	47.99	14.83	23.39	22.05	43.21	13.32	27.90	23.26
9	58.70	37.71	44.44	37.82	64.98	24.72	30.91	31.12	58.50	24.86	37.10	33.30
8	96.88	46.00	56.51	53.72	93.48	34.65	38.31	43.67	125.98	34.55	46.40	46.75
7	120.03	46.52	65.03	67.02	118.63	40.58	42.56	54.69	134.28	43.13	51.87	58.71
6	141.78	63.78	72.94	79.84	118.17	43.71	49.10	65.92	126.28	55.48	57.40	69.52
5	147.98	81.56	77.43	90.05	108.02	44.38	53.28	72.30	117.84	63.46	59.76	74.27
4	155.02	106.47	85.16	104.40	108.55	49.13	59.91	79.32	128.34	79.72	65.44	81.09
3	152.86	119.56	91.30	113.63	99.82	48.02	63.06	78.59	129.00	87.11	69.89	87.27
2	126.67	101.77	86.86	102.62	71.40	35.80	55.10	60.87	98.10	69.06	65.47	77.27
1	63.98	46.78	54.36	59.37	26.41	15.71	26.01	24.64	37.66	27.20	35.14	37.54

Table 5.4 Continued

Record	Northridge288				Imperial514				Imperial523			
Quantity	Floor Deflection (mm)				Floor Deflection (mm)				Floor Deflection (mm)			
Floor	MRF10	FD10	VE10	VD10	MRF10	FD10	VE10	VD10	MRF10	FD10	VE10	VD10
10	412.47	412.00	507.31	400.84	517.70	269.29	343.37	405.62	1390.40	495.84	582.64	856.88
9	400.27	399.04	479.13	377.71	497.06	257.54	323.99	386.00	1366.40	482.93	555.29	835.80
8	380.39	380.78	441.89	345.00	471.10	243.84	298.50	358.50	1320.30	464.84	518.89	804.77
7	341.07	350.04	395.02	302.80	429.86	222.22	266.47	322.13	1183.40	435.28	471.18	748.22
6	285.96	308.29	341.99	257.73	371.70	192.87	230.98	280.88	1009.20	393.68	414.06	662.09
5	221.15	253.64	282.79	210.39	294.50	157.78	191.97	233.27	807.50	331.52	346.76	549.41
4	167.99	194.59	221.51	164.03	210.57	123.75	151.61	181.94	591.78	255.50	272.84	418.30
3	114.49	128.51	155.74	115.96	131.38	85.59	107.32	124.19	373.90	168.61	190.77	274.89
2	60.30	64.72	87.95	64.85	64.15	45.57	60.89	66.27	176.42	83.30	105.81	136.79
1	17.93	18.23	28.32	19.97	17.33	13.87	19.79	19.64	29.00	21.84	33.19	33.50
Quantity	Interstory Drift (mm)				Interstory Drift (mm)				Interstory Drift (mm)			
Floor	MRF10	FD10	VE10	VD10	MRF10	FD10	VE10	VD10	MRF10	FD10	VE10	VD10
10	53.82	13.46	28.19	23.23	33.09	12.09	19.47	19.71	40.55	14.29	28.34	26.14
9	52.65	18.37	37.28	32.98	39.43	13.80	25.82	27.76	46.17	23.12	37.43	36.49
8	78.83	33.66	47.29	43.58	50.70	22.37	32.70	37.05	159.00	35.78	48.08	56.81
7	86.45	50.11	54.38	48.92	76.47	29.37	36.16	43.08	194.27	47.04	57.12	86.87
6	74.14	63.58	61.49	52.93	92.36	35.48	39.88	50.87	216.77	62.21	67.40	114.55
5	65.94	66.75	64.28	52.94	95.51	34.03	41.54	55.02	222.73	76.01	74.24	133.22
4	64.48	68.84	68.77	56.28	89.67	39.01	45.82	61.27	220.09	87.54	82.54	144.89
3	59.72	65.23	69.85	55.77	71.59	40.37	47.57	61.13	198.36	85.81	85.49	139.01
2	44.02	46.98	60.25	45.88	47.75	32.51	41.49	47.48	150.82	61.59	72.75	105.35
1	17.93	18.23	28.32	19.97	17.33	13.87	19.79	19.64	29.00	21.84	33.19	33.50

Table 5.5 Energy Calculations and Analysis of Different Models under Far-Fault and Near-Fault Ground Motions

Model	MRF10		FD10		VE10		VD10	
Earthquake Record	Yielding Energy Ratio (%)	Damping Energy Ratio (%)	Yielding Energy Ratio (%)	Damper Energy Ratio (%)	Yielding Energy Ratio (%)	Damper Energy Ratio (%)	Yielding Energy Ratio (%)	Damper Energy Ratio (%)
El-Centro	25	75	0	100	0	100	0	100
Coalinga270	19	81	0	100	0	100	0	100
Coalinga360	0	100	0	100	0	100	0	100
Parkfield	0	100	0	100	0	100	0	100
Lake-L-00	9	91	0	100	0	100	0	100
Lake-L-90	0	100	0	100	0	100	0	100
Lake-I-00	0	100	0	100	0	100	0	100
Northridge175	9	91	0	100	0	100	0	100
Northridge265	13	87	0	100	0	100	0	100
Northridge104	14	86	0	100	0	100	0	100
Lander000	39	61	0	100	0	100	1	99
Lander275	71	29	9	91	20	80	37	63
Northridge228	55	45	16	84	13	86	17	83
Northridge318	54	46	4	96	13	87	15	85
Northridge018	56	44	12	88	15	85	21	79
Northridge288	51	49	8	92	13	87	15	85
Imperial514	49	51	2	98	6	94	14	86
Imperial523	65	35	17	83	20	80	30	70

Yielding Energy Ratio = Yielding Energy / Total Input Energy
Damping Energy Ratio = Damping Energy/ Total Input Energy
Damper Energy Ratio = Damper Energy / Total Input Energy

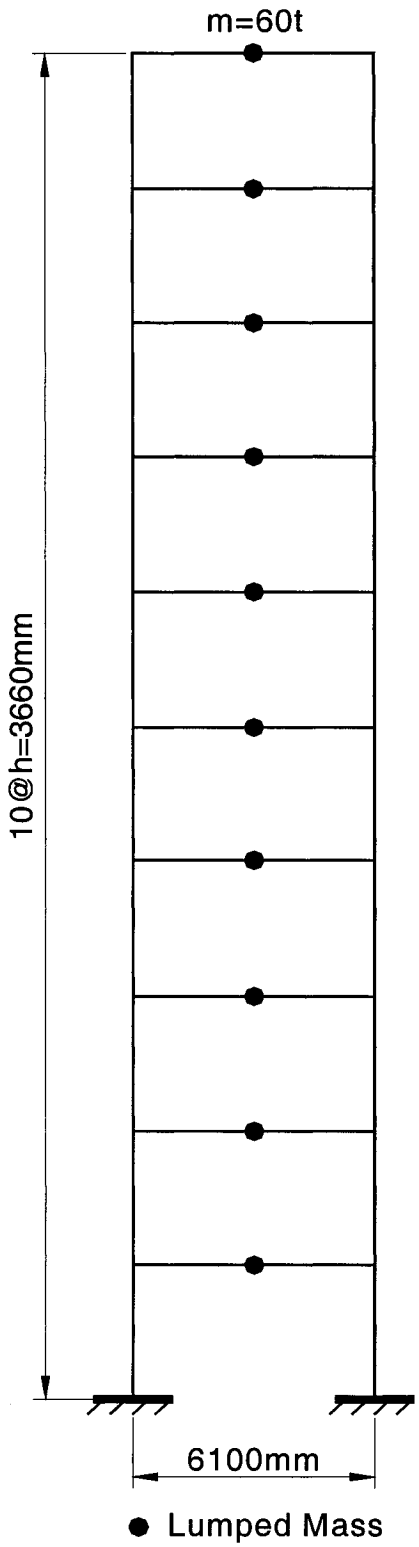

Properties of Cross Section of MRF10

Floor	Beam	Column
10	W460x74	W360x51
9	W460x74	W360x79
8	W460x74	W360x79
7	W460x74	W360x122
6	W460x74	W360x122
5	W460x89	W360x162
4	W460x89	W360x162
3	W460x89	W360x179
2	W460x89	W360x179
1	W460x113	W360x287

Fig. 5.1 Layout of Multi-Degree-of-Freedom MRF10

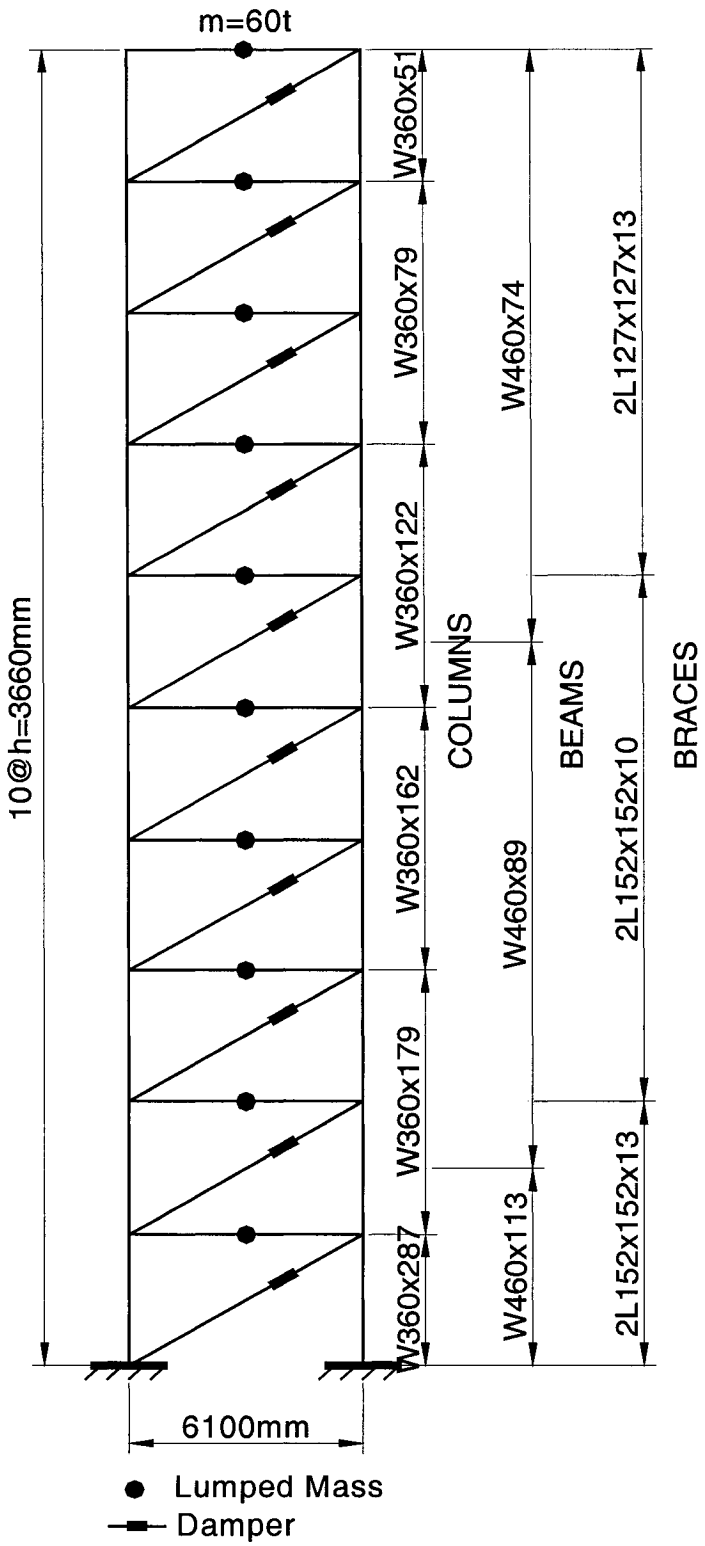

Properties of Brace

Floor	Brace
10	2L127x127x13
9	2L127x127x13
8	2L127x127x13
7	2L127x127x13
6	2L152x152x10
4	2L152x152x10
3	2L152x152x10
2	2L152x152x13
1	2L152x152x13

Fig. 5.2 Layout of Multi-Degree-of-Freedom Damped Frame

a.

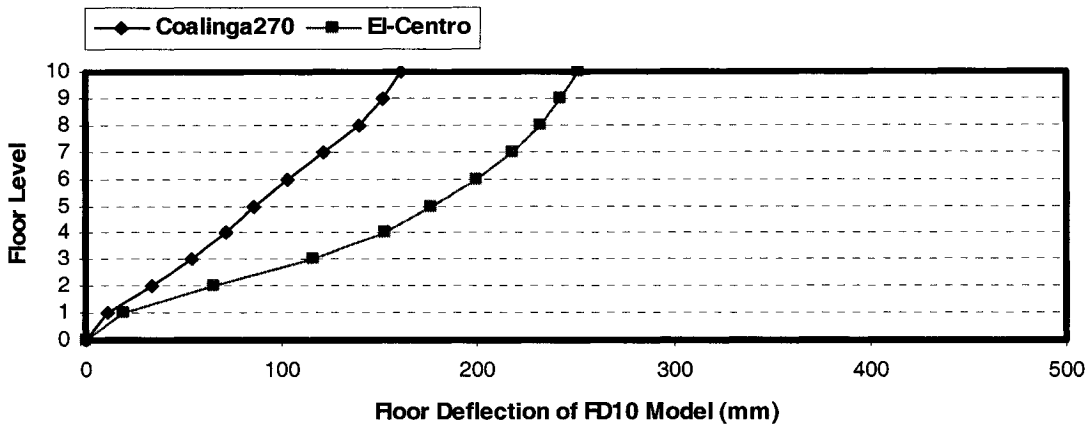

b.

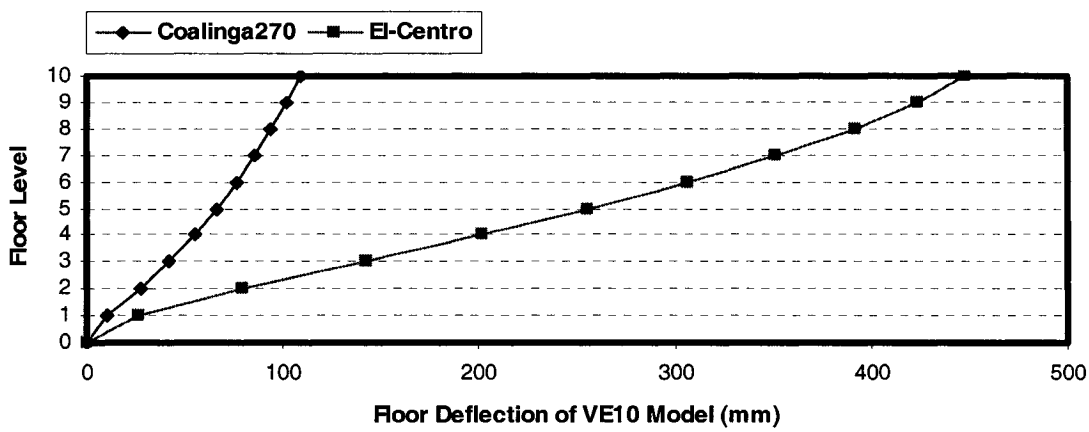

c.

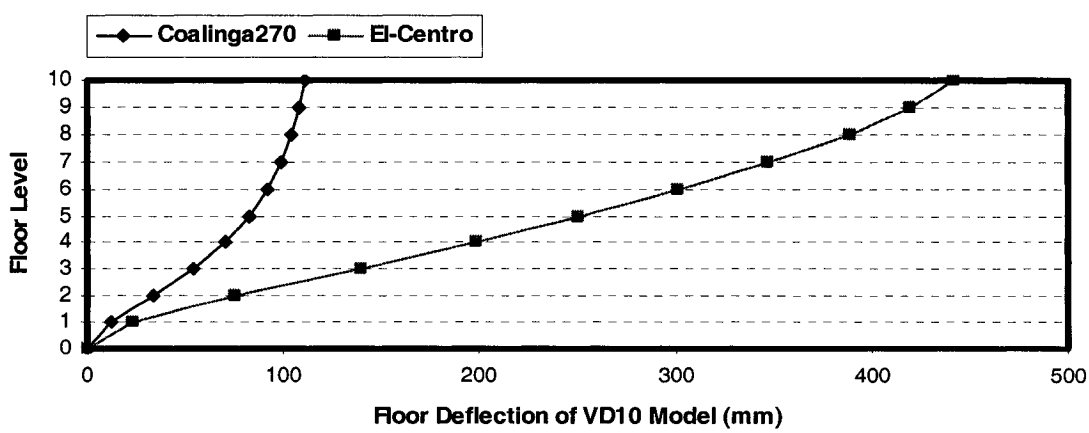

Fig. 5.3 Comparison of Floor Deflection of Models to El-Centro Earthquake and Coalinga270 Earthquake
a. FD10 Model b. VE10 Model c. VD10 Model

a.

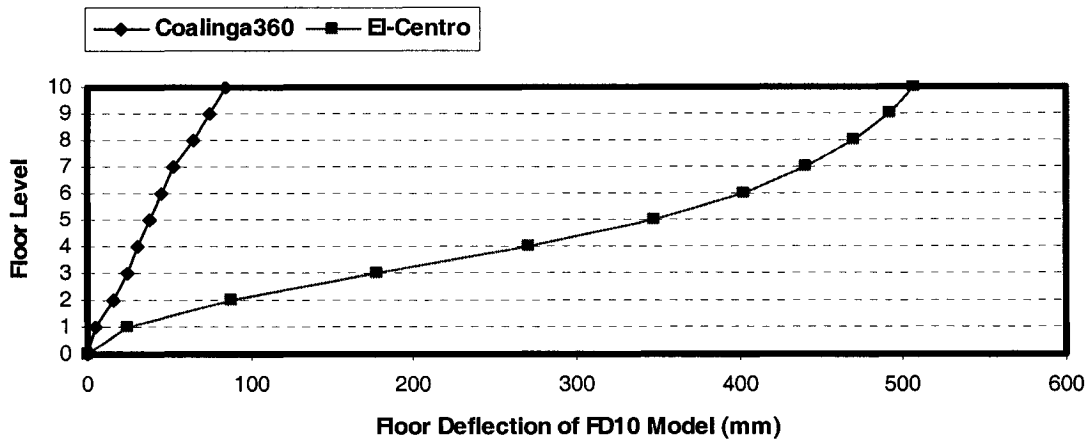

b.

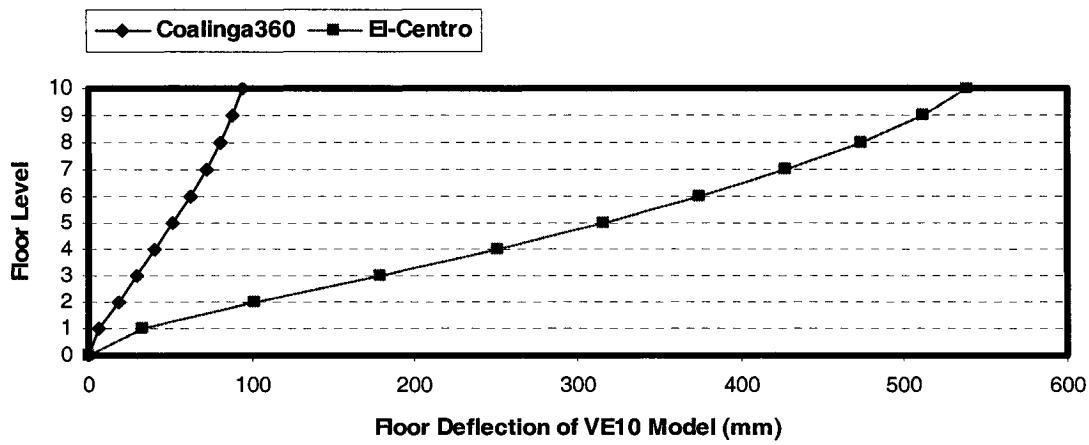

c.

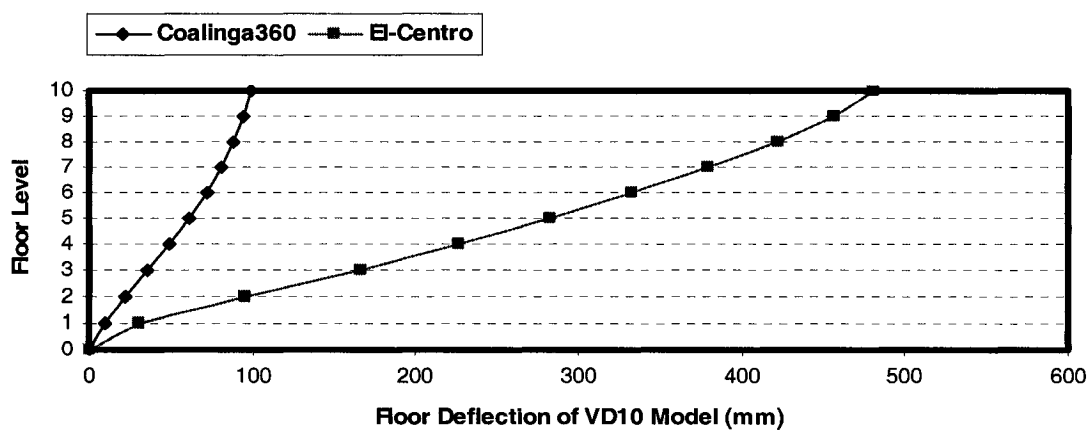

Fig. 5.4 Comparison of Floor Deflection of Models to El-Centro Earthquake and Coalinga360 Earthquake
a. FD10 Model b. VE10 Model c. VD10 Model

a.

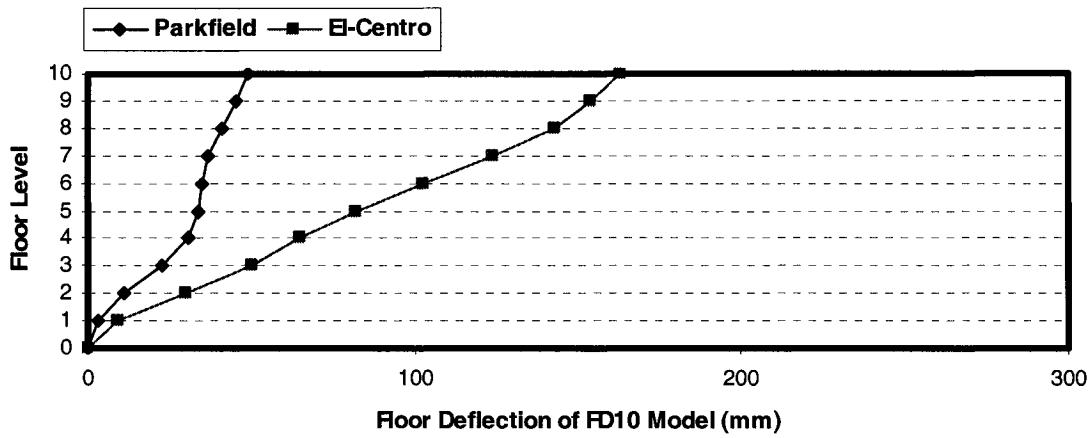

b.

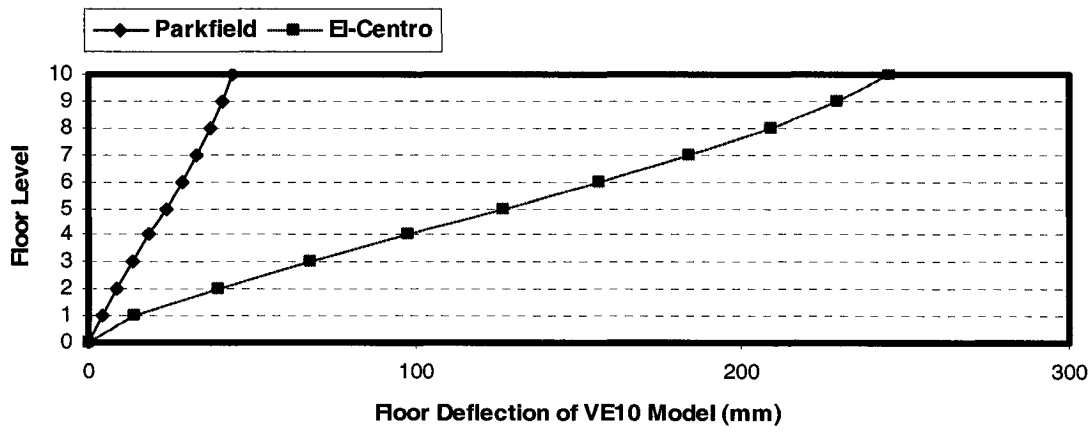

c.

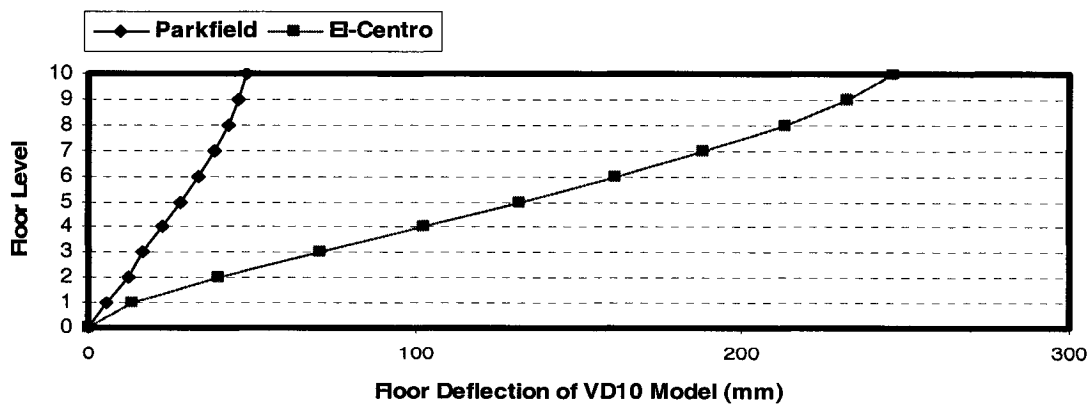

Fig. 5.5 Comparison of Floor Deflection of Models to El-Centro Earthquake and Parkfield Earthquake
a. FD10 Model b. VE10 Model c. VD10 Model

a.

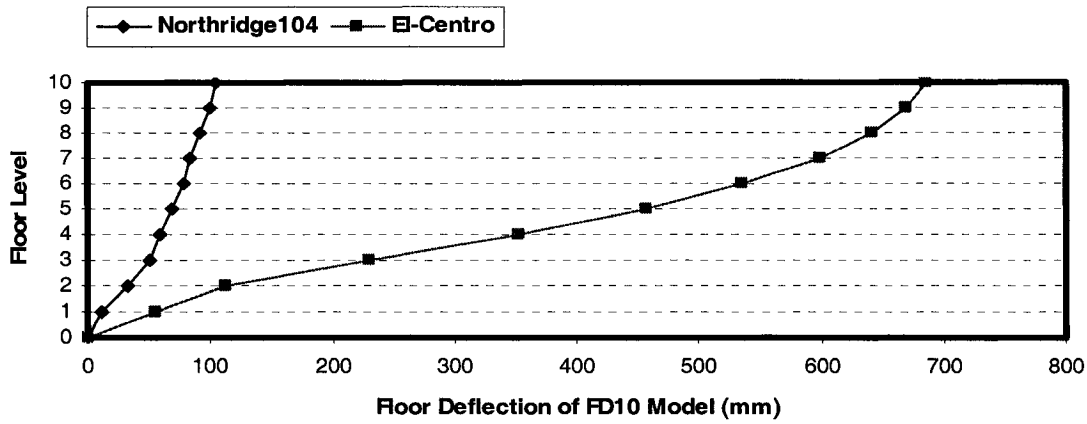

b.

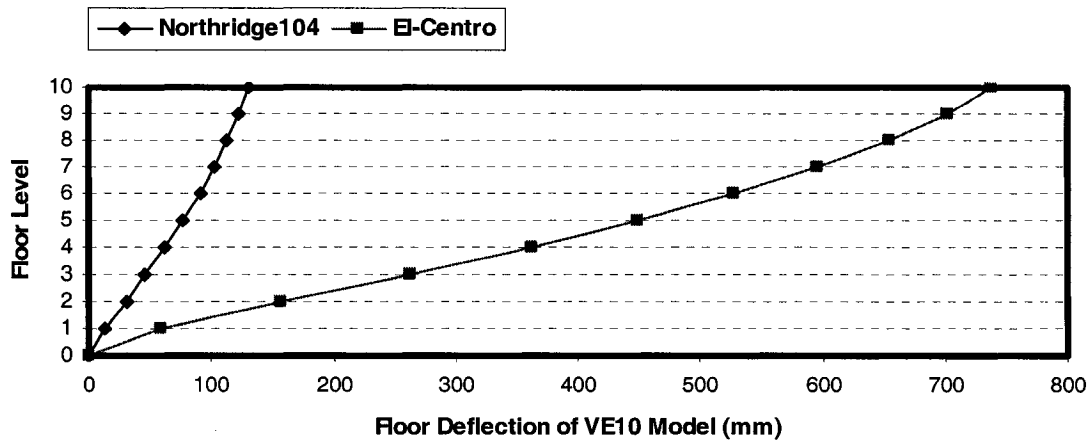

c.

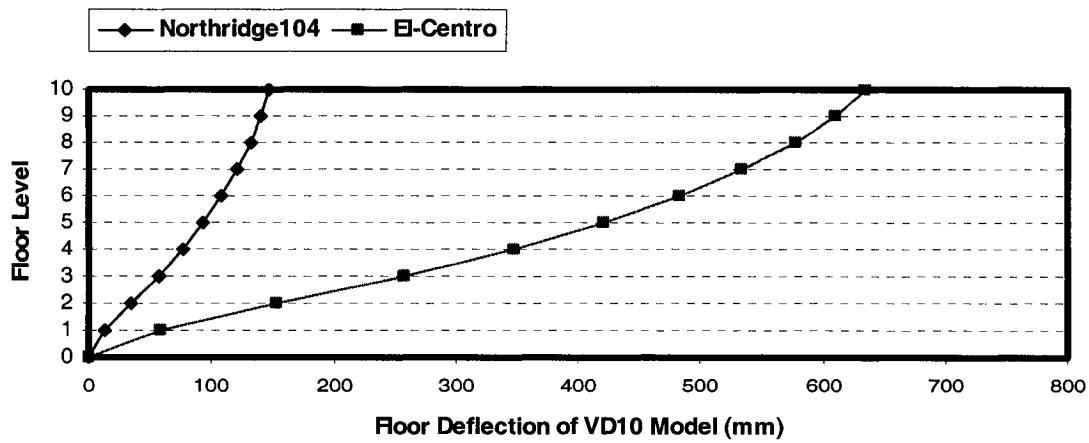

Fig. 5.6 Comparison of Floor Deflection of Models to El-Centro Earthquake and Northridge104 Earthquake
a. FD10 Model b. VE10 Model c. VD10 Model

a.

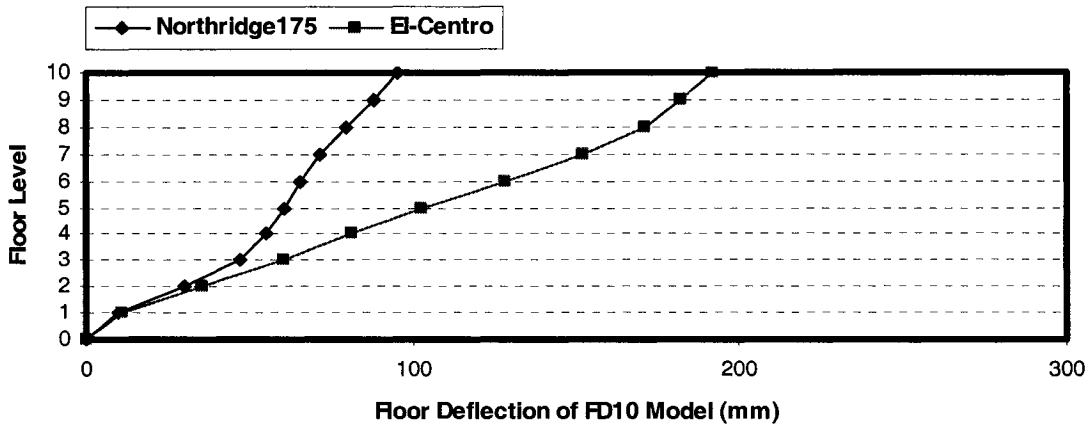

b.

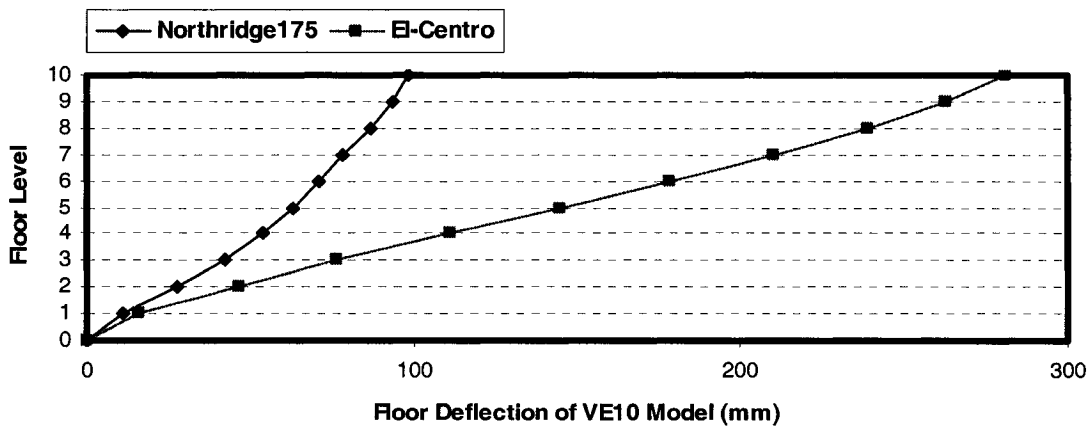

c.

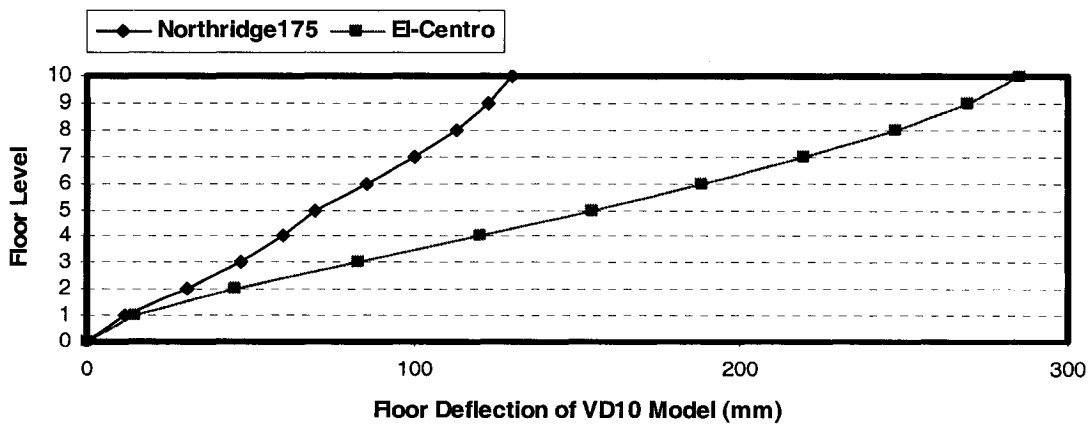

Fig. 5.7 Comparison of Floor Deflection of Models to El-Centro Earthquake and Northridge175 Earthquake
a. FD10 Model b. VE10 Model c. VD10 Model

a.

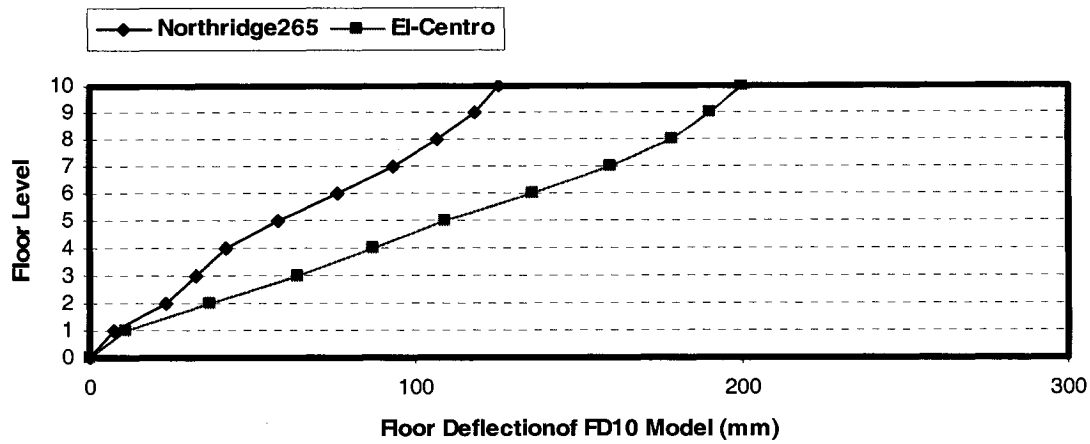

b.

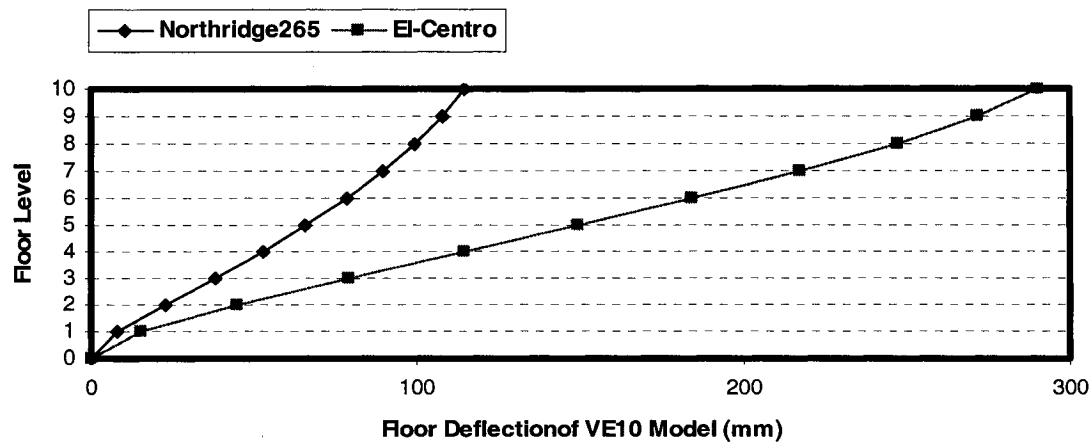

c.

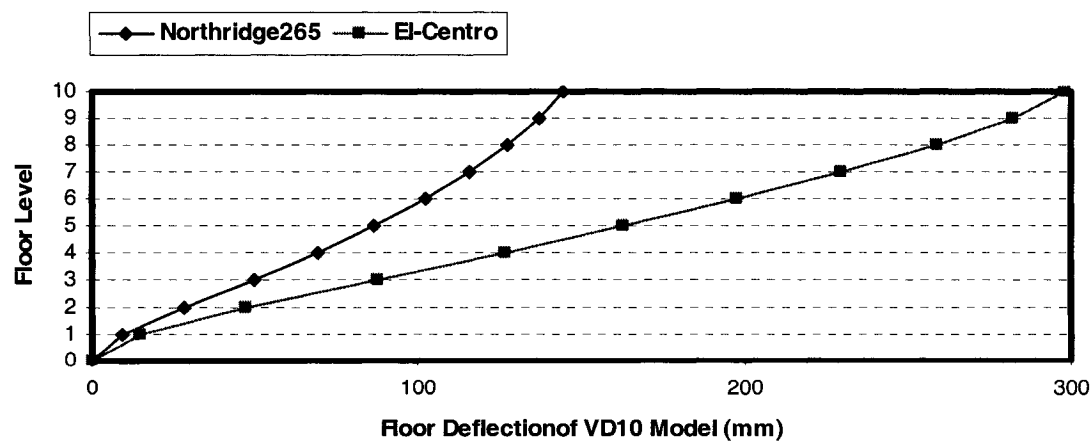

Fig. 5.8 Comparison of Floor Deflection of Models to El-Centro Earthquake and Northridge265 Earthquake
a. FD10 Model b. VE10 Model c. VD10 Model

a.

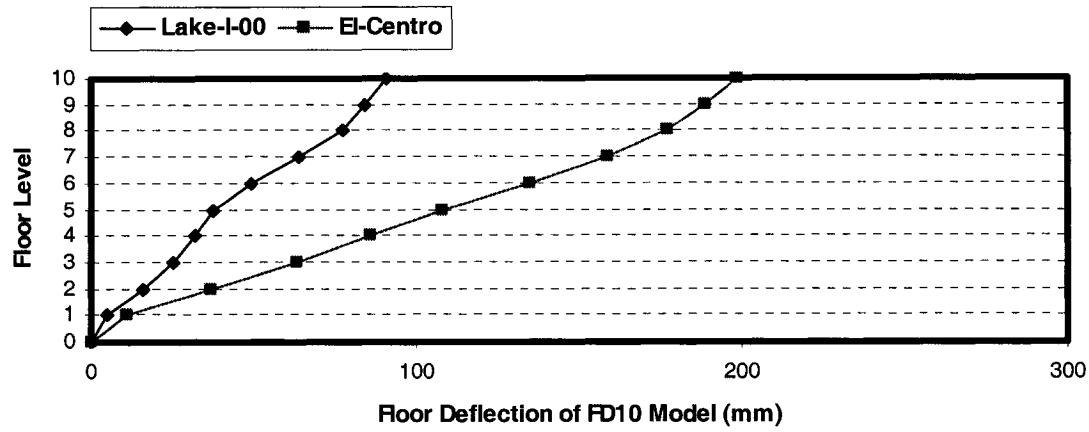

b.

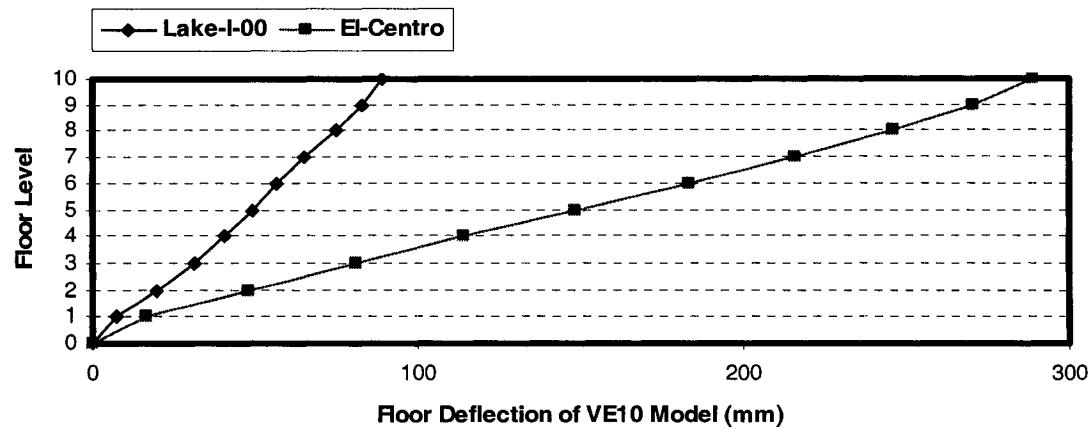

c.

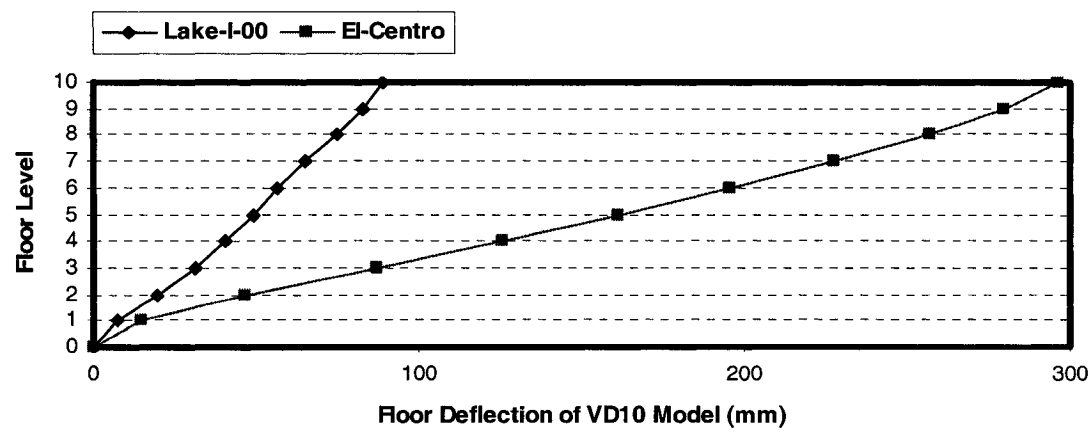

Fig. 5.9 Comparison of Floor Deflection of Models to El-Centro Earthquake and Lake-I-00 Earthquake
a. FD10 Model b. VE10 Model c. VD10 Model

a.

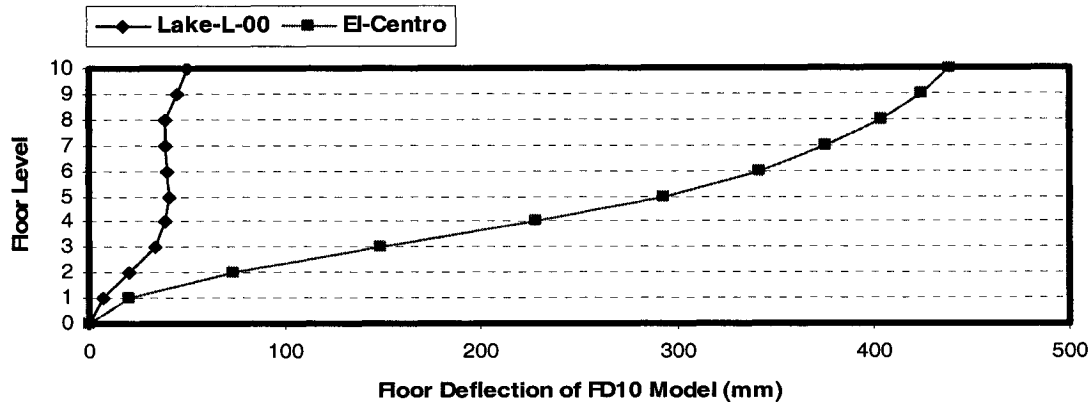

b.

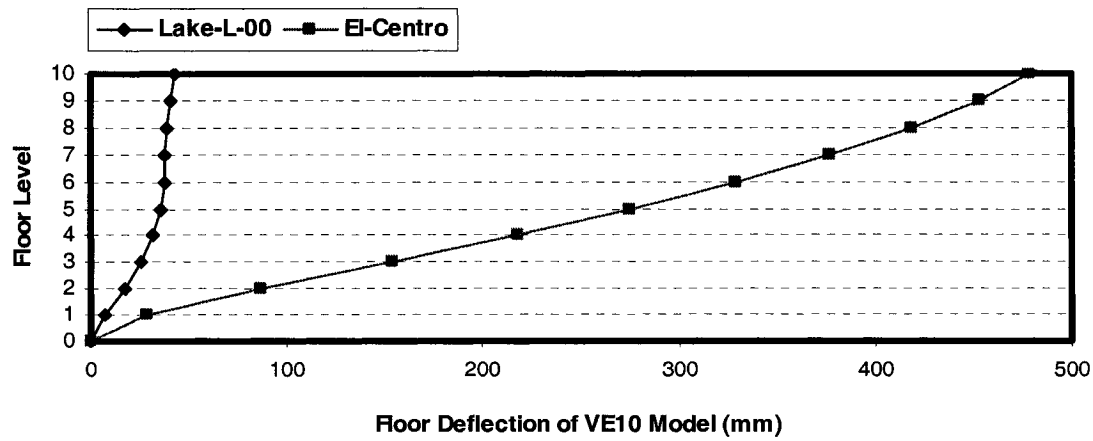

c.

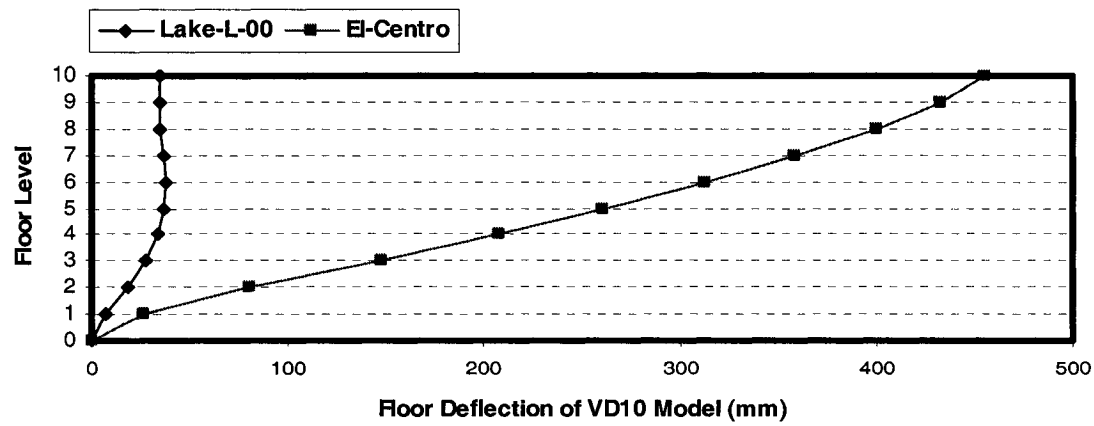

Fig. 5.10 Comparison of Floor Deflection of Models to El-Centro Earthquake and Lake-L-00 Earthquake
a. FD10 Model b. VE10 Model c. VD10 Model

a.

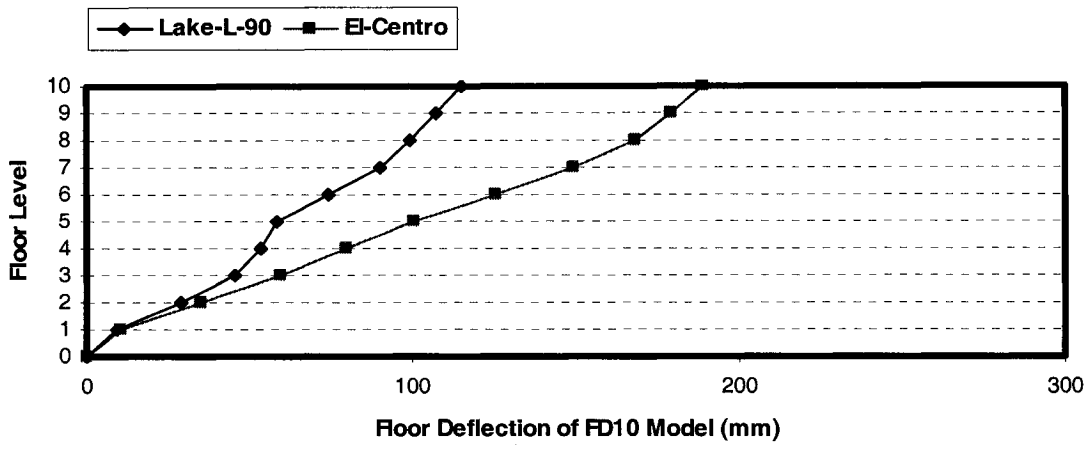

b.

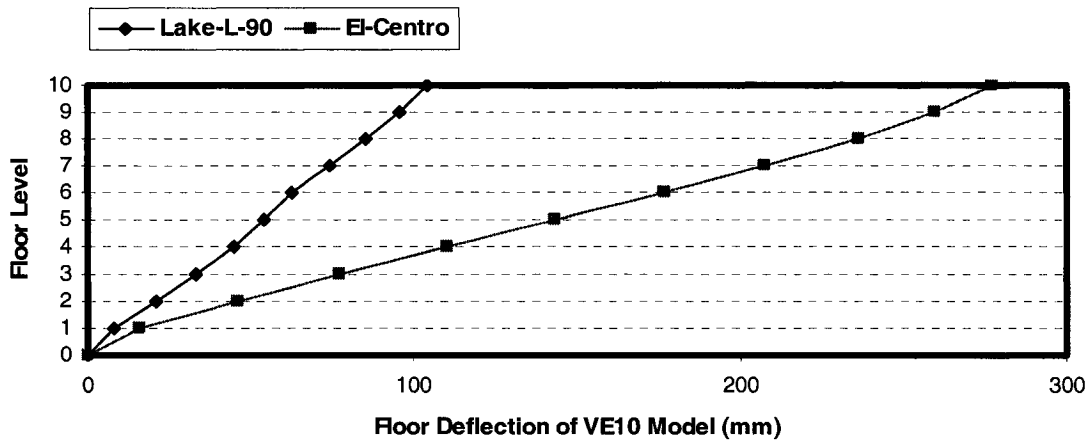

c.

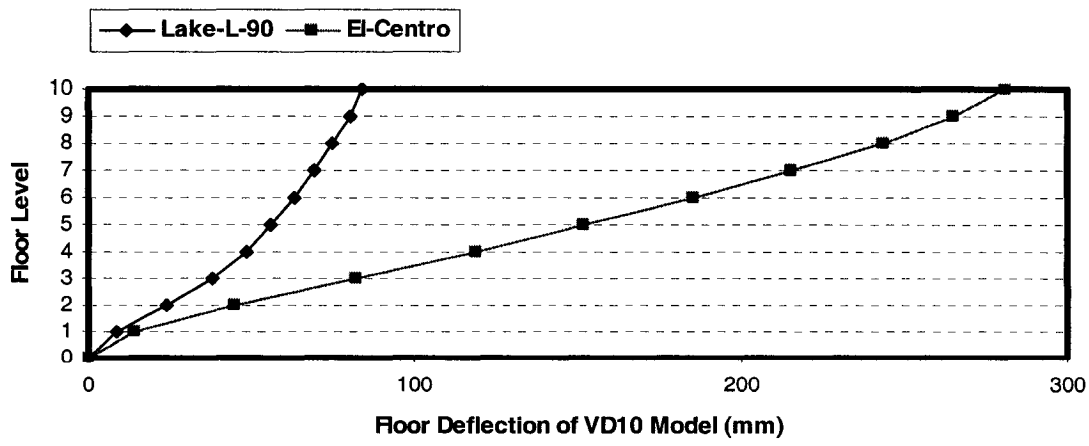

Fig. 5.11 Comparison of Floor Deflection of Models to El-Centro Earthquake and Lake-L-90 Earthquake
a. FD10 Model b. VE10 Model c. VD10 Model

a.

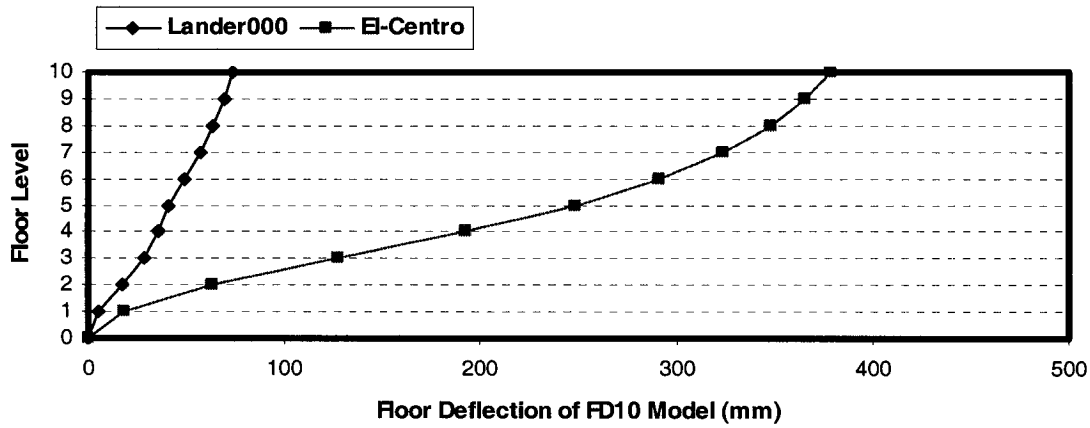

b.

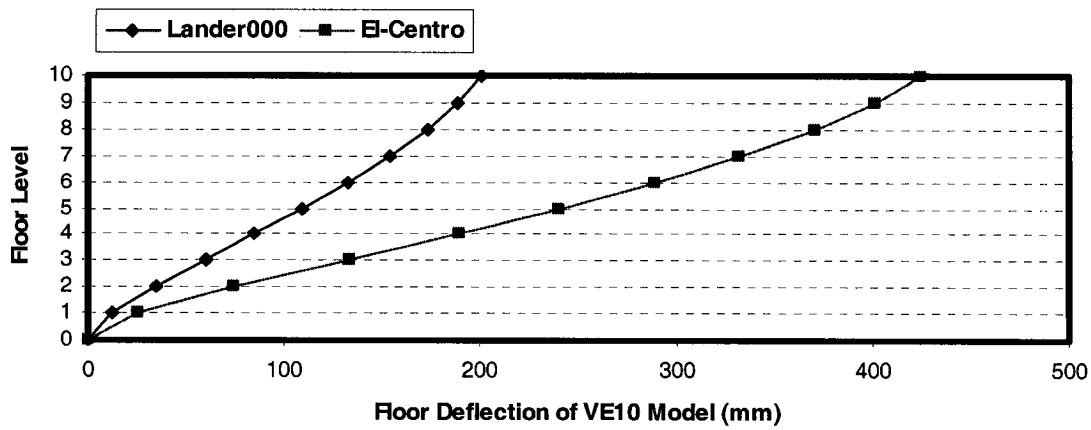

c.

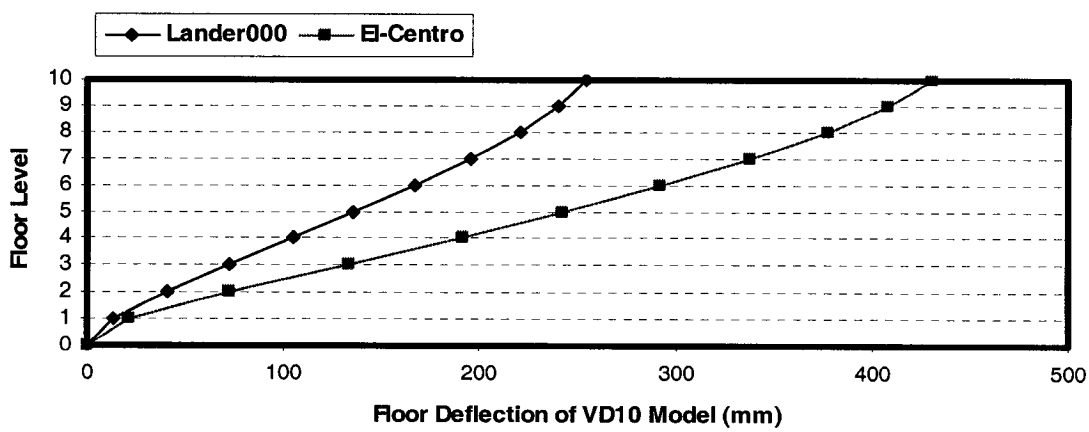

Fig. 5.12 Comparison of Floor Deflection of Models to El-Centro Earthquake and Lander000 Earthquake
a. FD10 Model b. VE10 Model c. VD10 Model

a.

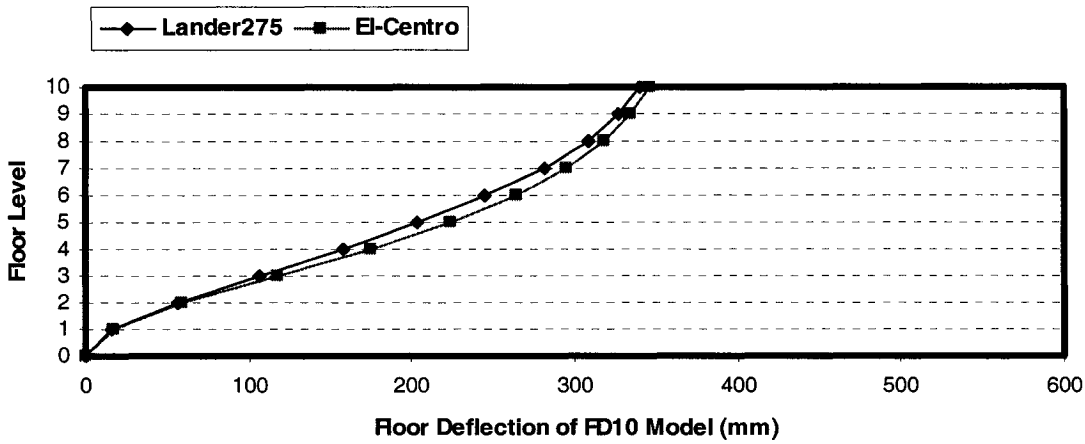

b.

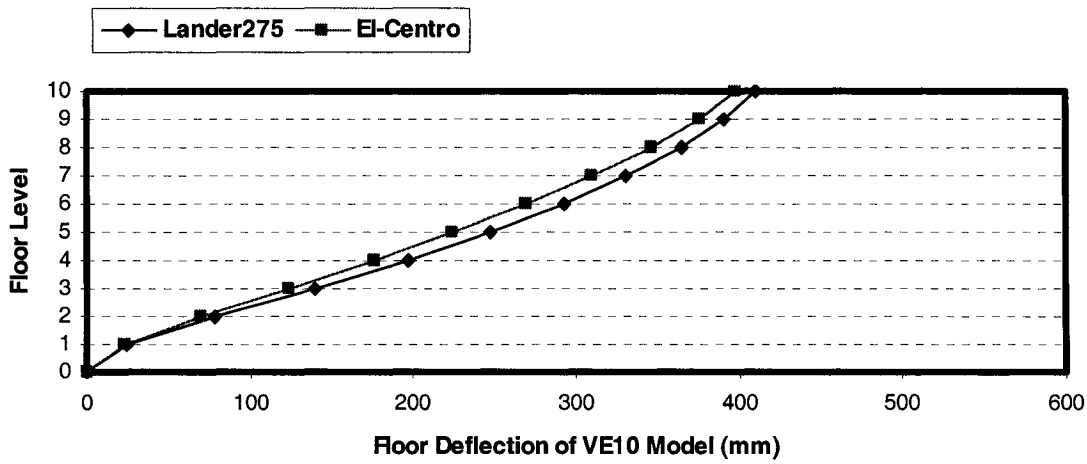

c.

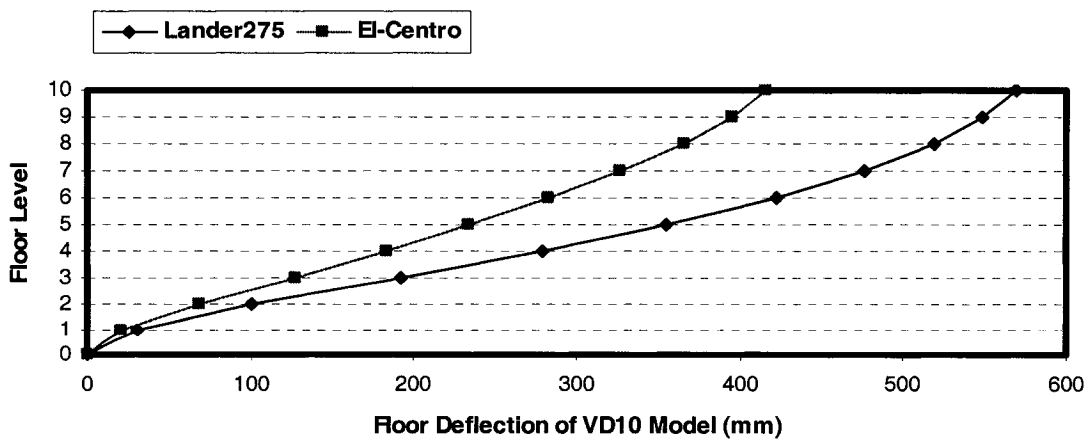

Fig. 5.13 Comparison of Floor Deflection of Models to El-Centro Earthquake and Lander275 Earthquake
a. FD10 Model b. VE10 Model c. VD10 Model

a.

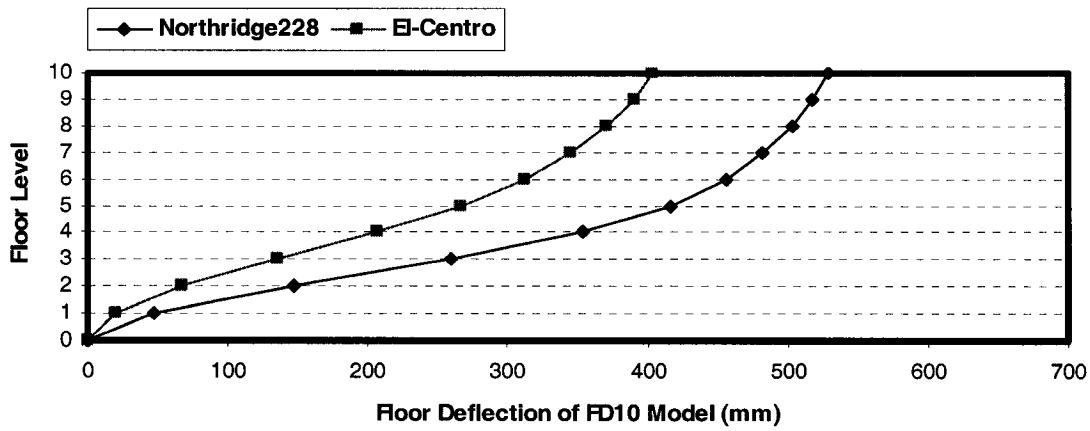

b.

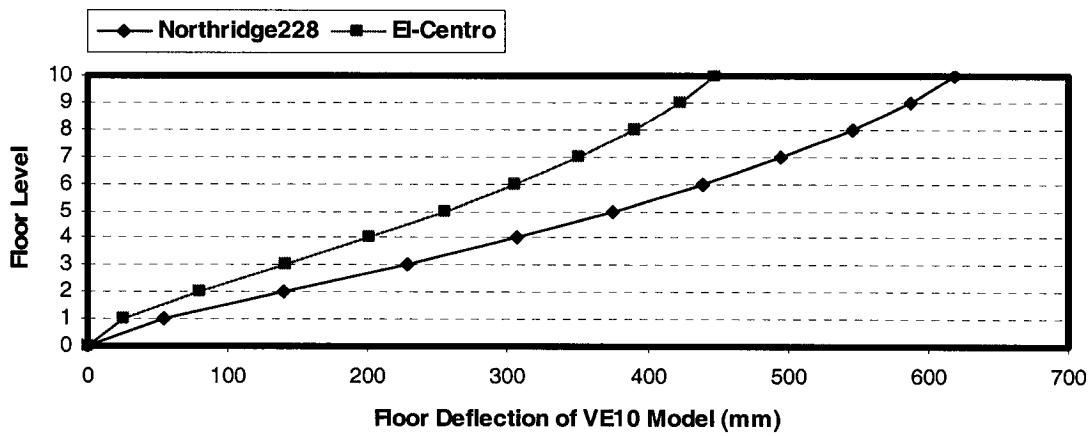

c.

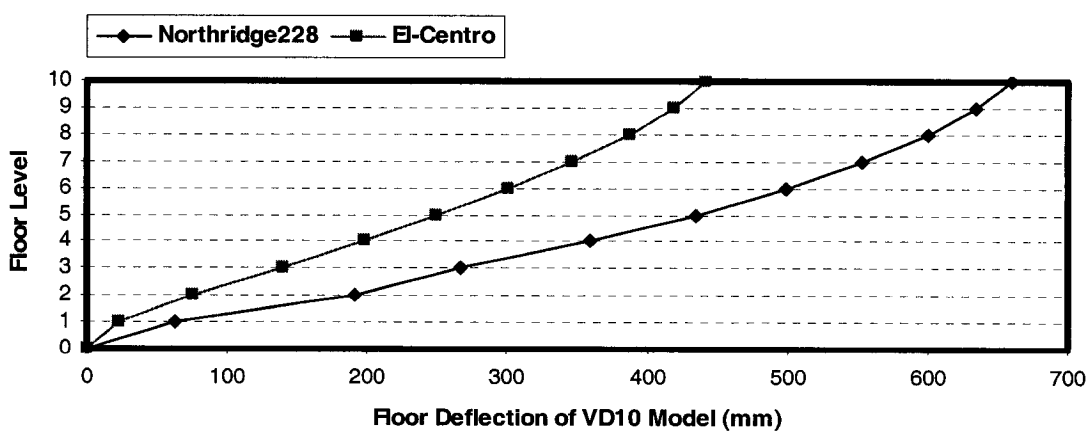

Fig. 5.14 Comparison of Floor Deflection of Models to El-Centro Earthquake and Northridge228 Earthquake
a. FD10 Model b. VE10 Model c. VD10 Model

a.

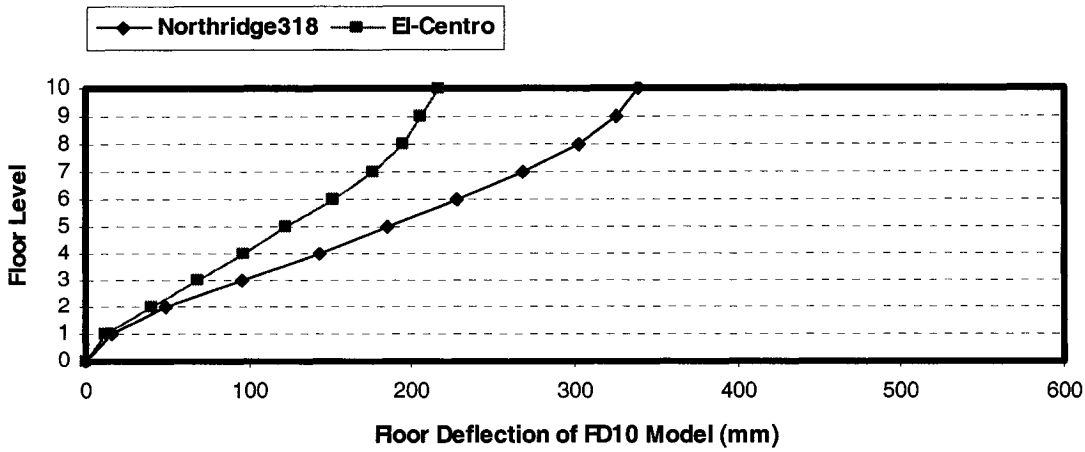

b.

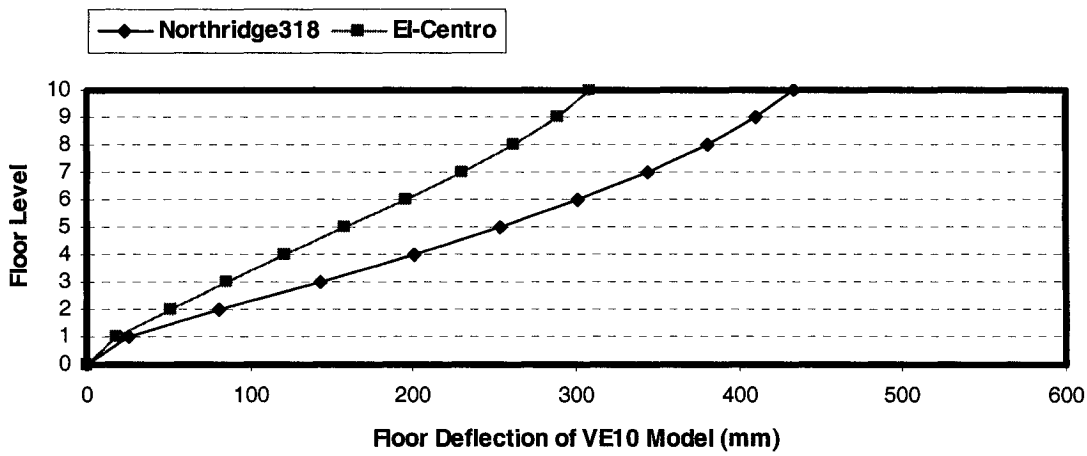

c.

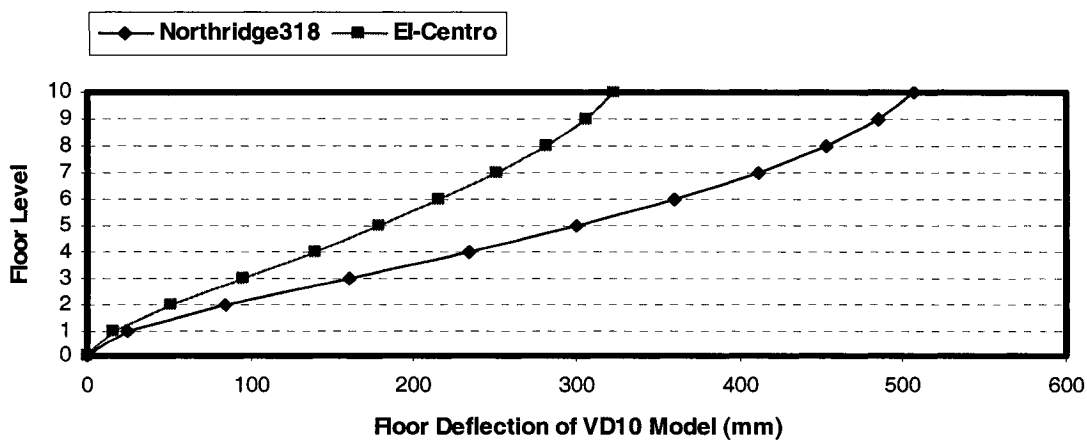

Fig. 5.15 Comparison of Floor Deflection of Models to El-Centro Earthquake and Northridge318 Earthquake
a. FD10 Model b. VE10 Model c. VD10 Model

a.

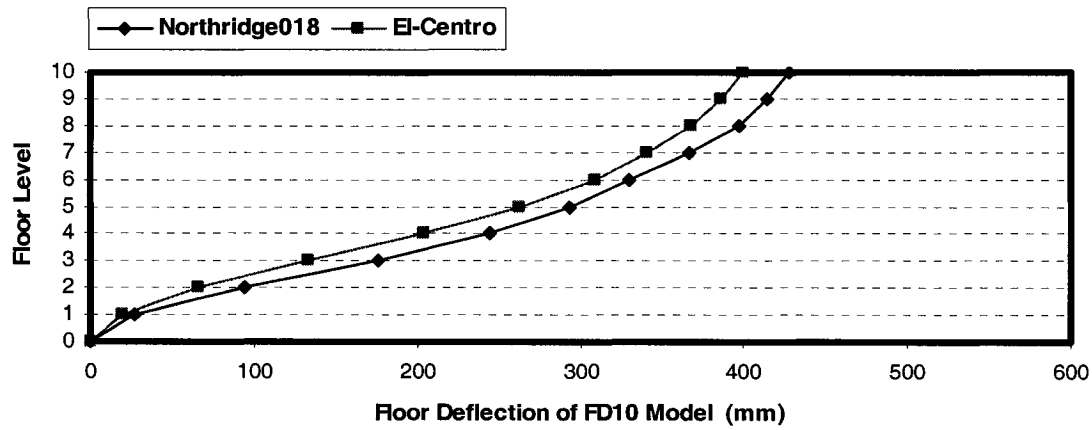

b.

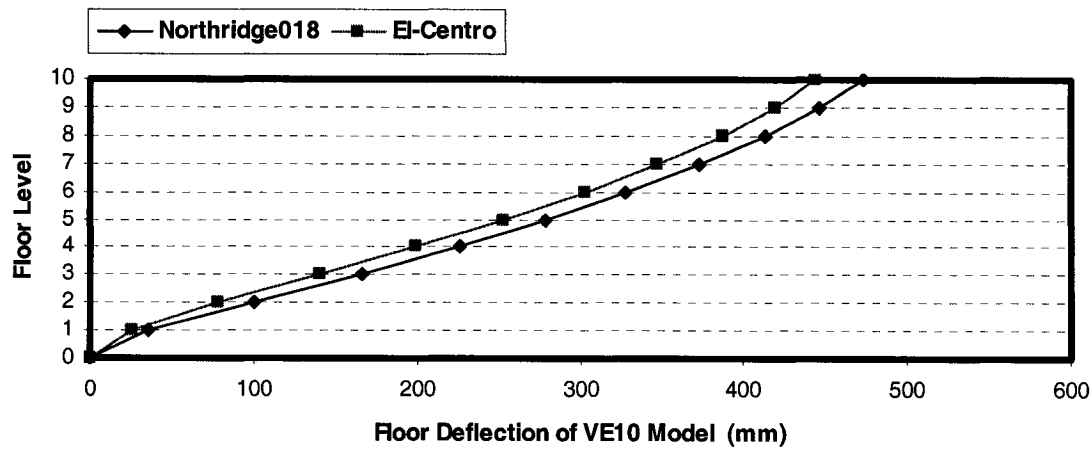

c.

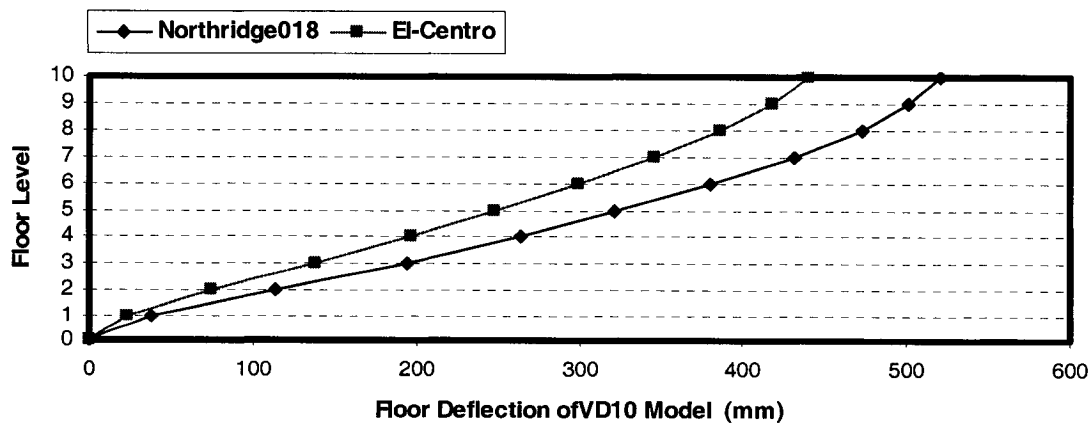

Fig. 5.16 Comparison of Floor Deflection of Models to El-Centro Earthquake and Northridge018 Earthquake
a. FD10 Model b. VE10 Model c. VD10 Model

a.

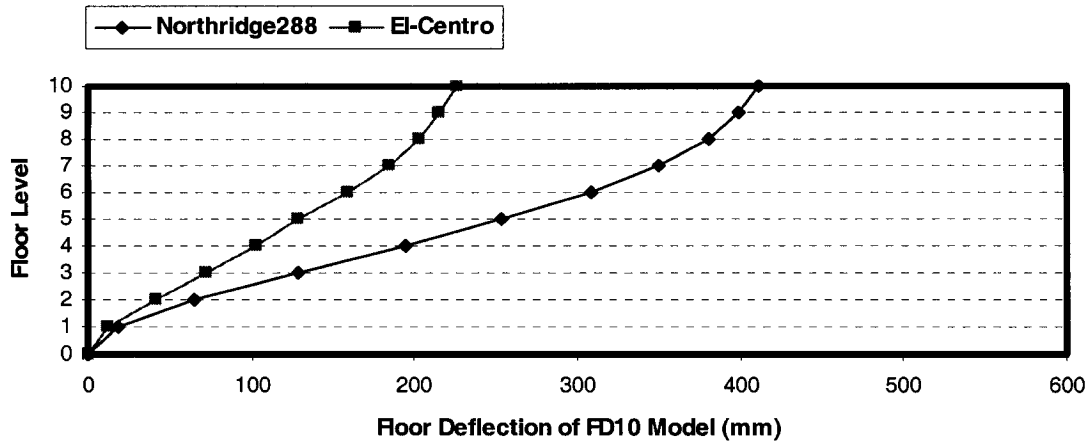

b.

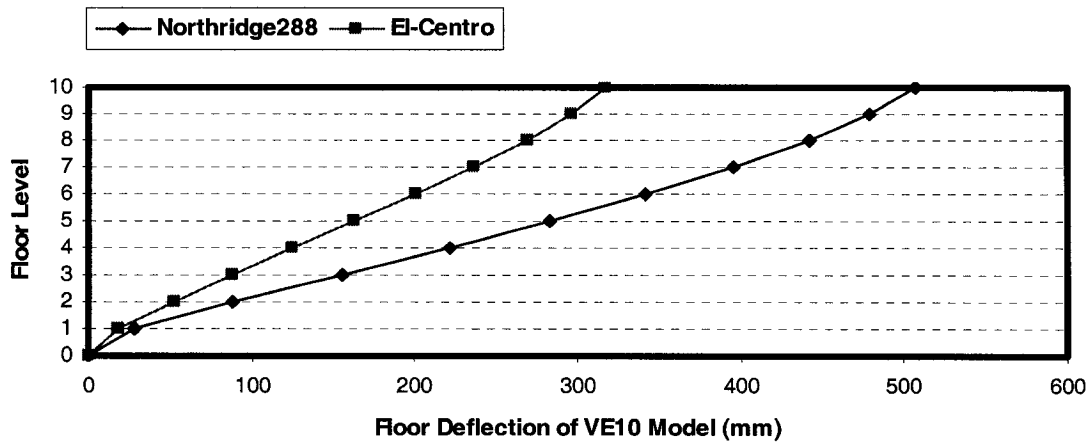

c.

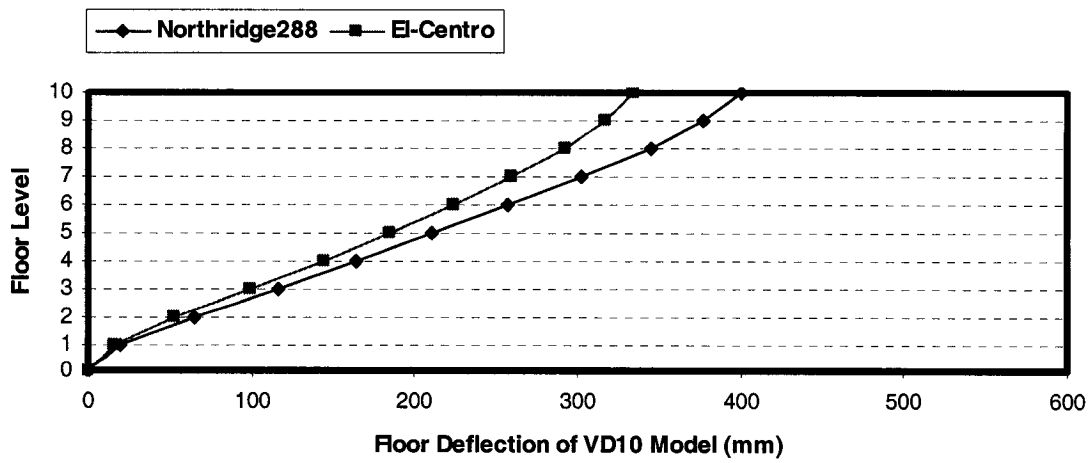

Fig. 5.17 Comparison of Floor Deflection of Models to El-Centro Earthquake and Northridge288 Earthquake
a. FD10 Model b. VE10 Model c. VD10 Model

a.

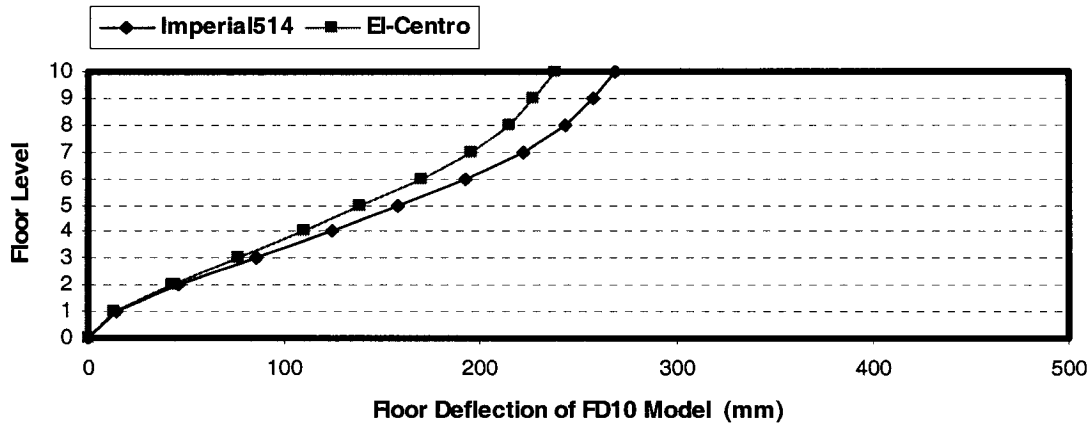

b.

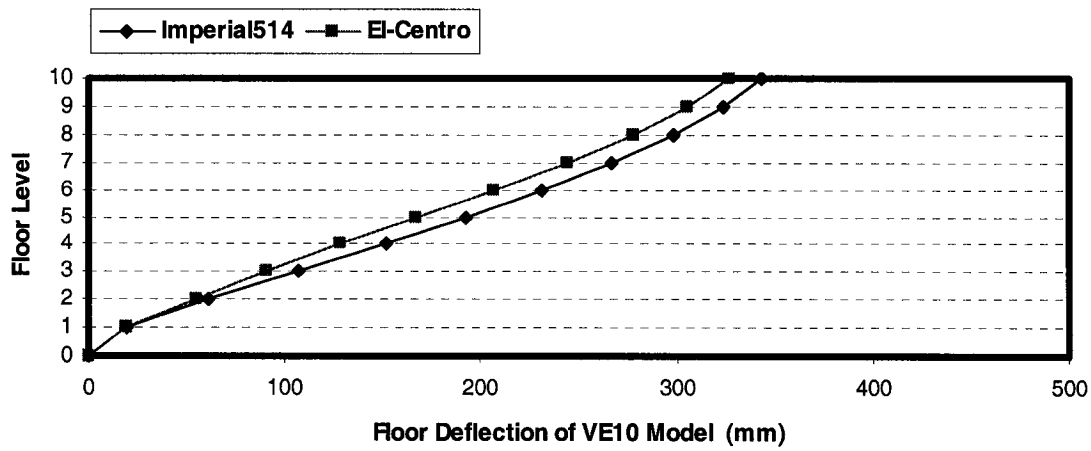

c.

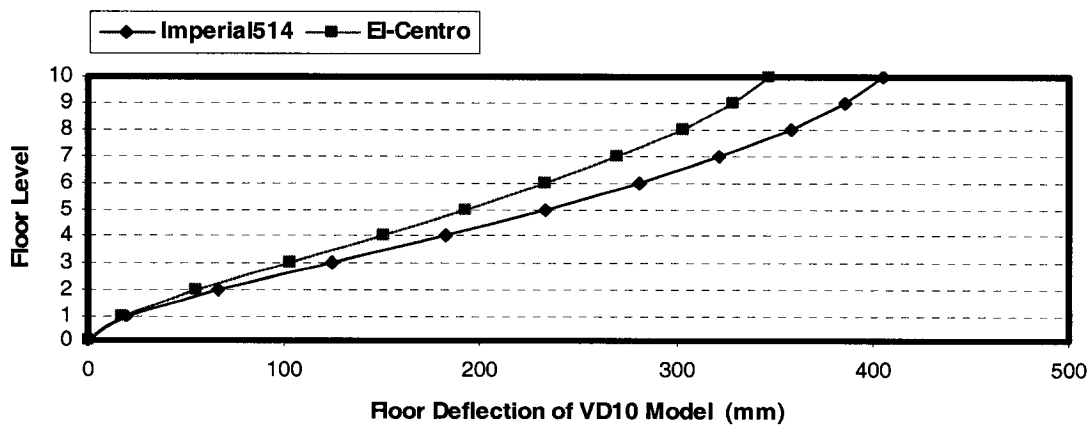

Fig. 5.18 Comparison of Floor Deflection of Models to El-Centro Earthquake and Imperial514 Earthquake
a. FD10 Model b. VE10 Model c. VD10 Model

a.

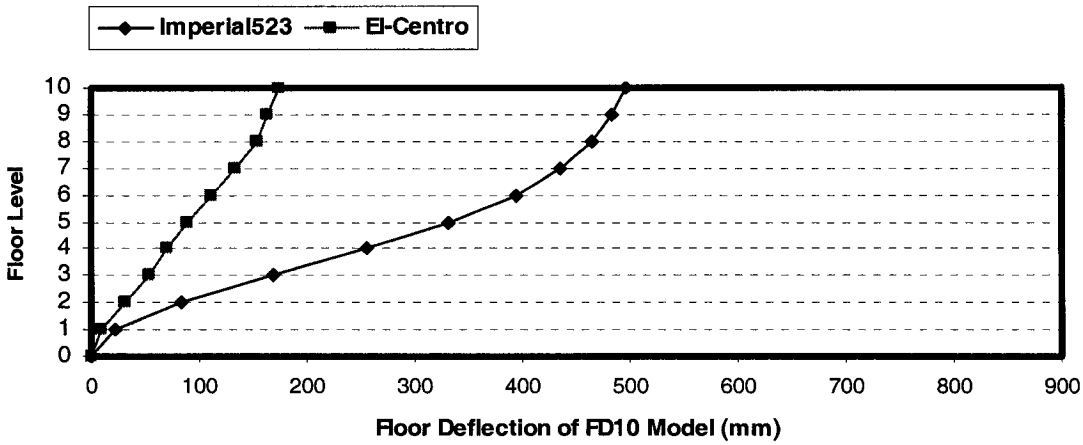

b.

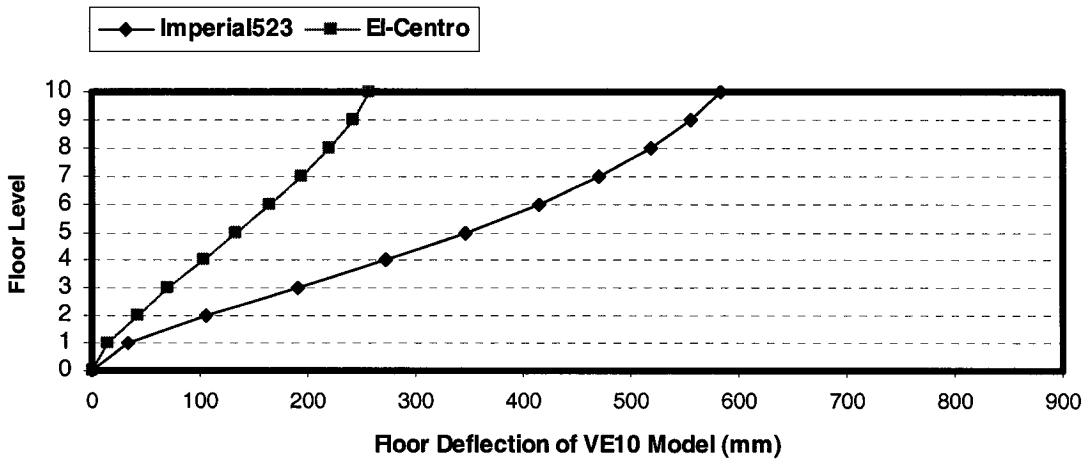

c.

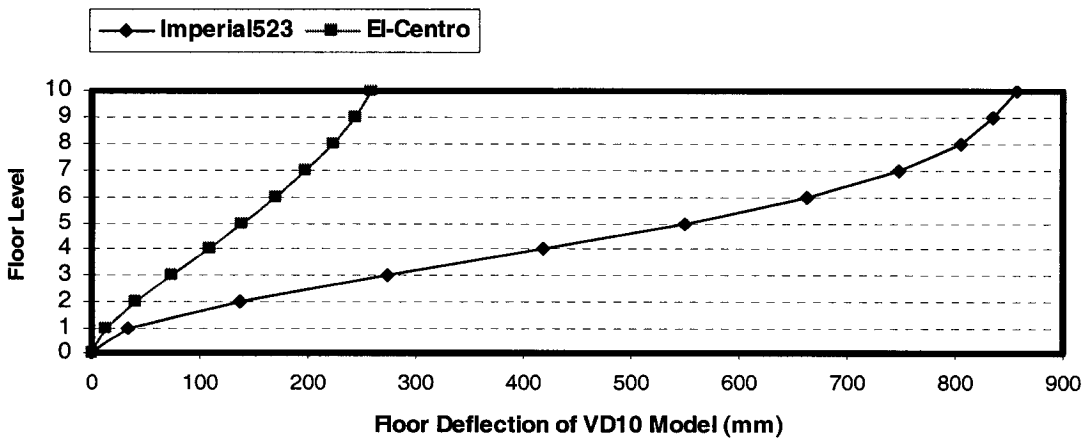

Fig. 5.19 Comparison of Floor Deflection of Models to El-Centro Earthquake and Imperial523 Earthquake
a. FD10 Model b. VE10 Model c. VD10 Model

a.

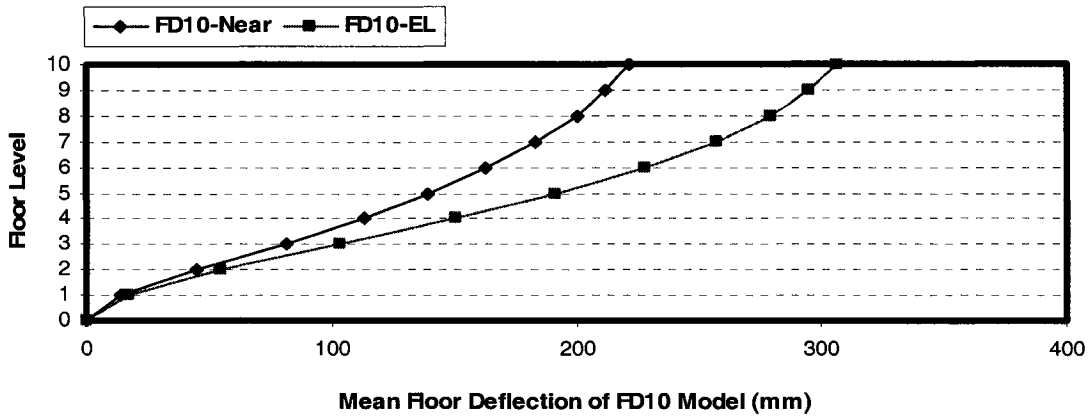

b.

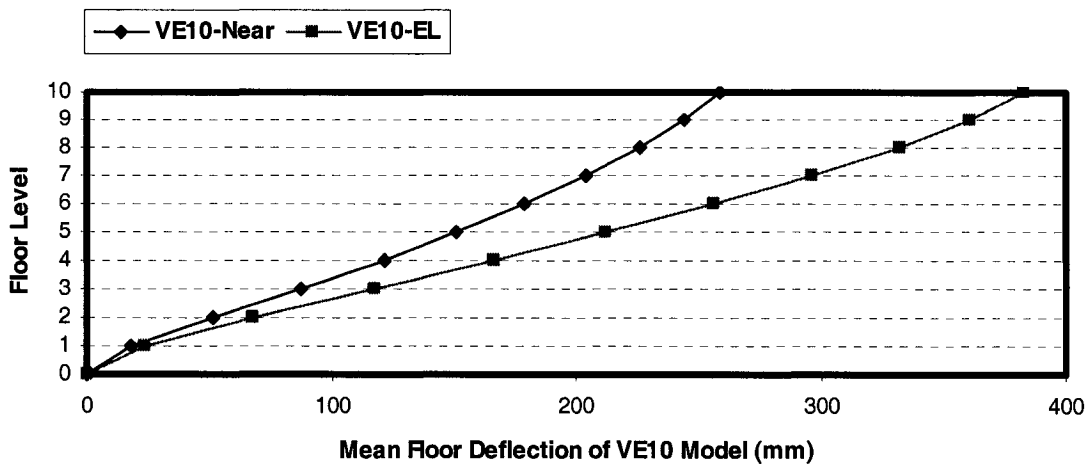

c.

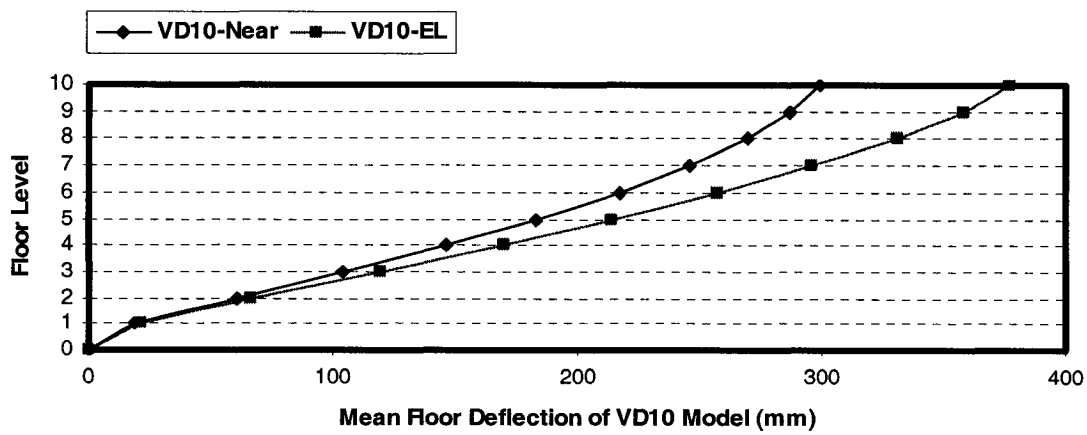

Fig. 5.20 Mean Floor Deflection of 10-Story Damped Model under 17 Near-Fault Earthquakes
a. FD10 Model b. VE10 Model c. VD10 Model

a.

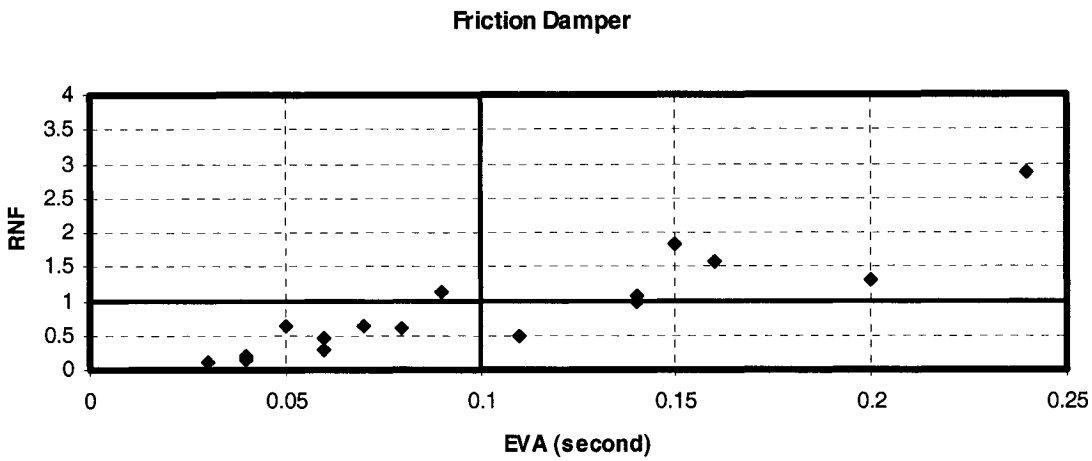

b.

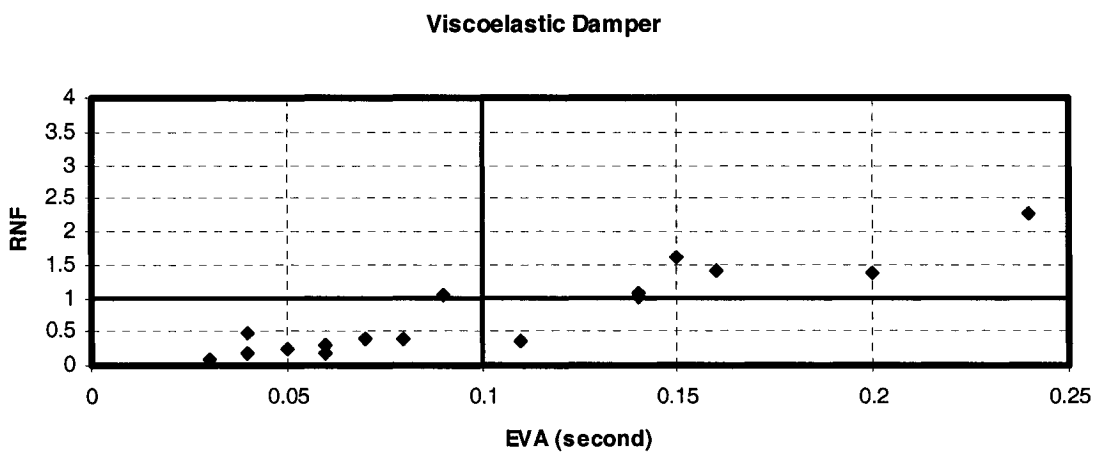

c.

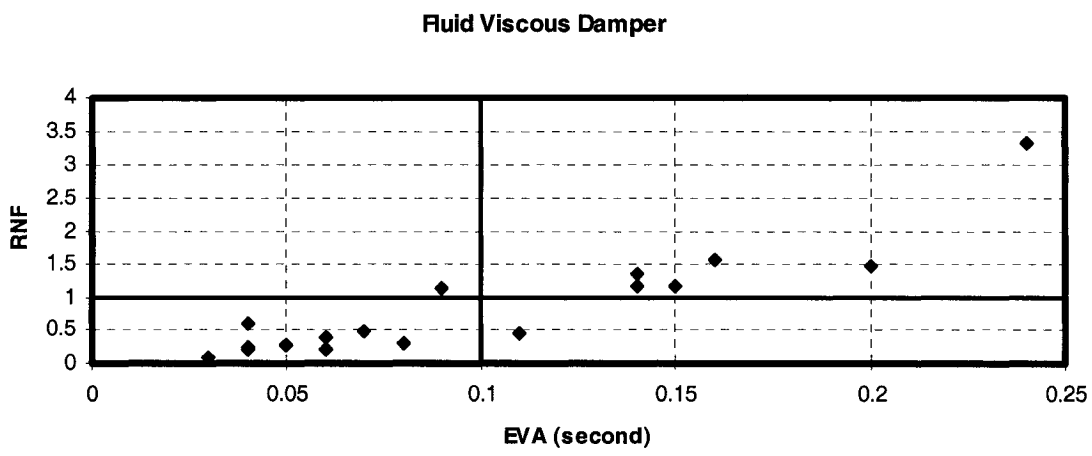

Fig. 5.21 Comparison of Roof Deflection under Near-Fault and Far-Fault Earthquakes a. FD10 Model b. VE10 Model c. VD10 Model

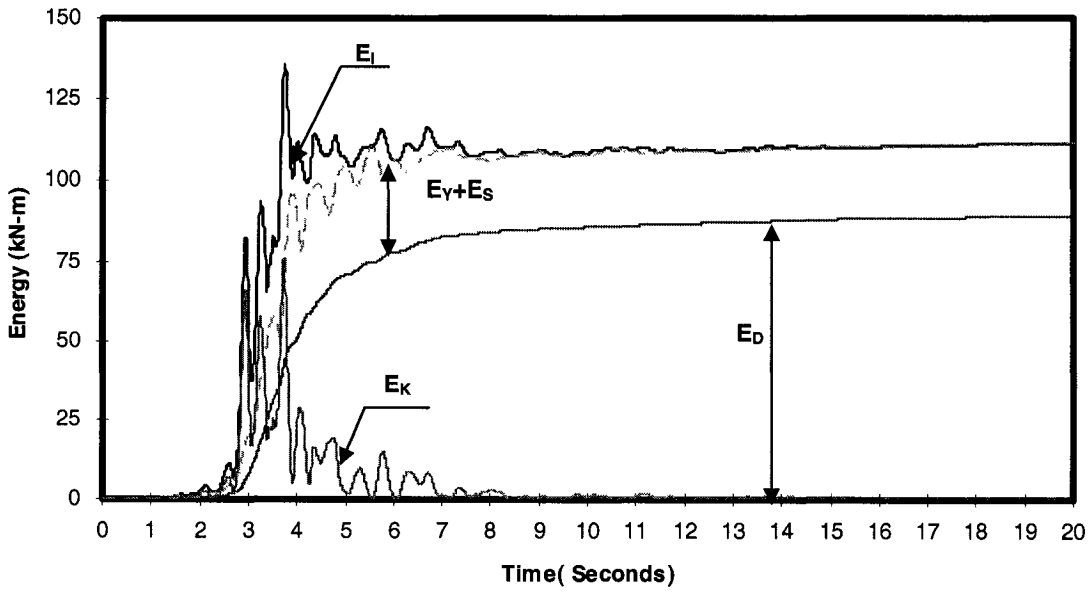

Fig. 5.22 Energy Time History of MRF10 Model to Coalinga270 Record
Note: E_I – Input Energy; E_k – Kinetic Energy; E_D – Damping Energy;
E_S – Strain Energy; E_Y – Yielding Energy

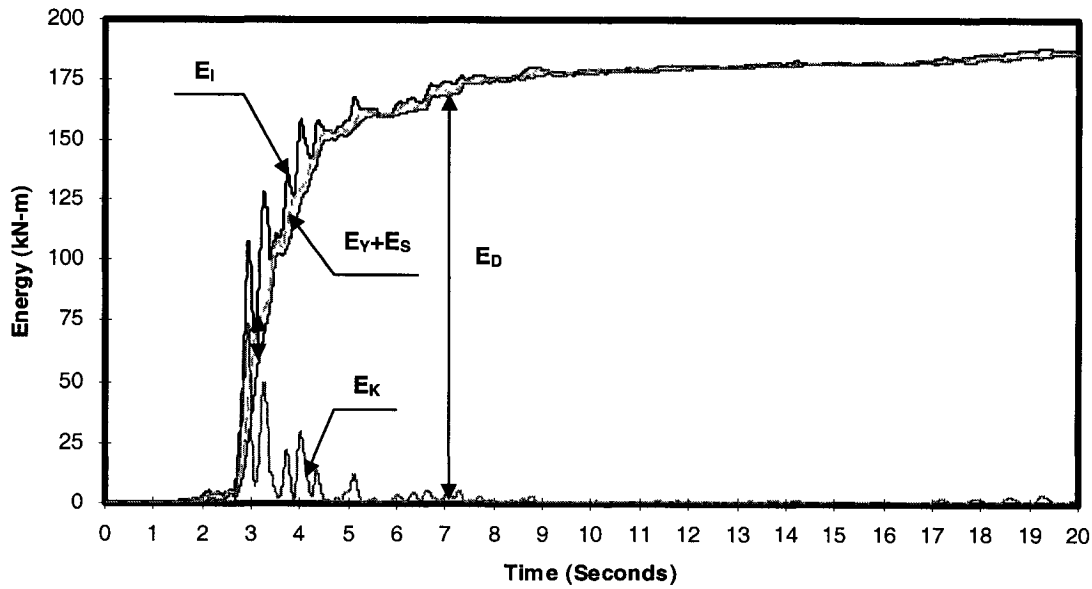

Fig. 5.23 Energy Time History of FD10 Model to Coalinga270 Record
Note: E_I – Input Energy; E_k – Kinetic Energy; E_D – Damper Energy;
E_S – Strain Energy; E_Y – Yielding Energy

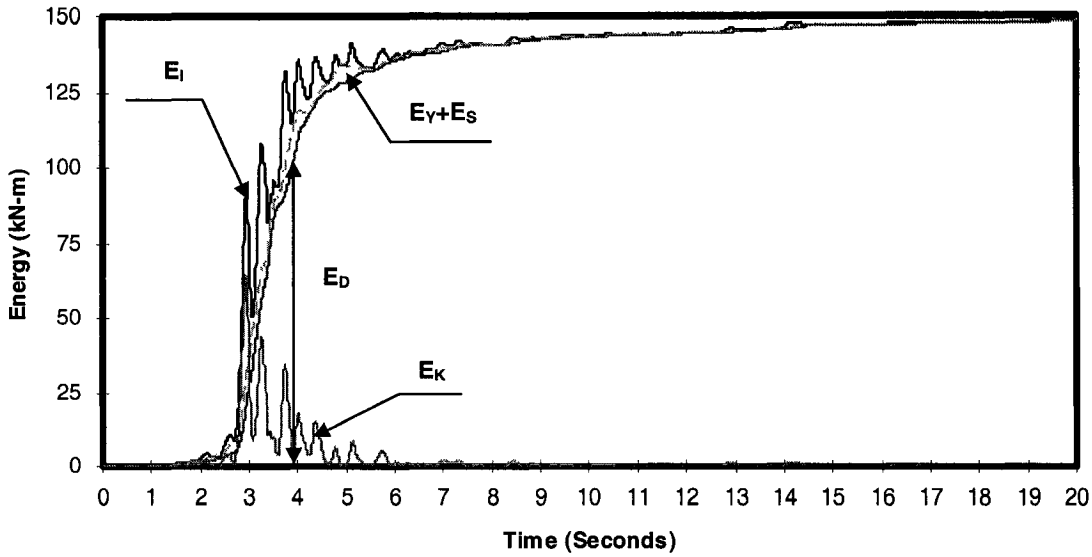

Fig. 5.24 Energy Time History of VE10 Model to Coalinga270 Record
Note: E_I – Input Energy; E_k – Kinetic Energy; E_D – Damper Energy;
E_S – Strain Energy; E_Y – Yielding Energy

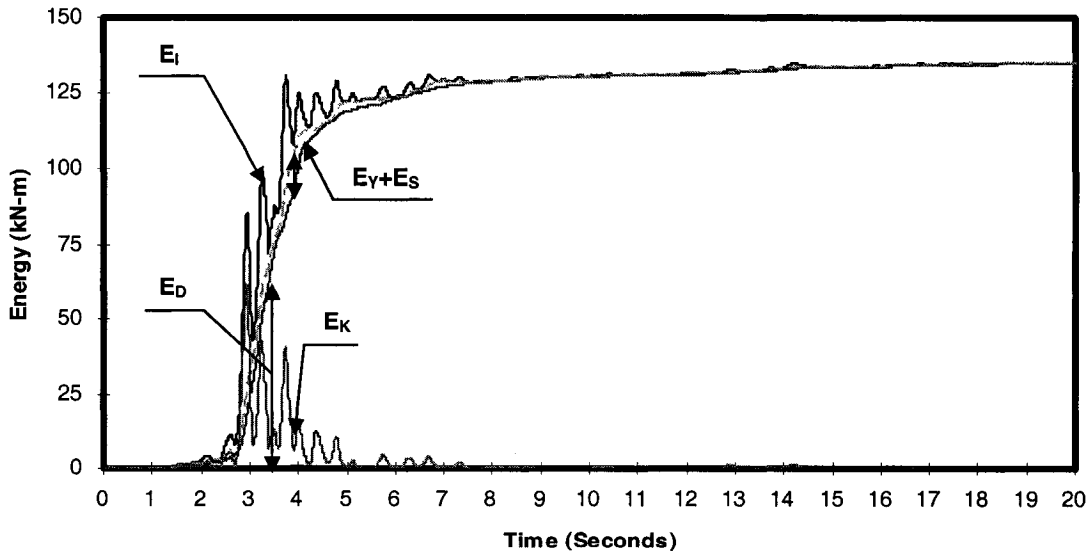

Fig. 5.25 Energy Time History of VD10 Model to Coalinga270 Record
Note: E_I – Input Energy; E_k – Kinetic Energy; E_D – Damper Energy;
E_S – Strain Energy; E_Y – Yielding Energy

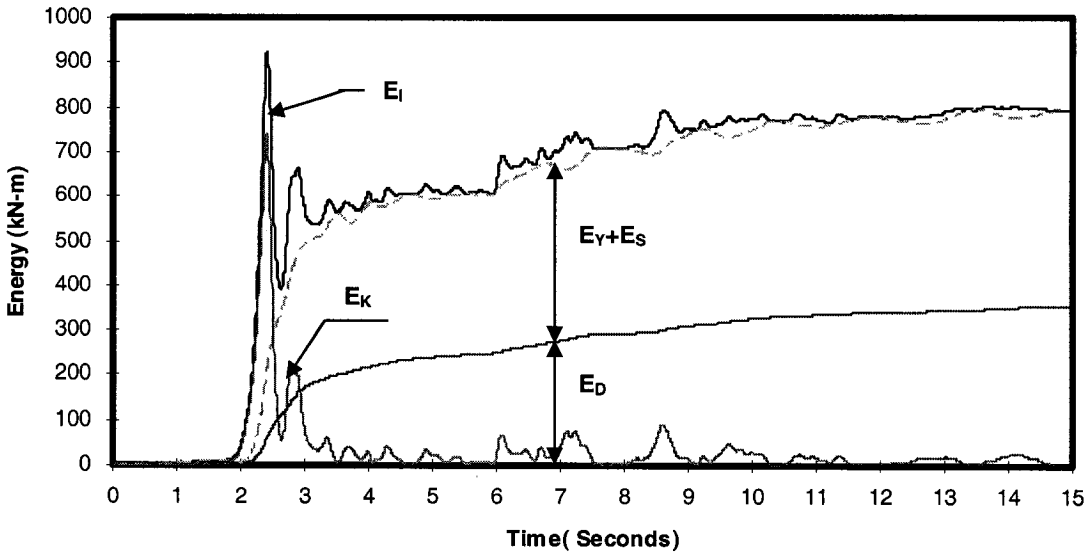

Fig. 5.26 Energy Time History of MRF10 Model to Northridge228 Record
Note: E_I – Input Energy; E_k – Kinetic Energy; E_D – Damping Energy;
E_S – Strain Energy; E_Y – Yielding Energy

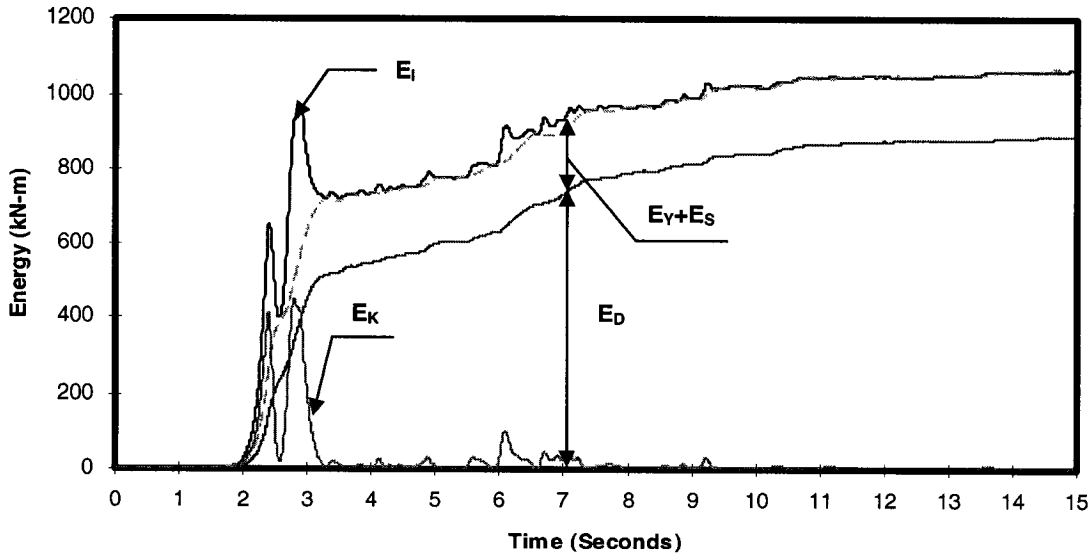

Fig. 5.27 Energy Time History of FD10 Model to Northridge228 Record
Note: E_I – Input Energy; E_k – Kinetic Energy; E_D – Damper Energy;
E_S – Strain Energy; E_Y – Yielding Energy

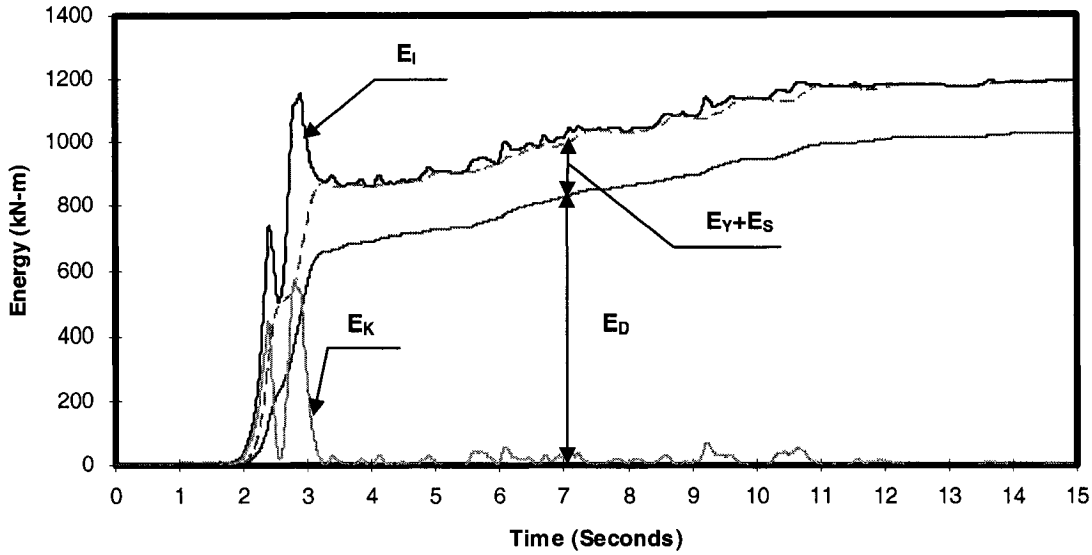

Fig. 5.28 Energy Time History of VE10 Model to Northridge228 Record
Note: E_I – Input Energy; E_k – Kinetic Energy; E_D – Damper Energy;
E_S – Strain Energy; E_Y – Yielding Energy

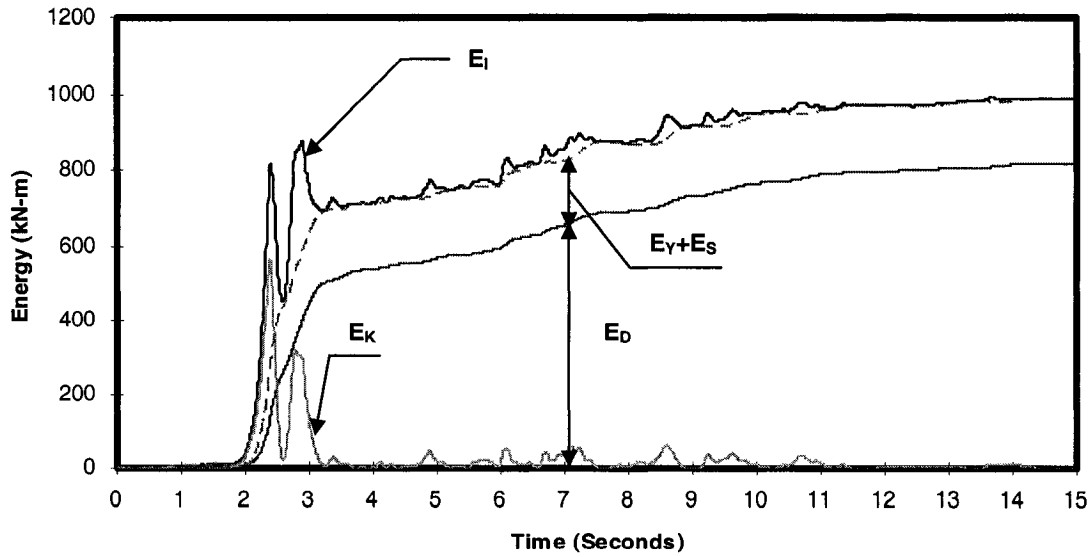

Fig. 5.29 Energy Time History of VD10 Model to Northridge228 Record
Note: E_I – Input Energy; E_k – Kinetic Energy; E_D – Damper Energy;
E_S – Strain Energy; E_Y – Yielding Energy

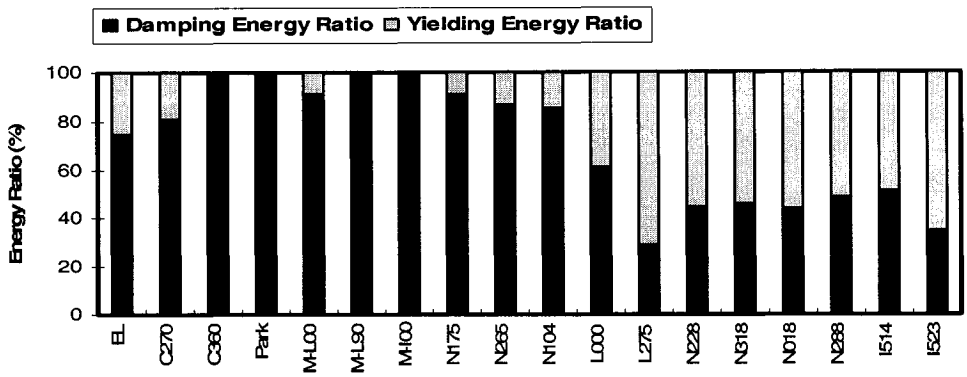

Fig. 5.30 Energy Ratio of MRF10 Model to Different Earthquakes (Evaluated at the end of the ground motion duration)

Damping Energy Ratio (%) = Damping Energy / Total Energy Input×100%
Yielding Energy Ratio (%) = Yielding Energy / Total Energy Input ×100%

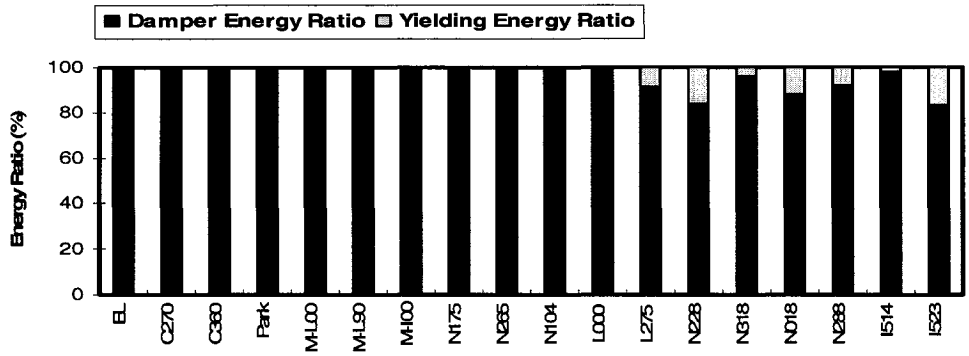

Fig. 5.31 Energy Ratio of FD10 Model to Different Earthquakes (Evaluated at the end of the ground motion duration)

Damper Energy Ratio (%) = Damper Energy / Total Energy Input ×100%
Yielding Energy Ratio (%) = Yielding Energy / Total Energy Input ×100%

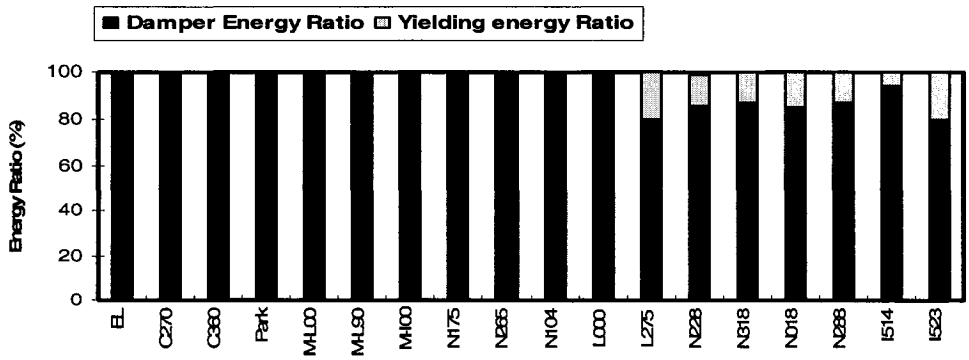

Fig. 5.32 Energy Ratio of VE10 Model to Different Earthquakes (Evaluated at the end of the ground motion duration)

Damper Energy Ratio (%) = Damper Energy / Total Energy Input ×100%
Yielding Energy Ratio (%) = Yielding Energy / Total Energy Input ×100%

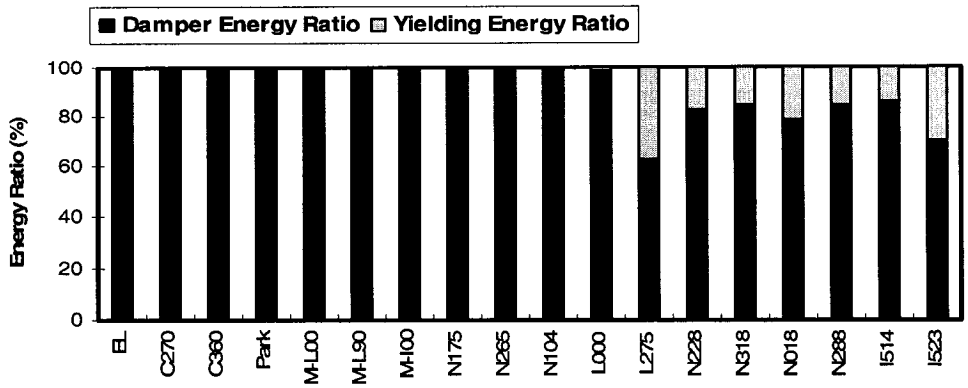

Fig. 5.33 Energy Ratio of VD10 Model for Different Earthquakes (Evaluated at the end of the ground motion duration)

Damper Energy Ratio (%) = Damper Energy / Total Energy Input $\times 100\%$

Yielding Energy Ratio (%) = Yielding Energy / Total Energy Input $\times 100\%$

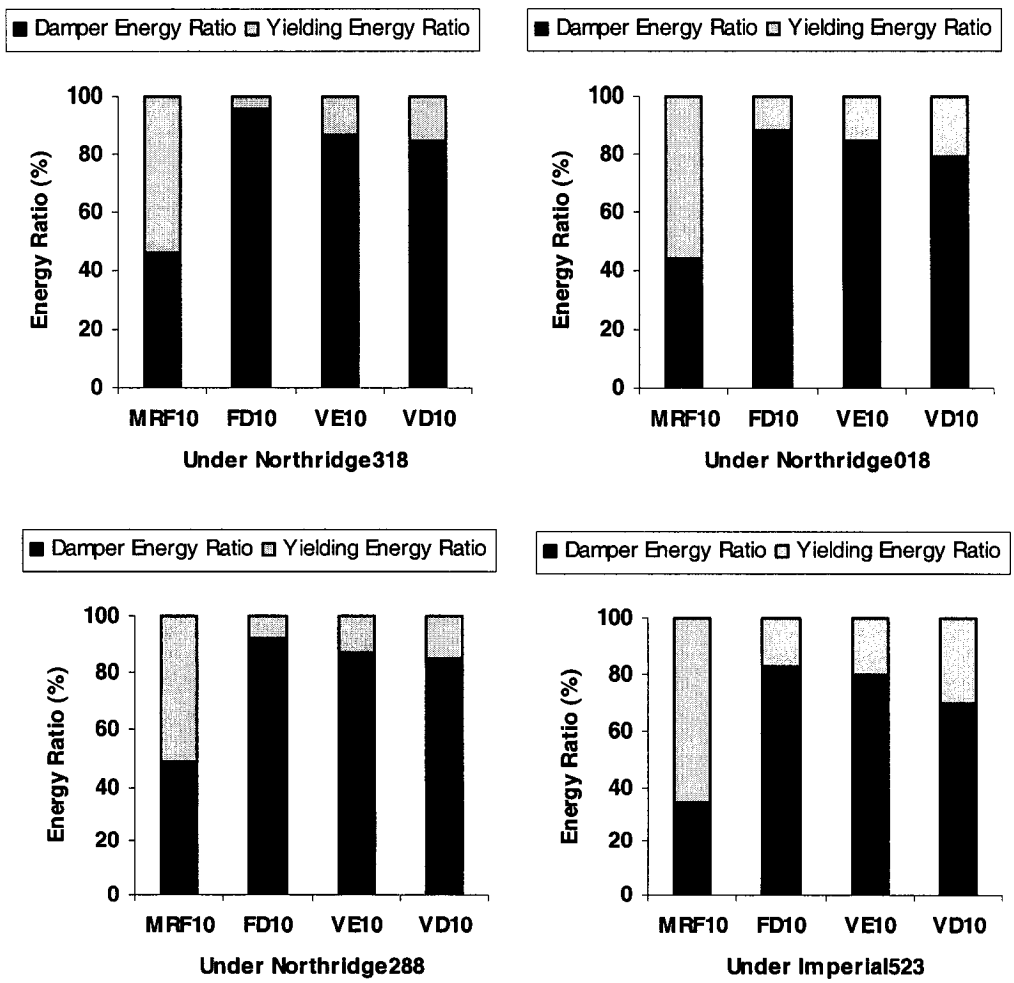

Fig. 5.34 Comparison of Energy Ratio for Different Damped Models

CHAPTER 6

CONCLUSIONS

6.1 CONCLUSIONS

As one of the natural hazards, the characteristics of earthquakes and dynamic responses of traditional frame systems have been studied by many researchers, especially for far-fault earthquakes. However, it is found that the damages due to near-fault earthquakes with pulse-type excitation seem more serious than those for far-fault earthquakes. On the other hand, as an alternative to reduce structural damage induced by ground motions, different types of dampers have also been proposed. The mechanism and effectiveness of dampers to mitigate the dynamic response of structures have been confirmed by large number of simulation tests and theoretical research. However, little research involves comparison of the dynamic response of structures to near-fault and far-fault earthquakes and the comparison of the effectiveness of different dampers. The objective of this thesis is to pay more attention to these two points.

In Chapter 4, using DRAIN-2DX program, dynamic responses of single-story, single-bay, single-degree-of-freedom frames with and without added friction damper, viscoelastic damper or fluid-viscous damper to near-fault and far-fault earthquakes are investigated. Dynamic response quantities such as floor displacements, moment in columns, column shear forces and energy time history are calculated and compared.

In Chapter 5, the dynamic response of single-bay, 10-story, multi-degree-of-freedom frames with and without added friction damper, viscoelastic damper or fluid-viscous damper to near-fault and far-fault earthquakes are studied. Structural response quantities of floor deflections, base shear force of columns, base moment of columns and energy time history are determined and compared. The DRAIN-2DX results are compared with those of dynamic analyses using SAP2000 program within the elastic state for details see Appendix C. It is found that close agreements are obtained between the two programs.

List of Assumption:

a. All the models with and without dampers have 5% inherent viscous damping;

b. All the dampers are distributed uniformly along the height of the building;

c. Only one far-fault earthquake record and 17 near-fault earthquake records are selected.

Based on selected near-fault and far-fault earthquakes and the assumption above, it is concluded that:

1. The structural dynamic responses of the model structures are quite complicated due to characteristics of different earthquakes, such as changes in frequency content, peak ground acceleration, peak ground velocity, peak ground displacement, pulse shape and overall duration of motion.
2. Although responses of different dampers are different under the same earthquake, all kinds of dampers being tested can be confirmed to reduce structural dynamic response effectively.
3. When compared with response to far-fault earthquake, the response of frames with added dampers to near-fault earthquakes with pulse-type excitation shows

similar response results. If a near-fault earthquake has high magnitude of pulse-type acceleration with relative small velocity, all kinds of dampers work better to near-fault earthquakes than to far-fault earthquakes. If a near-fault earthquake has relative high magnitude of pulse-type velocity compared with its acceleration, all kinds of damper work better under far-fault earthquakes than under near-fault earthquakes.

4. From a comparison of the energy time history for different dampers, it is found that the friction damper shows a more effective performance than the other two dampers based on the study of selected earthquake records.

6.2 RECOMMENDATIONS FOR FUTURE WORK

1. It is assumed that all dampers are uniformly distributed along the floor levels of the structure in the analysis. Optimum position of damper is neglected when comparing the effectiveness of dampers. However, it is an important factor and optimum position of the dampers can affect the structural response. Future work should consider the influence of this important factor.
2. Only linear fluid-viscous damper is considered due to restriction of the program. However, nonlinear fluid-viscous damper may be more effective than linear fluid-viscous damper. Therefore, it should be further considered in the future research.
3. The results obtained in this study are carried out under only one far-fault ground motion record. Therefore, more far-fault earthquake records are needed in the future research to compare different dynamic response under near-fault and far-fault earthquakes.

REFERENCE

1. Abrahamson, N. (2000). "Near-Fault Ground Motions from the 1999 Chi-Chi Earthquake", U.S.-Japan Workshop on the Effects of Near-Field Earthquakes Shaking, San Francisco, California.
2. Aiken, I. D., Kelly, M., and Mahmoodi, P. (1990). "The Application of Viscoelastic Dampers to Seismically Resistant Structures", Proceedings of Fourth U.S. National Conference on Earthquake Engineering, May20-24, 1990, Palm Springs, California.
3. Aiken, I. D., and Kelly, J. M. (1990). "Earthquake Simulator Testing and Analytical Studies of Two Energy-Absorbing Systems for Multistory Structures", EERC Report No. UCB03-90, Earthquake Engineering Research Center, University of California at Berkeley.
4. Aiken, I. D., Nims, D. K., Whittaker, A. S., and Kelly, J. M. (1993). "Testing of Passive Energy Dissipation Systems", Earthquake Spectra, Vol.9, No.3.
5. Aki, K. (1968). "Seismic Displacement near a Fault", Journal of Geophysical Research, Vol. 73, No. 16, pp.5359-5374.
6. Akkar, S., Yazgan, U. and Gulkan, P. (2005). "Drift Estimates in Frame Buildings Subjected to Near-Fault Ground Motions", Journal of Structural Engineering, Vol.131, No.7, pp.1014-1024.
7. Anderson, J. C., and Bertero, V. V. (1987). "Uncertainties in Establishing Design Earthquakes", Journal of Structural Engineering, Vol.113, No.8, pp.1709-1724.
8. Baktash, P. (1989). "Friction Damped Braced Frames", Ph.D. Thesis, Concordia University, Montreal.

9. Chang, K. C., Soong, T. T., and Oh, S. T. (1992). "Effect of Ambient Temperature on Viscoelastically Damped Structure", Journal of Structural Engineering, Vol.121, No.6, pp.1955-1974.

10. Chang, K. C., Soong, T. T., Oh, S. T., and Lai, M. L. (1995). "Seismic Behavior of Steel Frame with Added Viscoelastic Dampers", Journal of Structural Engineering, Vol.121, No.10, pp.1418-1426.

11. Chang, K. C., Chen, S. J., and Lai, M. L. (1996). "Inelastic Behavior of Steel Frames with Added Viscoelastic Dampers", Journal of Structural Engineering, Vol.122, No.10, pp.1178-1186.

12. Chang, K. C., and Lin, Y. Y. (2004). "Seismic Response of Full-Scale Structure with Added Viscoelastic Dampers", Journal of Structural Engineering, Vol.130, No.4, April, pp.600-608.

13. Chen, K. C., Huang, B. S., Wang, J. H., Huang, W. G., Chang, T. M., Hwang, R. D., Chiu, H. C. , and Tsai, C. C. P. (2001). "An Observation of Rupture Pulses of the 20 September 1999 Chi-Chi, Taiwan, Earthquake from Near-Field Seismograms", Bulletin of the Seismological Society of America, Vol. 91, No. 5, October.

14. Chopra, A. K., and Chintanapakdee, C. (2001). "Comparing Response of SDF Systems to Near-Fault and Far-Fault Earthquake Motions in the Context of Spectral Regions", Earthquake Engineering and Structural Dynamics, Vol.30, pp.1769-1789.

15. Chopra, A. K. (2001). "Dynamics of Structures: Theory and Applications to Earthquake Engineering", Prentice Hall: New Jersey.

16. Clough, R. W., and Penzien, J. (1993). "Dynamics of Structures", McGraw-Hill, Inc.

17. Colajanni, P., and Papia, M. (1995). "Seismic Response of Braced Frames with and without Friction Dampers", Engineering Structures, Vol.17, No.2, pp.129-140.

18. Colajanni, P., and Papia, M. (1997). "Hysteretic Behavior Characterization of Friction-Damped Braced Frames", Journal of Structural Engineering, Vol.123, No.8, pp.1020-1028.

19. Filiatrault, A., and Cherry, S. (1990). "Seismic Design Spectra for Friction-Damped Structures", Journal of Structural Engineering, Vol.116, No.5, pp.1334-1355.

20. Filiatrault, A. (2002). "Elements of Earthquake Engineering and Structural Dynamics", Second Edition, Polytechnic International Press.

21. Fu, Y., and Kasai, K. (1998). "Comparative Study of Frames Using Viscoelastic and Viscous Dampers", Journal of Structural Engineering, Vol.124, No.5, pp.513-522.

22. Gong, E. M. (2004). "Estimating Seismic Performance of Friction Damped Braced Frames by Pushover Analysis", M.A. Sc. Thesis, Concordia University, Montreal.

23. Hall, J. F. (1998). "Seismic Response of Steel Frame Buildings to Near-Source Ground Motions", Earthquake Engineering and Structural Dynamics, Vol.27, pp.1445-1464.

24. Kanitkar, R., Harms, M., Crosby, P., and Lai, M. L. (1998). "Seismic Retrofit of a Steel Moment Frame Structure Using Viscoelastic Dampers", ISET Journal of Earthquake Technology, Vol.35, No.4, pp.207-219.

25. Lai, M. L., Chang, K. C., and Soong, T. T. (1995). "Full-Scale Viscoelastically Damped Steel Frames", Journal of Structural Engineering, Vol.121, No.10, pp.1443-1447.

26. Levy, R., Marianchik, E., Rutenberg, A., and Segal, F. (2001). "A Simple Approach to the Seismic Design of Friction Damped Braced Medium-Rise Frames", Engineering Structures, Vol.23, pp.250-259.

27. Li, Y. and Mau, S. T. (1997). "Learning from Recorded Earthquake Motion of Buildings", Journal of Structural Engineering, Vol. 123, No.1, pp.62-69.

28. Lin, W. H., and Chopra, A. K. (2001). "Understanding and Predicting Effects of Supplemental Viscous Damping on Seismic Response of Asymmetric One-story Systems", Earthquake Engineering and Structural Dynamics, Vol.30, pp.1475-1494.

29. Lin, W. H., and Chopra, A. K. (2002). "Earthquake Response of Elastic SDOF Systems with Non-Linear Fluid Viscous Dampers", Earthquake Engineering and Structural Dynamics, Vol.31, pp.1623-1642.

30. Loh, C. H., Wan, S. and Liao, W. I. (2002). "Effects of Hysteretic Model on Seismic Demands: Consideration of Near-Fault Ground Motions", the Structural Design of Tall Buildings, Vol.11, pp.155-169.

31. MacRac, G. A., Morrow, D. V., and Roeder, C. W. (2001). "Near-Fault Ground Motion Effects on Simple Structures", Journal of Structural Engineering, Vol.127, No.9, pp.996-1004.

32. Mahmoodi, P. (1969). "Structural Dampers", Journal of the Structural Division, Vol.95, No.ST8, pp.1661-1672.

33. Makris, N., and Roussos, Y. S. (2000). "Rocking Response of Rigid Blocks under Near-Source Ground motions", Geotechnique 50, No.3, pp.243-262.

34. Makris, N., and Black, C. J. (2004). "Evaluation of Peak Ground Velocity as a 'Good' Intensity Measure for Near-Source Ground Motions", Journal of Engineering Mechanics, Vol.130, No.9, pp.1032-1044.

35. Malhotra, P. K. (1999). "Response of Building to Near-Fault Pulse-Like Ground Motions", Earthquake Engineering and Structural Dynamics, Vol.28, pp.1309-1326.

36. Min, K. W., Kim, J., and Lee, S. H. (2004). "Vibration Tests of 5-Story Steel Frame with Viscoelastic Dampers", Engineering Structures, Vol.26, pp.831-839.

37. Naeim, F., and Rhaman, M. A. (2000). "Structures 2000: Advanced Technology in Structural Engineering", Structures Congress 2000, Philadelphia, Pennsylvania, USA.

38. Onishi, Y., Horike, M., and Kawamoto, Y. (2004). "A Method for Simulating Three-Component, Near-Fault, Strong Ground Motions Using stochastic Green's Function", 13th World Conference on Earthquake Engineering, August 1-6, Vancouver, B.C., Canada

39. Pall, A. S., and Marsh, C. (1982). "Response of Friction Damped Braced Frames", ASCE, Journal of the Structural Division, Vol.108, No.ST6, pp.1313-1323.

40. Pekcan, G., Mander, J. B., and Chen, S. S. (1999). "Fundamental Considerations for the Design of Non-Linear Viscous Dampers", Earthquake Engineering and Structural Dynamics, Vol.28, pp.1405-1425.

41. Powell, G. H. (1993). "DRAIN-2DX Element Description and User Guide for Element Type01, Type02, Type04, Type06, Type09, and Type15", Department of Civil Engineering University of California Berkeley, California.

42. Prakash, V., Powell, G. H., and Campbell, S. (1993). "DRAIN-2DX Base Program Description and User Guide", Department of Civil Engineering University of California Berkeley, California.

43. Roberts, M. W., and Lutes, L. D. (2003). "Potential for Structural Failure in the Seismic Near Field", Journal of Engineering Mechanics, Vol.129, No.8, pp.927-934.

44. SAP2000 (1999). "Getting Started, Basic Analysis Reference, Tutorial Manuals", Integrated Finite Element Analysis and Design of Structures, Computers and Structures, Inc., California, USA.

45. SAP2000 (1999). "Analysis Reference", Integrated Finite Element Analysis and Design of Structures, Computers and Structures, Inc., California, USA.

46. Shen, K. L., Soong, T. T., Chang, K. C., and Lai, M. L. (1995). "Seismic Behaviour of Reinforced Concrete Frame with Added Viscoelastic Dampers", Engineering Structures, Vol.17, No.5, pp.372-380.

47. Shen, K. L., and Soong, T. T. (1995). "Modeling of Viscoelastic Dampers for Structural Applications", Journal of Structural Engineering, Vol.121, No.6, pp.694-701.

48. Soong, T. T., and Costantinou, M. C. (1994). "Passive and Active Structural Vibration Control in Civil Engineering", Springer-Verlag Wien, New York.

49. Soong, T. T., and Lai, M. L. (1991). "Correlation of Experimental Results with Predictions of Viscoelastic Damping of a Model Structure", Proceedings of Damping '91, Air Force Systems Command, Wright-Patterson Air Force Base, Ohio.

50. Symans, M. D., and Constantinou, M. C. (1998). "Passive Fluid Viscous Damping Systems for Seismic Energy Dissipation", ISET Journal of Earthquake Technology, Vol.35, No.4, pp.185-206.

51. Tan, M. H. (1992). "A Study on Friction-Damped-Frames", M.A. Sc. Thesis, Concordia University, Montreal.

52. Tezcan, S. S., and Uluca, O. (2003). "Reduction of Earthquake Response of Plane Frame Buildings by Viscoelastic Dampers", Engineering Structures, Vol.25, pp.1755-1761.

53. Tremblay, R., Filiatrault, A., and Kremmidas, S. (1998). "Near Field Seismic Response of Steel Moment Resisting Frame Retrofitted with Passive Friction Energy Dissipating Systems", ISET Journal of Earthquake Technology, Vol.35, No.4, pp.243-262.

54. Uang, C. M., and Bertero, V. V. (1990). "Evaluation of Seismic Energy in Structures", Earthquake Engineering and Structural Dynamics, Vol.19, pp.77-90.

55. Zhang, R. H., Soong, T. T., and Mahmoodi, P. (1989). "Seismic Response of Steel Frame Structures with Added Viscoelastic Dampers", Earthquake Engineering and Structural Dynamics, Vol.18, pp.389-396.

56. PEER Strong Motion Databases download from http://peer.berkeley.edu/smcat.

APPENDIX A

Application of the Modal Strain Energy Method in Viscoelastic Damper

A.1 Introduction

Experimental studies on mechanical properties of viscoelastic materials have been extensively carried out over the past twenty years by many researchers. Due to the fact that viscoelastic materials are sensitive to many factors such as environmental temperature, load frequency and amplitude of material strain, thus it is difficult to set up an accurate analytical model to simulate and analyze the behaviors of viscoelastic materials. Similar to the evaluation of the effect of complicated inherent structural damping, an energy method to determine the equivalent viscous damping ratio is needed to evaluate the effect of viscoelastic damping.

In the analysis of structural dynamics, modal analysis techniques have been widely used for linear behavior of multi-degree-of-freedom structures. Commonly, the total structural response is a combination of a finite number of uncoupled modal responses, which has been confirmed to be a very efficient and relatively accurate approach to solve dynamic problems.

In the early research of VE dampers, researchers paid more attention to the elastic behavior of viscoelastic-damped structures and found that the behavior of a VE damper also is quite linear; therefore, based on the concept of modal analysis, corresponding to

modal damping ratio, [Soong and Lai, 1991; Chang et al., 1992] applied the method of modal strain energy to comprehensively account for the effect of viscoelastic materials, which are affected by many factors. Later, this approximate method was further confirmed to be valid to predict the equivalent damping ratio of viscoelastic-damped structures [Zhang and Soong, 1989; Lai et al., 1995; Chang and Lin, 2004]. Through experiment of a 2/5-scale three-story model with added VE damper, Chang et al. [1995] found that the modal strain energy method was also validity to analyze the inelastic dynamic response of structures with added VE damper under strong ground motions.

A.2 Modal Strain Energy Method

Usually, equivalent viscous damping ratio of a SDOF system can be expressed as follows: [Chopra, 2001]

$$\zeta = \frac{1}{4\pi} \times \frac{E_d}{E_s} \tag{A1.1}$$

where E_d is energy dissipated by damping, E_s is strain energy of system. The formula (A1.1) is extended to a MDOF system by considering ζ as a modal damping ratio as follows:

$$\zeta_i = \frac{1}{4\pi} \times \frac{E_d^i}{E_s^i} \tag{A1.2}$$

where E_d^i is dissipated energy of *ith* mode by damping, E_s^i is maximum strain energy of system for *ith* mode. The relationship between damping energy and strain energy of the system is $E_d^i = 2\pi\eta_i E_s^i$ [Chopra, 2001], therefore, formula (A1.2) rewrites as follows:

$$\zeta_i = \frac{1}{4\pi} \times \frac{E_d^i}{E_s^i} = \frac{1}{4\pi} \times \frac{2\pi\eta_i E_s^i}{E_s^i} = \frac{\eta_i}{2} \tag{A1.3}$$

where η_i is loss factor of *ith* mode, which has the following relationship [Min et al., 2004]: $\eta_i = \frac{\phi_i^T K_I \phi_i}{\phi_i^T K_R \phi_i}$, for a viscoelastic damper and brace combined element. Its stiffness is complex, hence, $K_R = K_{frame} + K_{VED}$ and $K_I = \eta_{VE} K_{VED}$ refer to the real part and imaginary part of the complex stiffness matrix, respectively; K_{frame} is the stiffness matrix of system without VE damper; K_{VED} is the stiffness matrix of the system contributed only by VE damper; η_{VE} is loss factor of viscoelastic material and ϕ_i is *ith* mode shape vector. Therefore, for a viscoelastic-damped model, its equivalent viscous modal damping ratio can be developed as follows:

$$\zeta_i = \frac{1}{2} \times \frac{\phi_i^T K_I \phi_i}{\phi_i^T K_R \phi_i} = \frac{1}{2} \times \frac{\phi_i^T (\eta_{VE} K_{VED}) \phi_i}{\phi_i^T (K_{frame} + K_{VED}) \phi_i} = \frac{\eta_{VE}}{2} \times \frac{\phi_i^T (K_R - K_{frame}) \phi_i}{\phi_i^T (K_{frame} + K_{VED}) \phi_i}$$

$$= \frac{\eta_{VE}}{2} \times \left[1 - \frac{\phi_i^T K_{frame} \phi_i}{\phi_i^T (K_{frame} + K_{VED}) \phi_i} \right] = \frac{\eta_{VE}}{2} \times \left[1 - \frac{\phi_i^T K_{frame} \phi_i}{\phi_i^T K_{VE} \phi_i} \right] \tag{A1.4}$$

where K_{VE} is stiffness matrix of system with added VE damper.

A.3 Determination of Viscoelastic Damper Design Curve

From above formula (A1.4), the purpose of using modal strain energy method is to determine a relationship between viscoelastic damping ratio and equivalent stiffness of combined damper-brace element since the stiffness matrix of viscoelastic materials and systems are relatively easy to obtain. According to Formula (A1.4), a loss factor

$\eta_{VE} = 0.9$ is defined. The later stiffness matrix of the system with and without VE damper can be determined by the following conventional procedure: 1. Determination of lateral flexibility matrix of a system by using a unit lateral load applied at each story. 2. Determination of lateral stiffness matrix of a system by inverting lateral flexibility matrix. Therefore, different structures should have different VE damper design curves. In order to analyze the dynamic response of a one-bay, ten-story viscoelastic-damped model, two VE damper design curves, as shown in Fig. A.1 and Fig. A.2, are formed. Fig. A.2 is especially suitable for DRAIN-2DX program, and the other Fig. A.1 is suitable for general programs.

The following shows how to obtain a value in the plot of the VE damping ratio versus equivalent stiffness of VE-damped brace element.

Step 1: Determination of the lateral stiffness matrix K_{frame} without damper, detailed as shown as Table A.1.

Step 2: Assumption of equivalent axial area of VE damper-brace element $A_{eq} = 298mm^2$.

Step 3: Determination of the lateral stiffness matrix K_{VE} with VE damper, detailed as shown as Table A.1.

Step 4: Determination of first mode shape vector

$$\phi_1 = [0.05 \quad 0.15 \quad 0.27 \quad 0.40 \quad 0.52 \quad 0.64 \quad 0.76 \quad 0.86 \quad 0.94 \quad 1.00]$$

Step 5: Determination of damping ratio

$$\zeta_1 = \frac{\eta_{VE}}{2} \times \left[1 - \frac{\phi_1^T K_{frame} \phi_1}{\phi_1^T K_{VE} \phi_1} \right] = \frac{0.9}{2} \times \frac{922.7}{1384.0} \approx 0.15$$

Table A.1 Stiffness Matrix of Model with and without VE damper

$$K_{frame} = \begin{bmatrix} 1.2e5 & -6.0e4 & 1.4e4 & 692.2 & -1743 & 327.5 & -164.1 & 169.5 & -14.2 & 62.5 \\ -6.0e4 & 7.7e4 & -4.4e4 & 7084 & 1533 & -211.6 & -72.9 & -33.0 & -8.5 & -54.0 \\ 1.4e4 & -4.4e4 & 6.4e4 & -3.9e4 & 8693 & -1236 & 346.2 & 13.5 & -103.8 & 160.1 \\ 692.2 & 7084 & -3.9e4 & 6.3e4 & -4.0e4 & 8741 & -867.6 & -376.3 & 556.7 & -229 \\ -1743 & 1533 & 8693 & -4.0e4 & 5.6e4 & -3.2e4 & 6994 & 51.0 & -909.3 & 406 \\ 327.5 & -211.6 & -1236 & 8741 & -3.2e4 & 4.8e4 & -2.8e4 & 5104 & 221.5 & -286.8 \\ -164.1 & -72.9 & 346.2 & -867.6 & 6994 & -2.8e4 & 3.9e4 & -2.1e4 & 3824 & -134.8 \\ 169.5 & -33.0 & 13.5 & -376.3 & 51.0 & 5104 & -2.1e4 & 3.2e4 & -1.8e4 & 2750 \\ -14.2 & -8.5 & -103.8 & 556.7 & -909.3 & 221.5 & 3824 & -1.8e4 & 2.6e4 & -1.1e4 \\ 62.5 & -54.0 & 160.1 & -229 & 406 & -286.8 & -134.8 & 2750 & -1.1e4 & 8473 \end{bmatrix}$$

$$K_{VE} = \begin{bmatrix} 1.3e5 & -6.1e4 & 1.4e4 & -2587 & 1024 & -587.1 & 261.4 & -273 & 274.1 & -43.9 \\ -6.1e4 & 8.7e4 & -5.4e4 & 1.5e4 & -4337 & 1767 & -395.7 & 87.5 & -250.8 & 243 \\ 1.4e4 & -5.4e4 & 8.5e4 & -5.5e4 & 1.4e4 & -2753 & 163.3 & 184 & 598.9 & -449.9 \\ -2587 & 1.5e4 & -5.5e4 & 8.0e4 & -4.6e4 & 7835 & 202.4 & -1046 & -228.9 & 700.9 \\ 1024 & -4337 & 1.4e4 & -4.6e4 & 6.5e4 & -3.6e4 & 5178 & 1565 & -1190 & 157.9 \\ -587.1 & 1767 & -2753 & 7835 & -3.6e4 & 5.7e4 & -3.2e4 & 3292 & 872.2 & -219.5 \\ 261.4 & -395.7 & 163.3 & 202.4 & 5178 & -3.2e4 & 4.9e4 & -2.6e4 & 3743 & -298.9 \\ -273 & 87.5 & 184 & -1046 & 1565 & 3292 & -2.6e4 & 4.3e4 & -2.4e4 & 2866 \\ 274.1 & -250.8 & 598.9 & -228.9 & -1190 & 872.2 & 3743 & -2.4e4 & 3.7e4 & -1.7e4 \\ -43.9 & 243 & -449.9 & 700.9 & 157.9 & -219.5 & -298.9 & 2866 & -1.7e4 & 1.4e4 \end{bmatrix}$$

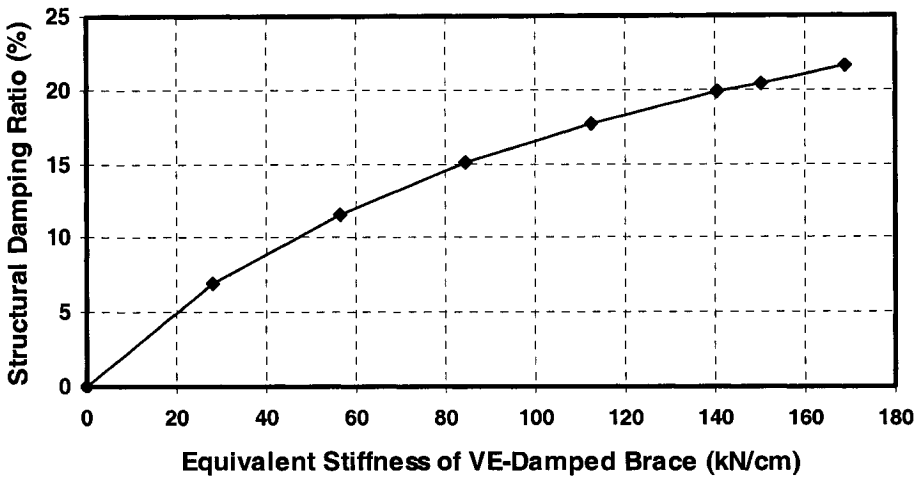

Fig. A.1 Viscoelastic Damper Design Curve 1 for a 10-story Frame (It can be used to determinate the dimension of VE damper)

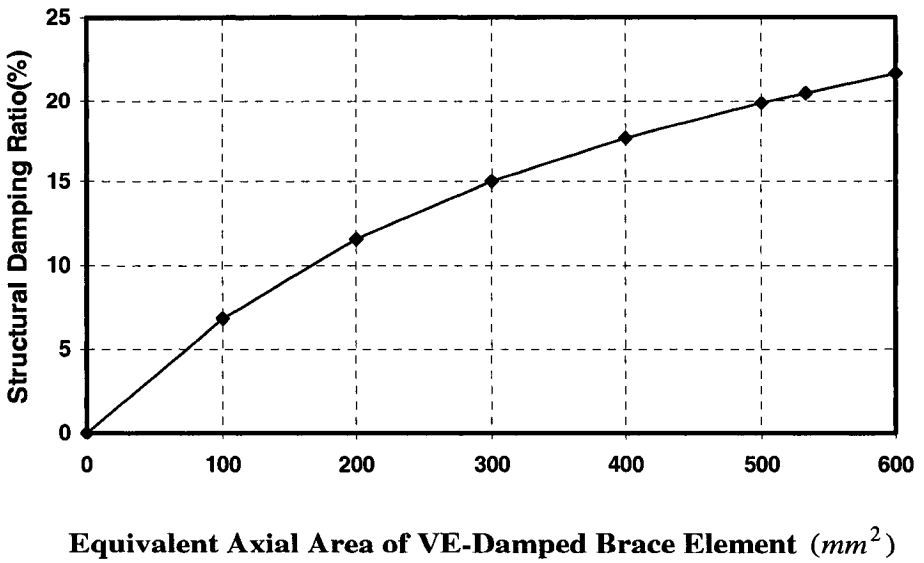

Fig. A.2 Viscoelastic Damper Design Curve 2 for a 10-story Frame (It is suitable for model analysis using Drain-2DX program)

APPENDIX B

Application of Energy Balance Equation in Seismic-Resistance Analysis

B.1 Introduction

The same as with solving equation of motion to study dynamic response quantities of systems, it is necessary to set up the energy balance equation to investigate the energy-dissipation ability of added damping and compare the effectiveness of different dampers from the energy point of view. Usually, for a specified system, its energy equation can be derived from its equation of motion. In the following, we take an inelastic SDOF system for example to discuss its energy mechanism.

B.2 Energy Balance Equation

The equation of motion of an inelastic SDOF system can be expressed as follows:

$$m\ddot{u}(t)+c\dot{u}(t)+f_s(u,\dot{u})=-m\ddot{u}_g(t) \tag{B.1}$$

The energy balance equation can be set up by integrating the forces in each term of Equation (B.1) through the distance du, moved in each time step and shown as follows:

$$\int m\ddot{u}(t)du+\int c\dot{u}(t)du+\int f_s(u,\dot{u})du=-\int m\ddot{u}_g(t)du \tag{B.2}$$

The first term on the left side of above Equation (B.2) is the kinetic energy $E_k(t)$ of mass associated with motion relative to the ground:

$$E_k(t)=\int m\ddot{u}(t)du=\int m\frac{d\dot{u}(t)}{dt}du=\int m\dot{u}(t)d\dot{u}=\frac{1}{2}m\dot{u}(t)^2 \tag{B.3}$$

The second term in Equation (B.2) is the damping energy $E_D(t)$:

$$E_D(t) = \int c\dot{u}(t)du = \int c\dot{u}(t)\cdot(\dot{u}\,dt) = \int c\dot{u}(t)^2 dt \tag{B.4}$$

The third term on the left side of Equation (B.2) is the sum of the energy absorbed as recoverable elastic strain energy $E_s(t)$ and the energy dissipated by irrecoverable yielding energy $E_Y(t)$:

$$E_s(t) + E_Y(t) = \int f_s(u,\dot{u})du = \int f_s(u,\dot{u})\cdot\dot{u}\,dt \tag{B.5}$$

and $$E_s(t) = \int f_s(t)du = \int k\,u(t)du = \frac{1}{2}k\cdot u(t)^2 = \frac{k}{2}\cdot\left[\frac{f_s(t)}{k}\right]^2 = \frac{f_s(t)^2}{2k} \tag{B.6}$$

$$E_Y(t) = \int f_s(u,\dot{u})du - E_s(t) \tag{B.7}$$

The term on the right side of Equation (B.2) is the input energy $E_I(t)$:

$$E_I(t) = -\int m\ddot{u}_g(t)du \tag{B.8}$$

Then, the energy equation of an inelastic SDOF system is set up as follows:

$$E_I(t) = E_k(t) + E_D(t) + E_s(t) + E_Y(t) \tag{B.9}$$

Equation (B.9) clearly indicates that the internal energy is composite of four parts: kinetic energy, damping energy, elastic strain energy and yielding energy. The total input energy is absorbed in the form of the kinetic energy and recoverable strain energy, and dissipated in the form of damping energy and yielding energy. Therefore, if incorporating additional damper, the damping energy will increase and other three types of energy will reduce correspondingly to meet principal of conservation of energy. The dynamic response of systems will reduce, which is the purpose of application of dampers.

APPENDIX C

Comparison with Models of SAP2000

C.1 STRUCTURAL MODELS OF SAP2000

In order to check the correctness of dynamic response of models using the DRAIN-2DX program, the SAP2000 program of three dimensional static and dynamic finite element analysis and design of structures is used to set up the same MDOF structural models with and without damper. However, in SAP2000 software only performs linear elastic analysis with definition of some special nonlinear elements. Conventional beam-column elements always remain elastic limit during the analysis. Therefore, only dynamic responses within the elastic state of two programs are selected to compare.

C.1.1 Model of Moment Resistant Frame

The basic material and cross section of the beam-column element are the same as the friction-damped model defined by Drain-2DX program. The modal damping ratios defined in the SAP2000 program are also the same as these calculated in the DRAIN-2DX program.

C.1.2 Model of Friction-Damped Frame

The basic material and cross section properties of the beam-column element are the same as for the friction-damped model defined by Drain-2DX program.

Model of friction damper: Friction dampers are modeled as ideal elastic-plastic elements.

C.1.3 Model of Viscoelastic-Damped Frame

The basic material and cross section of beam-column element are the same as the viscoelastic-damped model defined by Drain-2DX program.

Model of viscoelastic damper: Viscoelastic dampers are modeled as damper elements.

According to definition of cross section A of viscoelastic-damped brace element in Drain-2DX program, corresponding stiffness of viscoelastic-damped brace element is:

$A = 2.98 \times 10^{-4} m^2$, definition of stiffness $K = \frac{EA}{L} = 8377 kN/m$, damping $C = \beta K = 3517 kN/m$.

C.1.4 Model of Fluid-Viscous-Damped Frame

The basic material and cross section of beam-column element are the same as fluid-viscous-damped model defined by Drain-2DX program.

Model of fluid-viscous damper: Fluid viscous dampers are modeled as damper elements.

Effective stiffness of fluid-viscous damper element is zero, damping $C = \beta K = 2321 kN/m$.

C.2 COMPARISON OF MODEL

C.2.1 Comparison of Structural Period

Table c.1 clearly shows the structural period of model of Drain-2DX and model of SAP2000. For the same type of structure, the two models show almost the same period.

C.2.2 Comparison of Structural Floor Deflection Using Two Programs

Figs. C.1~C.4 show the structural response of floor deflection of the two models to El-Centro earthquake. It is found that the dynamic responses of two models are close.

It is confirmed that the calculating results using Drain-2DX are correct and can be reasonably extended to inelastic analysis, where SAP2000 program is not applicable.

Table c.1 Comparison of Periods of the MDOF Systems

MRF10		FD10		VE10		VD10	
PERIOD (sec)		PERIOD (sec)		PERIOD (sec)		PERIOD (sec)	
DRAIN-2DX	**SAP2000**	**DRAIN-2DX**	**SAP2000**	**DRAIN-2DX**	**SAP2000**	**DRAIN-2DX**	**SAP2000**
3.270	3.271	1.467	1.467	2.666	2.666	3.270	3.271
1.118	1.118	0.429	0.429	0.893	0.893	1.118	1.118
0.626	0.626	0.225	0.225	0.502	0.502	0.626	0.626
0.427	0.428	0.157	0.157	0.350	0.350	0.427	0.428
0.317	0.317	0.123	0.123	0.267	0.267	0.317	0.317
0.243	0.243	0.103	0.103	0.211	0.211	0.243	0.243
0.200	0.200	0.090	0.090	0.178	0.178	0.200	0.200
0.166	0.166	0.082	0.082	0.151	0.152	0.166	0.166
0.137	0.137	0.077	0.077	0.128	0.128	0.137	0.137
0.115	0.115	0.071	0.071	0.110	0.110	0.115	0.115

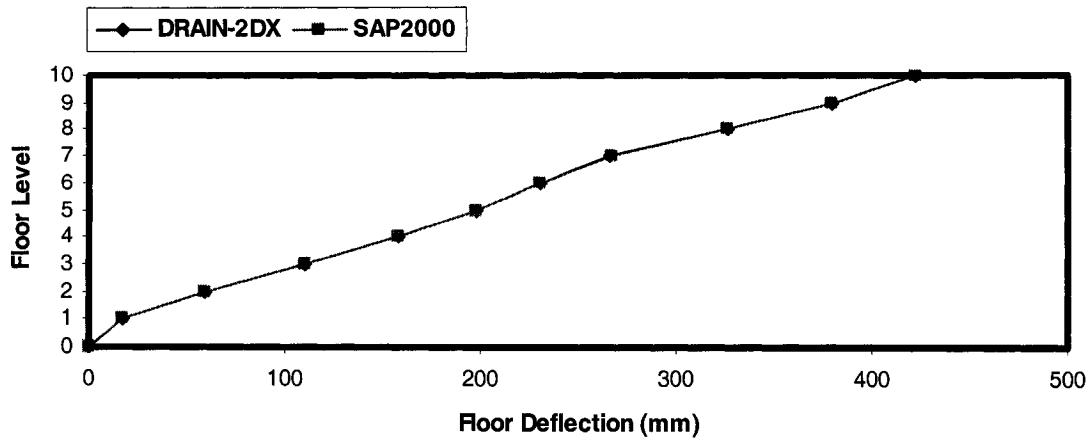

Fig. C.1 Comparison of Floor Deflections of Moment Resistant Frame Model to El-Centro earthquake

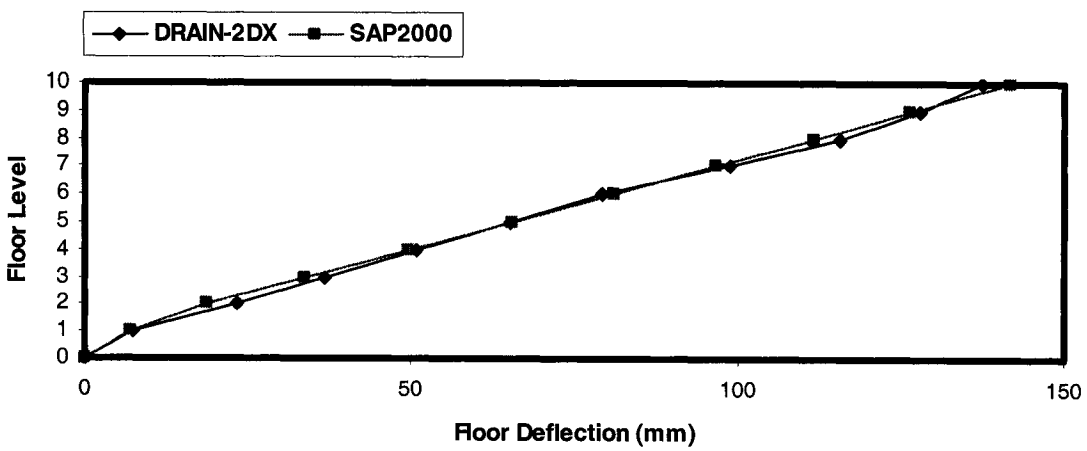

Fig. C.2 Comparison of Floor Deflections of Friction-Damped Model to El-Centro earthquake

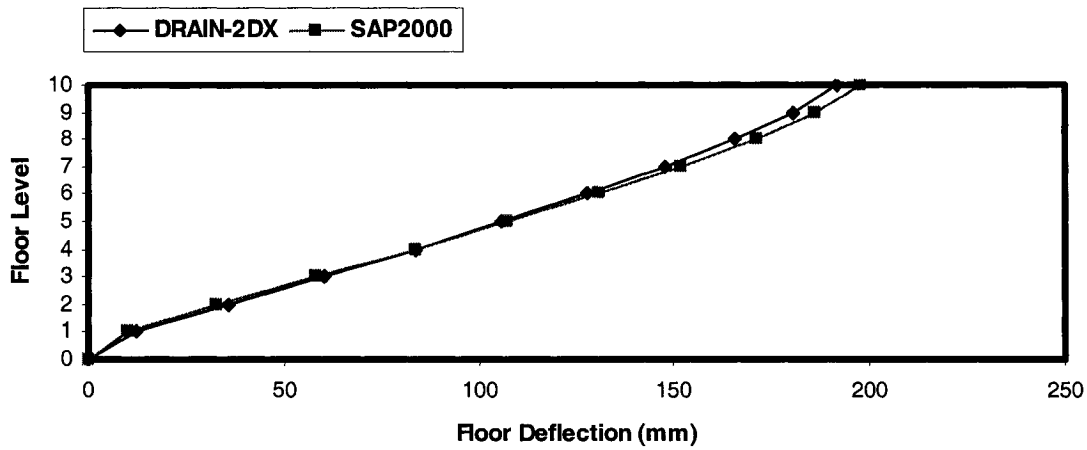

Fig. C.3 Comparison of Floor Deflections of Viscoelastic-Damped Model to El-Centro earthquake

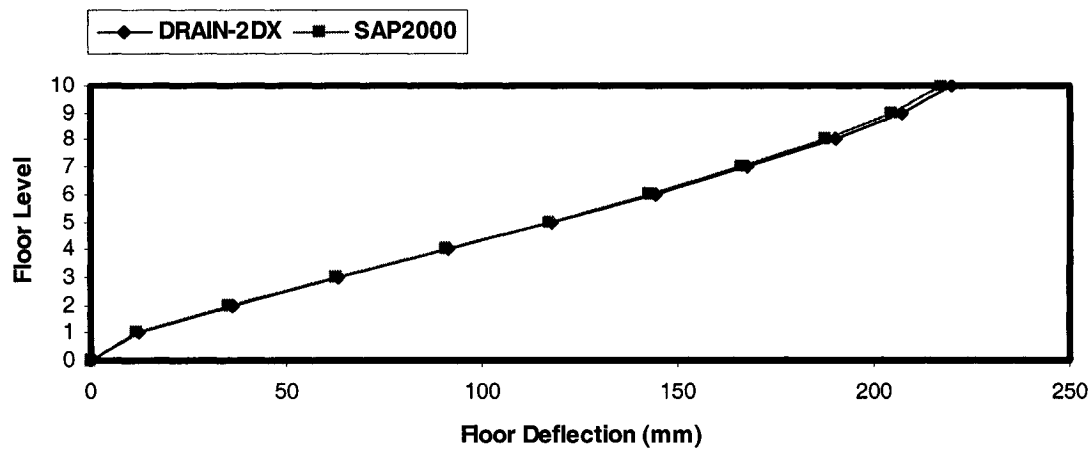

Fig. C.4 Comparison of Floor Deflections of Fluid-Viscous-Damped Model to El-Centro earthquake